AN ANALYTICAL AND EXPERIMENTAL INVESTIGATION OF THE HYDRAULIC TRANSPORT OF HIGH CONCENTRATION MIXED REGIME SLURRIES

by

A W SIVE

A thesis submitted in fulfilment of the requirements
for the degree of Doctor of Philosophy

Department of Civil Engineering
University of Cape Town

March 1988

DECLARATION

I, Anthony Wyndham Sive, declare that this thesis is essentially my own work and has not been submitted for a degree at another university.

Signed by candidate

A W Sive

March 1988

DEDICATION

For my Grandmother, Ilona Mandy

"Gott gibt die Nüsse aber er beisst sie nicht auf!"

J.W. v. Goethe

Weimar

October 1811

ACKNOWLEDGEMENTS

Professor John Lazarus, for his unfailing support and for the inspiration of his immense knowledge in the field of hydraulic transportation. No tribute I could write would convey my gratitude.

Dirk Streicher, for his master skills in helping to design and build the test facility. Dirk thought huge when everyone else thought big.

Mrs Shirley Breed, for her typing and layout *par excellence*.

The staff and postgraduate students of the Department of Civil Engineering for the stimulating working environment.

To my family and friends for their support.

For financial support :

The Council for Scientific and Industrial Research

The University of Cape Town.

The Chamber of Mines of South Africa.

Rössing Uranium, Namibia.

Mather and Platt, S.A.

Georgia Iron Works, U.S.A.

Krohne Instruments, S.A.

ABSTRACT

Mixed regime slurries are those slurries comprised of broad particle size distributions. Slurries of this type with volume concentration up to 50% (relative density of approximately 1.8) are considered. An analytical model has been developed for such slurries. The inputs to the model are mean mixture flow rate, delivered concentration and the particle and pipeline characteristics. In order to calculate *in situ* concentration, the concentration distribution is found by using a diffusion model. A logarithmic velocity distribution is also required and is used to ascribe velocity values to volume elements in a concentric computational grid. Calculated values of mean mixture flow rate and delivered concentration are compared to the input values and an iterative procedure is employed to ensure equality with a result being the computation of *in situ* concentration. The model is applicable over the complete range of flow regimes including stationary bed, sliding bed and suspended flow. The particular regime prevalent for the input values will be ascertained by the model and the energy gradient calculated.

The model is compared to 3 existing correlations in the literature, for mixed regime flow, using 1345 data points collected at the University of Cape Town test facility and 1630 data points from other institutions.

The test facility used comprises two systems each with two pipelines and separate centrifugal pumps. The four pipelines range from 50mm inside diameter to 140mm inside diameter. A data acquisition system continuously

monitors pressures, velocity and temperature. Mixture concentration and velocity are checked using a weigh tank which is filled over a time interval by diverting the slurry flow. Pressures are checked with water manometers. The data acquisition system is interfaced to a microcomputer that calculates required values and outputs tables and graphs of measured values. Detailed observations of the flow conditions are made through clear viewing sections in each pipeline.

A qualitative investigation of periodic flow phenomena observed is presented. These are a result of sliding bed flow and include dunes, waves and slugs. A two-fluid model is proposed and the mechanisms whereby these structures form, grow and eventually disperse is discussed.

TABLE OF CONTENTS

NOMENCLATURE

A	internal area of pipe	(m^2)
A_a	area of suspended load above bed	(m^2)
A_b	area of bed load	(m^2)
$A_{i,j}$	cross sectional area of volume element	(m^2)
a_{bed}	area of bed in pipe of unit radius	
A_*	constant	
B	constant	
c	wave celerity	(m/s)
C_a	concentration at reference level a	
C_b	concentration of solids in loose-packed bed to total volume of bed	
C_r	concentration ratio = C_{vtb}/C_b	
C_v	volumetric concentration	
C_{vd}	delivered volumetric concentration = Q_s/Q_m	
C_{vt}	*in situ* (spatial) volumetric concentration $\mathcal{V}_s/\mathcal{V}_m$	
C_{vtb}	volume concentration of solids in bed load to total mixture volume (*in situ*)	
C_{vtf}	volume concentration of suspended solids to total mixture volume (*in situ*)	
C_w	mass concentration = M_s/M_m	
C_D	particle drag coefficient	
C_{FP}	ratio of floc volume concentration to particle volume concentration	
$C_{FP,0}$	C_{FP} for the maximum degree of aggregation, $\frac{du}{dr} \rightarrow 0$	
$C_{FP,\infty}$	C_{FP} for the maximum degree of disaggregation, $\frac{du}{dr} \rightarrow \infty$	
C_{VF}	floc volume concentration	
d	particle size	(m)

d_{eff}	effective diameter found empirically from equns. (2.67) or (2.68)	(m)
d_i	particle size at which i per cent of the particles are smaller than d_i	(m)
d_{Lmax}	maximum particle size for laminar settling	(m)
d_{Tmin}	minimum particle size for turbulent settling	(m)
D	internal pipe diameter	(m)
e	distance of the point of maximum velocity from the pipe axis (eccentricity)	(m)
exp	basis of natural logarithm (= 2.718) raised to a power	
f	friction factor = $\frac{\tau_o}{\frac{1}{2}\rho V^2}$	
f_*	alternative description of friction factor = 4f	
f_b	friction factor (hydrodynamic) between bed and pipe wall	
f_I	friction factor for suspended portion at bed interface	
f_m	friction factor for mixture at pipe wall	
f_w	friction factor for water flowing at velolcity V_m in a pipe of diameter D	
fn	function of ...	
F_r	Froude number	
F_D	driving force on slurry (bed load plus suspended load)	(N)
$F_{D_{ST}}$	driving force for stationary bed flow	(N)
$F_{D_{SL}}$	driving force for sliding bed flow	(N)
$F_{D_{FS}}$	driving force for fully suspended flow	(N)
F_{HB}	hydrodynamic friction force between the sliding bed and the pipe wall	(N)
F_{RA}	resisting force for suspended load in contact with pipe wall	(N)
F_{RB}	resisting force for bed load portion	(N)
F'_{RB}	force resisting sliding bed including bed weight component (equn. 3.70)	(N)
F_{RI}	resisting force for suspended load in contact with bed interface	(N)

g	gravitational constant	(m/s^2)
G_d	grading coefficient = d_{90}/d_{10}	
h	dune height	(m)
h_b	maximum radial bed thickness	(m)
h_τ	height above pipe invert at which u = 0 , $h_\tau = h_b$ for stationary bed flow, $h_\tau = 0$ for sliding bed and suspended flow	(m)
ΔH	head loss	(m)
i_m	mixture head loss gradient in units of water per unit length of pipe	(m/m)
i_{mcal}	calculated value of i_m	(m/m)
i_{mobs}	observed value of i_m	(m/m)
i_p	head loss gradient for plug flow of solids	(m/m)
i_{susp}	head loss gradient for suspended load portion of flow	(m/m)
i_w	head loss gradient for water flowing at velocity V_m in pipe diameter D	(m/m)
j_m	head loss gradient in units of mixture per unit length of pipeline	(m/m)
k_1, k_2, k_3, k_4	constants defined by the equations in which they are used	
k_s	mean size of sand bed roughness	(m)
k_w	mean size of pipe roughness element	(m)
K	fluid consistency index	$(Pa\ s^n)$
log	decimal logarithm	
ln	natural logarithm	
L	length of pipeline measuring section	(m)
m_i	mass fraction of particles of size d_i	
M_s	solid mass flow rate	(kg/s)
M_m	mixture mass flow rate	(kg/s)
n	flow behaviour index	
n	number of	

n_v	number of particle size groups constituting vehicle	
N_P	number of particles contained in a floc	
p	perimeter	(m)
p_n	probability of grain erosion	
ΔP	pressure drop	(Pa)
q	local volumetric flow rate	(m^3/s)
q_{sb}	interface load rate per unit width	(N/ms)
q_{ss}	suspended load rate per unit width	(N/ms)
Q_m	volumetric flow rate of mixture	(m^3/s)
Q_s	volumetric flow rate of solids	(m^3/s)
Q_{sb}	interface load rate	(m^3/s)
Q_{ss}	suspended load rate	(m^3/s)
r	radial distance	(m)
r	correlation coefficient (equn. 4.13)	
r_F	floc radius	(m)
R	pipe radius	(m)
R_e	Reynolds number = $DV\rho/\mu$	
R_{ep}	particle Reynolds number	
R_{eplc}	power law Reynolds number	
R_f	ratio of mass of fines to total mass of particles	
Rh_a	hydraulic radius for suspended material = $\frac{A_a}{p_a + W_I}$	(m)
S	root mean square deviation or log standard error (equn. 6.1)	
S_F	particle shape factor	
S_m	relative density of mixture	
S_{mf}	relative density of suspended mixture	
S_s	relative density of solid	
S_v	slip velocity = $\lvert V_s - V_f \rvert$	(m/s)

SEC	specific energy consumption	(Ws/kg m)
SPC	specific power consumption	(Ws/Nm)
t	time	(s)
t_e	exchange time for bed particles	(s)
T	temperature	(°C)
T_β	surface tension between bed mixture and suspended mixture	(mN/m)
u	local velocity	(m/s)
u_*	shear velocity = $\sqrt{\frac{\tau}{\rho}}$	(m/s)
u^+	dimensionless local velocity = u/u_*	
u_{max}	maximum velocity in pipe flow	(m/s)
V_a	velocity in the area occupied by suspended portion above bed load	(m/s)
V_{crit}	laminar-turbulent transition velocity	(m/s)
V_{dep}	deposit velocity	(m/s)
V_m	mean mixture velocity = Q_m/A	(m/s)
V_{mt}	value of V_m at threshold of turbulent suspension	(m/s)
V_{suspi}	velocity for turbulent suspension of grain size d_i	(m/s)
V_t	particle settling velocity	(m/s)
V_t'	hindered particle settling velocity	(m/s)
$\mathcal{V}$	volume	(m^3)
$\mathcal{V}_b$	bed volume	(m^3/m)
$\mathcal{V}_m$	mixture volume	(m^3/m)
$\mathcal{V}_s$	solid volume	(m^3/m)
$\mathcal{V}_{si}$	total solid volume for each size group d_i	(m^3/m)
$\mathcal{V}_{sbi}$	interface load volume for each size group d_i	(m^3/m)
$\mathcal{V}_{ssi}$	suspended load volume for each size group d_i	(m^3/m)
$\mathcal{V}_{s\ bed}$	volume of solids in a stationary or sliding bed	(m^3/m)
w	weight	(kg)

W_I	bed interface width	(m)
x	ratio = τ_y/τ_o	
x	direction of the uniform flow	
X	characteristic grain size (equn. 3.25)	(m)
X	dimensionless particle size	
X	non dimensional hydraulic gradient parameter (equn. 1.23)	
X_S	X value from equn. (1.23) for incipient stationary bed condition	
y	direction perpendicular to x	
y	distance from pipe wall = R - r	(m)
y_a	height of reference level above bed/pipe invert (equn. 3.35)	
y_o	height of maximum velocity stream-line above bed interface	(m)
y^+	dimensionless distance from the wall = $yu_*\rho/\mu$	
Y	yield number	
Y	dimensionless terminal settling velocity	
Y	pressure correction factor (equn. 2.115)	
Y	non dimensional hydraulic gradient parameter (equn. 1.22)	
z	exponent in the suspension distribution	
α	exponent	
β	constant in equn. (2.14)	
γ_b	angle defining bed load portion	
δ	sublayer thickness	(m)
Δ	apparent roughness diameter (equn. 3.32)	(m)
ϵ_m	diffusivity of linear momentum	(m^2/s)
ϵ_s	diffusivity of solid particles	(m^2/s)
ζ_β	constant	
η_r	relative viscosity = K/μ_w	
θ	angle defining pipe slope	

θ'	angle between vertical axis and a point on the computational grid from the point of maximum velocity	
κ	von Karman constant	
λ	dune wavelength	(m)
μ	dynamic viscosity	(Pas)
μ_{mf}	viscosity of pseudohomogeneous suspension	(Pas)
μ_s	coefficient of sliding friction between bed load and pipe wall	
ν	kinematic viscosity = μ/ρ	(m^2/ms)
ξ	friction factor ratio = $2f_b/f_w$ (equn. 1.21)	
ξ	hiding factor (equn. 2.115)	
π	3.146	
ρ	density	(kg/m^3)
ρ_{mb}	density of bed material	(kg/m^3)
ρ_{mf}	density of suspended material	(kg/m^3)
τ	shear stress	(Pa)
τ_a	shear stress at pipe wall above interface	(Pa)
τ_b	shear stress at pipe wall below interface (hydrodynamic)	(Pa)
τ_I	shear stress at interface between bed load and suspension load	(Pa)
τ_o	wall shear stress	(Pa)
τ_y	yield shear stress	(Pa)
ϕ	$(i_m-i_w)/(C_{vd}\ i_w)$	
Φ	intensity of interface load transport	
Ψ	intensity of shear on individual particles	
Ψ_*	intensity of shear on individual particles located in the bed	

SUBSCRIPTS

a	lighter phase in 2 phase flow (suspended)
b	heavier phase in 2 phase flow (bed)

i	i-th component
m	mixture
o	pipe wall
c,f	coarse, fine
max	maximum value
v	volumetric basis
d	delivered (at outlet of pipe)
t	*in situ* (spatial)
f	fluid phase
s	solid phase
w	water
w	weight basis
ave	average

INTRODUCTION

The design of hydrotransport systems has historically been achieved by scaling the energy gradient and mixture flow rate obtained from a model or prototype pipeline. In the last two decades academic research has become more sophisticated, as shown in the proceedings of the numerous hydrotransport conference series, although the use of empirical design equations continues in industry. A major advance in hydrotransport research was the development of models that describe the internal mechanisms of pipeline flow. In the early 1970s this mechanistic approach produced a two-layer model which divided a slurry into a stationary or sliding bed with clear fluid flowing in the remaining pipe area.

By the late 1970s a method of quantifying the suspension of bed material improved the two-layer model. The two-layer two component model led to the development of a two-layer multicomponent model for mixed regime slurries.

At present problems still remain in the precise modelling of mixed regime slurries. Mixed regime slurries are composed of solids with well graded particle size distribution. The finest fraction often modifies the rheology of the fluid phase. The vehicle, produced by the fine fraction and the free fluid, and its effect on the transport mechanism has been neglected. The difference between *in situ* and delivered concentration has also been neglected.

1. The problem and its setting

This research identifies and evaluates a mathematical model for the hydrotransport of high concentration mixed regime slurries. A two-layer

Table 1 : Parameter range of the data base used to evaluate the mathematical model

Parameter	Range	
	Local data	Imported data
C_{vd} [%]	0% - 54.6%	4% - 51%
d_{50} [μm]	9 - 8280	9 - 4500
D [m]	0.045 - 0.142	0.052 - 0.315
S_s	1.90 - 2.96	1.34 - 5.25
Temp [°C]	16.7 - 58.7	17 - 42
V_m [m/s]	0.05 - 6.87	0.1 - 6.1
Number of data points	1345	1630

Table 2 : Mathematical models used for comparative purposes

	Author and Reference
1.	Wasp *et al.* (1963, 1970, 1971)
2.	Wilson (1974, 1976, 1978, 1979, 1980)
3.	Lazarus (1986)

The two-layer mechanistic model is a simplification of the physical flow condition. Periodic phenomena such as dune, wave and slug flow may occur. Detailed observations of the flow were made through viewing sections in all

is discussed for increasing mean mixture flow rate from stationary bed through part stationary bed, fully moving bed and fully suspended flow. Conclusions and recommendations arising from the literature review are drawn.

The second part presents the analytical and experimental investigation. A qualitative hypothesis for heterogeneous slurry flow for increasing mean mixture flow rate is presented. The analytical model and mathematical procedures employed are discussed in detail. The hydrotransport test facility is then presented. The experimental method is accompanied by a detailed error analysis. The data produced is then presented and discussed.

The third part presents an evaluation of the mathematical model. The mathematical description of the vehicle is evaluated against experimental data. The complete model is then compared to the other presented correlations on the basis of :

1. Energy gradient prediction.
2. *In situ* concentration prediction.
3. Flow regime classification.

Concentration and velocity profiles are presented for selected tests. A design example for constant solid mass flow rate and for constant concentration is presented to conclude the evaluation.

Conclusions and research recommendations complete the investigation.

Volume 2 contains the Appendices. A glossary is contained in Appendix 1. Appendices 2 to 5 present a detailed description of the test facility and

be undertaken without the use of a computer program and the output from the program can be tailored as required.

This research comprises a detailed investigation of mixed regime flow. It identifies and evaluates many of the phenomena present in the flow and suggests methods for modelling these. With careful evaluation conclusions are drawn and further research recommendations are made. As with research in any field this work represents a contribution to knowledge rather than a definitive study.

PART 1 : LITERATURE REVIEW

CHAPTER 1

EXISTING ANALYTICAL CORRELATIONS FOR MIXED REGIME FLOW

INTRODUCTION

Over the past 100 years a large body of literature on the hydraulic transport of solid-water mixtures has been produced. Significant contributions were made in the 1940s and 1950s by workers such as Durand in France and Newitt in England. Research became more sophisticated as shown in the proceedings of the numerous conference series begun in the 1970s namely the Hydrotransport series organised by the British Hydromechanics Research Association and the Slurry Transport Association conference series in America. The possibility of pipeline deregulation in the U.S.A. gave the industry new impetus at this time which was later to be destroyed by right of way and access disputes. Today significant work is still being produced by many prominent researchers.

1.1 DEFINITION OF MIXED REGIME FLOW

Mixed regime slurries, by definition, display heterogeneous and homogeneous flow phenomena simultaneously. Particle size distribution, volumetric concentration and mean flow velocity influence the regime ratio and hence energy gradient. Wasp *et al.* (1963) describes mixed regime flow as a two phase transporting medium (called the vehicle) with suspended solids carried

in this medium. The concentration and particle size distribution at the top of a horizontal pipeline define the vehicle for a particular flow velocity. The asymmetrical part of the concentration profile is ascribed to the heterogeneously transported coarse suspension (see Figure 1.1).

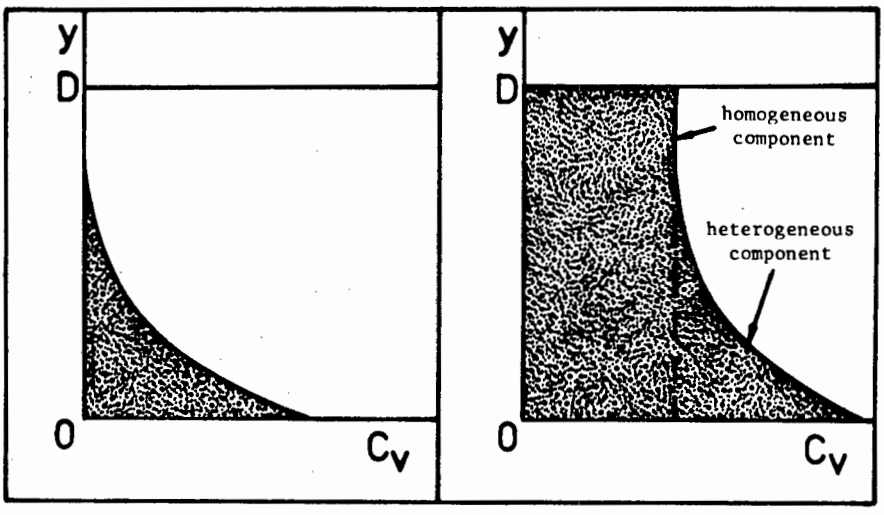

a) Heterogeneous b) Mixed regime

Figure 1.1 : Definition of mixed regime flow according to the concentration profile at constant mean velocity and particle size distribution

1.2 BENEFIT OF MIXED REGIME FLOW

Mixed regime flow results in a decreased energy gradient and a higher total solids concentration than an equivalent mixture of unisized particles. The increased concentration depends on particle size distribution. The increased carrying capacity results in a decrease in Specific Energy Consumption where

$$SEC = \frac{i_m \, g}{C_{vd} \, S_s} \qquad [Ws/kgm] \quad . \qquad (1.1)$$

This leads to an overall increase in the transport system efficiency. Abrasive wear and particle attrition are also reduced (Charles and Charles, 1971).

1.3 MECHANISMS DECREASING ENERGY GRADIENT

The mechanisms decreasing the energy gradient for equivalent concentrations of mixed regime slurries compared with unisized slurries are predominant at low velocities when the flow would be heterogeneous (Kazanskij *et al.*, 1974).

The mechanisms causing this decrease are listed below :

1.3.1 The fines content results in an increase in the apparent viscosity and a damping of turbulent eddies (Wasp *et al.*, 1970; Hanks, 1981).

1.3.2 There is a decrease in density differential between vehicle and suspended load (Hanks, 1981).

1.3.3 Mixed regimes eliminate, or significantly reduce coarse particle settling resulting in a decrease in the relative slip velocity of the coarse component and a decrease in turbulent suspension requirement (Wasp *et al.*, 1970; Hanks, 1981; Stepanoff, 1964). The vehicle may exhibit non Newtonian behaviour with a yield stress which results in a central core containing coarse solids (Stepanoff, 1964).

The increase in the mixture energy gradient over the carrier fluid (water) is due to a homogeneous non Newtonian vehicle with large particles being transported with little settling requiring low additional energy to keep them in suspension. Cheng and Whittaker (1972) exploited this fact in analysing mixed regime flow as a non Newtonian fluid if a specified settling interface criteria could be met.

1.3.4 There may be a reduction in pipe wall roughness due to the entrapment of fines in the pipe wall irregularities.

1.3.5 Plate and needle like fine particles ($d < 10\mu m$) cause a lubricating effect.

1.3.6 The ratio of particle size to the viscous sublayer thickness ($\delta = 5\mu/\rho u_*$), causes a pressure reduction if $d/\delta \geq 5$ for pseudohomogeneous flow which will occur if $V_t/u_* \leq 0.11$ (Thomas, A D, 1978).

Examples of the pressure reducing phenomena are :

1. At $C_{vd} = 15.7\%$ and $V_m = 1.5$ m/s
   For sand only $i_m = 0.012$ m/m
   For sand and bentonite $i_m = 0.008$ m/m (Kazanskij *et al.*, 1974).
2. An increase of up to 15% by volume of large particles in a mixture of fine particles has little influence on hydraulic gradient. An increase of up to 20% by volume of fines in a coarse mixture significantly reduces hydraulic gradient (Smoldyrev, 1982).

3. A clay content of 7% decreases the hydraulic gradient by 10% at $V_m \simeq V_{crit}$ and $C_{vd} \simeq 20\%$ (Smoldyrev, 1982).
4. Klose (1982) has reported a decrease in hydraulic gradient caused by the attrition of coal particles. Figure 1.2 shows the particle size distribution of the coking coal tested. Figure 1.3 shows the decrease in pressure loss associated with the change in particle size distribution.

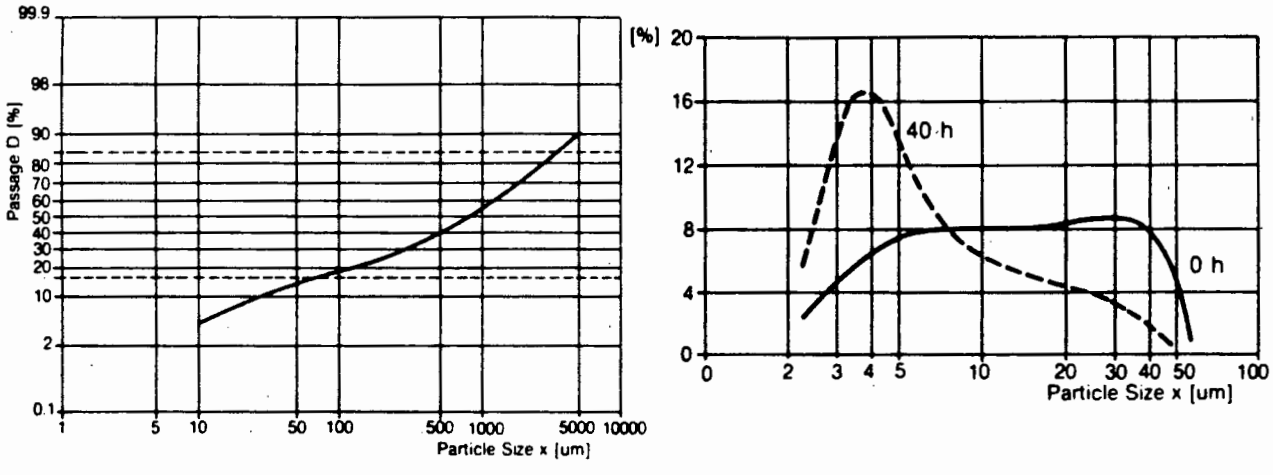

(a) (b)

Figure 1.2 : (a) Particle size distribution for coking coal
(b) Change in PSD for ultra fine fraction of coking coal
(from Klose, 1982)

1.4 EXISTING CORRELATIONS FOR HYDRAULIC GRADIENT PREDICTION

1.4.1 Introduction

Table 1.1 presents some correlations for mixed regime flow. The correlations used for analysis are marked by an asterisk. The models presented were chosen on the basis of requiring more information than a single particle size to describe the solid phase.

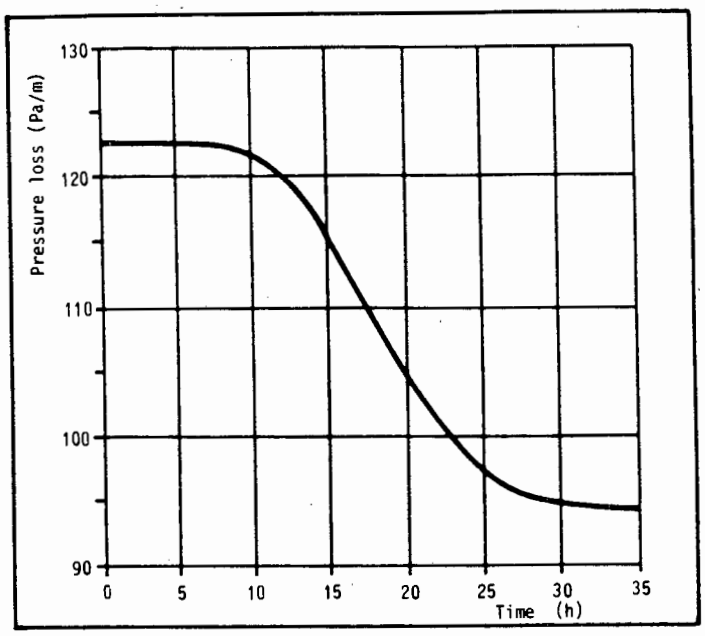

Figure. 1.3 : Changes in pressure loss for coking coal slurry with time (C_{vd} = 33%, V_m = 1.75 m/s, D = 400mm) (from Klose, 1982)

Table 1.1 : Some correlations for mixed regime flow

Type of Correlation	Author
1. Empirical non dimensional	Bonnington (1959) + Durand & Condolis □ + Zandi & Govatos □
2. Semiempirical non dimensional	Clift *et al.* (1982) Vocadlo & Charles (1972) + Smoldyrev (1982)
3. Two component	Faddick (1982b) + Hanks (1981) Newitt *et al.* (1955) + Wasp *et al.*(1963,1970,1971)*
4. Two layer, mixed regime	Wilson (1974, 1976) (1978, 1979, 1980) *
5. Two layer, multi-component, mixed regime	Lazarus (1986) *
6. Multi layer, multi-component, heterogeneous flow only	Roco & Shook (1982)

* - correlations used to analyse data in this thesis
+ - correlations compared by Wani *et al.* (1982)
□ - in Zandi (1971)

Hanks (1982) noted that the choice of a "favourite mean diameter" would not sufficiently describe the Particle Size Distribution (PSD) of any slurry. The only way to describe the PSD is by taking points along the distribution and actually using these in the analysis. The models presented fulfil this condition.

1.4.2 The Wasp *et al.* Model (1963, 1970, 1971)

Wasp *et al.* presented an iterative method for calculating the rheologically active part of a mixture. The procedure used is as follows :

1. Guess initial value of C_{vf} (say, $C_{vf} = C_{vd}$) .
2. $$S_{mf} = S_w + C_{vf}\,(S_s - S_w) \qquad (1.2)$$
   $$\mu_{mf} = \mu_w(1 + C_{vf}/C_b)^{-2.5} \; . \qquad (1.3)$$
3. Calculate f_m from Colebrook-White equation for $R_e = \dfrac{\rho_{mf} V_m D}{\mu_{mf}}$.
4. Calculate V_{ti} the settling velocity for each particle diameter for S_{mf} and μ_{mf} .
5. Calculate
   $$\log \left[\frac{C}{C_a}\right]_i = -\,1.8\,\frac{V_{ti}}{\kappa\,\beta\,V_m\sqrt{f_m/2}} \text{ where } \beta \simeq 1 \; . \qquad (1.4)$$
6. Sum all the values obtained in 5 as follows :
   $$C_{vf} = \sum_i \left[\frac{C}{C_a}\right]_i m_i\, C_{vd} \qquad (1.5)$$
   $$C_{vb_i} = \left[1 - \left[\frac{C}{C_a}\right]_i\right] m_i\, C_{vd} \qquad (1.6)$$
   m_i = percentage of each particle size retained.
7. Compare C_{vf} in Step 6 to C_{vf} in Step 1 and if C_{vf} (from 6) minus C_{vf} (from 1) is greater than 0.001 then recalculate from Step 2 using new C_{vf} from Step 6.

8. Calculate: $$i_{mf} = \frac{2f_m S_{mf} V_m^2}{gD} . \quad (1.7)$$

9. $$\phi' = 82\, C_{vb_i} \left[\frac{gD(S_s - S_w)}{V_m^2 \sqrt{C_{D_i}}}\right]^{1.5} . \quad (1.8)$$

10. $$\Psi = \Sigma \phi_i' . \quad (1.9)$$

11. $$i_m = i_{mf} + i_w \Psi . \quad (1.10)$$

12. The equation for stationary deposit is given by :

$$V_D = F_L' \left[2gD(S_s - S_w)\right]^{1/2} \left[\frac{d}{D}\right]^{1/6} \quad (1.11)$$

where $F_L' = fn(C_v)$

if $V_m \leq V_D$ then a stationary bed exists.

1.4.3 The Wilson Model (1974, 1976, 1978, 1979, 1980)

Wilson presented a mechanistic model for the analysis of sliding bed flow. The analysis has an inherent method for stationary bed classification. Wilson presented nomographic charts to alleviate the need for a computer analysis. The analysis presented here is for a computer and required considerable interpretation of Wilson's papers.

1. Calculate the bed load concentration C_{vb} by averaging the equation

$$\frac{C_{vb}}{C_v} = \left[\frac{V_{mt}}{V_m}\right]^{\alpha} . \quad (1.12)$$

This was interpreted (Sive and Lazarus, 1986) as

$$\frac{C_{vb}}{C_v} = \left[\frac{\Sigma\left[\frac{V_{mti}}{V_m}\right]^2}{n}\right] \text{ for } \frac{V_{mti}}{V_m} > 1 \quad \text{let } \frac{V_{mti}}{V_m} = 1 \quad (1.13)$$

where $V_{mti} = 0.6\ V_{ti}(2/f_w)^{\frac{1}{2}} \exp \frac{45d_i}{D}$ (1.14)

and n - number of groups with particle size d_i .

2. $a_{bed} = \pi\ C_r$ the bed load area (1.15)

where $C_r = \frac{C_{vb}}{C_b}$. (1.16)

C_{vb} is obtained from equn. (1.13).

3. Calculate γ (see Figure 1.4) for a given bed load using an iterative method where

$a_{bed} = \gamma - \cos \gamma \sin \gamma$. (1.17)

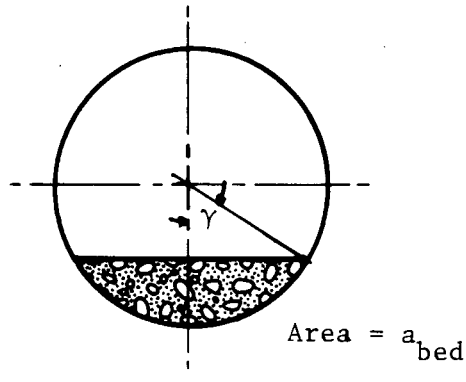

Figure 1.4 : Definition of terms

4. Determine the friction factor associated with the interface

$$f_b = \left[4 \log \left[\frac{3.7D}{d_{50}}\right]\right]^{-2} .$$ (1.18)

5. Calculate the head loss gradient for the suspended load portion

$i_{susp} = ((S_s - S_w)(C_v - C_{vb}) + 1)\ i_w$. (1.19)

6. Calculate the head loss gradient for plug flow of solids from

$$i_p = 2\,\mu_s(S_s - S_w)C_b \,. \qquad (1.20)$$

7. Calculate the ratio (ξ) from

$$\xi = 2\,f_b/f_w \,. \qquad (1.21)$$

8. Wilson defined non dimensional hydraulic gradient parameters given by

$$Y = \frac{i}{i_p} = \frac{\sin\gamma - \gamma\cos\gamma}{1 - a_{bed} + \dfrac{a_{bed}\,\xi\sin\gamma}{\pi - \beta + \xi\sin\gamma}} \qquad (1.22)$$

and

$$X = \frac{i_{susp}}{i_p} \,. \qquad (1.23)$$

9. The total hydraulic gradient is calculated from

$$i_m = Y\,S_m\,i_p + i_{susp}\,\frac{(1 - a_{bed})}{\pi} \,. \qquad (1.24)$$

10. The value of X at the bed slip point is calculated from

$$X_s = \frac{(\sin\gamma - \gamma\cos\gamma)(1 - a_{bed})^2}{\xi\sin\gamma} \,. \qquad (1.25)$$

If $X \leq X_s$ then a stationary bed exists.

1.4.4. The Lazarus Model (1986)

Lazarus presented a modification of Wilson's method. The three component model consists of the vehicle plus suspended load portion and a stationary bed load portion.

1.4.4.1 **The vehicle portion**

The initial separation of solids is arbitrary and is carried out using a grading curve and selecting all those particles which are less than the particle size corresponding to hindered settling particle Reynolds number of unity.

The following steps are followed in the calculation procedure :

The value for d_{Lmax} is obtained from

$$d_{Lmax} = \left[\frac{18\mu^2 S_w}{\rho\,(S_s - S_w)g}\right]^{1/3} . \qquad (1.26)$$

The ratio (R_f) of fine material in the vehicle portion to the total solids component carried as suspension or bed load is

$$R_f = \frac{1}{10}\left[i - 1.5 + \log\left[\frac{d_{Lmax}}{d_{i-1}}\right]/\log\left[\frac{d_i}{d_{i-1}}\right]\right] \qquad (1.27)$$

where i = integer number of components of particle size just greater than d_{Lmax}

and d_i = particle size of component i .

The relative density (S_{mf}) and viscosity (μ_{mf}) of the fines and water (i.e. the vehicle) arising from this initial separation is calculated, assuming a Newtonian vehicle for the first trial from

$$S_{mf} = \frac{S_w + C_{vd}\,(R_f\,S_s - S_w)}{1 - C_{vd}\,(1 - R_f)} , \qquad (1.28)$$

and

$$\mu_{mf} = \mu_w(1 - C_{vf}/C_b)^{-2.5} \qquad (1.3)$$

where $C_{vf} = \dfrac{S_{mf} - S_w}{S_s - S_w}$. (1.29)

The friction factor (f_m) for the assumed Newtonian vehicle is determined from the Colebrook-White equation with the relative density and viscosity calculated for the fine particles (i.e. ρ_{mf} and μ_{mf}) .

1.4.4.2 The suspended portion

The suspended portion is obtained by dividing each size fraction into a suspended portion and a bed load portion using the mean mixture velocity at the threshold of turbulent suspension as the criterion.

The threshold of turbulent suspension is given for each particle size d_i ,

$$V_{mti} = 0.6\ V'_{ti}\ \sqrt{2/f_m}\ \exp(45\ d_i/D) \qquad (1.14)$$

V'_{ti} = hindered settling velocity for the i-th size fraction.

The ratio of solids in the bed load for each size fraction (C'_{ri}) is found from

$$C'_{ri} = (V_{mti}/V_m)^2 \quad . \qquad (1.30)$$

The value of (V_{mti}/V_m) must be less than unity.

The fraction (C_{vbi}) of each solid size fraction m_i in bed load is

$$C_{vbi} = C'_{ri} * m_i \quad . \tag{1.31}$$

The total fraction of solids in bed load is

$$C_{vb} = \Sigma \left[C'_{ri} * m_i \right] = \Sigma\, C_{vbi} \quad . \tag{1.32}$$

The above procedure is repeated for each size fraction.

The total fraction of bed load solids in the mixture is

$$C_{vbm} = C_{vb} * C_{vd} \quad . \tag{1.33}$$

The value of C_{vbm} must be less than C_{vd} .

By subtraction the concentration of fines is given as

$$C_{vf} = C_{vd} - C_{vbm} \quad . \tag{1.34}$$

A new value for the relative density of fines in the suspended portion (S_{mf}) and the viscosity (μ_{mf}) may now be determined from this new value of C_{vf} and equns. (1.29) and (1.3) respectively.

The values of S_{mf} and μ_{mf} for the suspended portion are used in an iterative procedure for determining a new friction factor (f_m), a new hindered settling velocity (V'_t) , a new fraction of solids in bed load (C_{vb}) and a new fraction of bed load solids in mixture (C_{vbm}) .

The above procedure is continued until the change in the concentration of the suspended portion for successive iterations is less than a prescribed tolerance

$$|C_{vf}(New) - C_{vf}(Old)| < 0.01$$

or $C_{vb} > 0.99$,

where $C_{vf}(New) = C_{vf}$ for the latest iteration

and $C_{vf}(Old) = C_{vf}$ for the previous iteration .

1.4.4.3 The bed load portion

Once the suspended portion has been finalised, the bed load portion is determined.

The area occupied by the bed of solids is given by

$$A_b = A \frac{C_{vbm}}{C_b} \quad . \qquad (1.35)$$

1.4.4.4 The two component model

The three component model is reduced to a two component model by combining the vehicle and suspended load portion as one component occupying the area above the bed, and the bed load portion as the other component.

1.4.4.5 Calculation of shear stresses at the pipe wall and interface

The shear stress on the vehicle plus suspended portion at the pipe wall above the interface is given by

$$\tau_a = f_m \rho_{mf} V_m^2/2 \quad . \tag{1.36}$$

The shear stress at the interface between the bed load and suspended load is given by

$$\tau_I = f_I \rho_{mf} V_a^2/2 \tag{1.37}$$

$$\text{where} \quad f_I = (4 \log 3.7\ D/d_{50})^{-2} \quad . \tag{1.18}$$

1.4.4.6 Force balance for two component mechanistic model

Application of a force balance to a control section of slurry is shown in Figure 1.5 and represented by

$$F_D = F_{RH} + F_{RB} + W \sin \theta \quad . \tag{1.38}$$

The resisting force for a pseudohomogeneous suspension above the bed load may be found from

$$F_{RH} = \tau_a (\pi D - D \gamma) \quad . \tag{1.39}$$

The weight component down the slope of an upward sloping pipe is determined from

$$W \sin \theta = \rho_m A g \sin \theta \quad . \tag{1.40}$$

The bed resistance in a horizontal pipeline is integrated to yield

$$F_{RB} = g\,(\rho_s - \rho_w)\,C_b\,\mu_s\,A_b\cos\theta \quad . \tag{1.41}$$

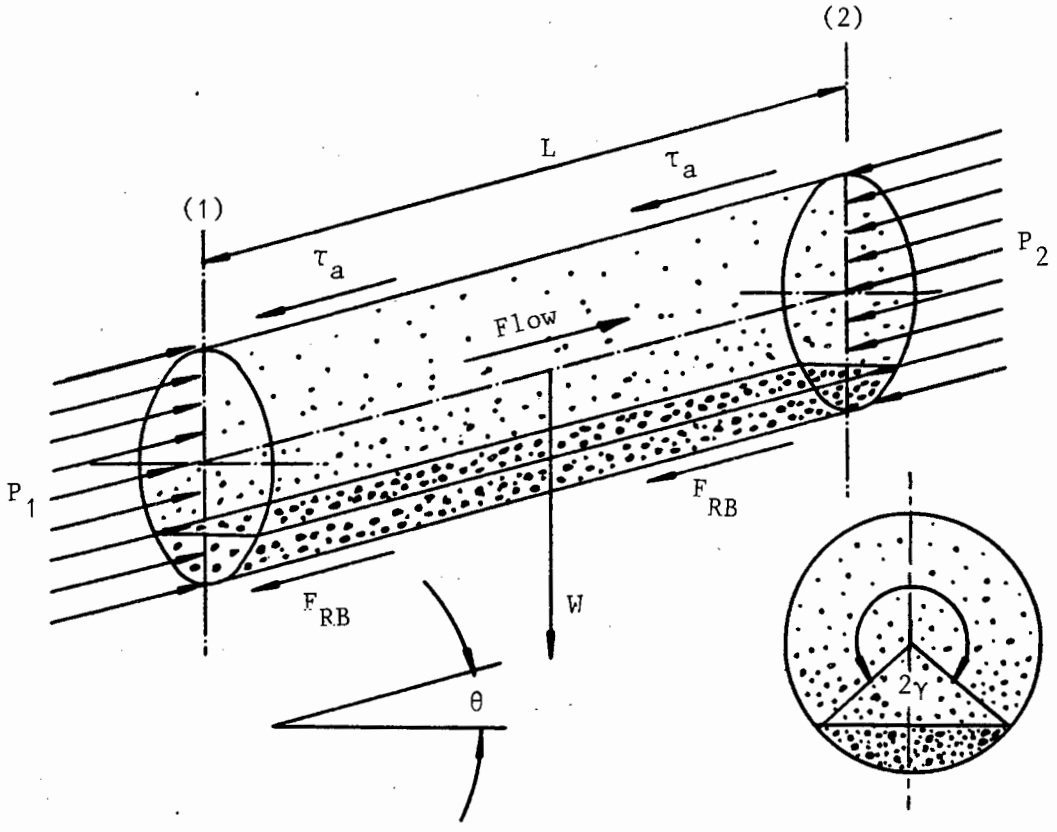

Figure 1.5 : Force balance on control section of three component two-phase flow (Lazarus 1986)

1.4.4.7 Equations for the four modes of flow

1. Stationary bed with suspended portion above

In the region above the bed Lazarus (1986) presents a force balance on the suspension enabling the pressure gradient $\frac{\Delta P}{L}$ to be

calculated

$$\frac{\Delta P}{L'} A = \tau_a (\pi D - D \gamma) + F_{RB} + (A - A_b) \sin \theta \rho_{mf} g \quad . \qquad (1.42)$$

2. Incipient sliding bed

A force balance on the bed yields

$$\frac{\Delta P}{L} A_b + \tau_I D \sin \gamma = F_{RB} + W_b \sin \theta \qquad (1.43)$$

where $W_b = A_b \rho_{mb} g$. (1.44)

When an incipient sliding bed exists, equn. (1.43) is true and may be used to find the incipient sliding bed velocity (V_{dep}) .

If the left hand side is less than the right hand side then the bed is stationary and $\frac{\Delta P}{L}$ is given by equn. (1.42). However, if the left hand side is greater than the right hand side then the bed is sliding and equn. (1.45) is used.

3. Dynamic condition with sliding bed

A force balance on the entire flow with a sliding bed yields

$$\frac{\Delta P\, A}{L} = \tau_a(\pi D - D \gamma) + F_{RB} + W_b \sin \theta \quad . \qquad (1.45)$$

4. Fully suspended flow with no bed load

A force balance for fully suspended flow yields

$$\frac{\Delta P\, A}{L} = \tau_a \pi D + W_b \sin \theta \quad . \qquad (1.46)$$

This occurs when

$\gamma \to 0$ and $A_b \to 0$

i.e. $F_{RB} \to 0$ and $\tau_a(\pi D - D \gamma) \to \tau_a \pi D$.

In this case $\frac{\Delta P}{L}$ is determined from equn. (1.46).

1.4.4.8 Friction head loss gradient

The head loss gradient may be found for all modes of flow from

$$i_m = \frac{\Delta P}{\rho_w g L} . \qquad (1.47)$$

1.5 CONCLUSIONS

An understanding of mixed regime flow phenomena may encompass single regime flow as a special case. The method ascribed to Wilson and presented in this chapter was adapted from a correlation for heterogeneous flow of unisized particles. The concentration equation used by Wasp *et al.* (1.4) was also developed for unisized particles by Ismail (1951). This study of mixed regime flow phenomena is an attempt to produce a unified model.

The three models selected represent those which use a full description of the particle size distribution. The models are also all computer based and can therefore be used to assess any further analytical computer based models developed in this thesis. The models presented are not considered to be the only available but are considered to be representative of those available.

CHAPTER 2

ANALYSIS OF HIGH CONCENTRATION MIXED REGIME FLOW

INTRODUCTION

This chapter is divided into four sections :

2.1 Flow observations

2.2 Particle properties

2.3 Vehicle properties

2.4 Two phase flow

2.5 Conclusions

The first section serves to define the region of interest. The flow phenomena observed will suggest the active flow mechanisms and indicate the *modus operandi* for the analytical investigation. The next two sections analyse the major constituents of the mixture. The last section investigates the physical phenomena that exist in pipeline flows and forms a basis for the analytical model presented in Chapter 3.

2.1 FLOW OBSERVATIONS

Flow observations are an essential part of any hydrotransport system investigation. A qualitative understanding of the flow phenomenon serves as a basis for the analytical model. Care must be taken to ensure that the clear viewing section used does not interfere with the slurry flow (i.e.

changes in diameter, pipe joint misalignment). The length of the viewing section is important in that the flow condition observed must be extrapolated for the complete pipeline. This means that periodic phenomena observed at the viewing section will be part of a more complex overall system.

The flow observations of several authors are presented in this section. The literature presented was chosen because of the similarity to materials tested at the University of Cape Town.

Boothroyde *et al.* (1979) presented a description of the flow of solids with two different size ranges in a 200mm nominal bore pipe (see Table 2.1) and found that material moved in contact with the bed invert up to the highest velocity tested (7 m/s). A description of the flow is presented in Table 2.2.

Table 2.1 : Materials tested by Boothroyde *et al.* (1979)

Material descriptions			
Gravel	: d_{50}	=	4.3mm
	S_s	=	2.55
Granite	: d_{50}	=	12mm
	S_s	=	2.80
Markham fines	: d_{50}	=	200μm
	S_s	=	1.50

Table 2.2 : Description of flow of coarse particles after Boothroyde *et al.* (1979)

Velocity V_m [m/s]		Flow description
Gravel	Granite	
7.0	7.0	Some particles slide on pipe invert.
3.5	4.3	Fully moving bed - uniform velocity.
3.2 - 3.3	4.0	Some material stops instantaneously. Velocity of continuously moving material fluctuates.
2.9 - 3.0	3.8	Velocity V_1 . Bed moves in jerky fashion described as "slip-stick" behaviour.
2.5	3.0	Velocity V_2 . The whole bed remains stationary from 1 to 5 seconds and moves again. A build up of "dunes" is apparent. "Dunes" move downstream. More conspicuous at low concentration.
1.5	2.3 - 2.5	Stationary bed.

Boothroyde *et al.* (1979) also presented results for mixtures of solids comprising 14mm granite and "Markham" fines. Table 2.3 presents the velocity values V_1 and V_2 , described in Table 2.2, for the coarse mixture.

Baker and Jacobs (1979) presented a set of diagrams, reproduced as Figure 2.1, for the flow regimes observed in a mixture. The figure presented by Baker and Jacobs (1979), when compared with the descriptions of Boothroyde *et al.* (1979), appears to be simplistic. The non uniform, unstable flow conditions that prevail between heterogeneous flow and stationary bed flow are neglected.

Table 2.3 : Effect of fine particles on the transition velocities as described by Boothroyde *et al.* (1979)

Volume percentage of coarse material (Granite)	V_1 [m/s]	V_2 [m/s]
4.3	4.30	2.62
11.0	3.03	2.50
20.0	3.30	2.50

Coarse material only C_v (Granite)	V_1[m/s]	V_2[m/s]
4.6	3.30	3.00
9.3	3.50	3.00
20.2	3.80	3.00

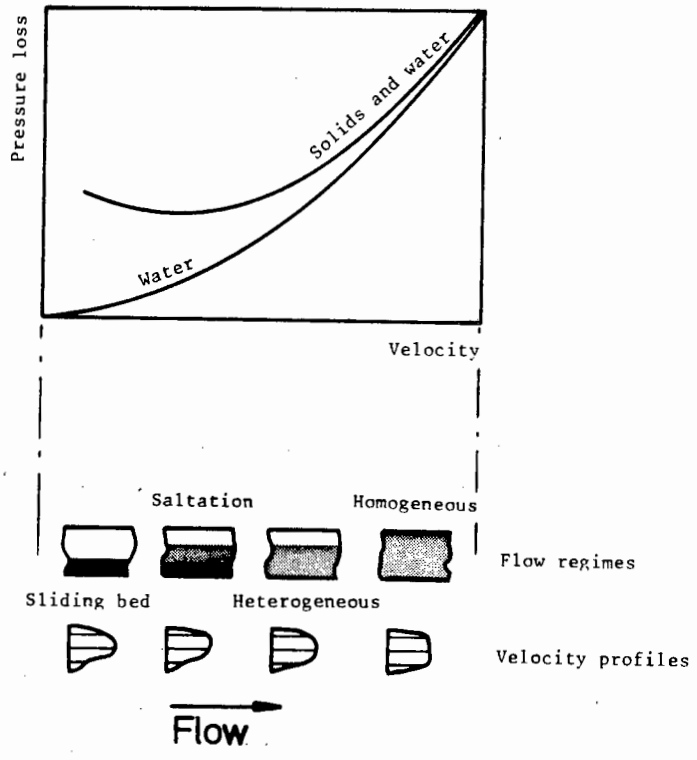

Figure 2.1 : Description of flow regimes after Baker and Jacobs (1979)

2.1.1 Periodic Flow Phenomena

Early researchers such as Howard (1939), Smith (1955), Sinclair (1962) and D.G. Thomas (1964a), (1964b) noted flow instabilities but none except Thomas advanced an explanation. Howard (1939) distinguished "three types (*sic.*)" of transportation one of which was described as "spasmodic movement" in which sand layers moved forward slightly and then stopped. Smith (1955) found particles "sliding slowly and jerkily over the bottom" prior to any particle settling. He expressed a difficulty in finding a deposit velocity, especially for particles with d > 1 - 2mm since "these tended to collect momentarily into batches which either slid or rolled into motion again". Finer particles with d < 300μm settled into "evenly spaced mounds which slowly moved along the pipe". Thomas (1964a) described the motion of "clumps or islands" which formed within seconds to minutes of the flow rate being adjusted to a value "at which a single particle is transported without saltation and without obvious rolling or bouncing on the bottom of the pipe". Table 2.4 presents some of the results Thomas (1964a) found from his experimentation. Thomas conducted tests with two sizes of glass bead (S_s = 2.65) in pipelines ranging in diameter from 25mm to 100mm. Particles with diameter greater than 750μm did not form dunes.

Various terms are used for the non uniform flow condition described by Thomas (1964a). These include islands, clumps, mounds, ripples or dunes. It is also important to note that the formation of these occur both above and below the velocity associated with particles remaining completely stationary at the pipe invert. These terms therefore are used in a very loose context to describe any bedform or instability observed.

Table 2.4 : Dune (island) formation in pipelines after Thomas (1964a)

a) Typical dune dimensions for material tested

Particle diameter d [μm]	Mean dune wavelength λ [mm]	Dune velocity [m/s]	Mean velocity V_m [m/s]
565	100	0.01230	0.45
100	46	0.00045	0.33

b) Average velocity range for dune formation. A small diameter dependence was found

Particle diameter d [μm]	Velocity range V_m [m/s]
565	0.30 → 0.65
100	0.15 → 0.45

c) Dune dimension ratios

$9 \leq \frac{\lambda}{h} \leq 40$	Wavelength to height ratio of dune
$0.06 \leq \frac{h}{D} \leq 0.7$ $\frac{h}{D} \simeq 0.2$ average	Dune height to pipe diameter ratio

Figure 2.2 presents a graph produced by Shook *et al.* (1973). The formation of "dunes" occurs above the velocity associated with the formation of a stationary bed. Figure 2.3 presents similar graphs produced by the CSIR in South Africa (1975). Ponce-Campos and Wall (1984) conducted tests above the part stationary bed condition and found that dunes formed on a slow moving bed with saltating particles overhead. The mixture was a sand-water slurry with 92% of particles between 0.8mm and 1.2mm.

Wallis (1969) suggested that the motion of particle clusters as described by Shook *et al.* (1973), the CSIR (1975) and Ponce-Campos and Wall (1984) resemble a Helmholtz instability in the flow. This form of instability is associated with wave motion and in the case of two-phase pipeline flow, with interfacial waves. Wallis (1969) observed pressure fluctuations caused by this instability at velocities "above the deposit velocity and below the velocity at which stratification disappears". Wallis (1969) simulated the phenomenon by using a model with two inviscid fluid layers flowing between infinite parallel flat plates. Televantos *et al.*(1979) confirmed this approach and found that the bed load in a pipeline would slide *en bloc* before being dispersed. In their description of the phenomenon Televantos *et al.* (1979) reported a distinct change in the velocity profile visible near the midpoint of the pipeline ($C_v \simeq 20\%$). The interface between the two layers seemed to occur higher than the point of abrupt velocity change. This phenomenon can be interpreted as a shear stress distribution acting in the bed layer causing it to flow much like a fluid with density greater than the overhead mixture.

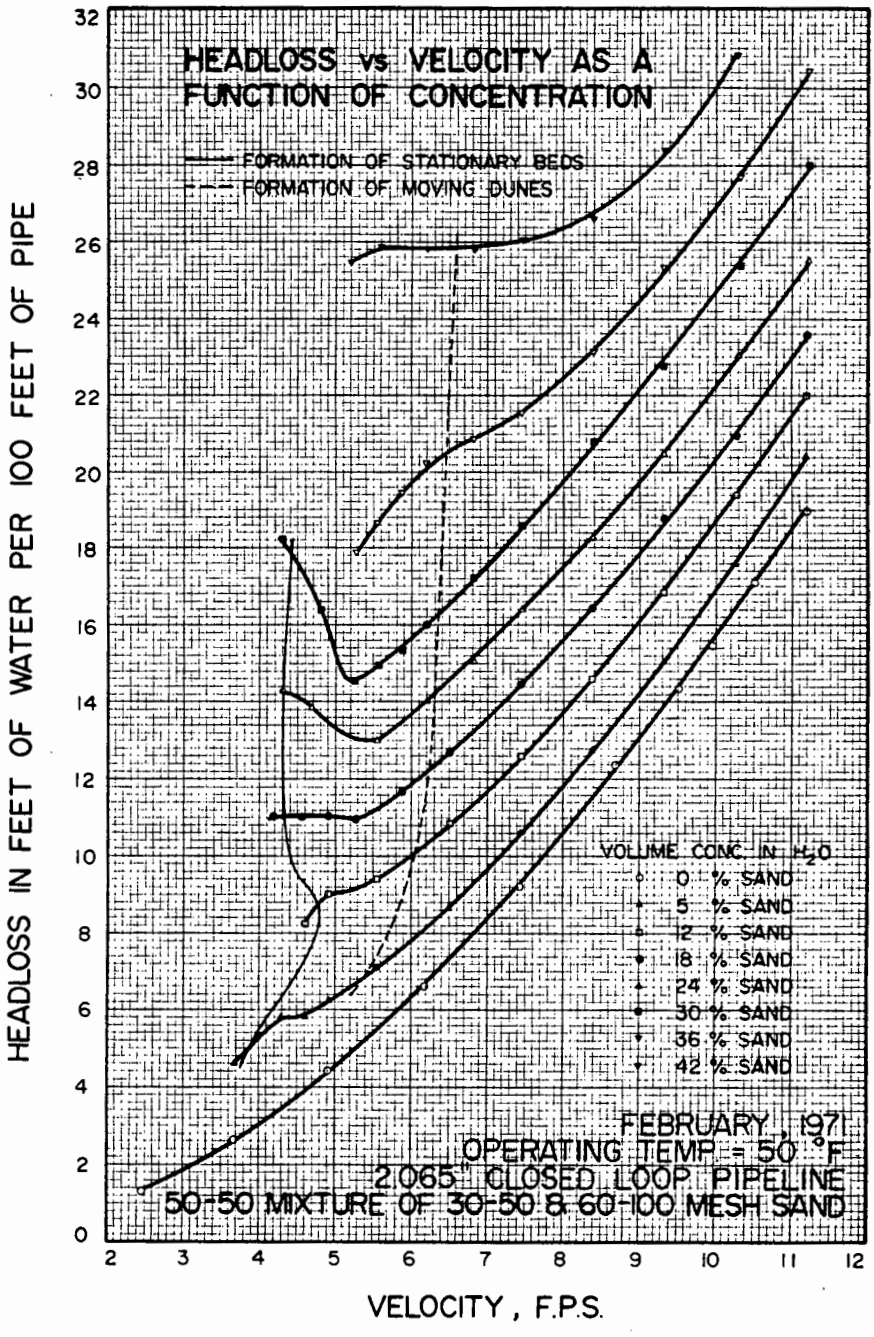

Figure 2.2 : Locus of dune formation (reproduced from Shook *et al.* (1973))

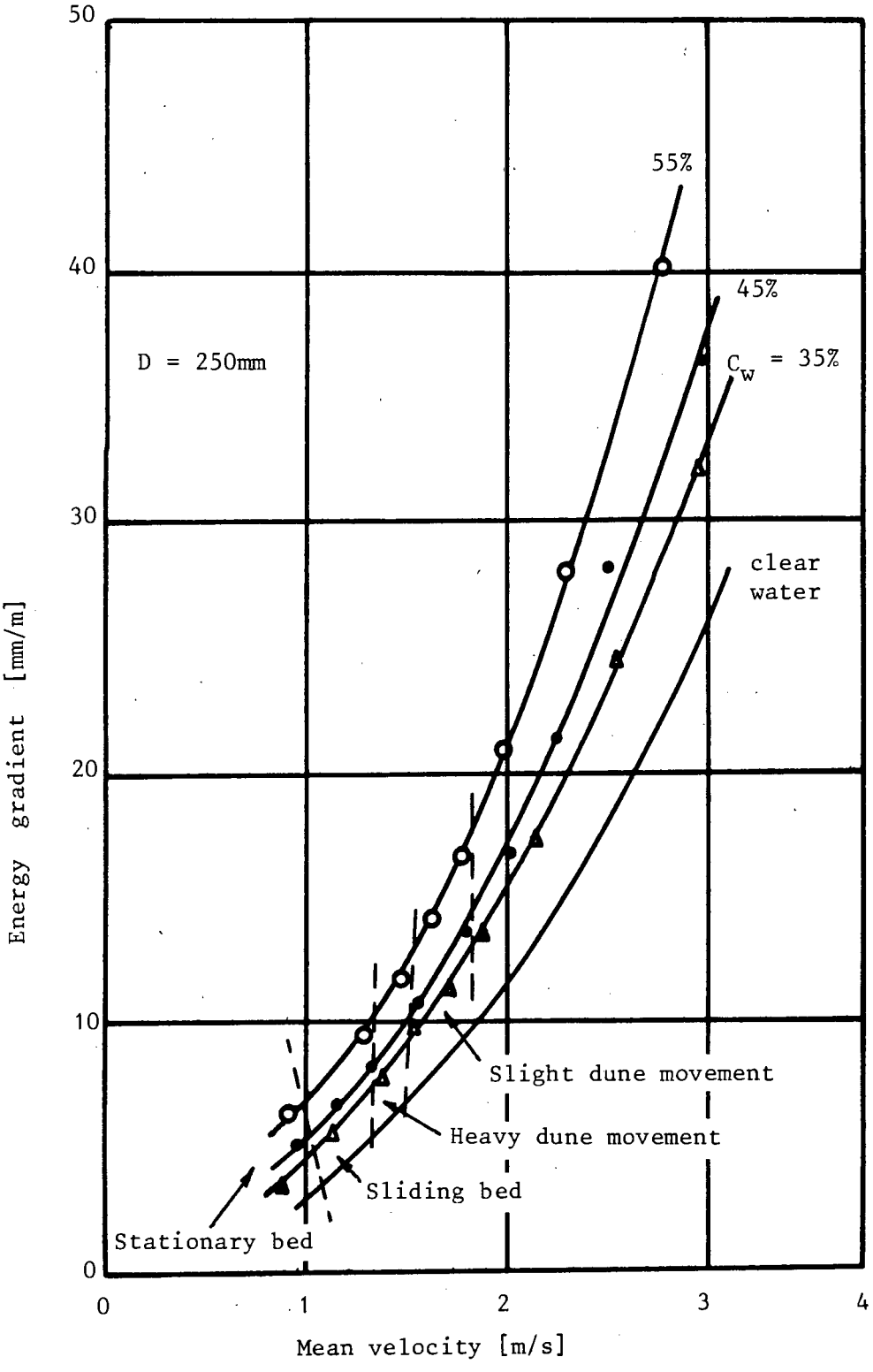

Figure 2.3 : Flow patterns associated with particular flow rates (after CSIR Report ME 1386 (1975))

Gold slime tailings :
Particle size tested: $d_{50} \simeq 50\mu m$
$d_{100} \simeq 3mm$ ($d_{99} \simeq 1mm$)

At velocities below which some material remains stationary Newitt *et al.* (1955), Acaroglu and Graf (1968), Shen and Wang (1970) and Wan (1985) reported ripple and dune formation. These formations are associated with the ripple and dune formations observed in open channel flow.

Newitt *et al.* (1955) described a rippled surface, that moved slowly downstream, on a stationary bed with low solid mass flow rate. Acaroglu and Graf (1968) presented their observations at various values of a shear intensity parameter. Table 2.5 presents these results. The definition given for ripples and dunes is of triangular shaped bedforms with gentle upstream and steep downstream slopes travelling in the direction of flow. These bedforms are associated with weak sediment motion.

Table 2.5 : Observations made by Acaroglu and Graf (1968) for uniform gravel (S_s = 2.67) in a pipeline of 76mm diameter at various values of shear intensity

$\Psi = \frac{(S_s - S_w)\, d}{u_*^2}$		Flow description
d = 2.00mm	d = 2.78mm	
> 23	-	liquid flow only
23	21	Few particles move, no bed forms. Considered "critical shear intensity"
16.4	-	Longitudinal 'waves' $\lambda \simeq 0.5$ m
4.9	-	Dunes more pronounced $\lambda \simeq 0.5$ m . Particle sliding and saltation.
2.3	2.5	Limit of dune formation. Plane bed forms.
1.35	1.35	Flat bed, particles move in suspension. Bed moves slowly and intermittently.
< 1.35	-	Solids gradually suspended, bed disappears.

Shen and Wang (1970) observed ripple formation at the velocity for incipient particle motion for 0.2mm sand particles. No ripples formed for a particle mixture with uniform diameter greater than 0.6mm, or if the overhead fluid was in laminar flow although "long low amplitude dunes eventually appear". Ripple formation was therefore associated with the fluctuating flow component in turbulent flow.

Wan (1985) associated ripples with the presence of a viscous layer and dunes with the presence of hydraulic roughness. Wan (1985) found that an increase in the suspended load over a bed favoured the transition from dune formation to plane bed at lower flow intensities.

Wan (1985) observed that the flow of a bentonite mixture over a granular bed resulted in differences when compared with clear water flowing over a granular bed. These include :

1. Incipient particle motion occurred at higher velocities.
2. Dune formations transformed to plane bed at lower velocities. For a bentonite concentration of greater than C_v = 1% , no dunes formed.
3. Dunes are smoother in shape and are symmetrical.

Kazanskij *et al.* (1974) presented observations in the form of flow pattern maps (Figure 2.4 and Table 2.6). The complexity of these flow pattern maps substantiates the difficulty in defining a single velocity that is associated with a stationary deposit.

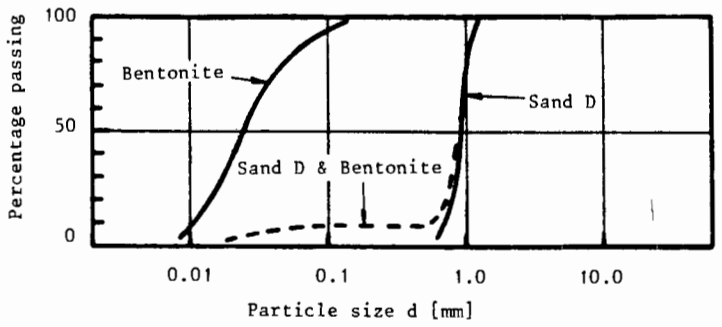

(a) : Particle size distribution

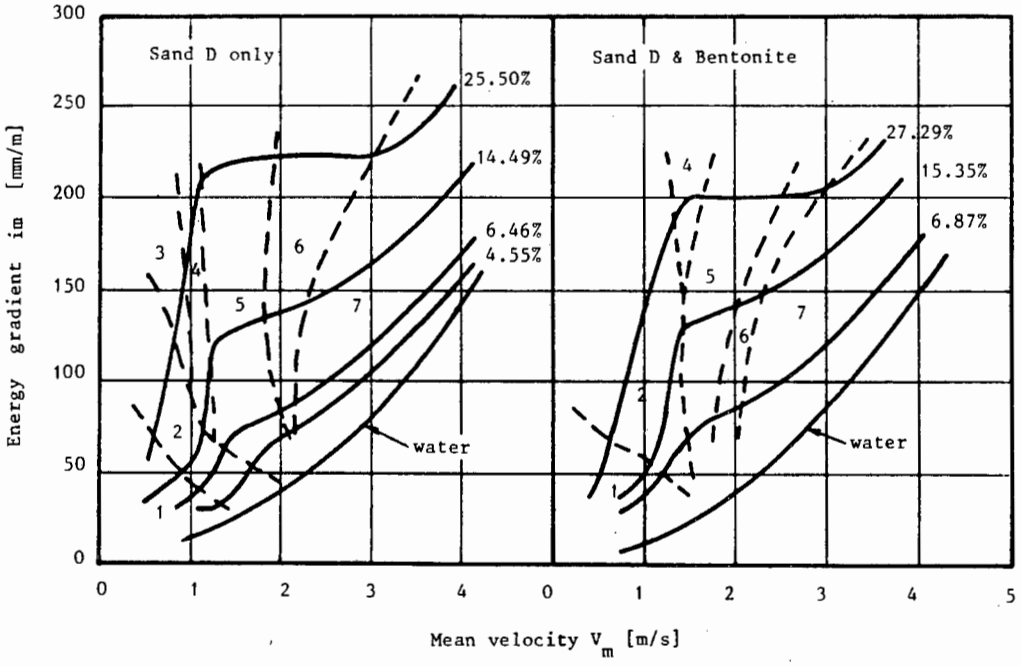

(b) : Influence of concentration and velocity of flow regime

Figure 2.4 : Flow pattern maps after Kazanskij *et al.* (1974)

Table 2.6 : Description of regions shown in Figure 2.4

Region	Description
1	Stationary bed with ripples.
2	Flat stationary bed.
3	Stationary bed with macroturbulence
4	Slug flow.
5	Sliding bed with sand waves, macro-turbulence and saltation.
6	Saltation.
7	Heterogeneous suspension

2.1.2 Stationary Deposit Velocity

The concept of a deposit velocity has received significant attention by researchers in the field of hydraulic transportation. The subjective nature of the measurement of deposit velocity by observations has been discussed by Sinclair (1962), Kazanskij *et al.* (1974), Shook (1976), Goedde (1978) and Carleton *et al.* (1978).

Sinclair (1962) overcame the problem of dune formation, if it occurred, by defining the deposit velocity at a value just above that at which dunes formed. The velocity at which "flow particles remained stationary" was otherwise used. Kazanskij *et al.* (1974) noted the fundamentally different

behaviour of medium (d_{50} > 500μm) and coarse (d_{50} > 1mm) slurry flows and commented on the difficulty of defining "the well known and often used critical velocity of deposition". Shook (1976) suggested that the discrepancy in observation and measurement of the deposit velocity could be found in :

1. Subjectivity of observation.
2. Difference in roughness for the pipeline and observation sections.
3. The fact that the minimum energy gradient point was taken as the deposit velocity point without observation.
4. Pressure fluctuations can become pronounced especially in stratified flows.

Goedde (1978) also discussed the subjective nature of the observation of deposit velocity and devised a method for measuring the bedload height at different stationary bed load velocities. By extrapolating the linear relationship to zero bed height, the deposit velocity was ascertained. Carleton *et al.* (1978) found that their deposit velocity measurements could vary widely due to "jerky, unstable" motion as the bedload started to move. No clear definition for deposit velocity exists except for single particles in water and even then problems of definition and observation occur (Zenz, 1964).

In an effort to simplify the analysis of hydraulic transport modelling in the past the observations made in pipelines have been largely neglected. A simple deposit velocity has been used to describe the complex flow changes that occur as material is initially taken into suspension and until stratification finally disappears. It is suggested that a region of flow

velocity exists in which particles may become stationary. This region is associated with periodic phenomena. The use of a single "deposit velocity" is discouraged and the use of a velocity range suggested. If particles exist in the flow that remain completely stationary then stationary bed flow exists. If all particles move, albeit intermittently, sliding bed flow exists. Sliding bed flow will persist until no periodic phenomena are observed. At this and higher velocities fully suspended flow occurs. Fully suspended flow may be heterogeneous or pseudohomogeneous.

The loose usage of the term "dune" in describing any periodic bed form has led to confusion since the phenomenon below the point at which particles remain stationary is very different from that which occurs if all particles are moving albeit intermittently. Dune flow may occur in the stationary bed flow region. Wave and slug flow may occur in the sliding bed flow region. These terms are used in this thesis and are described in detail in Chapter 3.

2.2 PARTICLE PROPERTIES

Particle size and particle size distribution can be measured and presented in many different ways. The degree of sophistication increased significantly with the advent of particle image analysis (Kesten and Klose, 1982). The number of different dimensional measurements made on a sample of particles is limited only by the ingenuity of the operator using an image analyser. The measurements required for analysing slurry flow systems are somewhat less sophisticated.

Particle properties and mixture concentration are the two essential elements that govern the mechanisms in slurry flow. A thorough investigation of particle properties is the key to understanding the differences in the flow regimes encountered.

2.2.1 Particle Size

Two aspects of particle size are important :

1. A satisfactory definition.
2. The maximum permissible size for any particular transport system.

For spherical particles a definition of size is inherent. For non spherical particles many definitions exist. The following three are commonly used :

1. The particle whose volume or mass is equal to the average volume of all the particles. This may be measured by fluid displacement of a known number of particles.
2. For sieved particles the average size between two consecutive sieve sizes or the geometric mean size.
3. A percentage passing size. This is a diameter (d_i) such that i per cent of the particles in the distribution will be smaller or would pass through a screen having openings that size. This is the preferred definition.

The essential requirement for maximum particle size is that there should be sufficient room above a sliding or stationary bed for the largest particles to turn over freely. For example, in a 150mm diameter line with the flow condition being such that the delivered concentration (C_{vd}) is 20% and the

in situ concentration (C_{vt}) is 28%, coal will occupy a depth slightly more than half the pipe diameter for a loose packed concentration (C_b) of 50%. The 75mm clear space above the bed will therefore accommodate a particle with a maximum diameter of about 50mm.

2.2.2 Particle Shape

Particle shape affects two parameters required in the description of hydraulic transport systems :

1. Particle packing density.
2. Settling velocity.

The effect of particle size alone on packing density is complicated. The effect of including particle shape can only be found by experimental measurement of the packing density. A statistical approach can be used with some success in analytical computations (see Section 2.2.5).

Particle shape has a marked effect on settling velocity. The particle shape is taken into account when comparing spherical and non spherical particle settling. Reliable methods exist for calculating spherical particle settling velocities but no agreement has been reached on the analysis of non spherical particles, particularly those of complex shape. An effective way of accounting for particle shape is by using a particle shape factor defined as

$$(V_t)_{actual} = S_F(V_t)_{spherical} \qquad (2.1)$$

where

$(V_t)_{spherical}$ - calculable settling velocity for spherical particles

$(V_t)_{actual}$ - actual settling velocity of the particle investigated

S_F - particle shape factor.

A complication in the definition of particle shape is the result of particle surface interactions with a carrier fluid. These interactions are governed by complex phenomena such as zeta-potential[1] and the adsorption layer. Dabak and Yucel (1986) point out that "the effective shape of a solid particle thus formed in a fluid could be drastically different from its original dry shape". These phenomena will affect particles in inverse proportion to their diameter.

The non spherical particle shape factor can be found experimentally by defining a percentage passing spherical particle diameter and then comparing the theoretical spherical settling velocity to the actual settling velocity from experiment.

2.2.3 Relative Density

In any material comprised of a range of particles, variations will exist in the relative density of each particle. The variation may be based on

---

[1] 'zeta-potential' is a measure of the small electrostatic charge that inherently adheres to particles in a suspension. Since all charges are of the same sign (usually negative) they have the effect of causing the particles to repel each other. This enables free liquid to occupy the spaces between the particles therefore increasing fluidity. The smaller the particles the greater the effect.

particle size or it may be based on a difference in chemical composition of the particles. The concept of a global relative density is therefore not accurate but may be *realistic* or *convenient*. The variation can be taken into account by careful investigation of the particle size distribution or may be included in the distribution of settling velocity where each particle group can be ascribed its unique relative density. A global relative density is however needed for the calculation of concentration and mass flow rate.

2.2.4 Distribution of Particle Properties

2.2.4.1 Distribution of size

Various single values have been used to describe particle size distribution. The simplest of these is to define a representative size for the sample viz. d_{50} or d_{85} . This value on its own gives no information as to the shape of the particle size distribution curve. A single value that can be used to describe the shape of a well graded[2] distribution curve is the grading coefficient (G_d) . The grading coefficient is defined by the ratio of two particle sizes that represent the cumulative percentage passing equal to some small and some large value.

---

[2]By a well graded sample is meant one that exhibits a particle size distribution curve that spans particle diameters of more than one order of magnitude (see Figure 2.5).

Examples are the ratio

$$G_d = \frac{d_{10}}{d_{90}} \qquad (2.2)$$

or the reciprocal,

$$G_d = \frac{d_{90}}{d_{10}} \quad .$$

The grading coefficient is of limited use since it gives no account of the quantity of the fine or coarse material in the sample.

Shook *et al.* (1973) used the empirical Rosin-Rammler equation

$$m_i = \exp(-z) \qquad (2.3)$$

where $z = \left[\frac{d_i}{B}\right]^n$

and m_i - mass fraction coarser than d_i ,

d_i - i-th particle diameter .

The constants n and B can be found for a particular sample. The breadth of the size distribution is governed by the exponent n . Examples of possible values of n are;

n = 5 commercially screened sand (narrow)

n = 0.7 single stage grinding process (broad).

Shook *et al.* (1973) maintain that the Rosin-Rammler distribution "has been shown to represent the output from commercial grinding circuits reasonably well". The Rosin-Rammler distribution is restricted since it cannot accommodate bimodal distributions, a feature Hanks and Hanks (1982) maintain is advantageous in slurry pipeline transport.

There is no generally acceptable theoretical correlation which can satisfactorily describe particle size distributions and for this reason Hanks and Hanks (1982) suggest that "the safest and simplest method of presentation of particle size distribution data is graphical".

Two graphical presentations are shown in Figure 2.5 :

1. Cumulative percentage passing.
2. Percentage retained.

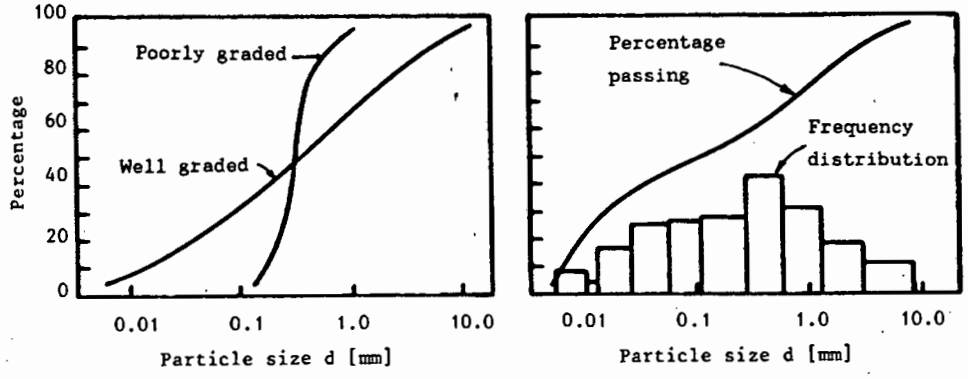

Figure 2.5 : Graphical presentation of particle size distribution

spheres that filled the voids left by the next larger size of spheres that the final filled material was somewhat higher in packing concentration than a mixture comprised of mid-size particles only. Table 2.7 presents the findings of Elliot and Gliddon (1970).

Table 2.7 : Properties of densist possible packing of spheres (Rhombohedral Arrangement) from Elliot and Gliddon (1970)

	Primary	Secondary	Tertiary	Quaternary	Quinary	Filler
Radius of Sphere	R	0.414R	0.225R	0.177R	0.116R	Very small
Relative number of spheres	1	1	2	8	8	Volume added = $.622\ r^3$
Voidage of packing*	25.95	20.7	19.0	15.8	14.9	3.9
% Weight of spheres in mixture	77.1	5.5	1.7	3.3	0.97	11.4

* - voidage of packing = $1 - C_b$

The particle packing concentration can be found experimentally or analytically. Two methods of experimental determination are by sedimentation or by centrifuge action. Dabak and Yucel (1986) point out that "it is not really known as to which of these methods determines the true value" of C_b . An analytical analysis can only be achieved by making certain simplifying assumptions. The most important assumption is that the particles are nearly spherical, non porous and have negligible surface chemistry effects. Experimental constants are usually also required making the use of analytical analyses of C_b limited.

2.2.6 Unhindered Particle Settling Velocity

The settling of single particles in fluids can be analysed theoretically for laminar settling only. In the transition and turbulent settling regions a mechanistic or continuum approach is required.

It can be found from a force balance on a sphere moving through a viscous fluid that the drag coefficient (C_D) is related to the particle Reynolds number (R_{ep}) only

$$C_D = fn(R_{ep})$$

and $$R_{ep} = \frac{\rho_f V_t d}{\mu_f} \quad . \tag{2.7}$$

The variation of drag coefficient (C_D) with Reynolds number (R_{ep}) , obtained from experiments involving a variety of Newtonian fluids and a range of particle diameters, is shown in Figure 2.6. Graf (1971) stressed that this curve applies only to smooth, non rotating spheres, moving in a fluid free of disturbances with a constant relative velocity.

The variation of C_D with R_{ep} is not a simple one. It is possible to approximate the variation by fitting several straight lines to the curve shown in Figure 2.6. Three convenient straight lines are given by

$$C_D = 24/R_{ep} \quad \text{Stokes' law} \tag{2.8}$$

$$C_D = 14/(R_{ep})^{½} \quad \text{Intermediate law} \tag{2.9}$$

$$C_D = 0.44 \quad \text{Newton's law} \quad . \tag{2.10}$$

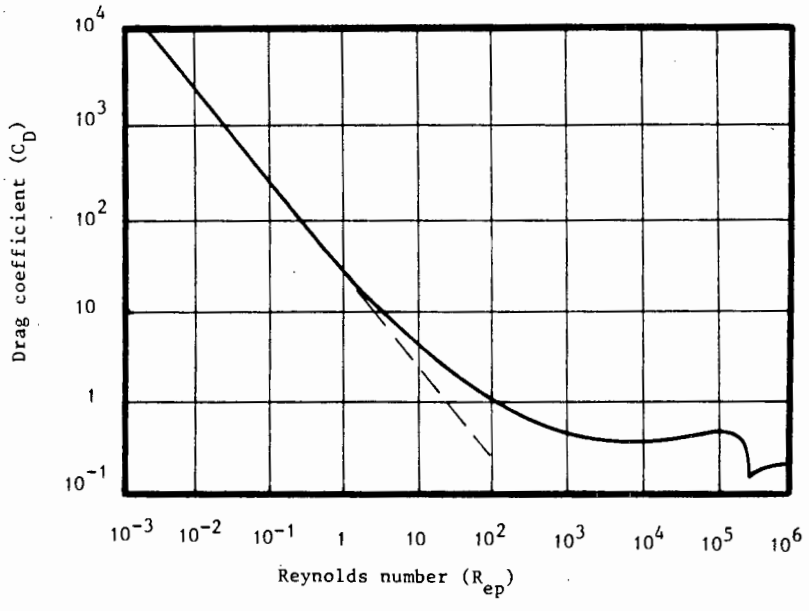

Figure 2.6 : Drag coefficient as a function of particle Reynolds number for spheres

The terminal settling velocity may be calculated by using the applicable drag laws at various particle Reynolds numbers. The terminal settling velocity is calculated from a force balance on a sphere moving with constant velocity,

$$V_t = \sqrt{\frac{4}{3}\frac{gd}{C_D}(S_s - S_w)} \quad . \tag{2.11}$$

It is possible by making V_t and d dimensionless, in an appropriate manner, to present the information of particle settling in the three regions (defined by equns. 2.8, 2.9 and 2.10) by a curve as shown in Figure 2.7.

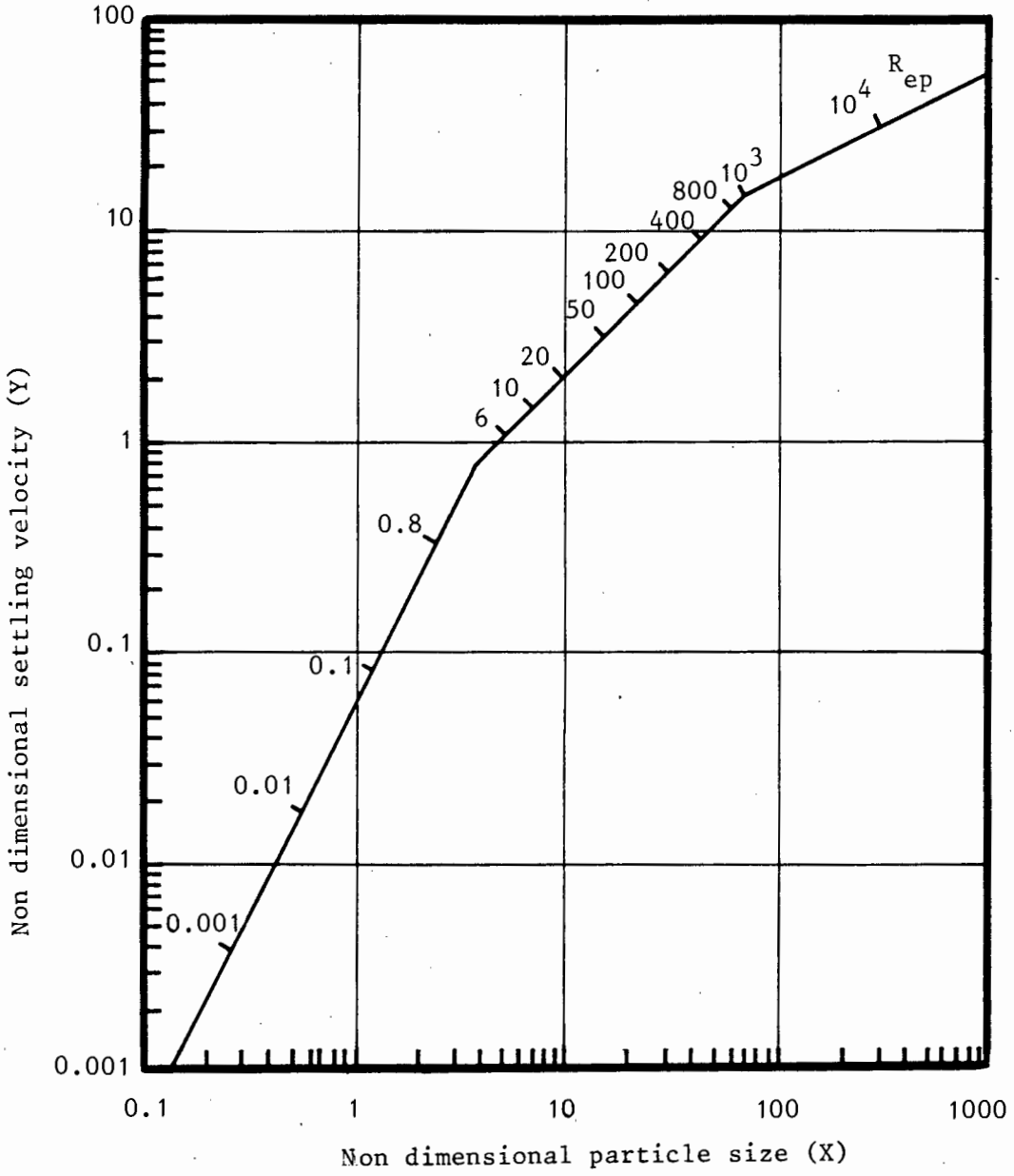

Figure 2.7 : Non dimensional terminal settling velocity (Y) as a function of non dimensional particle size (X)

In Figure 2.7

$$X = d\left[\frac{(S_s - S_w)\,\rho^2 g}{\mu^2}\right]^{1/3} \qquad (2.12)$$

$$Y = V_t\left[\frac{\rho}{\mu\, g(S_s - S_w)}\right]^{1/3} . \qquad (2.13)$$

For Stokes' law $X < 3$; $Y = 0.0556\, X^2$ (2.14)

Allen's law $3 < X < 70$; $Y = 0.21\, X$ (2.15)

Newton's law $X > 70$; $Y = 1.739\, \sqrt{X}$. (2.16)

2.3 THE VEHICLE

Mixed regime slurries are comprised of mixtures with a rheologically active component. The rheologically active part or *vehicle* can be thought of as a fictitious, new, conveying fluid composed of some of the particles and all the free liquid, in which the remainder of the particles are heterogeneously or pseudohomogeneously suspended. The *vehicle* produced has very different flow characteristics from the free liquid used to mobolize the solid.

It is important that the flow characteristics and vehicle-particle interaction are well understood for a description of the flow of mixed regime slurries.

It is expedient then to investigate the following topics :

2.3.1 Physico-chemical effects.

2.3.2 Rheological parameters.

2.3.3 Rheological equations.

2.3.4 Hindered terminal settling velocity.

2.3.5 Definitions for the coarse-fine particle split.

2.3.6 Velocity distribution for the flow of vehicle in pipes.

2.3.7 Vehicle friction factors.

2.3.1 Physico-chemical Effects

As particle size is reduced toward colloidal dimensions D G Thomas (1963b) points out that physico-chemical effects become significant and that, in the absence of a stabilizing electrolyte, particles agglomerate into flocs. A floc is a network of solid particles enclosing water in the interstitial spaces. A floc can be considered an integral unit causing an increase in the effective diameter of particles in the mixture. Floc formation or particle dispersion of colloidal size particles is manifest by particle surface and body electric charges.

Particles will be attracted to one another by van der Waals forces (body charge), but a dominating repulsive component (surface charge or zeta-potential) may also be present, preventing coagulation. Molecules dispersed in water can acquire surface charge, dependent on the acidity of the dispersion medium, by ionization. Due to the strong electrostatic interaction between ions, whichever ionic group is present will have it

counterions of opposite charge giving an electric double layer. Figure 2.8 is a schematic representation of the region very close to a solid.

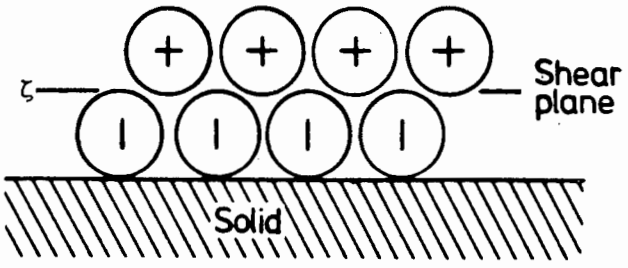

Figure 2.8 : Schematic representation of the region very close to a solid, showing the shear plane where the potential is ζ (zeta) (from Murrel and Boucher, 1982)

The specific adsorption of hydrated ions affects the mobility of the surface relative to the liquid, since movement is expected to occur at the shear plane where the potential is ζ. The zeta potential is the most important single measurable characteristic of charged surfaces. A rapid decay in the surface potential associated with a compression of the double layer leads to colloid instability and flocculation.

Horsley and Reizes (1978) and Horsley (1982) reduced the yield stress of gold slime slurries by dispersion of the floc structure. This was achieved by modifying the zeta potential using sodium hexametaphosphate. This resulted in a substantial reduction in the laminar flow energy gradient. The effect could be reversed using calcium hydroxide. Their work shows the importance of zeta potential on the formation of flocs.

Horsley and Reizes (1978) found that for slurries with volume concentration less than 30% and for turbulent flow that the zeta potential modification had no effect. They suggested that an equilibrium floc size might develop that persists in turbulent flow. Reich and Vold (1959) found in contrast that at a certain turbulence level any floc formation, in any slurry, will break down completely.

Another method of zeta potential modification is by a change in acidity. Duckworth *et al.* (1983a) found a strong relationship between yield stress and acidity. Figure 2.9 shows this relationship. Table 2.8 presents the particle characteristics for the material tested.

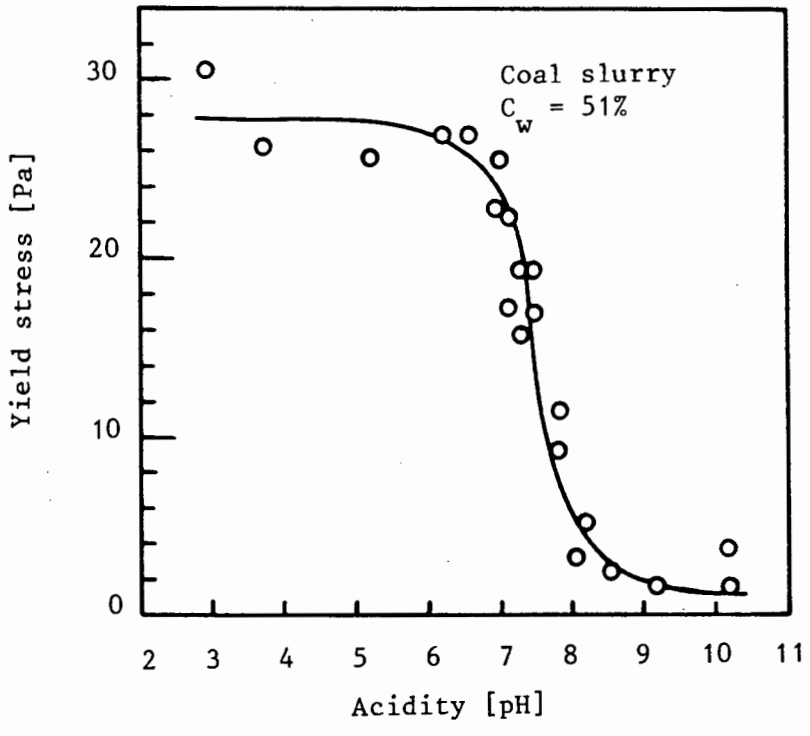

Figure 2.9 : Yield stress versus acidity for fine coal slurry (from Duckworth *et al.* 1983)

Table 2.8 : Particle size distribution for fine coal tested in Figure 2.9 above (from Duckworth *et al.* 1983)

d [μm]	Cumulative percentage passing
80	99.2
50	96.3
35	89.4
25	72.8
20	54.2
15	0

D G Thomas (1963b) found a contradiction to the work of Duckworth *et al.* (1983) when testing a range of slurries including kaolin. He found that for a variation in acidity from pH 4 to pH 10 the rheological parameters varied by less than 20%. He concluded that acidity was of secondary importance.

Duckworth *et al.* (1983) derived Figures 2.10(a) and 2.10(b) from Elliott and Gliddon (1970). The effect of acidity on two different coal water mixtures is shown, one having properties highly dependent on acidity, the other having weak dependence. It should be noted that the slurry that exhibits a yield stress shows a high degree of dependence on acidity.

The complexity of physico-chemical effects is evident. These effects account for the difference between theoretically and experimentally determined rheological parameters such as yield stress (τ_y) , fluid consistency index (K) and flow behaviour index (n).

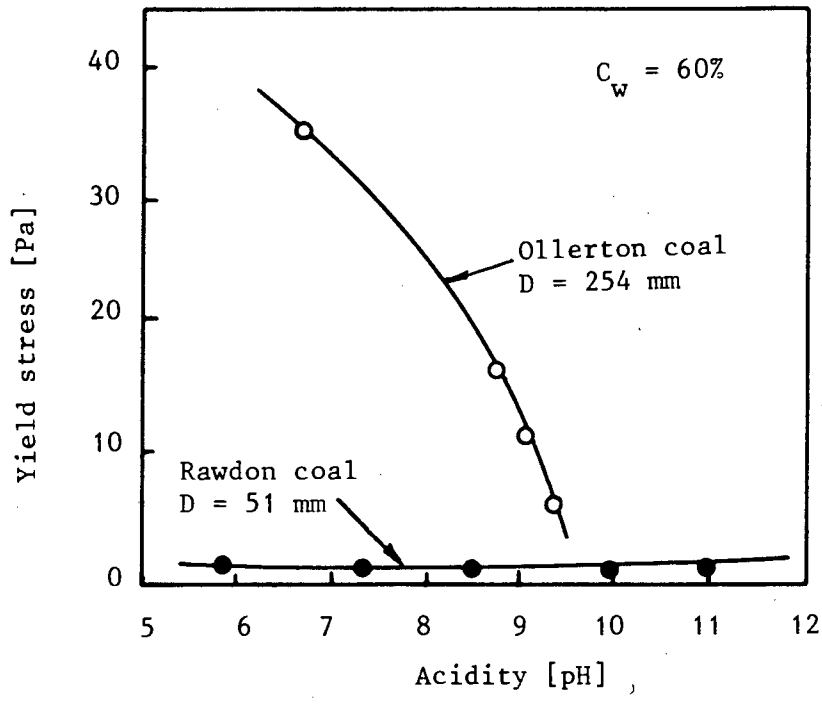

(a)

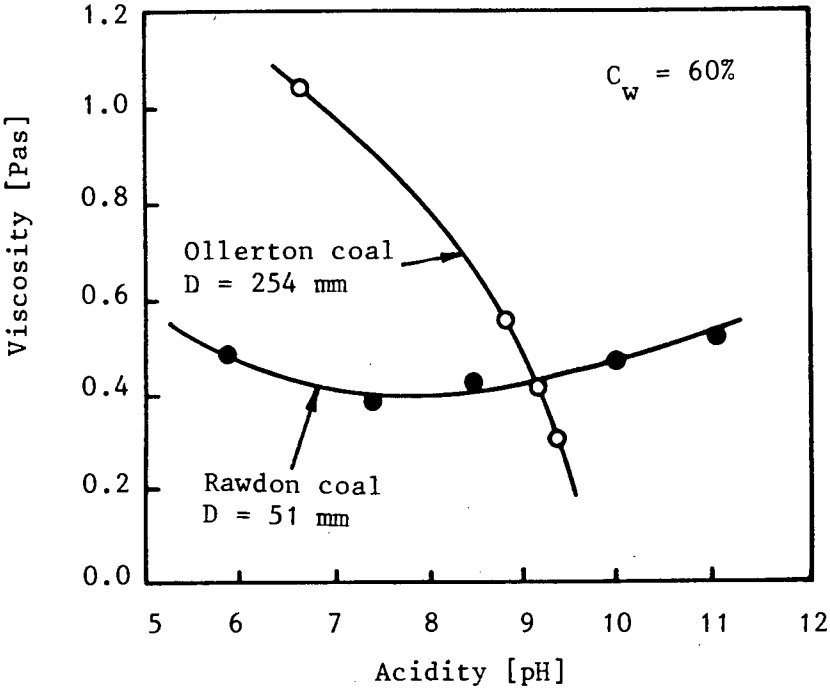

(b)

Figure 2.10 : Effect of acidity on (a) yield stress and (b) viscosity for two coal types (after Duckworth *et al.* (1983))

D G Thomas (1963a) described the laminar flow characteristics of a particular slurry by using the true volume concentration or particle diameter and floc structure and found that satisfactory definitions could be found from either. It seems justified that an analysis of the fine material can be made by rheological considerations only without the necessity to account for acidity and zeta potential as long as these remain essentially constant for all tests.

2.3.2 Rheological Parameters

2.3.2.1 Fluid consistency index (K)

The fluid consistency index (K) of a fluid is a measure of its fluidity. The larger the value of K the *thicker* or *more viscous* or *less mobile* the fluid.

Fluid consistency index is effected by the following :

1. Particle size

   Decreasing particle size increases the degree of non Newtonian behaviour of a mixture affecting both the fluid consistency index (K) and the flow behaviour index (n). Resistance to flow increases as particle size decreases.

2. Particle solid density

   Particle density is significant and smaller particle sizes and higher concentrations are necessary for homogeneous flow as particle density increases. This required increase in mixture concentration results in increased values of the fluid consistency index (K).

3. Shape

Particle shape has the single greatest influence on K . The particle shapes that will result in decreasing K are :

1. Glass rods
2. Glass plates
3. Quartz grains
4. Glass spheres

↓ Decreasing fluid consistency index

The rotation of non spherical particles in a velocity gradient causes an increase in the frequency of interparticle contacts and an apparent increase in the effective concentration and hence fluid consistency. At low concentrations where hydrodynamic effects predominate this effect is small.

4. Particle roughness

Rough grains do not slip or roll easily over one another. The effect of adding a lubricant (e.g. soap) to the mixture demonstrates this. The lubricant will cause a substantial change in K for rough particles but will have a limited effect on smooth spheres.

5. Size distribution

The addition of a relatively small quantity of fine particles to a mixture of coarse particles will result in a significant decrease in K. Addition of a small quantity of coarse particles to a mixture of fines will produce very little change in the value of K .

Castillo and Williams (1979) found that the functional relationship between relative viscosity[3] and concentration (η_r = fn (C_{vt})) has a steeper slope in general for narrow size distributions than for broad size distributions that contain fine particles. A broad particle size distribution results in a mixture with a higher packing density C_b so that at a given concentration C_{vt} the mixture exists in a lower C_{vt}/C_b state than a narrow distribution mixture. The dependence of η_r on C_{vt} is therefore best correlated in terms of C_{vt}/C_b if C_b can be realistically evaluated in a fluid medium.

6. Particle interactions

Particle interactions cause discrete particles to be sporadically retarded and then accelerated again. In both stages inertia affects the amount of energy required by the interaction. This dissapation of energy is manifest as an increase in fluid consistency.

Clarke (1967) found that for granular materials a critical concentration of $C_{vt} \simeq 25\%$ existed below which the increase in the value of K with concentration was small but above which K increases rapidly with increasing concentration. He associated this with the fact that particles would undergo impacts above this

---

[3] η_r - relative viscosity = $\frac{K}{\mu_w}$.

critical concentration below which particles could move freely. From his experimental work he found the critical concentrations shown in Table 2.9.

Table 2.9 : Critical concentrations after Clarke (1967)

C_{vt}	Material
15%	Glass rods
40%	Plastic beads

Castillo and Williams (1979) reported the same critical concentration phenomenon which they found to occur above $C_{vt} \simeq 30\%$.

Ward and Whitmore (1950) suggest that the increase in relative viscosity (η_r) of a suspension arises from :

1. The presence of the particles in the liquid.
2. The immobile liquid layer held in the irregularities of the particle surface which leads to an increase in the effective volume concentration.

The liquid layer has the following characteristics :

1. For a particular material it remains at uniform thickness over a wide concentration range.
2. For coarse particles the layer is practically of the same thickness for a broad range of particle sizes.

3. For fine particles the layer thickness decreases with decreasing particle size but the relative thickness increases continuously with decreasing size.
4. The layer thickness is substantially independent of the mobilizing liquid viscosity.

2.3.2.2 **Evaluation of fluid consistency index**

Table 2.10(a) contains the mathematical correlations considered for the calculation of relative viscosity in dispersed systems.

Hirshfelder *et al.* require evaluation of an empirical function of concentration (see Table 2.10(a)) for the calculation of relative viscosity. For $C_v > 0.1$ Table 2.10(b) is used.

D G Thomas' (1963b) correlation for relative viscosity using the true volume concentration and particle diameter (equn. 2.20) or the floc characteristics (equn. 2.31), has inherent the fact that the volume concentration and particle diameter are related to the floc characteristics of a mixture. Alessandrini *et al.* (1985) presented a means for relating these two groups using a ratio of volume concentrations where this ratio is defined as

$$C_{FP} = \frac{C_{vF}}{C_{vt}} \qquad (2.28)$$

and C_{vF} - floc volume concentration

C_{vt} - particle volume concentration.

Table 2.10(a) : Relative viscosity correlations for dispersed suspensions

Correlation	Original Author	Equation number
1. $\eta_r = 1 + 2.5C_v$ for $C_v < 2\%$, monomodal rigid spheres with no surface charge	Einstein[1]	(2.17)
2. $\eta_r = 1 + 22.4C_v$ for $C_v < 15\%$, clay-water slurries only	Michuyoshi *et al.* 1966)	(2.18)
3. $\eta_r = 1 + 2.5C_v + 14.1C_v^2$ for $C_v < 20\%$, conditions as for 1) above	Guth & Simha[1]	(2.19)
4. $\eta_r = \exp(k_2 C_v)$ $k_2 = 2.5 + (14/\sqrt{d})\Phi_2$ $\Phi_2 = \sqrt{s/s_o}$ where s = surface area of actual particle for $C_v < 30\%$ $s_o = d/6$	D G Thomas (1961)	(2.20)
5. $\eta_r = 1 + 2.5C_v + 10.05C_v^2 + 2.73\ 10^{-3} \exp(16.6C_v)$ for full range of C_v	D G Thomas (1965)	(2.21)
6. $\eta_r = 4C_v(0.8 + 0.767(fn(C_v) - 1) + (fn(C_v) - 1)^{-1})$ $fn(C_v) = 1 + 1.4C_v + 10C_v^2 + 18.36C_v^3 + 29.44C_v^4$ for $C_v < 0.1$ $fn(C_v)$ from Table 2.10(b) for $C_v > 0.1$	Hirshfelder *et al.*[2]	(2.22)
7. $\eta_r = \left[1 - C_v/C_b\right]^{-2.5}$	Landel *et al.*[1]	(2.23)
8. $\eta_r = \left[1 + 0.75\ \frac{C_v/C_b}{1 - C_v/C_b}\right]^2$	Chong *et al.*[3]	(2.24)
9. $\eta_r = \frac{9}{8}\left[\frac{(C_v/C_b)^{1/3}}{1 - (C_v/C_b)^{1/3}}\right]$	Frankel and Acrivos[1]	(2.25)
10. $\eta_r = \left[1 + \frac{[\eta]C_bC_v}{n(C_b - C_v)}\right]^n$ $n = fn(du/dr)$ $[\eta] = \lim_{C_v \to 0}\left[\frac{\eta - 1}{C_v}\right]$ - intrinsic viscosity Find $[\eta]$ from $\eta_\infty = \left[1 + \frac{[\eta]C_bC_v}{2(C_b - C_v)}\right]^2$	Dabak and Yucel (1986)	(2.26)
11. $k = (\mu + A)\exp(BC_v)$	Weltmann and Green (1943)	(2.37)

1. from Govier and Aziz (1981); 2. from Givler *et al.* (1986); 3. from Castillo and Williams (1979)

Table 2.10(b) : $fn(C_v)$ for $C_v > 0.1$ for use with equn. (2.22)

C_v	$fn(C_v)$
0	1
0.0884	1.44
0.1583	1.91
0.2128	2.39
0.2618	2.89
0.3060	3.40
0.3443	3.91
0.3818	4.43
0.4160	4.93
0.4513	5.44
0.4835	5.95
0.5145	6.46
0.5400	6.99
0.5695	7.50
0.5968	7.93
0.6390	∞

Alessandrini *et al*. (1985) confirming the work of D G Thomas (1963b) stated that "under varying shear conditions the flow units (or flocs) of a suspension undergo deformation as well as aggregation-disaggregation processes". In steady state the shear dependence can be adequately described by equations of the form

$$\eta_r = fn(C_{vF}) = fn(C_{FP}C_{vt}) \qquad (2.29)$$

and $$C_{FP} = fn\left[\frac{du}{dr}\right] \qquad (2.30)$$

where η_r - relative viscosity of the suspension.

Table 2.11 presents three sets of equations of the form of equn. (2.29) and (2.30). In Table 2.11 the following nomenclature applies :

$C_{FP,0}$ - C_{FP} for the maximum degree of aggregation, $\frac{du}{dr} \rightarrow 0$

$C_{FP,\infty}$ - C_{FP} for the minimum degree of disaggregation, $\frac{du}{dr} \rightarrow \infty$

K' , K'' - constant based on particle shape and electric charge

$\left[\frac{du}{dr}\right]_c$ - shear rate beyond which the disaggregation process of the disperse phase prevails over aggregation.

Table 2.11 : Viscosity correlations for flocculated suspensions, after Alessandrini *et al.* (1985)

Correlation	Original Author	Equation No.
1. $\eta_r = 1 + 2.5C_{FP}C_{vt} + 10.5(C_{FP}C_{vt})^2 + 0.00273 \exp(16.6C_{FP}C_{vt})$ $C_{FP} = C_{FP,\infty} + K\left[\frac{du}{dr}\right]^{-m}$ Under certain conditions m = 1/2 Three adjustable parameters	D G Thomas	(2.31)
2. $\eta_r = \exp\left[k_1 + k_2\left[\frac{du}{dr}\right]^{-n}\right]$ $0.09 \leq n \leq 1$ $k_1 = 2.5C_{FP,\infty}C_{vt}/(1 - C_{vt}/C_b)$ The k_1 value is lowest for $k_2 = 2.5K''C_{vt}/(1 - C_{vt}/C_b)$ $C_{FP,\infty} = 1$ and $C_b = 1$ $n = B\left[3 - \frac{1}{A}\right]$ Three adjustable parameters where $0.3 \leq B \leq 1$ $0.05 \leq A \leq 0.37$	Smith and Bruce	(2.32)
3. $^{*}\eta_r = \left[(1 - K_\infty C_{vt}/2)\left[\frac{du}{dr}\right]^P / \left[\left[\frac{du}{dr}\right]^P + \left[\frac{du}{dr}\right]_c^P\right]\right]^{-2}$ Under certain conditions P = 1/2 $K_\infty = K'C_{FP,\infty}$ $C_{FP,0} \simeq \frac{2}{K'C_{vt}}$ Three adjustable parameters	Quemada	(2.33)

* Alessandrini *et al.* (1985) found this set of equations to give the best fit for their data

Two approaches to evaluating the fluid consistency index are presented. The first is based on the particle characteristics, the second on the floc characteristics. The equations based on floc characteristics rely on the evaluation of the ratio C_{FP} at zero and at infinite rate of strain (i.e. $C_{FP,0}$ and $C_{FP,\infty}$) as well as the *in situ* concentration of the mixture. The first approach requires the evaluation of a maximum packing concentration and *in situ* concentration.

The equations presented in this section for fluid consistency index are evaluated and compared in Section 2.3.2.6.

2.3.2.3 Flow behaviour index (n)

The floc radius (r_F) can be related to the particle radius (r) by the equation

$$r_F = r\, N_p^{A} \qquad (2.34)$$

where $0.05 \leq A \leq 0.37$

N_p - number of particles contained in the floc

r - particle radius.

Combining equns. (2.28) and (2.34)

$$C_{FP} = \left[\frac{r_F}{r}\right]^3 / N_p = \left[\frac{r_F}{r}\right]^{(3 - 1/A)} . \qquad (2.35)$$

The floc radius is dependent on the rate of strain such that

$$r_F \propto \left[\frac{du}{dr}\right]^{-B} \qquad (2.36)$$

$$0.3 < B < 1 \ .$$

The flow behaviour index (n) , therefore has some physical meaning (i.e. n = -B in equn. (2.36)).

2.3.2.4 Evaluation of yield stress

Yield stress is a phenomenon closely associated with electrical attractions of particles and hence flocculation. The existence of a yield stress is therefore exclusive to flocculated mixtures. Tadros (1985) suggested an equation for yield stress of the form

$$\tau_y = \frac{3C_{vt}n}{8\pi r^3} E_{sep} \qquad (2.37)$$

r - particle radius

n - average number of contacts per particle

≃ 8 for random close packing

≃ 12 for hexagonal close packing

E_{sep} - energy required to totally separate the flocs into single units.

Equn. (2.37) is presented because it shows the essential relationship between yield stress and floc strength.

This model assumes that at shear stress values above the yield stress all contacts are broken. Most estimates of E_{sep} result in τ_y predictions that are high except for low values of C_{vt} . The assumption is therefore only valid for low concentration. Although it is all but impossible to calculate E_{sep} this equation serves as an indication of the nature of the yield stress and emphasizes the fact that the yield stress is a direct consequence of a floc structure in a fine particle mixture.

D G Thomas suggested two equations for yield stress : the first based on the particle parameters (D G Thomas, 1963a) i.e.

$$\tau_y = k_1 C_{vt}^3 \qquad (2.38)$$

where

$$k_1 = \frac{2.1\ 10^{-3}}{d_{50}^2} \Psi_1 \quad ,$$

$$\Psi_1 = \exp 0.7((s/s_o) - 1) \quad ,$$

and

s/s_o - actual particle surface area per spherical particle surface area ($s_o = 6/d$) .

k_1 is a constant for a particular mixture.

The second based on the floc parameters (D G Thomas, 1963b) i.e.

$$\tau_y = k_1 C_{FP,0}^4 C_{vt}^3 \qquad (2.39)$$

$$k_1 = 0.7421\ N/m^2$$

$$\frac{d_F}{d_{app}} = \left[1 + C_{FP,0}\right]^2 \qquad (2.40)$$

$$d_{app} = d(s/s_o)\ \exp\ (-\tfrac{1}{2}\ \ell n^2\sigma) \qquad (2.41)$$

d_{app} - apparent particle diameter

d_F - floc diameter

σ - logarithmic standard deviations of particle size distribution.

Another approach to the calculation of yield stress is by empirical correlations derived from experimentation. Caldwell and Babitt (1941) presented an equation which, when converted to S.I. units, is given as

$$\tau_y = 47.88\ \left[10^{(0.078\ C_w\ -\ 2.32)}\right] \quad , \qquad (2.42)$$

where $C_w = \dfrac{S_s C_{vt}}{S_m}$ the weight concentration.

2.3.2.5 **Empirical evaluation of rheological parameters**

Slatter (1987) tested kaolin slurries in the Balanced Beam Tube Viscometer developed at the University of Cape Town (Lazarus and Sive (1984), Lazarus and Slatter (1986) and Slatter (1986)). Table 2.12 shows the results obtained for these tests.

Table 2.12 : Rheological parameters for kaolin test by Slatter (1987)

C_{vt} (%)	τ_y [Pa]	K [Pas^n]	n	S_m
17.71	80.00	2.290	0.430	1.256
14.88	44.00	1.170	0.490	1.215
12.08	23.00	0.500	0.500	1.175
5.88	3.00	0.201	0.474	1.085
4.03	1.40	0.061	0.593	1.058
2.05	0.60	0.018	0.663	1.030

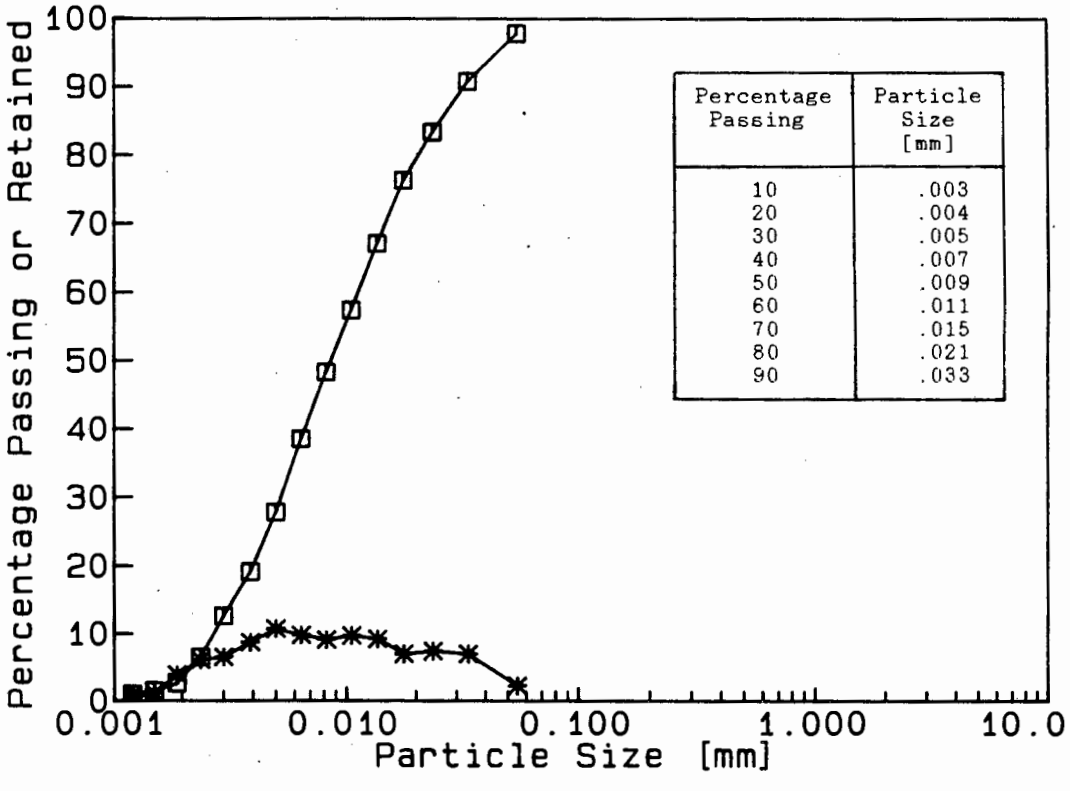

Figure 2.11 : Particle size distribution of kaolin

The kaolin tested has a relative density of 2.445. The particle size distribution is shown in Figure 2.11. The mixture pH of 6.8 was maintained throughout the tests.

Slatter (1987) proposed the following empirical correlations for the rheological parameters for kaolin mixtures

$$\tau_y = \exp\,(-\,0.7851 - 0.1133\,\ell n(C_v) + 0.6687\,(\ell n(C_v))^2) \qquad (2.43)$$

$$K = \exp\,(-\,6.7970 + 1.4628C_v - 0.1207C_v^2 + 3.545.10^3C_v^3) \qquad (2.44)$$

$$n = \exp\,(-\,0.2222C_v + 0.2163C_v^2 - 6.640.10^{-4}C_v^3) \quad . \qquad (2.45)$$

In all three equations C_v is entered as a percentage value. These equations are only valid in the concentration range tested viz. $2.0\% < C_v < 18.0\%$.

Hisamitsu *et al.* (1978) presented experimental data for a clay and a limestone slurry. The data is presented in Table 2.13 and Table 2.14.

Table 2.13 : Experimental results of Hisamitsu *et al.* (1978)

C_{vt} [%]	τ_y [N/m^2]	K [Pas]
6	0.88	$4.1\ 10^{-3}$
8.3	2.84	$7.0\ 10^{-3}$
10	5.20	$9.0\ 10^{-3}$
12	9.81	$10.5\ 10^{-3}$
14.5	17.66	$14.0\ 10^{-3}$

Table 2.14 : Relative viscosity (η_r) as a function of concentration from Hisamitsu *et al.* (1978)

C_{vt} [%]	Relative viscosity (η_r)	
	Clay	Limestone
0	1	1
1.0	1.08	1.07
2.0	1.19	1.15
3.0	1.32	1.21
4.0	1.50	1.28
5.0	1.70	1.34
6.0	1.91	1.42
7.0	-	1.49
8.0	-	1.55
9.0	-	1.61
10.0	-	1.69

The clay used (Table 2.13 and 2.14) has a relative density, S_s = 2.65 and mean particle size $d_{50} < 1\mu m$.

The limestone powder (Table 2.14) has a relative density, S_s = 2.74 and mean particle size $d_{50} = 7\mu m$.

2.3.2.6 **Comparison of evaluation methods for rheological parameters**

Figure 2.12 shows a plot of equns. (2.17) through (2.25) (Table 2.10(a)). Equns. (2.26) and (2.27) are correlations that require experimental results in order to evaluate the relevant constants ($C_{FP,0}$ and $C_{FP,\infty}$) and are therefore not considered. Figure 2.13 shows the data of Slatter (1987) and

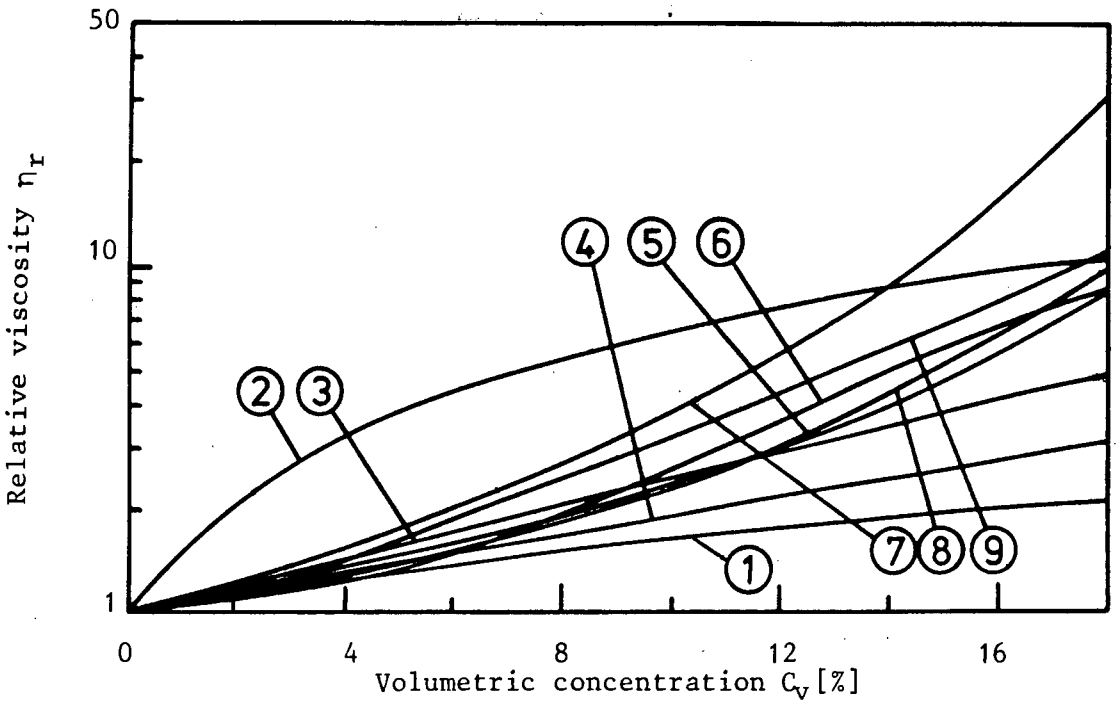

Figure 2.12 : **Comparative plot of relative viscosity equations presented in Table 2.10(a). The numbers presented refer to the equation number given in Table 2.10(a).**

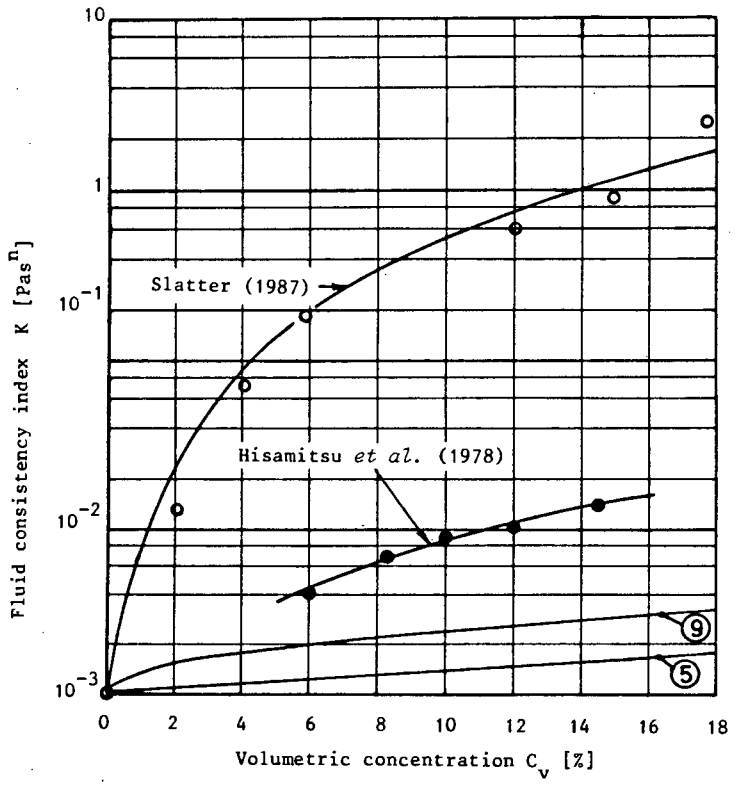

Figure 2.13 : **Comparative plot of fluid consistency index from the data of Slatter (1987) and Hisamitsu *et al.* (1978)**

Hisamitsu *et al.* (1978) for fluid consistency index compared to equns. (2.21) and (2.25). The significant difference in the equations taken from Table 2.10(a) and the data of Slatter (1987) can be accounted for by the flow behaviour index (n) . The equations of Table 2.10(a) have inherent in them that n = 1 where Slatter (1987) has n = fn(C_v) . Slatter (1986) made the assumption that the kaolin slurries he tested were best represented by a yield pseudoplastic rheology. The values for yield stress (τ_y) , flow behaviour index (n) and fluid consistency index (K) were treated as constants to be found from a best fit of the experimental data. Figure 2.14 shows the data of Hisamitsu *et al.* (1987) for relative viscosity (Table 2.14) compared to equns. (2.17) and (2.18).

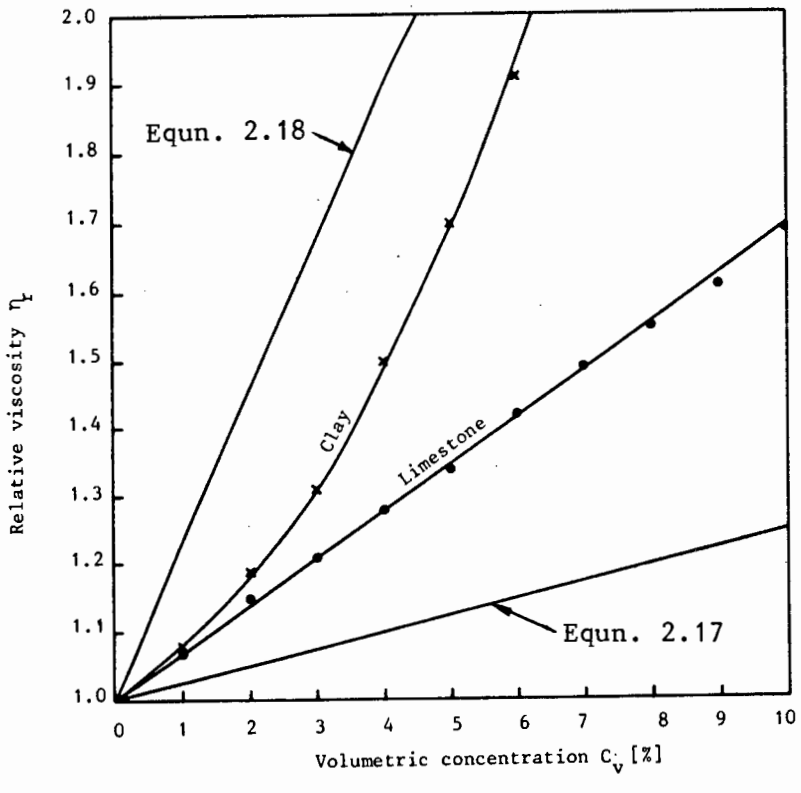

Figure 2.14 : Comparative plot of relative viscosity from the data of Hisamitsu *et al.* (1978)

Figure 2.15 shows a plot of yield stress versus concentration for equns. (2.38) and (2.43) and the experimental data of Tables 2.12 and 2.13.

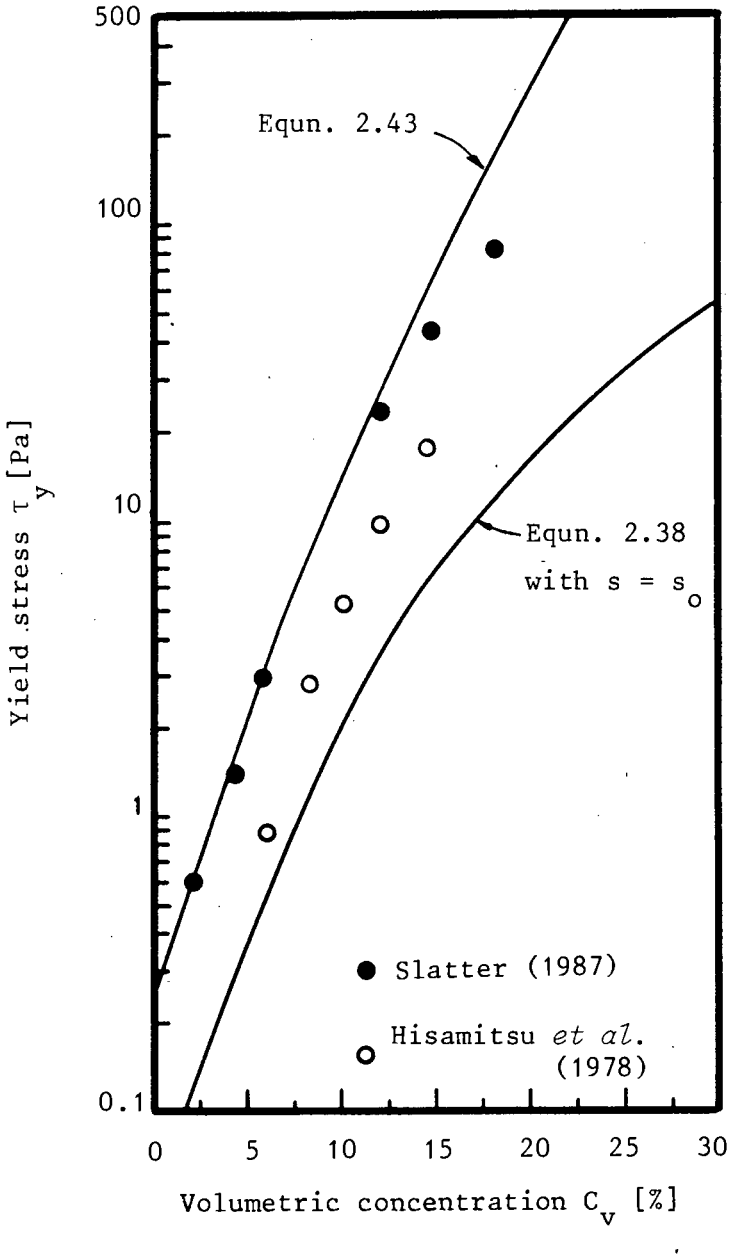

Figure 2.15 : Comparative plot of yield stress from equns. (2.38) and (2.43) and the experimentdal data of Slatter (1987) and Hisamitsu *et al.* (1978)

From a comparison of the fluid consistency index prediction equations two types are apparent. One for which the flow behaviour index is unity (i.e. Table 2.10(a)) and a second for which the flow behaviour index is less than unity (i.e. the data of Slatter (1987)). Figure 2.13 shows the difference between these two prediction types. It is suggested that experimental data be used for the rheological characterisation of the vehicle if such data is available. If not, the flow behaviour index should be assumed equal to unity and one of the equations in Table 2.10(a) should be used. Equation (2.23) is suggested because of its simplicity and the fact that the maximum particle packing density will ensure that relative viscosity values tend to infinity as C_v tends to C_b .

The equations for predicting yield stress are not considered reliable and should not be used. Experimental data should be used to predict the yield stress. If no experimental data is available the yield stress should be taken as zero. For the turbulent flow conditions that exist in the slurry systems investigated herein, the floc structure will probably be completely dispersed so that the yield stress will be zero.

2.3.3 Rheological Equations

"The central problem in the field of rheology," states D G Thomas (1963a), "is the derivation of general equations of state relating the rate of shear strain, the shear stress, the composition and time". Newton postulated that fluids might be expected to respond to an applied shearing stress by flowing in a manner such that the velocity gradient is strictly proportional to the

applied stress. Pseudohomogeneous suspensions of smooth, spherical particles in simple liquids will behave as Newtonian fluids (Govier and Aziz, 1981). Any fluid that has a nonlinear relationship between shear stress and rate of strain is called a non Newtonian fluid. Table 2.15 presents the rheological equations considered herein.

Hershel and Bulkley proposed an equation for a general non Newtonian fluid that described the behaviour of yield pseudoplastics reasonably well except at high strain rates. Cross (1965) and Wilson (1986) proposed equations that overcame this problem and predicted yield pseudoplastic flow over the entire measurable range. The model proposed by Newton is a special case of that proposed by Hershel and Bulkley. Cross (1970) presents an even more generalized model for viscoelastic, time independent fluids. Using a kinematic interpretation of non Newtonian flow, Cross (1970) proposed a model for a given system which "may exhibit shear thinning in one range of shear rate and shear thickening in another". Aqueous suspensions of titanium dioxide and fine coal (Hanks, 1982) have this characteristic. Each stage of sophistication includes those previous models as special cases. A description of each model is presented in the following section. It is important to remember that none of the presented equations are laws, states Schowalter (1960), "but merely an empirical description" which in some cases is not entirely adequate.

Table 2.15 : Rheological equations

Model	Equation	Comments
Newtonian	$\tau = \mu \left[-\frac{du}{dr}\right]$ (2.60)	Proposed by Newton
Yield pseudoplastic	$\tau = \tau_y + K \left[-\frac{du}{dr}\right]^n$ (2.61)	Proposed by Hershel and Bulkley
Cross model (1965)	$K = \eta_\infty + \frac{(\eta_o - \eta_\infty)}{1 + \alpha_1 \left[-\frac{du}{dr}\right]^m}$ (2.62)	- $K = \tau / \frac{du}{dr}$ - η_∞, η_o = apparent viscosity at infinite and zero rate of strain respectively - $\tau \rightarrow \tau_y$ as $K \rightarrow \eta_o$ - α_1 = constant - n = exponent which is a function of size distribution grading
Wilson model (1986)	$\tau = \tau_i + K\left[-\frac{du}{dr}\right]^n - (\tau_i - \tau_y) \ldots \exp\left[-\alpha_2 \frac{du}{dr}\right]$ (2.63)	- τ_i = intercept of high strain rate rheogram asymptote - τ_y = yield stress - α_2 = rheogram shape factor

Wilson (1986) pointed out the two main shortcomings of equn. (2.61) :

1. The tangent is vertical at a strain rate value of zero, while actual mixtures typically have a non vertical tangent at this location.

2. The viscosity decreases indefinitely with increasing strain rate leading to inaccuracy at high strain rates. Cross (1965) and Wilson (1986) proposed methods to overcome these problems.

Flocculation behaviour provides a qualitative explanation of yield pseudo-plastic flow which Cross (1965) considers the largest and most important class of non Newtonian fluids. Under steady state shear conditions there is an average floc size dependent on the magnitude of the strain rate. Cross assumed that at very high rates of shear the system would become completely dispersed.

The Cross model is presented in terms of viscosity (K) which is the ratio of shear stress to rate of strain (equn. (2.62), Table 2.15).

The index 2/3 was found to be applicable over a large range of mixtures although no physical reason is apparent. Cross found that in fact m = 1 for uniform sized particulate mixtures and varied as a continuous fraction for well graded systems.

At low shear rates it is possible to make the assumption that $K >> \eta_\infty$. It is further usual that α_1 is very large for particulate mixtures so that a plot of low strain rate data can be approximated by

$$K = \eta_\infty + \alpha_1 \left[-\frac{du}{dr}\right]^m$$

$$\Rightarrow \quad K \simeq \alpha_1 \left[-\frac{du}{dr}\right]^m \quad .$$

A graph of log K against log $\left[\frac{du}{dr}\right]$ should be linear at low shear rates with a slope (- m) . Equn. (2.62) can be solved using three data points forming three simultaneous equations once the value of m has been found.

Wilson's model uses a description of the rheological function at the extremes of the range tested and fits an exponentially decreasing function to join these extremes. Figure 2.16 defines the term τ_i in equn. (2.63).

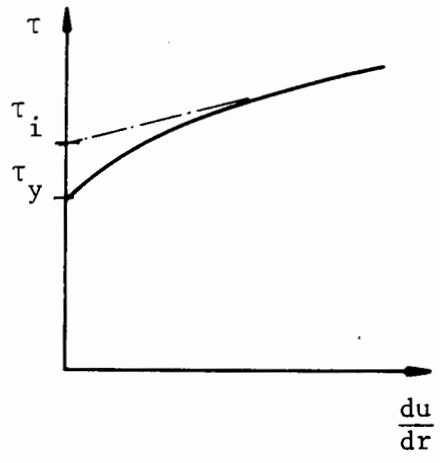

Figure 2.16 : Definition of term τ_i in Wilson model

At high strain rates

$$\tau = \tau_i + K \frac{du}{dy} \quad .$$

At zero strain rate

$$\tau = \tau_y \quad .$$

The resultant equation is shown in Table 2.15.

Equation (2.63) can be solved by using viscometer data to form three simultaneous equations for the three unknown constants.

The Cross (1965) model and the Wilson (1986) model are in fact equivalent except for the functional form of the rheogram. Cross used a power law where Wilson used an exponential function. This equivalence is shown below.

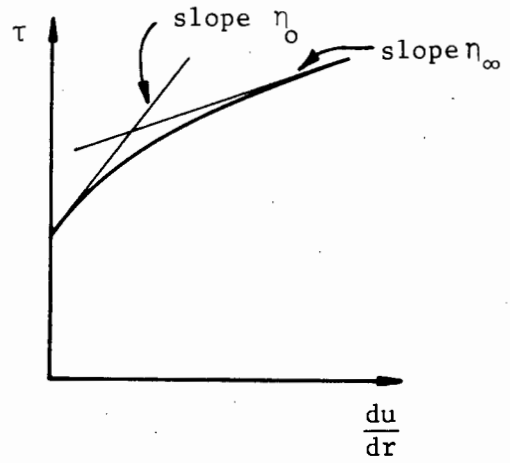

Figure 2.17 : Definition of terms to assist in understanding the transformation from η to τ in the Cross model

From the tangent at

$$\frac{du}{dr} = 0 \quad , \quad \tau = \tau_y + \eta_o \frac{du}{dr}$$

and $\frac{du}{dr} = \infty \quad , \quad \tau = \tau_i + \eta_\infty \frac{du}{dr}$.

Figure 2.17 shows the viscosity values η_o and η_∞ .

Substituting for η_o and η_∞ in equn. (2.62)

$$K = \frac{\tau - \tau_i}{D} + \frac{1}{D} \frac{\tau_i - \tau_y}{1 + \alpha_1 \left[\frac{du}{dr}\right]^m} \quad .$$

Rearranging

$$\tau = \tau_i + K \frac{du}{dr} - \frac{(\tau_i - \tau_y)}{1 + \alpha_1 \left[\frac{du}{dr}\right]^m} \quad . \qquad (2.63a)$$

Equation (2.63a) is therefore of a similar form to equn. (2.62) except for the functional form of the intermediate portion of the curve.

Rheological equations are significant for two reasons :

1. They embody a description of the viscous forces in a fluid that are needed to describe turbulent flow;
2. They describe conditions in the laminar sublayer of turbulent flow.

If it is presumed that if the fluid under investigation does not change fundamentally when changing from laminar to turbulent flow then rheological parameters found for laminar flow always embody a description of the viscous forces in the fluid. Turbulent flow data of fine particulate slurries is important so that the usefulness of the rheological equations presented can be ascertained. Such tests will also result in an understanding of the vehicle in mixed regime flow. The results for tests conducted on turbulent flow kaolin clay slurries are presented in Chapter 5 and discussed in Chapter 6.

2.3.4 Hindered Settling Velocity

The free terminal settling of particles in fluids is discussed in Section 2.2.6. As the concentration of particles settling in a fluid increases so the settling path of a particle is interrupted and its average settling velocity changes. O'Brien and Folsom (1937) concluded from their work that terminal settling velocity (V_t) of solid particles in a transporting fluid was an important variable in understanding the flow of slurries. The fact

that a calculation of the settling velocity includes the difference in solid-liquid relative densities, the particle size and shape in a single quantity make it essential to any correlation for slurry flow. A theoretical model for hindered settling can be found if C_v < 2% or 3% . Higher than this, too many effects are present and a mechanistic or continuum approach is required. Figure 2.18 shows a relational diagram for particle settling in fluids and a list of the authors work discussed in this section.

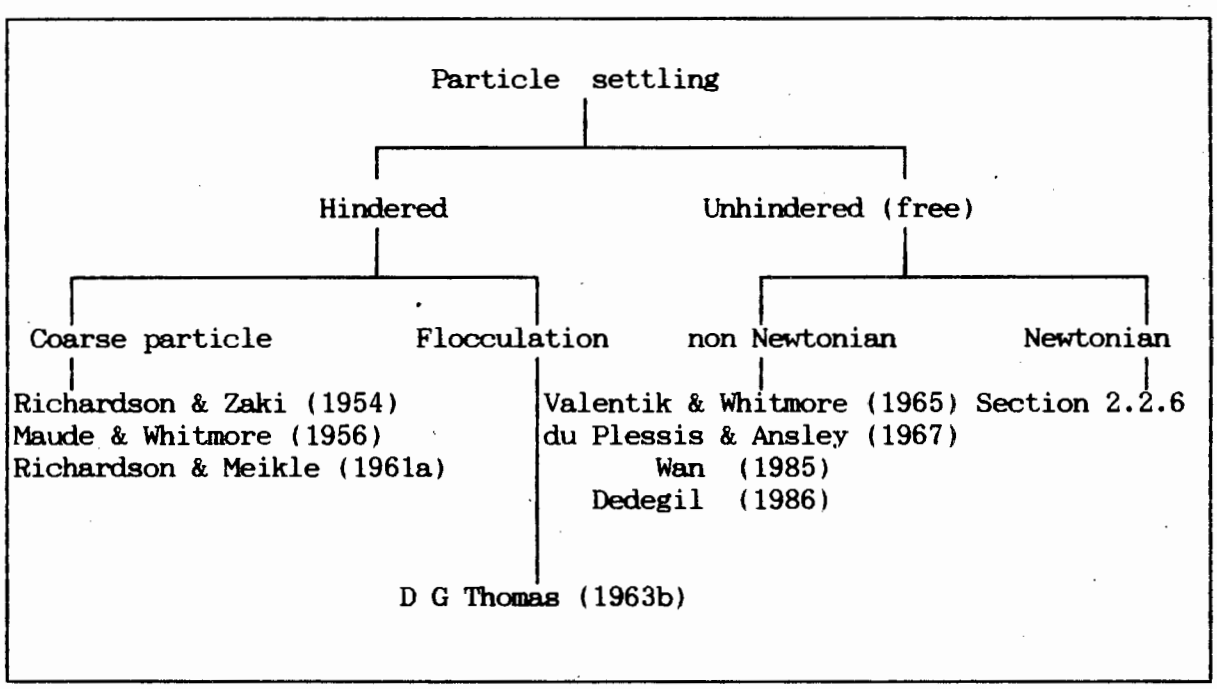

Figure 2.18 : Relational diagrams for particle settling listing authors cited in this section

Table 2.16 presents the equations for hindered settling velocity.

For non spherical particles or particles with large surface roughness the value of k_1 (equns. 2.64 and 2.65) will increase compared to those in Table

2.16. The suggested reason for this increase is that suspended liquid will be trapped by the particle surface increasing its apparent diameter[4]. The increase in the value of k_1 will be mediated by a decrease in the relative density of the particle.

Thomas (1963b) in his investigation of flocculated suspensions found that the attractive forces associated with flocculation modify laminar flow settling properties and increase the settling rate of dilute suspensions (C_v < 5%) by a factor of 10 to 100 over the Stokes settling for single particles of which the flocs are comprised.

Equn. 2.66 is only valid for C_{vf}< 2.5% above which the floc interaction becomes complex and the "unique characterization of floc properties"[5] is not valid.

Valentik and Whitmore (1965) drawing on earlier work suggested that when a body moves in a yield pseudoplastic "some of the suspension may be carried along with the body, increasing its effective size (d_{eff})". From their experimental results this concept of an envelope of suspension was confirmed. The value d_{eff} (equn. 2.67) is therefore always greater than the diameter of the settling particle.

The shortcomings of this approach are :

1. The need for experimental results to define d_{eff} (see equn. 2.67).
2. The choice of Reynolds number.

---

[4] cf Valentik and Whitmore (1965).

[5] D G Thomas (1963b).

Table 2.16 : Hindered settling velocity equations

Non dimensional parameter	Drag coefficient	Hindered settling velocity	Material tested and comments	Author	Equation No.
$R_{ep} = \frac{\rho_f V_t d}{\mu_f}$		$V_t' = V_t(1 - C_v)^{k_1}$ where $R_{ep} \leq 0.2$; $k_1 = 4.6$ $0.2 < R_{ep} \leq 1$; $k_1 = 4.4\ R_{ep}^{-0.03}$ $1 < R_{ep} \leq 500$; $k_1 = 4.4\ R_{ep}^{-0.01}$ $500 < R_{ep} \leq 7000$; $k_1 = 2.4$	Richardson & Meikle (1961a) tested these equations for $d \geq 5\ \mu m$. Valid for all macro-particles not subject to Brownian motion.	Richardson & Zaki (1954)	2.64
$R_{ep} = \frac{\rho_f V_t d}{\mu_f}$		$V_t' = V_t(1 - C_v)^{k_1}$ where $R_{ep} \leq 0.2$; $k_1 = 4.65 + 19.5\ d/D$ $0.2 < R_{ep} \leq 1$; $k_1 = (4.36 + 17.6\ d/D)\ R_{ep}^{-0.03}$ $1 < R_{ep} \leq 500$; $k_1 = 4.45\ R_{ep}^{-0.01}$ $R_{ep} > 500$; $k_1 = 2.39$	Hindered settling of particles with diameter d in a vessel of diameter D .	Richardson & Meikle (1961a)	2.65
		$\ell n \left[\frac{V_t'}{V_t}\right] = -5.6\ C_v$ for $1 \leq \frac{V_t'}{V_t} \leq 0.08$	Valid for spherical particles $C_v = C_{vf}$ for flocculated mixtures C_{vf} - floc volume concentration	Thomas (1963a)	2.66

Table 2.16 contd.

Non dimensional parameter	Drag coefficient	Hindered settling velocity	Material tested and comments	Author	Equation No.
$R_{ep} = \frac{\rho_f V_t d_{eff}}{K}$	C_D from Figure 2.6 for settling in Newtonian fluids	$V_t' = \left[\frac{4}{3C_D}(S_s - S_f)gd\right]^{1/2}$	Kaolin clay, C_v = 8.5% to 17.1% S_s = 2.64 , d_{80} = 1 μm d tested, 9.5mm to 54mm	Valentik & Whitmore (1965)	2.67
$R_{ep} = \frac{\rho_f V_t d_{eff}}{\frac{7\pi}{24}\tau_y + \frac{V_t}{d}}$	$C_D = 3\pi K d V_f' + \frac{7\pi}{8} d^2 \tau_y$	$V_t' = \left[\frac{4}{3C_D}(S_s - S_f)gd\right]^{1/2}$	Sand grains and plastic beads in vertically upward flowing bentonite suspension	Wan (1985)	2.68
$P\ell = \frac{\tau_y + \frac{K V_t}{d}}{\rho_f V_t^2}$	$C_D = 5.0(P\ell)^{0.5}$	$V_t' = \left[\frac{4}{3C_D}(S_s - S_f)gd\right]^{1/2}$	Kaolin clay d tested $\leq$ 1 μm	du Plessis & Ansley (1967)	2.69
$R_{ep} = \frac{(V_t')^2 \rho_f}{\tau}$ where $\tau = fn\left[\frac{du}{dr}\right]$	$R_{ep} \leq 8$; $C_D = 24/R_{ep}$ $8 < R_{ep} \leq 150$; $C_D = \frac{22}{R_{ep}} + 0.25$ $R_{ep} > 150$; $C_D = 0.4$	$V_t' = \left[\frac{2}{C_D}\left[\frac{2}{3}(S_s - S_f)gd - \frac{\pi \tau_y}{\rho_f}\right]\right]^{1/2}$	Used results of Valentik & Whitmore (1965). Equation solved by successive approximation.	Dedegil (1986)	2.70

The Reynolds number chosen will not produce a unique function of C_D since the large transition region from laminar to turbulent settling and the yield stress effect are not included.

Wan (1985) found that his data lay on a line for typical natural sand settling in a Newtonian fluid. Wan suggested that "a particle settling in a Bingham fluid obeys the same law as one settling in a Newtonian fluid if a proper universal Reynolds number is adopted". The implication of this is studied by Dedegil (1986). Wan (1985) conducted his tests for particles settling in a fluid that undergoes shear. This shear may have destroyed the floc structure and hence produced a Newtonian fluid. Dedegil (1986) used the data of Valentik and Whitmore (1965) for which the fluid was quiescent.

Dedegil's (1986) method is analogous to settling in Newtonian fluids. It is important, to complete this analogy, that the correct definition of the Reynolds number is used. This definition is in fact what Wan (1985) should have used,

$$R_{ep} = \frac{(V_t')^2 \rho_f}{\tau} \qquad (2.71)$$

where τ = fn $\left[\frac{du}{dr}\right]$ the rheological equations discussed in Section 2.3.3.

A representative shear gradient can be given by

$$\frac{du}{dr} \simeq \frac{V_t'}{d} \quad . \tag{2.72}$$

For a Bingham plastic the appropriate Reynolds number is then

$$R_{ep} = \frac{(V_t')^2 \rho_f}{\tau_y + K(V_t'/d)} \quad . \tag{2.73}$$

This is the reciprocal of the plasticity number of du Plessis and Ansley (1967). For a Newtonian fluid the Reynolds number is given by

$$R_{ep} = \frac{(V_t')^2 \rho_f}{\mu\left[\frac{V_t'}{d}\right]} \quad .$$

$$\text{So} \quad R_{ep} = \frac{V_t d \rho_f}{\mu} \quad \text{the familiar form.} \tag{2.7}$$

Both Steinour (1944b) and Richardson and Meikle (1961a) found that the buoyancy force on a sedimentary particle in a suspension is determined by the *density of the suspension* and not by the density of the pure liquid. Richardson and Meikle (1961a) conducted some tests on a system with two distinct particle sizes to confirm this. The free settling velocity must therefore be calculated for settling in the suspension.

Maude and Whitmore (1958b) made the implicit assumption, in studying the sedimentation of complex mixtures, that no ordering of particles would occur. They gave two reasons for this :

1. If one portion of the mixture forms an array which settles at a different rate to the rest of the mixture it would mix with further particles as it settles and so destroy the array.
2. Any particle system will contain particles with slightly different settling rates which would ensure that no possible pattern could develop.

If the mixture comprises 2 sets of uniform particles that are similar in size but have different free settling velocities then stratification will occur[6]. An explicit assumption in this thesis will be that no ordering of particles will occur on sedimentation.

The equations for settling velocity and hindered settling velocity can be compared using some of the data available in the literature. Valentik and Whitmore (1965) produced data that Dedegil (1986) considers reliable. An extract from the data of Valentik and Whitmore (1965) is presented in Table 2.17.

The data of Table 2.17 is presented graphically in Figure 2.19. The correlations for hindered particle settling presented in Table 2.16 are also shown. No correlation fits the data although two equations (2.69 and 2.70) show the correct trend.

---

[6]Richardson and Meikle (1961a).

Table 2.17 : Settling velocity data for a sphere of 57.1mm diameter ($S_s \simeq 2.7$) settling in kaolin clay, after Valentik and Whitmore (1965). All tests were conducted for a quiescent mixture.

Fines concentration [%]	Coarse settling velocity [m/s]
10.35	1.51
12.78	1.57
14.38	1.45
15.69	1.33
17.64	1.14
19.44	0.51

Equations (2.69) and (2.70) include a term for the mixture yield stress. The data of Valentik and Whitmore (1965) was obtained for particles settling in a quiescent kaolin mixture. For a mixture of kaolin which undergoes shear the floc structure may break up reducing the yield stress and allowing the particles to settle more quickly. For this reason two equations are required for the calculation of hindered particle settling.

The non dimensional approximation for particle settling (equns. 2.12 to 2.16) with increased relative density and fluid consistency index is recommended for use with mixtures that have no yield stress or mixtures undergoing shear. For unsheared mixtures with a yield stress, the correlation of Dedegil (1986) is recommended.

2.3.5 Vehicle Concentration

In Section 2.3.4 a conclusion reached by both Steinour (1944b) and Richardson and Meikle (1961a) was that the buoyancy force on a settling

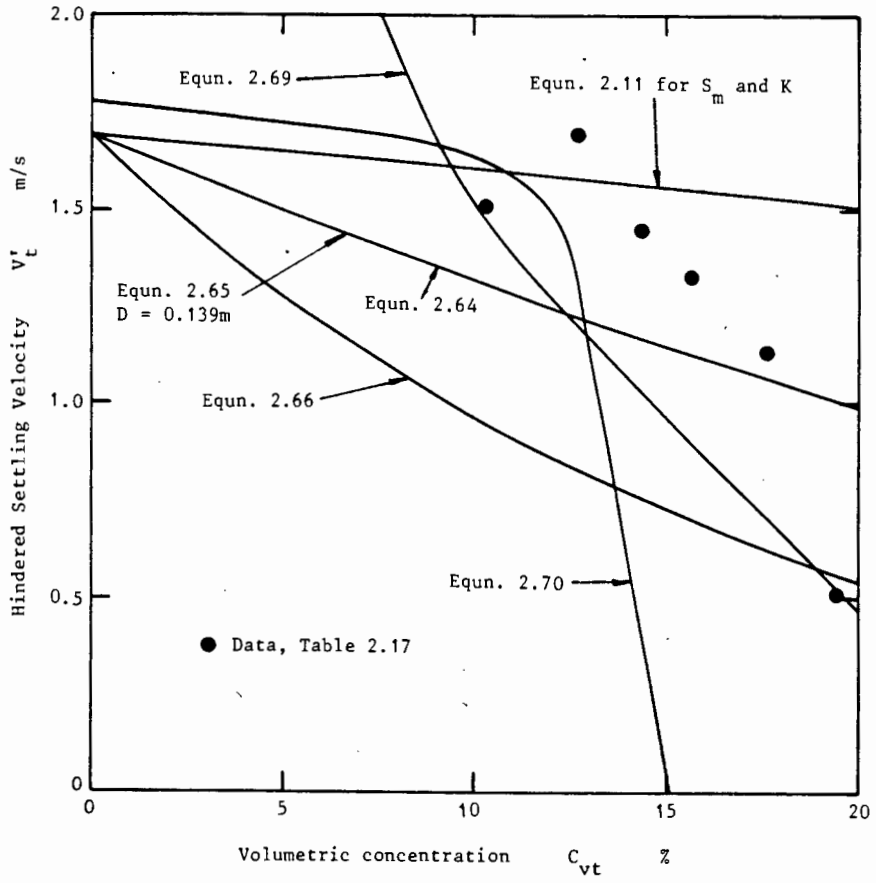

Figure 2.19 : Hindered velocity equations for 57.1mm diameter sphere settling in a kaolin mixture

particle is determined by the density of the suspension and not by the density of the liquid. A method for calculating the fluid consistency of the suspension, an integral part of settling calculations, was not suggested. In the analysis of suspensions with broad particle size distributions only a certain quantity of the mixture will be rheologically active and contribute to the fluid consistency of the mixture. The remaining particles constitute the coarse fraction and have no effect on the viscosity of the vehicle but contribute to the particle interactions and mixture density.

Table 2.18 lists some of the fine-coarse split definitions that have been proposed. The ratio of fine material, or material that contributes to the vehicle can be calculated from equn. (2.74) which relates to the particle size distribution

$$R_f = \frac{1}{10}\left[F - 1 + \log\left[\frac{d^*}{d'(F-1)}\right] / \log\left[\frac{d'(F)}{d'(F-1)}\right]\right] \qquad (2.74)$$

where F - integer number of components of particle size distribution just greater than d^*

$d'(I)$ - particle size for 10% passing

R_f - ratio of fine material to total solids content

d^* - diameter defining coarse-fine split.

This equation was proposed by Streicher (1984). Figure 2.20 presents a graph to aid in the understanding of equn. (2.74) which simply calculates the correct ratio between intermediate size groups and adds it to the previous highest fraction.

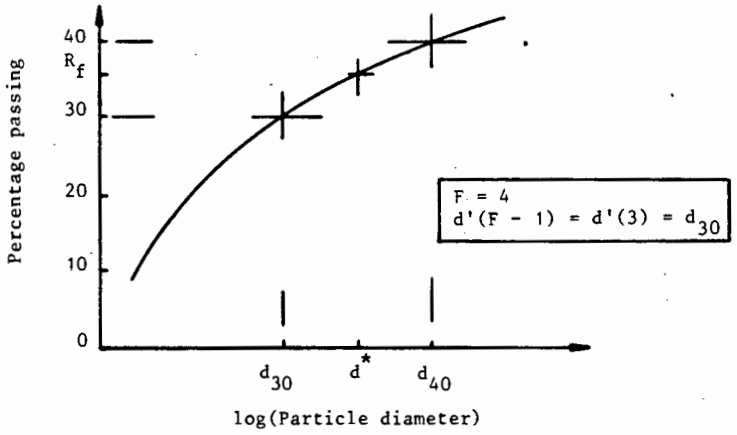

Figure 2.20 : Definition graph for equn. (2.74) showing R_f as a percentage

Table 2.18 : Criteria for distinguishing vehicle in a mixture with a broad particle size distribution

Definition	Remarks	Reference
1. $25\mu m \leq d$ Homogeneous suspension $25\mu m < d \leq 50\mu m$ Intermediate $d > 50\mu m$ Heterogeneous suspension (2.75)		Durand (1953)
2. $R_{ep} \leq 2$ (2.76)	$R_{ep} = \frac{\rho_f V_m d}{K}$ so $d \leq \frac{2K}{\rho_f V_m}$	Duckworth (1978)
3. $d \leq 1mm$	Conservative estimate C_{vtf} predicted will be high as will K	Boothroyde *et al.* (1979)
4. $d_{Lmax} = \left[\frac{18\,\nu^2\,S_w}{g(S_s - S_w)}\right]^{1/3}$ $d \leq d_{Lmax}$ (2.77)	Maximum particle diameter for Stokes' settling i.e. $R_{ep} \leq 1$	Faddick (1982b)
5. $d \leq \left[\frac{3}{4}\frac{28}{g}\frac{0.0056\,\nu\,V_m}{S_s - S_w}\right]^{1/2}$ (2.78)	Transition diameter a function of material density, mixture velocity and fluid consistency	Weber (1986)

D G Thomas (1962) proposed a method for distinguishing the fine component or suspended component of a slurry by using the shear velocity as parameter.

The minimum transport velocity for flocculated particles which are both smaller than the laminar sublayer and settle according to Stokes' law is

$$\frac{V_t}{u_o^*} = 0.0083 \left[\frac{du_o^*\rho}{K}\right]^{2.61} \qquad (2.79)$$

where $R_{ep} \leq 1$

and u_o^* = friction velocity for minimum transport condition for the limiting case of infinite dilution.

The value of u^* can be specified in eqn. (2.79) and a particle diameter calculated. The functional relationship between u^* and V_m must be known. For equn. (2.79) $d \leq \delta$ is a condition so the functional relationship between u^* and V_m is

$$u^* = y^*$$

$$\Rightarrow \quad V_m = \frac{yu_*^2\rho}{K}$$

$$\text{and} \quad \delta = \frac{11.6\,\nu}{u_*} \quad .$$

For particles larger than the laminar sublayer D G Thomas (1962) gave two equations :

1. For infinite dilution

$$\frac{V_t}{u_o^*} = 4.90 \left[\frac{du_o^*}{\nu}\right] \left[\frac{\nu}{Du_o^*}\right]^{0.60} \left[S_s - S_f\right]^{0.23} \qquad (2.80)$$

2. For concentration dependence

$$\frac{u_c^*}{u_o^*} = 1 + 2.8 \left[\frac{V_t}{u_o^*}\right]^{1/3} \sqrt{C_v} \qquad (2.81)$$

u_c^* = friction velocity at minimum transport condition

u_o^* must be calculated from equn. (2.80) and then substituted into equn. (2.81).

The vehicle definition (equn. 2.77) proposed by Faddick (1982b) can be extended to a broad particle size distribution system. Figure 2.21 presents a plot of hindered settling velocity as a function of particle diameter with concentration as parameter. The points corresponding to a particle Reynolds number of unity are connected forming a boundary between particles that are rheologically active (crosshatched region) and coarse suspended solids.

This approach supposes that the flow velocity of a mixture has no effect on the vehicle constitution. This may be a shortcoming of the method but it could serve well as a first approximation.

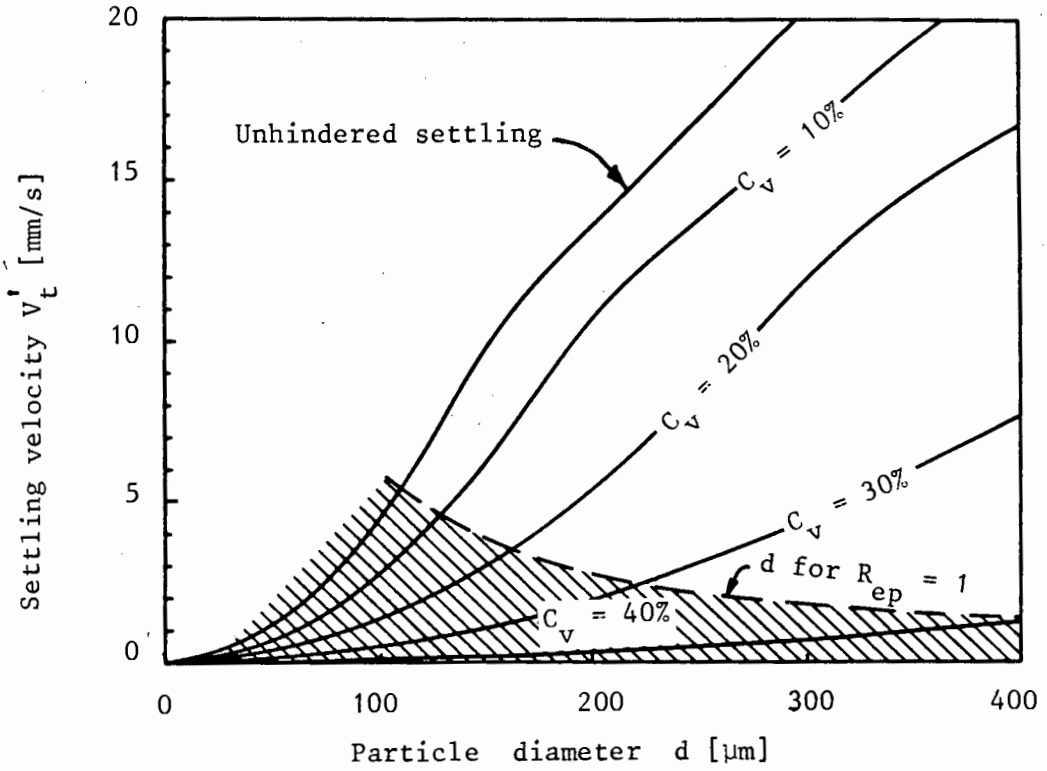

Figure 2.21 : Hindered settling velocity (V_t') as a function of particle diameter (d) with concentration as parameter. Region of particle suspension shown crosshatched.

Wilson (1972) investigated the velocity for particle suspension and arrived at an equation of the form

$$V_{susp} = k_2 \frac{V_t d}{\sqrt{f_w}\, D} \qquad (2.82)$$

k_2 = 100 , a constant

f_w = friction factor for clear fluid flowing at velocity, V_{susp}

V_{susp} = velocity for initiation of turbulent suspension of particle size d .

This equation can be represented by a graph shown in Figure 2.22 with the region of suspension marked by crosshatching. A particle diameter can be selected and the corresponding velocity calculated or the maximum suspended particle size can be found for a particular velocity.

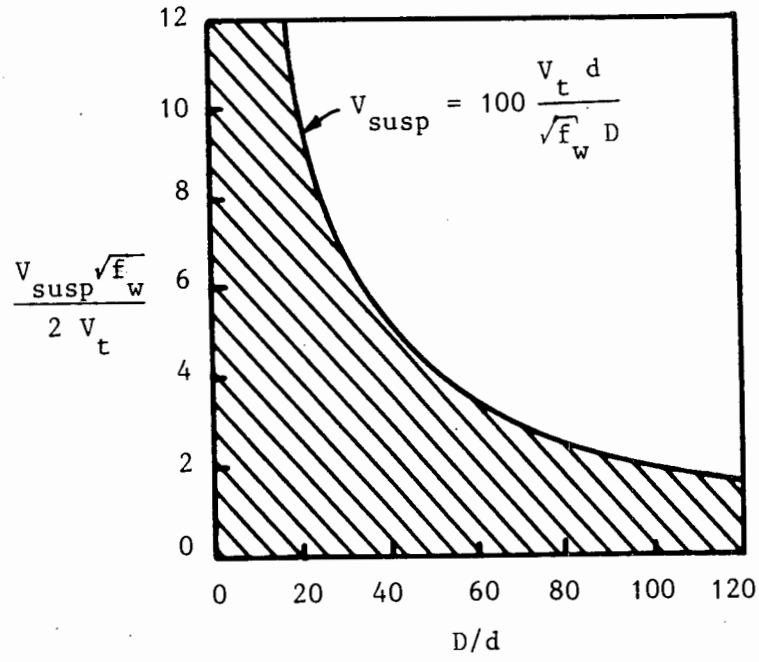

Figure 2.22 : Suspension region after Wilson (1972) shown crosshatched

Wilson and Watt (1974) extended this work and suggested a threshold velocity for turbulent suspension of the form

$$\frac{V_{susp}}{V_t}\sqrt{\frac{f_w}{2}} = k_1 \exp\,[k_2\ d/D] \qquad (2.83)$$

where $k_1 = 0.6$

$k_2 = 45$.

The constants were considered only provisional values by Wilson and Watt(1974) because of the limited experimental data used in their assessment.

Equation (2.83) is a generalised equation for predicting the velocity for turbulent suspension. It is recommended that this equation be used for calculation. Equation (2.78) is for the specific test conditions encountered by Weber (1986). The method of Thomas (1962) is useful only if a relationship between the shear velocity and the mean velocity can be found.

Wilson (1976) completed his analysis of the split between suspended and contact load material by suggesting that for values of the mean velocity progressively higher than the suspension velocity, a greater fraction of the particles in the system are suspended. For particles of uniform size

$$1 - \frac{C_{vtf}}{C_v} = \left[\frac{V_{susp}}{V_m}\right]^{k_1} \qquad (2.84)$$

k_1 - constant with a value just less than 2 ($\simeq$ 1.9)

C_{vtf} - concentration by volume of suspended material.

V_{susp} is calculated from equn. (2.83). This equation (2.84), for uniform sized particles, can be used for a mixture of sizes in the form

$$1 - \frac{C_{vtf}}{C_v} = \frac{\sum_{i=1}^{n}\left[\frac{V_{susp\ i}}{V_m}\right]^{k_1}}{n} \quad \text{for} \quad \frac{V_{susp\ i}}{V_m} > 1\ , \ \frac{V_{susp\ i}}{V_m} = 1 \qquad (2.85)$$

where n - number of particle size groups

$V_{susp\ i}$ - V_{susp} for particle size d_i .

Hanks (1982) presented a method for determining the effect of particle size distribution on the rheology of a slurry, based on his work using pulverized coal mixtures. Hanks (1982) stated that "the key concept [in slurry flow analysis] is that the division between 'vehicle' and 'coarse' material should be based upon rheological behaviour, and not upon any arbitrary dry solid size measure". The concept of an equivalent slurry concentration was introduced for this purpose.

Hanks defined a value for the fraction of rheologically active slurry where

$$\alpha = \sum_{i=1}^{n} m_i$$

and n - maximum size group of rheologically active particles

m_i - mass fraction of particles of size d_i .

The volume concentration of rheologically active material (C_{vtf}) can be calculated from the sum of the product of the ratio α and the total weight of solids plus the water of saturation and all the free water.

$$\text{So} \quad C_{vtf} = \frac{\alpha\, C_v}{1 - (1 - \alpha)C_v} \quad . \qquad (2.86)$$

Changing the subject of this equation we obtain the equivalent slurry concentration

$$C_v' = \frac{C_{vtf}}{\alpha + (1 - \alpha)C_{vtf}} \qquad (2.87)$$

C_v' - equivalent slurry concentration for a given value of α and C_{vtf} .

The equivalent slurry concentration (C_v') is the total slurry concentration that is equivalent to the concentration of fine (C_{vtf}) , or rheologically active material for which viscometer data has been obtained.

Hanks suggests its use in the following way :

1. Divide the material to be transported into various size groups in which the particle diameter can be considered constant.
2. Test the finest component in a viscometer at various mixture concentrations. For this finest fraction $\alpha = m_1$, the mass fraction of the smallest size group. The test concentration equals C_{vtf} so an equivalent concentration (C_v') can be calculated (equn. 2.87). Tests should be conducted at various values of C_{vtf} .
3. Add to the first size fraction the next highest size fraction in correct proportion to the particle size distribution. Now $\alpha = m_1 + m_2$ and C_{vtf} is obtained from the concentrations at which the mixture is tested. More C_v' values can be obtained from this set of tests.
4. A rheological equation that best describes the mixture must now be chosen and the rheological parameters plotted as a function of equivalent concentration in each case.

5. The size fraction after which no change in the rheological parameters is apparent with the addition of even larger fractions is the maximum size fraction that is rheologically active.

Figures 2.23 is extracted from Hanks (1982) for coal-water slurries that exhibit a rheology best described by the Cross (1970) model. Only the $d < 44\ \mu m$ fraction is rheologically active since the rheological parameters are effectively constant for the addition of larger fractions. This is seen in the graphs by virtue of their particle diameter independence. The nomenclature used in the graphs is ascribed to Hanks (1982).

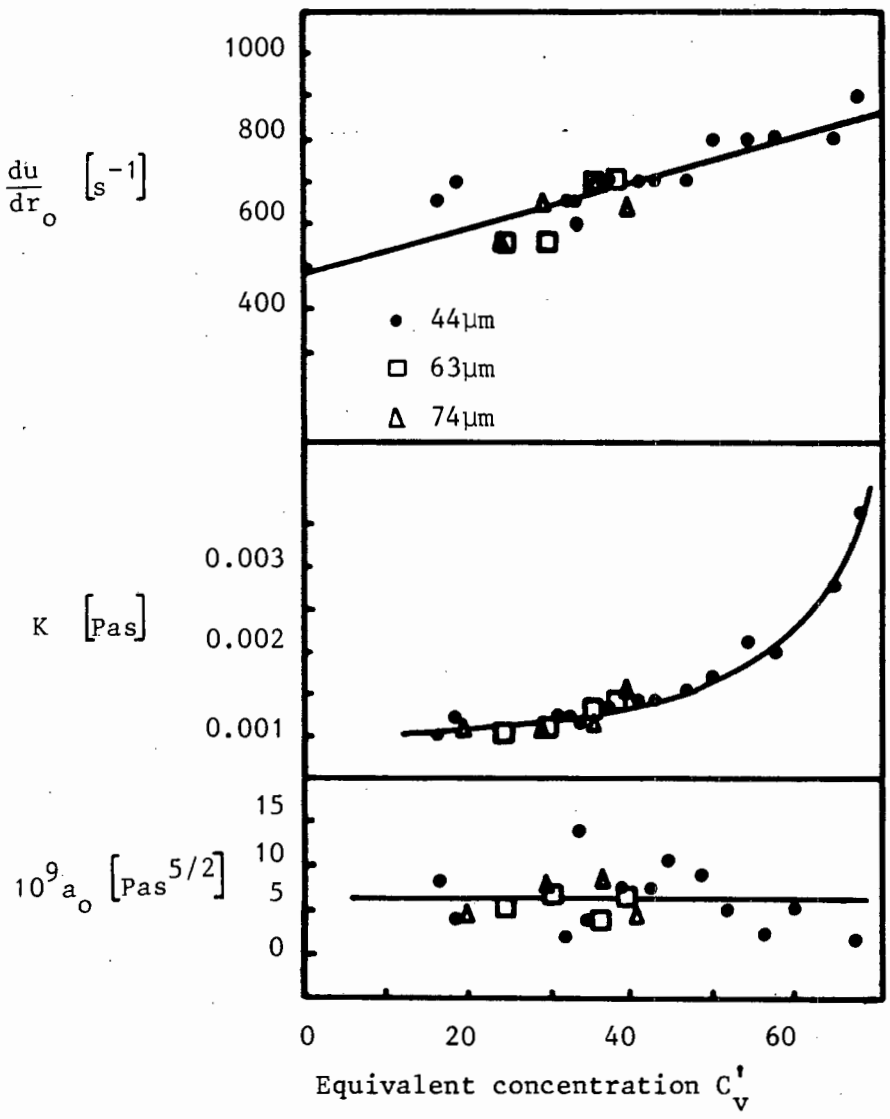

Figure 2.23 : Summary of results for rheological parameters as defined by Hanks (1982) for three partaicle size groups of a coal sample

The method of distinguishing the rheologically active part of a slurry according to Hanks (1982) is not discussed further herein. The method requires that the material investigated needs to be carefully tested in a laboratory. For select cases this may be possible but for the development of an analytical model for generalised mixed regime flows this method would be impractical.

2.3.6. Vehicle Velocity Distribution

The velocity distributions considered are quasi-one-dimensional descriptions of the flow since velocities are only allowed to exist in the principle direction of motion. Any motion across the pipe is either neglected or accounted for by parameters such as the eddy diffusivity, associated with turbulent mixing, or the mixing length.

Table 2.19 presents the velocity distribution equations considered. The distributions fall into two broad catagories; power law or logarithmic distributions. The shape of the distributions presented can be modified by changing the Newtonian value (κ = 0.38) for the von Karman constant (Vanoni (1946), Ismail (1951)). Einstein and Chien (1954) correlated the reduction in the von Karman constant (κ) by the amount of turbulent energy spent per unit weight of fluid per unit time in supporting a sediment suspension. Figure 2.24 presents a graph of the variation of (κ) .

A reduction in the value of (κ) has been ascribed to :

1. a less effective momentum exchange due to a reduction of mass of the exchange flow in the presence of a heavy fluid zone;

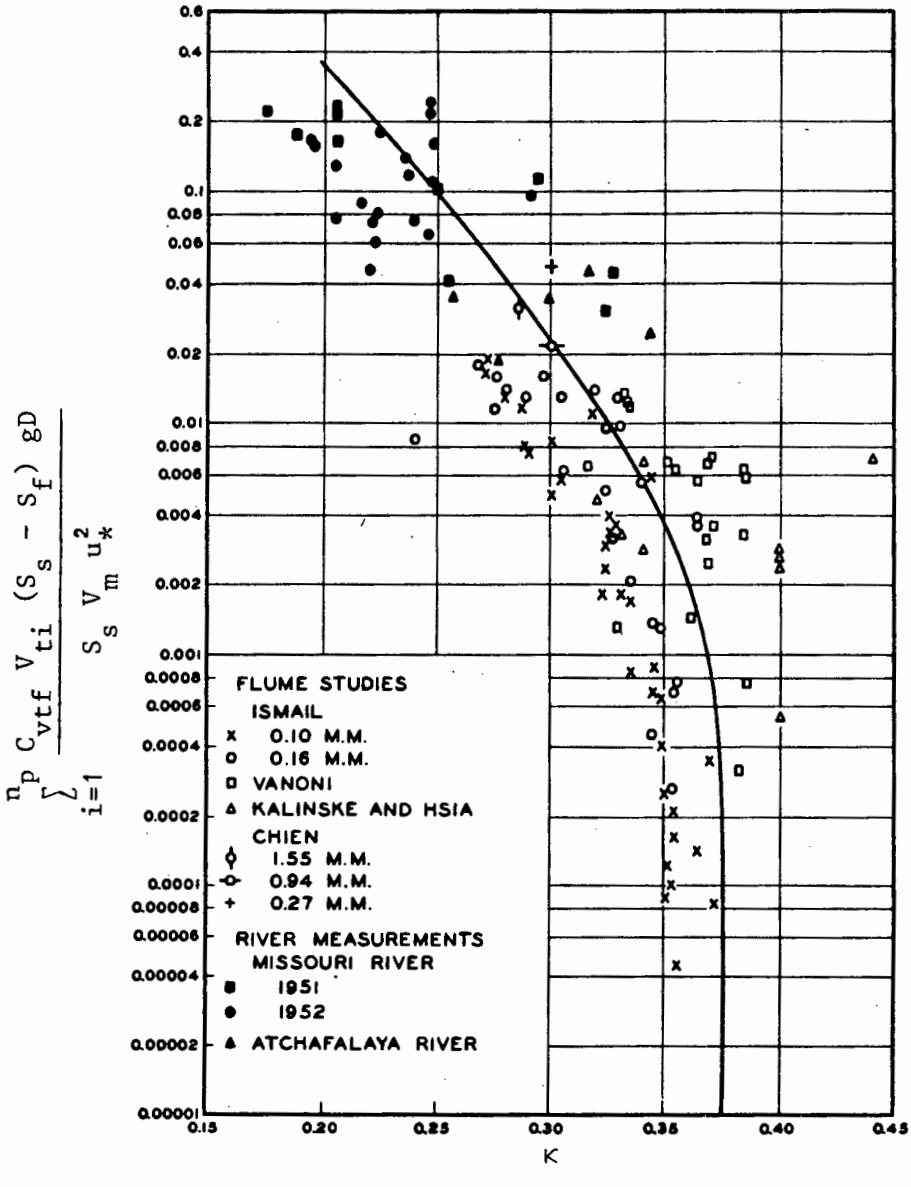

Figure 2.24 : Turbulent energy parameter versus von Karman constant (κ) (after Einstein and Chien (1954))

2. a transmission of shear to the boundary partly through sediment particles in motion;
3. a decrease in turbulence levels because of the energy spent in keeping sediment in suspension.

A comparison of the equations presented in Table 2.19 is required. This could best be achieved by using actual data rather than by creating fictitious 'constants' to be substituted into the equations. This comparison will need to form part of future research work. In order to limit the number of constants required equns. (2.88), (2.89) and (2.90) were selected for calculating U_{max} . The velocity defect law (equn. 2.94) was selected for developing the velocity profile.

2.3.7 Vehicle Friction Factor

Table 2.20 presents the friction factor equations considered for the vehicle. A comparison of these equations will best be achieved with actual data derived from a test facility. The comparison is presented in Chapter 6. Equations (2.99) and (2.104) can be used as a first approximation in the solution of a friction factor.

2.4 TWO PHASE SOLID LIQUID FLOW

Soo (1986) suggested that three general slurry flow regions can be identified with low, intermediate and high concentrations of solid. For low concentration (dilute) suspensions the fluid motion is essentially unaffected by the particles. The very dense suspensions tend to be in a

Table 2.19 : Velocity distribution equations

Velocity distribution equations	Author	Equation No.
Universal velocity profile $u^+ = y^+$ for $y^+ < 5$		2.88
$u^+ = \frac{2.0}{\kappa} \ell n\ y^+ - 3.05$ for $5 \leq y^+ \leq 30$		2.89
$u^+ = \frac{1}{\kappa} \ell n\ y^+ + 5.5$ for $y^+ > 30$		2.90
$u^+ = \frac{u}{u_*}$ and $y^+ = \frac{u_* \rho y}{K}$		
For pseudoplastic fluids $u^+ = (y^+)^{1/n}$ for $0\ y^+ < 5^n$		2.91
$u^+ = \frac{5.0}{n} \ell n\ y^+ - 3.05$ for $5^n \leq y^+ \leq y_2^+$		2.92
$u^+ = \frac{2.78}{n} \ell n\ y^+ + \frac{3.8}{n}$ for $y^+ > y_2^+$	Clapp (from Govier and Aziz, 1981)	2.93
y_2^+ found from experimentation		
where $u^+ = \left[\frac{u}{u_*}\right]$ and $y^+ = \frac{(u_*)^{2-n} \rho y^n}{K}$		
Defect velocity law For $\epsilon_m = 0$ at $y = R$		
$\frac{U_{max} - u}{u_*} = \frac{1}{\kappa} \ell n \frac{R}{y}$ $\quad \delta \leq y < R$		2.94

Table 2.19 contd.

Velocity distribution equations	Author	Equation No.
Defect velocity law For $\epsilon_m \neq 0$ at $y = R$ $\frac{U_{max} - u}{u_*} = \begin{cases} \frac{1 - a}{2\kappa a} + \frac{1}{K} \ell n \frac{aR}{y} & \delta \leq y < aR \\ \frac{1}{2\kappa a(1 - a)} \left[1 - \frac{y}{R}\right]^2 & aR \leq y < R \end{cases}$ $a = 0.7$ to 0.97	Zhaoyin and Ning (1984)	2.95 2.96
Distribution including concentration gradient and particle lift effects at bed interface For $0.05\ R \leq y < aR$ $\frac{U_{max} - u}{u_*} = \frac{1 - a}{2\kappa a} + \frac{1}{\kappa} \ell n \frac{aR}{y} - \frac{5\ d^2}{\kappa^3 y^2} \left[\frac{R + 2y}{R} - \frac{1 + 2a}{a^2} \frac{y^2}{R^2}\right]$ For $aR \leq y \leq R$ $\frac{U_{max} - u}{u_*} = \frac{1}{2\kappa a(1 - a)} \left[1 - \frac{y}{R}\right]^2$ $a = 0.7$ to 0.97	Zhaoyin & Ning (1984)	2.97 2.98

Table 2.20 : Friction factor equations for pseudohomogeneous mixtures

Friction factor equations	Equation No.
Blasius (1913)	
$f = 0.079\ R_e^{-0.25}$ for $3000 < R_e < 100\ 000$	2.99
Colebrook-White equation after Colebrook (1939)	
$\frac{1}{\sqrt{f}} = -4 \log \left[\frac{k}{3.7\ D} + \frac{1.26}{Re\sqrt{f}}\right]$	2.100
Torrence equation (1963)	
$\frac{1}{\sqrt{f}} = \frac{2.687}{n} - 2.949 - \frac{1.966}{n} \ell n\ (1 - \alpha)$ $+ \frac{1.966}{n} \ell n\ (1 - \alpha) \left[Re\ \sqrt{f^{2-n}}\right]$ $+ \frac{0.682}{n} (5n - 8)$	2.101(a)
$\alpha = \frac{\tau_y}{\tau_o}$ and $Re = \frac{D^n\ V^{2-n}\ \rho}{K\ 8^{n-1}}$	2.101(b)
Rough wall Rek > 70	
$\frac{1}{\sqrt{f}} = 1.767\ \ell n \frac{D}{2k} + 6 - \frac{2.65}{n}$	2.102
$Rek = \frac{k}{D} Re \sqrt{\frac{f}{2}}$	2.103
Govier and Aziz (1981)	
$\frac{fm}{fw} = \left\{\frac{\mu_m \rho_w}{\mu_w \rho_m}\right\}^{0.25}$	2.104

state of pseudo-non Newtonian viscous motion . Both the dilute and the very dense suspensions can be modelled mathematically[7]. Steady motion is sustained by a balance between diffusion, shear lift and gravity effects. Table 2.21 presents some information on the low and high concentration regions.

At intermediate concentrations between these two extremes Soo (1986) suggests that the situation becomes complicated. Steady flow is replaced by wavy stratified flow in a horizontal pipeline. Availability of vacant spaces in the suspension for relative motion among particles as well as multiple interactions between the particles and the fluid become important.

The intermediate concentrations range is that in which most industrial hydraulic transport systems operate. It is therefore important that this region of flow is investigated.

2.4.1 Stationary Bed

2.4.1.1 Particle suspension mechanism

The entrainment of particles into a turbulent flow stream is considered to be related to the turbulent fluctuating flow components rather than the average values. Sumer and Oguz (1978), proposed a mechanism for particle suspension close to the bottom of a smooth channel.

---

[7] Dilute phase, Shih and Lumley (1986).
Dense phase, Elliot and Gliddon (1971), Shook (1985), Streat (1986) Thomas (1979).

Table 2.21 : Comparison of dilute and dense suspensions
After Soo (1986)

	DILUTE SUSPENSION	DENSE SUSPENSION
Relative motion between particles	Large	Small
Particle-particle interaction	Weak	Strong
Particle diffusivity[8], ϵ_s	Large	Small
Apparent viscosity[9]	Due to particle fluid interaction, $\mu_{PL} = C_v \rho_s \epsilon_s$	Due to particle-particle interaction $\mu_{pp} \alpha \frac{1}{\epsilon_s}$
Flow regime in application	Steady, Turbulent	Pseudolaminar
Motion above minimum transport velocity	Stable	Stable
Volumetric concentration range	$C_v \leq 10\%$	$C_v > 40\%$ to 75% depending on particle size distribution

Sumer and Oguz (1978) suggested that the turbulent fluctuations at the bottom of a smooth channel take the form of a "bursting" (ejection) and a "sweeping" process. The observed repetitive nature of the flow patterns

---

[8]Diffusion refers to the net transport of material in the absence of mixing (by mechanical means or by convection). The proportionality constant between the flux and potential is the diffusivity.

[9]See Glossary, Appendix 1, for definition of apparent viscosity.

suggest a quasicyclic process[10]. A bursting process is initiated by the upwelling motion of fluid in the subboundary layer. This upwelling is caused by an adverse pressure gradient in the subboundary layer. A local convected recirculation cell will immediately form below the lifted fluid (see Figure 2.25). As the ejection progresses the lifted fluid and the recirulation cell will move away from the wall and grow in size. The flow along the lowest portion of the recirculation will be in the reverse direction with respect to an observer moving with the cell. The relative reverse flow near the wall implies a temporary local adverse pressure gradient. When the correct conditions exist the next ejection will occur as the existing structure continues to pass overhead. The previously lifted fluid then breaks up as it interacts with the next burst. Some fluid from both bursts returns to the wall where it spreads out sideways. This sideways spread gives the flow in the viscous sublayer ($0 \leq y^+ \leq 5$) a streaky character with lateral variation in the streamwise direction of the velocity. Sumer and Oguz (1978) viewed the streaks of high and low speed fluid as a subboundary layer phenomenon. A burst will occur from a low speed streak. The fluid returning from the burst to the wall is called a sweep process. The burst and sweep processes, although discussed in a two dimensional sense, are in fact three dimensional.

A generation region ($5 \leq y^+ \leq 70$) coincides with the position of the majority of so called fluid burst and sweep phases. In the burst phase low

---

[10] A deterministic sequence that occurs randomly in space and time.

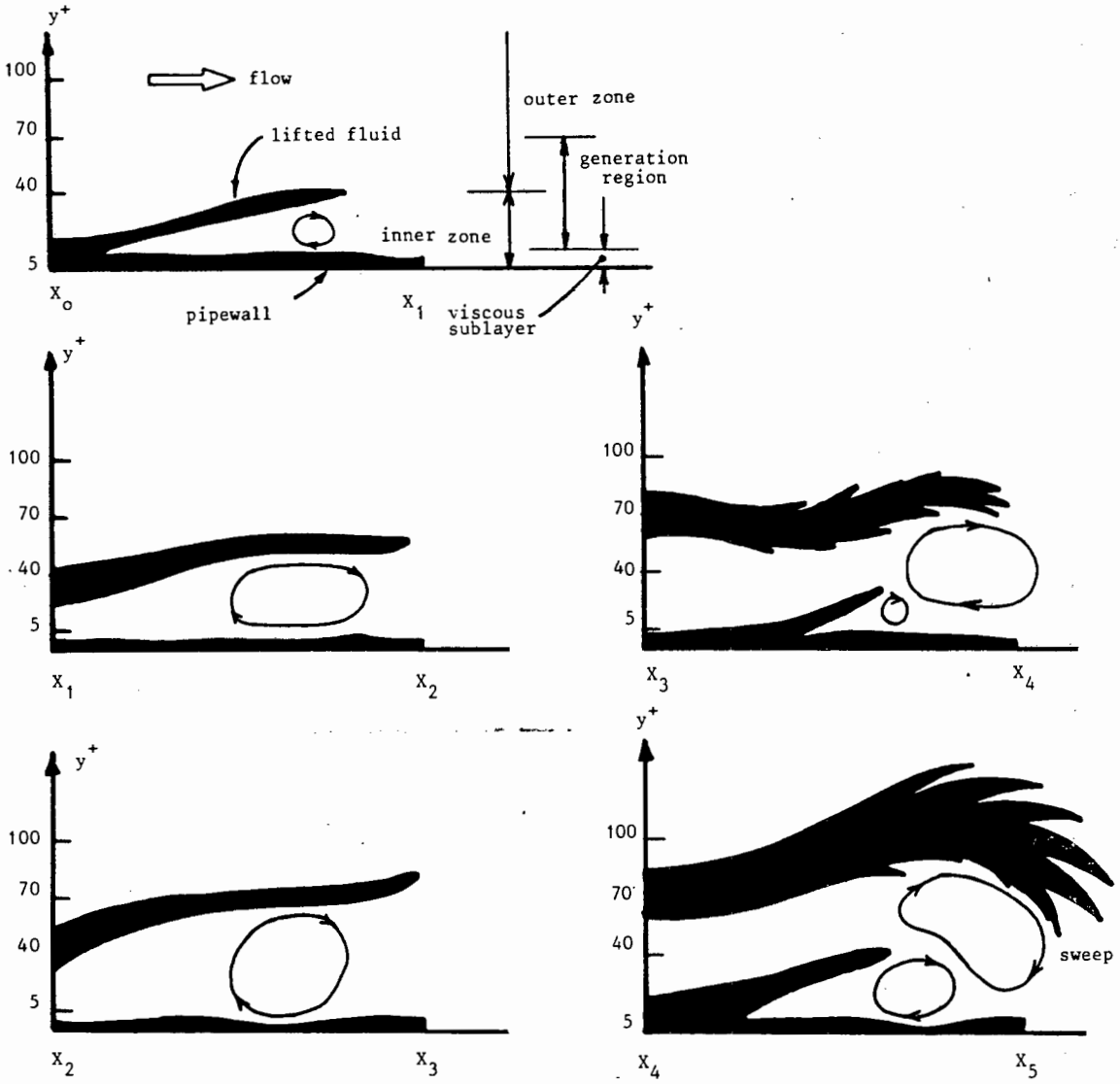

Figure 2.25 : Instantaneous views of a burst as it progresses downstream. Local convected recirculation cell forming below fluid lifted by an adverse pressure gradient.

speed fluid is ejected away from the lower zone of the generation region. This burst can have an instantaneous velocity component perpendicular to the wall which is as high as 30% of the longitudinal component. Shear varies as

a square of the velocity so the instantaneous shear can be up to 70% higher than the average.

The fluid returning to the wall from a sweep will quickly be retarded and may be the source of new low speed streaks further downstream. Sweeps therefore represent the passage of a previous burst from further up the stream. Sumer and Ozuz (1978) reported the distance between low speed wall streaks to be $\frac{100\nu}{u^*}$. The spreading fluid in a sweep pushes particles (wandering in the immediate vicinity) to an adjacent low speed wall streak. If the particle size is such that it projects above the edge of the viscous sublayer, particularly above the passive region ($0 \leq y^+ \leq 2.5$), it will be exposed to the pressure gradient in this region and therefore the mechanism which brings about bursting. If the particle size is less than the thickness of the viscous sublayer it is not expected to be lifted into the body of the flow (i.e. $d < \frac{2,5\nu}{u^*}$) .

Observations showed that a particle originating in the region $0 \leq y^+ \leq 50$ could reach y^+ values of 100 to 200 which is the height at which the bursts break up. Most ejected particles observed reached at least y^+ values of 80 to 100. From this position the particle returns to the region near the bottom. In the downward motion the fluid instantaneously in the particles' vicinity consists of high speed flow penetrating towards the wall (sweep phenomenon). A particle on the way back to the wall is expected to meet the next ejection which may cause the particle to have another upward motion.

If the particle reaches the bottom it will eventually be lifted again by the process described.

Sumer and Deigaard (1981) extended this work to account for heavier particles and wall roughness. In the case of a rough wall the theoretical bottom was found to be located at a distance of $0.25k$[11] below the roughness tops. For rough wall flow particles, in a single continuous motion achieve much higher average elevations than in the case of smooth wall flow. The streamwise distance travelled is found to be slightly smaller. The mean 'rise' time also appears to be smaller for the rough wall case. Particle upward velocity in the case of a rough bottom is appreciably greater. In the rough wall case the lateral flow of fluid along the neighbouring sides of two adjacent high speed zones is likely to be retarded by the roughness form drag thus causing the disappearance of the smooth boundary wall streaks. Particles will be swept laterally from a high momentum fluid environment into a localized low momentum zone (known as the 'crossing trajectories effect') from where the lift mechanism is similar to that of a smooth wall case. The bursting period shows no sign of dependency upon the bed roughness. The mean burst periodicity and the mean characteristic wavelength of the bursting process seem to scale with the outer flow parameters V_m and D irrespective of the bed roughness.

---

[11] k - mean height of roughness tops above base plate ($k \simeq d$) .

Particles that are relatively heavy[12] yet still not heavy enough to move constantly in contact with the bottom by rolling or sliding trace a path pattern of short 'hops'. These particles reach only low values of y^+ since an appreciable slip between the fluid and the particle exists. The particle cannot be maintained in the lifted fluid of the accompanying burst and leaves the main body of the lifted fluid due to gravity before the accompanying burst breaks up (see Figure 2.26).

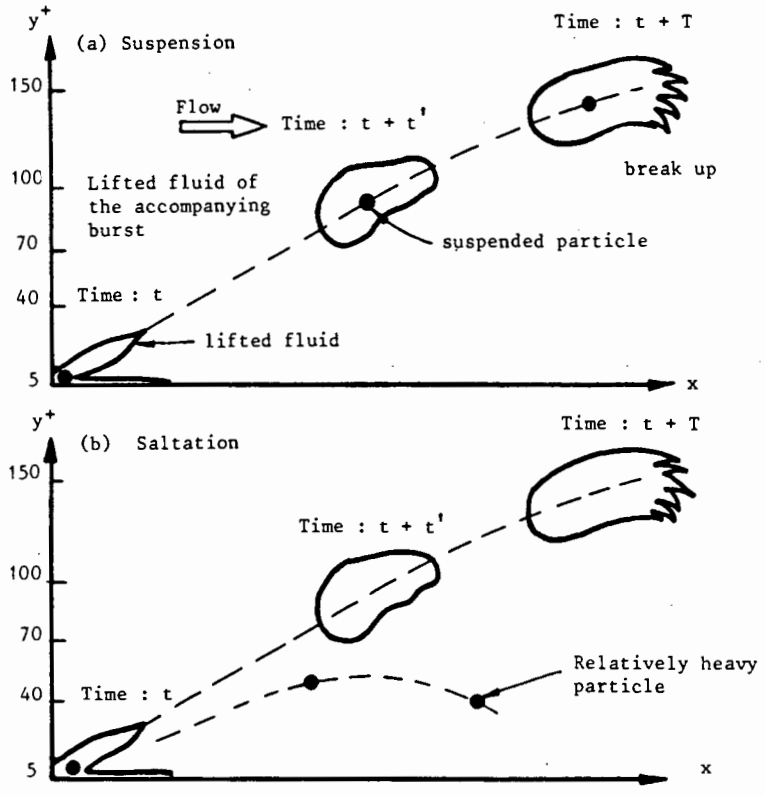

Figure 2.26 : Fluid burst process showing a) the path of a particle small enough to remain entrained, b) a particle undergoing saltation

---

[12] Rizk and Elghobashi (1985);
Particles with $d^+ = \frac{du_*}{\nu} = 0.02$ follow exactly the fluid path in the wall region.

It should be noted that the bursting event is not of constant cycle but rather is highly irregular both in time and space and is interactive with similar surrounding structures. Particles entrained by one bursting cycle can be intercepted by similar surrounding structures.

2.4.1.2 Incipient particle motion

Shields' criterion for incipient suspension of uniform, spherical particles is presented in Figure 2.27. This is considered to be of the most reliable criterion by Shen and Wang (1970), Graf (1971), Francis (1973) and Bonapace (1981). Shields' criterion is based on the bed interface shear which was shown by Sumer and Oguz (1978) to reach 70% of its average value due to turbulent flow fluctuations.

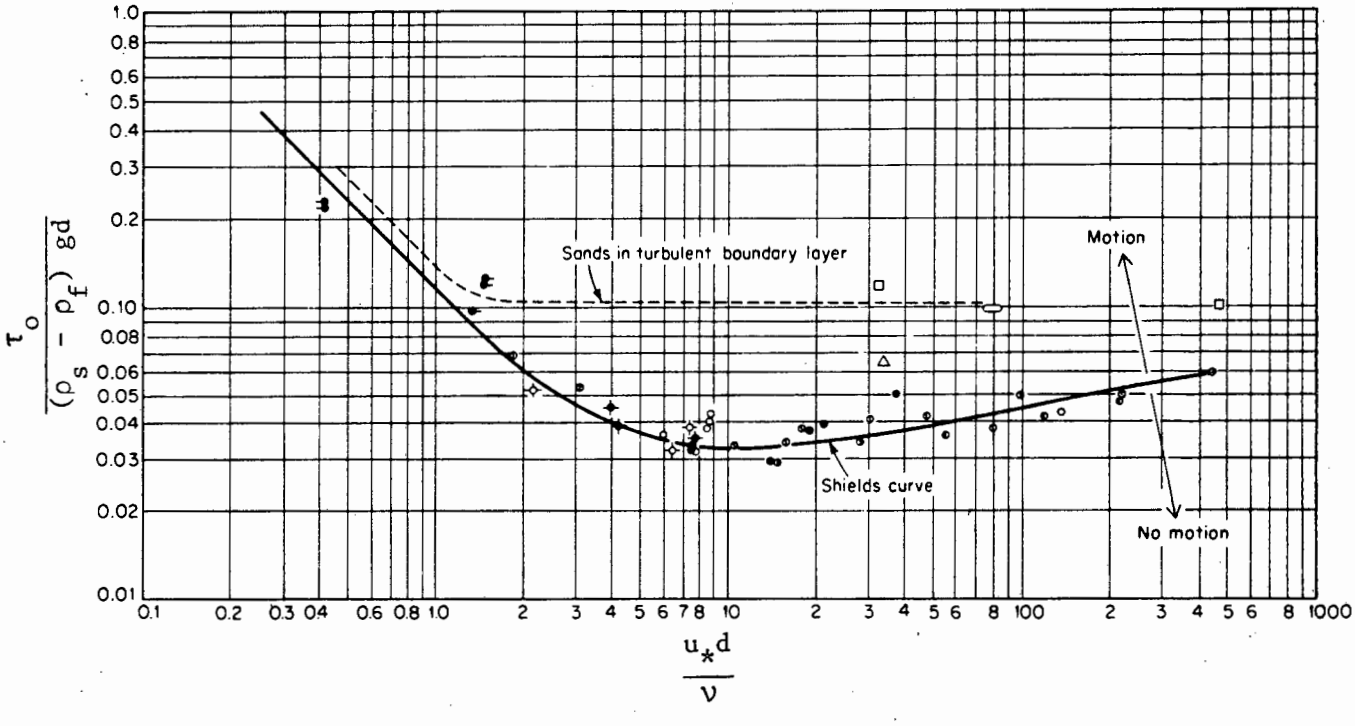

Figure 2.27 : Shields' diagram; dimensionless critical shear stress vs. shear Reynolds number for fully developed turbulent velocity profile (after Vanoni, 1964)

The Shield criterion for incipient particle suspension is

$$\frac{(\tau_o)_{crit}}{(S_s - S_w)d} = fn\left[\frac{du_*}{\nu}\right] \qquad (2.105)$$

where $R_{e*} = \frac{du_*}{\nu}$.

The shear Reynolds number can be presented in terms of the laminar sublayer thickness δ by the relationship

$$\frac{du_*}{\nu} = 11.6\,\frac{d}{\delta} \quad . \qquad (2.106)$$

Three zones are recognized in Figure 2.27. These are discussed in Table 2.22.

The line represented in the Shield diagram is the line for the minimum shear stress required to move a particle. For any particular system the actual shear stress required to move a particle may be well above this line.

Ippen and Verma (1953) find the Shield diagram untenable for beds where the particle size in the bed is of a different size and texture to material carried as suspended load. Extreme density differences between the fluid and the bed are also considered to cause anomalies. For material that is well graded, non spherical, sticky or flocculated the critical shear stress for suspension will be higher than that suggested.

Table 2.22 : Zones distinguishable in the Shield diagram

Zone	Particle size	Shear Reynolds Number	Comments
1	$d < \delta$	$R_{e*} \leq 2$	Particles enclosed in laminar sublayer. Movement is mainly due to viscous action and independent of turbulence.
2	$d \simeq \delta$	Intermediate	Laminar sublayer partially covers particle. Curve (Figure 2.27) has a minimum at $R_{e*} \simeq 10$ $\frac{(\tau_o)_{int}}{(\rho_s - \rho_w)dg} \simeq 0.03$ Below this value no scour should occur.
3	$d >> \delta$	High	Dimensionless shear stress independent of shear Reynolds number for $R_{e*} \geq 400$ $\frac{(\tau_o)_{int}}{(\rho_s - \rho_w)dg} = 0.06$

Egiazaroff[13] (1965) presented a modification to overcome the anomaly for a well graded mixture where

$$\frac{(\tau_o)_{int}}{(\rho_s - \rho_w)dg} = \frac{0.1}{\left[\log 19 \frac{d}{d_{50}}\right]^2} \qquad (2.107)$$

d - diameter of particle in the bed to be "picked up".

For particles smaller than d_{50} the resistance to particle motion will be increased, for coarse particles ($d > d_{50}$) the opposite is true.

Other phenomena not taken into account by the Shield criterion are :

1. Small particles are subject to cohesive forces.
2. Large particles are less readily eroded than smaller particles. The top layer will form a protective layer over the underlying particles. This is known as "armouring of the bed".

A mathematical description of incipient particle motion is very complex for all but the simplest case of uniform spherical particles on a flat bed. It is therefore desirable to use a bed scour model that does not require the calculation of incipient particle motion conditions.

---

[13] from Graf (1971).

2.4.2 Part Stationary Bed

2.4.2.1 Interface load model

The interface load is the sediment material the weight of which while in motion is supported by the non moving material or pipe bottom. Individual particles move by rolling, sliding and occasionally saltation.

Graf (1971) found that all interface load equations predict the maximum interface load that a stream in equilibrium can possibly carry. The transport capacity may or may not be equal to the actual load. Most of the work done on interface load flow[14] is for open channels. This work is directly applicable to pipeline flow since the free surface has no effect on interface load flow. This condition holds true only until the stationary bed begins to move and does not apply to the suspended load above the bed.

A comprehensive interface load model was developed by Einstein (1942), Einstein (1948) and Einstein (1950). Ashida and Fugita (1986) have extended this model suggesting advances that can be incorporated but need a computer to obtain the solution.

Einstein's model has the following benefits :

1. It avoids the difficulty of defining a critical value for initiation of sediment motion.

---

[14] In the open channel flow literature this term is called *bed load* flow. A change in terminology herein is to avoid confusion with the stationary *bed load*.

2. It suggests that the interface load transport is related to the velocity fluctuations in turbulent flow rather than the average.

From experimental observation the following was found :

1. Intensive exchange of particles is observed between the interface load and the bed.
2. The interface load moves slowly downstream, the motion of individual particles is one of quick steps with intermediate rest periods.
3. Average step length is independent of flow conditions.
4. Different transport rates are achieved by changing the average time between successive steps and by a change in the thickness of the moving layer.

For interface load equilibrium the number of particles deposited per unit time must equal the number of particles eroded per unit time. This is taken to occur over a unit bed area.

The number of particles deposited per unit time and unit area is given by

$$\frac{q_s X_s}{A_L k_2 d^4} \quad . \tag{2.108}$$

The number of particles eroded per unit time and unit area is given by

$$\frac{X_b p_n}{k_1 d^2 t_e} \tag{2.109}$$

where X_s - fraction of interface load of a given grain size

X_b - fraction of bed material in a given grain size

p_n - probability of grain being eroded

t_e - time for each exchange

q_s - bed load rate in volume per unit time and width

A_L - step length constant, where step length = dA_L

k_2 - constant of particle volume

k_1 - constant of grain area.

Einstein suggested a dependency of t_e on the settling velocity of the particles V_t such that

$$t_e \alpha \frac{d}{V_t} = k_3 \sqrt{\frac{d\rho_f}{g(\rho_s - \rho_f)}} \tag{2.110}$$

and k_3 - a constant of time scale.

The rate of deposition is equal to the rate of erosion so

$$\frac{q_s X_s}{A_L k_2 d^4} = \frac{X_b p_n}{k_1 k_3 d^2} \sqrt{\frac{g(\rho_s - \rho_f)}{d\rho_f}} \quad . \tag{2.111}$$

This then is Einstein's bed load equation.

The exchange probability p_n has the following effect;

If p_n is small => low sediment transport

p_n is high => high sediment transport

so p_n can be used to calculate the distance $A_L d$.

For small p_n , i.e. single particles being transported

$A_L d = \lambda_b d$ where from experiment $\lambda_b \simeq 100$

If p_n is large, $(1 - p_n)$ particles find a chance of deposition after travelling $\lambda_b d$ while p_n particles stay in motion. At another step again some particles will be able to settle i.e. $(1 - p_n)$ in $2\lambda_b d$ but p_n will stay in motion for another step. This distance travelled can be expressed by a series relationship as

$$A_L d = \sum_{k=0}^{\infty} (1 - p_n) p_n^k (k + 1) \lambda_b d = \frac{\lambda_b d}{1 - p^n} \quad . \tag{2.112}$$

Substituting this equation into equn. (2.111) yields

$$\frac{p_n}{1 - p_n} = \left[\frac{k_1 k_3}{k_2 \lambda_b}\right] \left[\frac{X_s}{X_b}\right] \left[q_s \sqrt{\frac{\rho_f}{(\rho_s - \rho_f)}} \sqrt{\frac{1}{gd^3}}\right] \tag{2.113}$$

Einstein introduced three correction factors :

1. ξ - hiding factor. This takes into account the fact that small particles tend to "hide" between larger ones or in the laminar sub layer. The function for ξ is given in Figure 2.27.

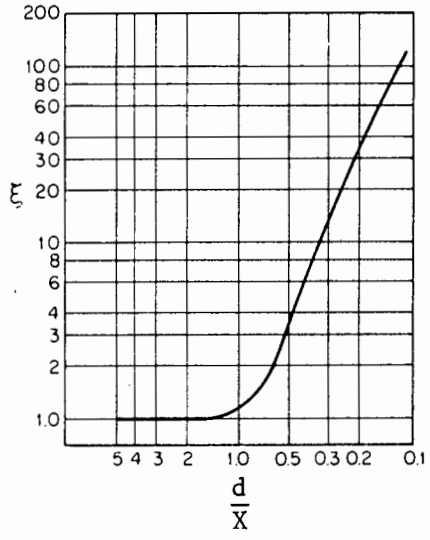

Figure 2.27 : Hiding factor as used in equn. (2.115) Einstein (1950)

2. h - a logarithmic velocity distribution correction factor shown in Figure 2.28.

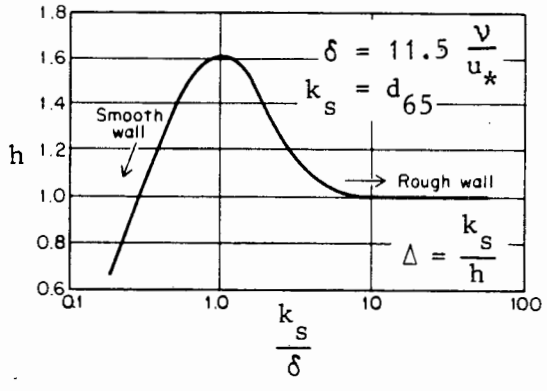

Figure 2.28 : Correction factor in the logarithmic velocity distribution (Einstein (1950))

3. Y - pressure correction factor. This correction factor describes the change of lift coefficient in mixtures with various grain roughnesses. Y is given in Figure 2.29. For uniform sized grains ξ and Y are both unity.

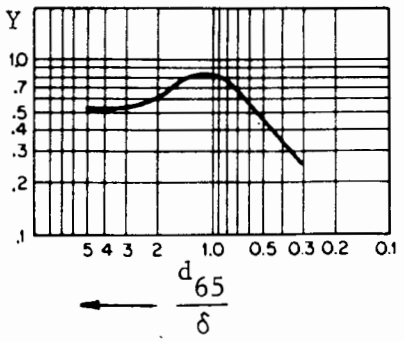

Figure 2.29 : Pressure correction factor as used in equn. (2.115) (Einstein (1950))

The final analytical equation presented by Einstein (1950) is given by

$$1 - \frac{1}{\sqrt{\pi}} \int_{-B_* \Psi_* - 1/k_1}^{+B_* \Psi_* - 1/k_1} e^{-t^2} \, dt = \frac{A_* \Phi_*}{1 + A_* \Phi_*} \quad . \tag{2.114}$$

A_* , B_* and k_1 are universal constants where

$$A_* = \frac{1}{0.023} = 43.5$$

$$B_* = \frac{1}{7} = 0.143$$

$$k_1 = \tfrac{1}{2}$$

The shear intensity on individual particles located in the bed is given by

$$\Psi_* = \xi \; Y \left[\frac{B^2}{B_x^2}\right] \Psi \qquad (2.115)$$

where $\Psi = (S_s - S_f) \dfrac{dg}{u_*^2}$

$B = \log 10.6$

$B_x = \log (10.6 \; X/\Delta)$

and Δ is given in Figure 2.28.

The intensity of interface load transport on individual particles in the bed is given by

$$\Phi_* = \frac{q_s X_s}{X_b} \sqrt{\frac{1}{(S_s - S_w) \; gd^3}} \qquad (2.116)$$

This method gives the transport rate of individual components $\dfrac{X_s}{X_b}$ within a mixture. The total transport rate of the mixture as *interface load* can be determined by summing up these fractions for the complete particle size distribution.

Wilson (1966 and 1987) suggested that the predictions of equn. (2.114) may be incorrect at the high shear rates encountered in pipe flow and suggested

the use of the Meyer-Peter and Muller (1948) equation. This is an empirical equation given by

$$\phi_* = \left(\frac{4}{\Psi_*} - 0.188\right)^{3/2} \quad . \tag{2.117}$$

Figure 2.30 shows a comparison of these two equations.

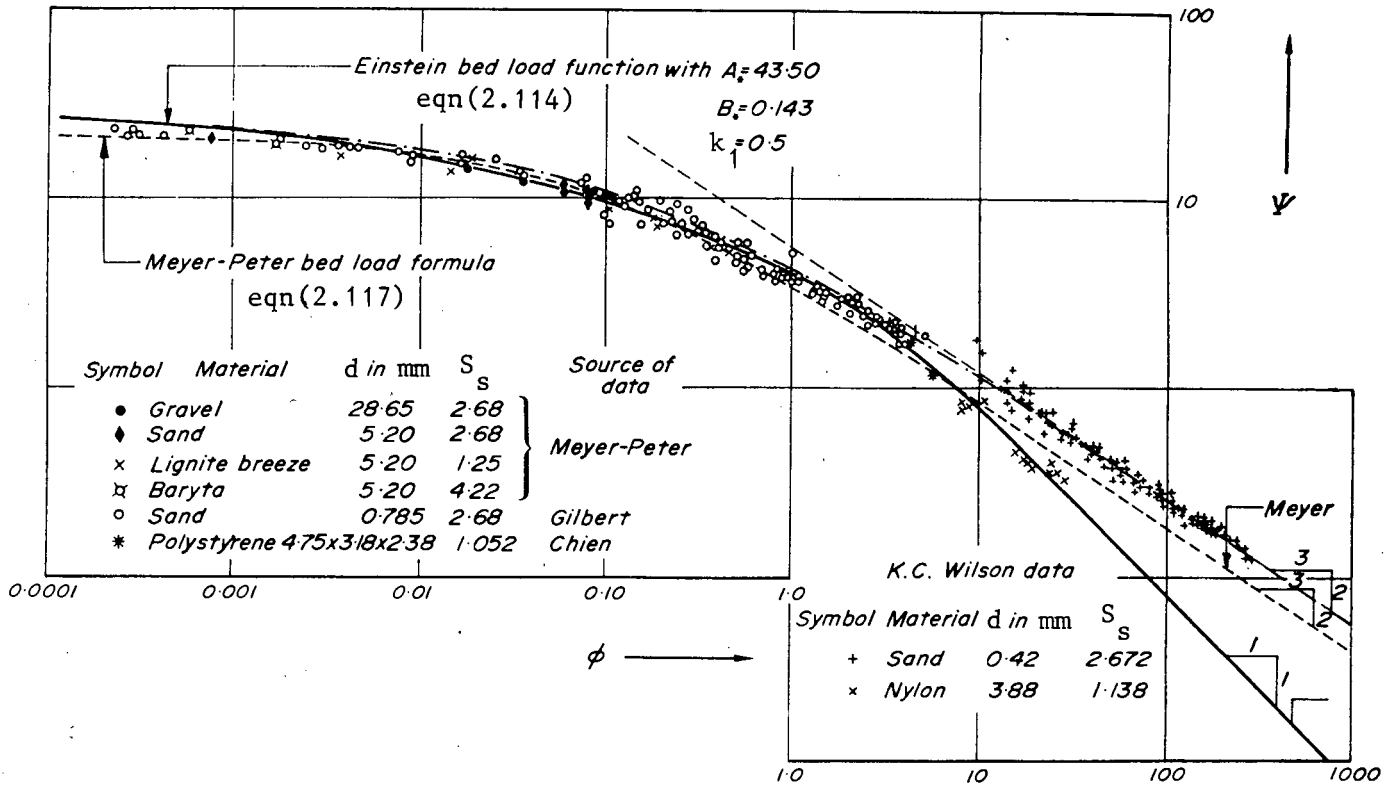

Figure 2.30 : Comparison of the bedload transport intensity equations of Einstein (1950) and Meyer-Peter and Muller (1948) (from Yalin, 1972)

2.4.2.2 Bed forms

Bed form geometry in open channel flow is critical to an understanding of the friction losses associated with these bed forms. In pipeline flow dunes will form but only at low Froude numbers. Graf (1971) suggested that dunes would form at

$$F_r \leq 1 \ .$$

For a pipeline of D = 0.139 m

$$\bar{u} = \sqrt{gD}$$

$$= 1.17 \text{ m/s.}$$

2.4.2.3 Interface friction factor

The resistance to flow of the mixture over a bed is the sum of the surface drag and form drag. The reistance to flow caused by the pipe perimeter above the bed can be calculated by using the fully suspended flow equations.

1. Lazarus (1986) and Doron *et al.* (1986) used the Colebrook-White friction factor equation for rough wall flow (equn. 2.100 for $Re \rightarrow \infty$) and partially rough wall flow (equn. 2.100) respectively. Doron *et al.* (1986) suggested that this friction factor might in fact be doubled to achieve the correct value.

2. Richardson and Simons (1967) broke the friction factor prediction equation into regions. For a plane bed with no sediment transport

$$\sqrt{\frac{2}{f_I}} = 1.475 \ln \frac{D}{d_{85}} + 1.36 \quad . \qquad (2.118)$$

For a plane bed with appreciable sediment transport

$$\sqrt{\frac{2}{f_I}} = 1.85 \ln \frac{D}{d_{85}} \quad . \tag{2.119}$$

2.4.2.4 Bed fluidization

The plane bed created by dune "wash out" will be fluidized and begin to move. This designates the transition from part stationary bed flow to fully moving bed flow. Two mechanisms may be responsible for this fluidization either occurring exclusively or simultaneously :

1. Force balance on the bed

   Consider a force balance on the bed shown in Figure 2.31.

$$\frac{\Delta P}{L} A_b + \tau_i D \sin \gamma = F_{RB} + W_b \sin \theta \tag{2.120}$$

   γ - bed half angle

$$F_{RB} = N\mu_s = \rho g (S_s - S_w) C_b \mu_s A_b \cos \theta \tag{2.121}$$

$$W_b = A_b S_b \rho g \quad . \tag{2.122}$$

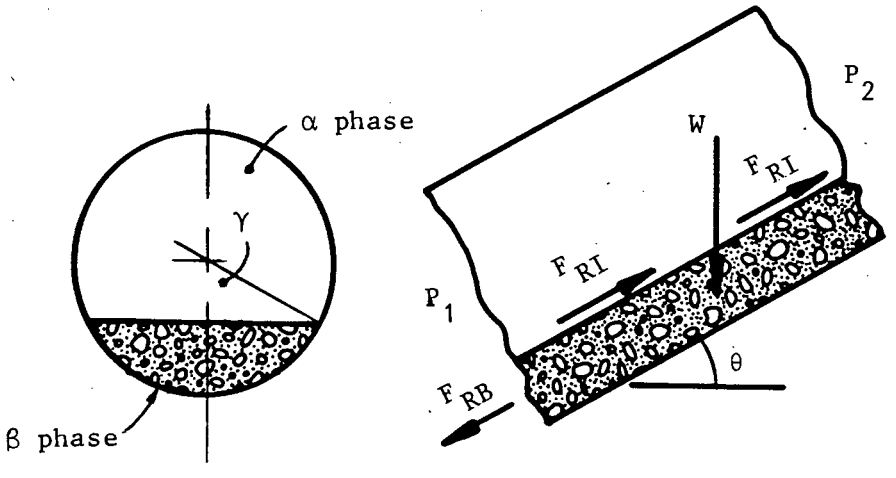

Figure 2.31 : Force balance on an incipient stationary bed

When equn. (2.120) is true then the incipient sliding bed condition exists. If the left hand side of the equation is less than the right hand side the bed will be stationary. The incipient sliding bed condition is considered to be the incipient bed fluidization condition as well.

2. Percolation flow

The pressure drop along the pipe will cause a pressure drop along the bed. This pressure drop will be manifest as percolation flow through the bed.

2.4.3 Fully Moving Bed

2.4.3.1 Two-fluid approach

In particulate fluidization the particles are uniformly dispersed in an expanded mixture. The mixture expands because the particles no longer rest on one another but are partially supported by the interstitial fluid and are free to move about. This freedom of movement will allow a shear field to be created in the fluidized material. For a fluidized bed, which is considered to occur when the stationary bed starts to move, the bed will act as a fluid of a higher density than the overhead suspended mixture. A two-fluid model is then applicable. No mass transfer between the phases is considered because any movement of one phase into another will cause an equal and

opposite migration back to occur. In the two-fluid system described the force per unit volume on the fluid or particles is a function of the velocity, concentration and concentration gradient. These are necessary and sufficient conditions for dynamic and continuity waves to occur simultaneously (Wallis (1969)). A mixture of these waves will cause the interface to develop ripples and "roll" waves which may become unstable and disperse or cause slug flow.

Figure 2.31 shows the convention used in describing the two-fluid phase.

The flow of α phase liquid over β phase affects the interface by the presence of tangential forces (interfacial shear) and normal forces which develop due to variation of pressure in the flow due to turbulence. Many investigators consider the effects of shear to be secondary. The pressure variations caused by turbulent fluctuations normal to the interface will cause the interface to develop small ripples. These small ripples may grow to form a wavy interface depending on the stability criterion for wave formation.

The small ripples will cause pressure variations in the α phase which are in phase with the slope of the ripple. This pressure variation will cause the ripple to grow into a wave structure and will eventually be accompanied by a pressure variation 180° out of phase with the wave. This second pressure variation may cause a further interfacial instability and cause exponential amplitude growth leading to slug flow or β phase dispersion. This exponential growth is attributed to a Kelvin-Helmholtz instability.

2.4.3.2 Fluid phase distinction

A slurry comprised of a well graded material in water will produce a mixture with some part of the particle size distribution contributing toward the vehicle on α phase and the rest contributing to the bed material on β phase. Three methods of distinguishing between the α and β phase are :

1. Hindered settling velocity (Figure 2.21).
2. Method ascribed to Wilson (1976) (Equn. 2.84).
3. Method ascribed to D G Thomas (1962) (Equn. 2.79).

2.4.3.3 Wall shear stress

The stratified flow of the two fluid components will produce a wall shear stress component for each phase. Different mechanisms creating this shear stress are active for each phase.

1. α phase or suspended material

   Three different approaches have been proposed for describing the α phase hydrodynamic wall shear stress (see Table 2.20) :

   1. Blausius type (Equn. 2.99)
   2. Colebrook-White equation (Equn. 2.100)
   3. Torrence (1963) equation (Equns. 2.101, 2.102)

2. β phase or sliding bed material

   The shear stress of the β phase is more complicated than that of the α phase since it is comprised of two components. One due to the mechanical friction of the bed material sliding along the pipe and the other due to hydrodynamic friction effects.

Doron *et al.* (1986) presented a method for calculating the force required to drive a moving bed

$$F_{RB} = \tau_\beta p_\beta \tag{2.123}$$

F_{RB} - force resisting bed load motion

τ_β - shear stress between bed material and pipe wall

p_β - pipe perimeter in contact with bed load.

$$F_{RB} = F_{bd} + F_{bL} \tag{2.124}$$

$$F_{bd} = \eta_s N \tag{2.125}$$

$$\Rightarrow \quad F_{bd} = \eta_s \left\{ 2(\rho_s - \rho_\alpha) g C_b R^2 \left[\left[\frac{h_b}{R} - 1 \right] \left[\gamma + \frac{\pi}{2} \right] + \cos \gamma \right] + \frac{\tau_B w_I}{\tan \phi} \right\} \tag{2.126}$$

The first term in equn. (2.126) is the normal force caused by the hydrostatic weight of the bed material. The second term is the normal force on the bed surface created by the material impacting with the bed. This contribution to the normal force was first described by Bagnold (1954).

The Bagnold stress can be described by the equation

$$\tau_B = P_B \tan \phi \tag{2.127}$$

where $\tan \phi$ = coefficient of dynamic friction

= 0.32 for $G^2 > 3700$

= fn (G^2) for $28 < G^2 < 3700$

= 0.75 for $G^2 < 28$

G^2 - dimensionless group = $\dfrac{\rho_s d P_B \sigma}{\mu^2}$

σ - average distance between particle surfaces

$$\sigma = d\left[\left[\frac{C_b}{C_v}\right]^{1/3} - 1\right]^{-1} . \qquad (2.128)$$

The hydrodynamic force on the bed material due to the presence of the pipe wall is given by

$$F_{bL} = \tau_{\beta L} p_\beta$$

$\tau_{\beta L}$ is described by a Blausius type friction factor (Doron *et al.* 1986)

$$\tau_{\beta L} = \frac{1}{2} f_\beta \rho_\beta V_\beta^2$$

where

$$f_\beta = 0.046 \, (R_{e\beta})^{-0.25}$$

$$R_{e\beta} = \frac{\rho_\beta V_\beta Rh_\beta}{\mu_\beta}$$

and $Rh_\beta = \dfrac{4A_\beta}{p_\beta + w_i}$ - the hydraulic radius of the bed material.

2.4.3.4 Wave stability

Figure 2.32 presents the data of Hanratty and Engen[15] for the interface structure of stratified flow.

---

[15] From Govier and Aziz (1981).

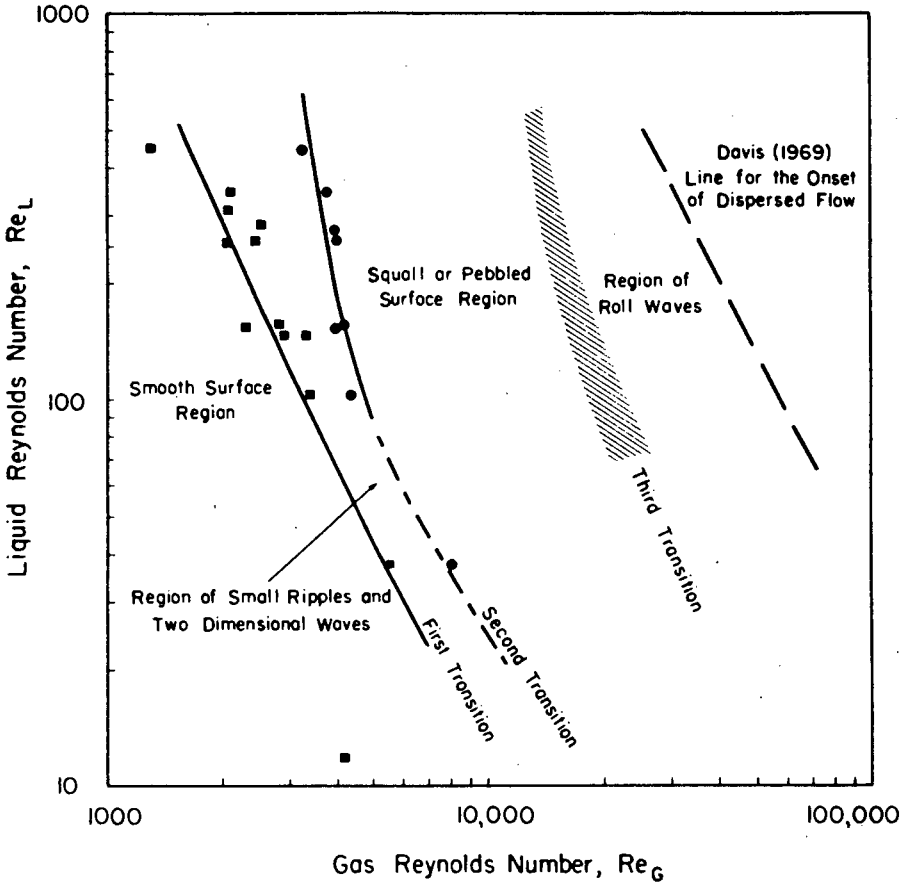

Figure 2.32 : Interface structure in stratified flow (after Hanratty and Engen in Govier and Aziz (1981, p.573)

Kordyban (1985) suggested that the tangential force at the interface between α and β phase contributed only slightly to the formation of waves and can be neglected. Normal forces on the interface caused by turbulent eddies manifest as pressure variations in the α phase. These pressure variations bear a definite phase relationship to interfacial waves and may be considered to consist of two components; one 180^{o} out of phase with the wave and one in phase with the wave slope.

1. Pressure variation 180° out of phase

Figure 2.33 shows the flow configuration for interfacial waves.

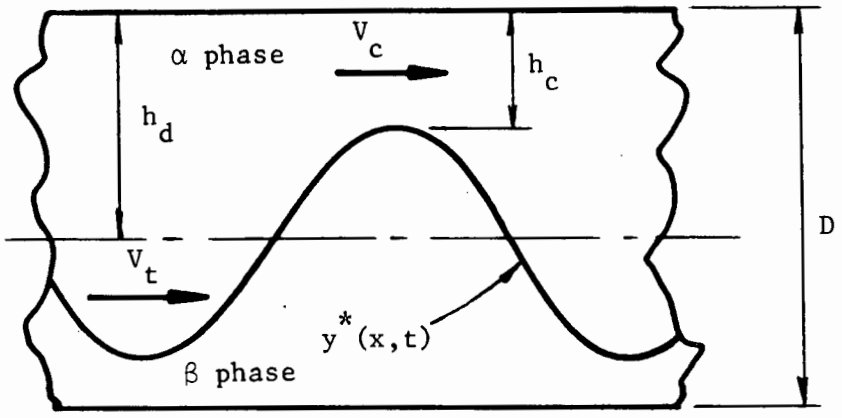

Figure 2.33 : Flow configuration for interfacial waves

From Figure 2.33 a defining equation for the wave may be written as

$$\frac{\rho_\beta}{k}\frac{\partial^2 y^*}{\partial t^2} + (\rho_\rho g + T_\rho k^2)y^* = -P_\alpha \qquad (2.129)$$

where k - wave number

y^* - wave profile

T_β - surface tension between an air-water interface in the original derivation. For slurry flow it is difficult to conceive of a surface tension as such but a generalized term must be included in the equation to allow for a discontinuity in the fluid shear stress at the interface.

The pressure in the α phase

$$P_\alpha = -\varsigma_\alpha y^*$$

ς_α = constant.

Substituting this into equn. (2.129)

$$\frac{\rho_\beta}{k}\frac{\partial^2 y^*}{\partial t^2} + (\rho_\beta g + T_\beta k^2 - \varsigma_\alpha)y^* = 0 \quad . \tag{2.130}$$

This equation has a periodic form of solution if

$$\varsigma_\alpha < \rho_\beta g + T_\beta k^2 \quad . \tag{2.131a}$$

The solution is exponential if

$$\varsigma_\alpha > \rho_\beta g + T_\beta k^2 \quad . \tag{2.131b}$$

Thus equating the two sides of equn. (2.131) represents the onset of instability which is known as a Kelvin-Helmholtz instability.

The Kelvin-Helmholtz instability may be interpreted physically as the instability of the wave which occurs when the low pressure at the crest, resulting from higher α phase velocity there, overcomes the stabilizing effect of gravity.

The celerity of the waves is given by

$$c = \left[\frac{g}{k} + \frac{T_\beta k}{\rho_\beta} - \frac{\varsigma_\alpha}{\rho_\beta k}\right] \tag{2.132}$$

At the point of instability $c = 0$ and the wave should travel at the liquid velocity.

2. Pressure variation in phase with wave slope

Kordyban (1985) presents the component of pressure in phase with the wave slope as

$$P_\alpha = \varsigma_\beta \frac{\partial y^*}{\partial x} \quad .$$

If ς_β is small

$$P_\alpha = - \frac{\varsigma_\beta}{c} \frac{\partial y^*}{\partial t} \tag{2.133}$$

where c - wave celerity

and ς_β - constant.

Substituting this value of P_α into the initial equn. (2.129)

$$\frac{\rho_\beta}{k} \frac{\partial^2 y^*}{\partial t^2} - \frac{\varsigma_\beta}{c} \frac{\partial y^*}{\partial t} + (\rho_\beta g + T_\beta k^2) y^* = 0 \quad . \tag{2.134}$$

This has a solution of the form

$$y^* = a \exp \left[\frac{\varsigma_\beta kt}{2c\rho_\beta} \right] \sin k (x - ct) \quad . \tag{2.135}$$

The wave stability is dependent on the value of ς_β as shown in Table 2.23.

The waves will retain their periodic characteristics as the amplitude changes slowly. This mechanism describes the generation and at least the initial growth of interfacial waves.

Table 2.23 : ς_β as a measure of wave stability

ς_β	Stability
Positive	Unstable, slow growth
0	Stable
Negative	Unstable, slow attenuation

2.4.3.5 **Slug flow pattern**

Govier and Aziz (1981) present the work of Hubbard and Dukler on Slug Flow. A schematic representation of the slug flow pattern is shown in Figure 2.34. The length of the β phase slug is significantly smaller than that for the α phase "bubble". This is shown distorted in Figure 2.34 to facilitate explanation.

Slug flow is a consequence of interfacial waves. The waves may, under certain conditions, grow in amplitude and eventually bridge the pipe blocking the stream of α phase flow. The β phase material in the bridge is then accelerated uniformly to the velocity of the overhead flowing α phase. A consequence of this acceleration is that more β phase material is picked up and the slug develops further. As the slug moves down the pipe β phase liquid is shed from the trailing edge of the slug and falls under the influence of gravity to the bottom of the pipe. A following slug will pick up material from the base of the pipe. Since this material is only the amount that the preceeding slug deposited the slug length will eventually

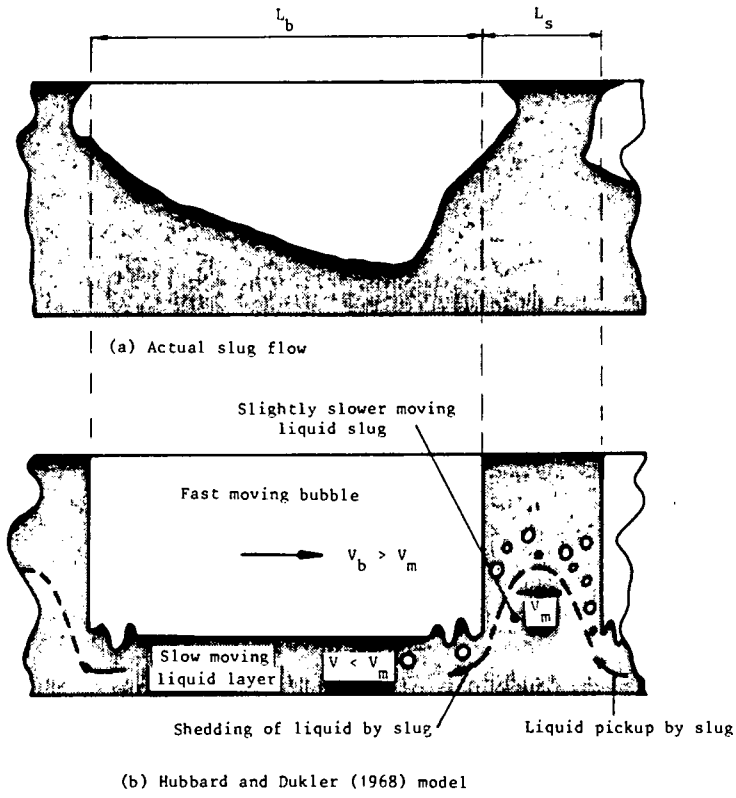

Figure 2.34 : Schematic representation of slug flow after Govier and Aziz (1981))

stabilize. A consequence of the accelerating film ahead of the slug is that it will penetrate a short distance into the slug as it is accelerated to the slug velocity. A mixing vortex is therefore developed at the front of the slug in the absence of a pressure gradient. α phase material will therefore be entrained into the slug. As the slug velocity is increased the entrainment of α phase liquid into the slug will eventually form a continuous α phase stream along the top of the slug. The slug no longer maintains a bridge across the pipe and slug "blow through" occurs. The slug

velocity begins to decrease but the β phase material dissipates by entrainment due to the high velocity of the α phase. This entrainment begins the transition to heterogeneous flow and the two-fluid analogy breaks down.

2.4.3.6 **Slug stability**

1. Slug formation

Slug flow develops as a result of Kelvin-Helmholtz instability of the interfacial waves enhanced by the presence of the top of the pipe.

Once waves have formed and grow they begin to occupy a significant portion of the pipe cross section and the pressure distribution in the α phase deviates considerably from the smooth interface or open channel flow cases. From the Bernoulli equation, if the velocity of the α and β phase differ, the pressure component 180^{o} out of phase with the wave increases rapidly. As the wave crest approaches the top of the pipe they must eventually reach a condition at which the Kelvin-Helmholtz instability may occur.

Various authors, listed by Kordyban (1985), have found that slug flow occurs somewhat before the pressure variation, due to a velocity difference between the crest and the trough, is sufficiently high to overcome the effect of gravity.

At the point of instability the celerity c = 0 and the waves should travel with the liquid velocity. The stationary wave requirement for

the Kelvin-Helmholtz instability has never been observed experimentally when applied to the whole wave. Kordyban (1985) suggested that it may occur locally over a small part of the wave.

Consider the vertical forces on a liquid element (shown in Figure 2.35).

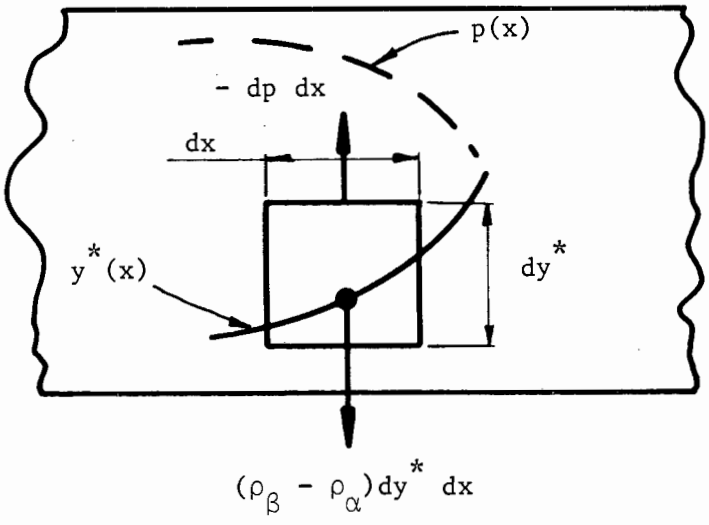

Figure 2.35 : Forces on a liquid element

At the point of instability

$$(\rho_\beta - \rho_\alpha)g dy^* dx = - dp\, dx$$

$$\Rightarrow \quad - \frac{dp}{dx} / \frac{dy^*}{dx} = (\rho_\beta - \rho_\alpha)g \quad . \qquad (2.36)$$

The interface is particularly susceptible to instability at locations where the profile $\frac{dy^*}{dx}$ is high.

The one dimensional Bernoulli equation can be used to determine the pressure of any point at the interface

$$p - p_o = \frac{K\rho_\alpha}{2}(V_\alpha^2 - V_\beta^2) \qquad (2.137)$$

K - constant allowing for the effect of velocity distribution

p_o - reference pressure .

Differentiating for p with respect to x and after some manipulation the stability criterion becomes

$$(\rho_\beta - \rho_\alpha)g = K\rho_\alpha V_\beta \frac{V_\alpha h_\alpha}{(h_\alpha - y^*)^2} \quad . \qquad (2.138)$$

Applying this equation to a wave approaching the top wall of the pipe the crest will become unstable before the main portion of the wave since both the velocity V_β and the wave profile y^* have the highest values there.

Kordyban (1985) investigated this wave crest phenomenon using a series of motion picture photographs. A wavelet was found to appear on the wave crest of the smooth face wave approaching the conduit upper surface. This was proposed as the onset of Kelvin-Helmholtz instability.

Kordyban (1985) found that the velocity of the wave trough (considered to represent the whole wave velocity) had practically the same velocity as the wavelet on the wave crest. The disturbance therefore fulfills the requirement that the celerity c = 0 when the Kelvin-Helmholtz instability occurs.

Kordyban (1985) stressed the importance of including the interfacial surface tension term in the analysis of stability at the interface. The wavelets are small and their stability will be affected strongly by this surface tension.

The value of K (in equn. (2.138)) can be estimated at the crest from data collected by Kordyban on the transition to slug flow. Kordyban found a value

$$K = 1.80 \ .$$

This value may be high because the waves considered in calculations were the highest waves just prior to the formation of slugs and it was usually the next highest wave that produced the slug.

Kordyban (1985) conducted his experiments using air-water flow. Viscosity does not enter the analytical considerations and it was assumed by Kordyban that the results should be valid for a broad band of viscosities. Interfacial surface tension tends to stabilize the liquid surface. For liquids with small interfacial surface tension (such as in the case of the proposed slurry system) the mechanism

should be valid. For greater surface tension it is possible that the instability of the whole wave will occur before formation of the crest wavelets.

2. Slug dispersion

Slug dispersion occurs where 'blow-through' becomes pronounced due to increasing entrainment of α phase into the β phase slug. This entrainment begins the transition from slug flow to heterogeneous flow. No method based on the mechanics of flow exist for predicting this transition. The equations developed for predicting the limit of heterogeneous flow can be used for this prediction.

2.4.4 Fully Suspended Flow

Heterogeneous flow has been well studied by many authors. The particles are considered to remain in suspension at all times due to the turbulent mixing of the surrounding fluid. The concentration distribution will asymmetrically increase towards the bottom of the pipe. This regime has been considered to be the operating regime of slurry transport systems conveying settling particles. This is however not necessarily the case. A complex analysis is required to find the best operating point for a pipeline system.

2.4.4.1 Concentration profile

For open channel flow the vertical diffusion equation for particles can be written

$$\epsilon_s \frac{dC}{dy} + V_t C = 0 \quad . \tag{2.139}$$

This equation has been used and is found to be satisfactory if a description of both ϵ_s and V_t can be found. Vanoni (1946), Ismail (1951), Einstein (1950) amongst others have made use of this description.

For pipeline flow the diffusion equation is represented by a second order homogeneous differential equation of the form

$$\epsilon_s \frac{d^2C}{dy^2} + V_t \frac{dC}{dy} = 0 \quad . \tag{2.140}$$

This is confirmed by Ismail (1951), Okuda (1980) and Doron *et al.* (1986). The differentials in the equation should be partial differentials but two dimensional flow is assumed and the full differential applies.

The settling velocity can be found for particles in quiescent Newtonian or non Newtonian fluids. The settling velocity found can be modified to take into account the concentration and a hindered settling value found. The diffusivity is more difficult to define.

The diffusivity for various sytems (i.e. heat flow, fluid flow, sand movement by wind) has been found to be of a similar form although not necessarily having the same value. The diffusivity for turbulent fluid flow (called the eddy viscosity) can be related to the particle diffusivity in a slurry by the equation

$$\epsilon_s = \beta\epsilon \quad . \tag{2.141}$$

It is now generally agreed that the value of β is close to unity.

For fine particles

$$\beta \simeq 1 \quad \text{or } \epsilon_s = \epsilon \ .$$

For coarse particles

$$\beta < 1 \quad \text{or } \epsilon_s < \epsilon \ .$$

If the particles are fine enough they will follow the fluid turbulence exactly and $\beta = 1$. The value of ϵ for turbulent fluid flow can now be found.

In a two dimensional flow situation which is approximated in a pipeline the shear stress between the wall and the point of maximum velocity in the pipe is given by

$$\frac{\tau}{\tau_w} = 1 - \frac{y}{y_m} \tag{2.142}$$

where y_m - distance from the wall to the point of maximum velocity.

Boussinesq suggested a relationship between the turbulent stress and the gradient of the mean velocity, analogous to the laminar flow relationship. The turbulent stress is written in the form

$$\tau = \rho \epsilon \frac{du}{dy} \ . \tag{2.143}$$

Assuming a logarithmic velocity distribution of the form

$$u = \frac{u^*}{\kappa} \ell n\ y + A$$

Differentiating gives

$$\frac{du}{dy} = \frac{u^*}{\kappa y} \quad . \tag{2.144}$$

Combining equns. (2.141) to (2.144) inclusive, for $\beta = 1$ it is found that

$$\epsilon_s = \kappa u_* (y_m - y) \frac{y}{y_m} \quad . \tag{2.145}$$

A plot of this equation is shown in Figure 2.36 for a symmetrical velocity distribution.

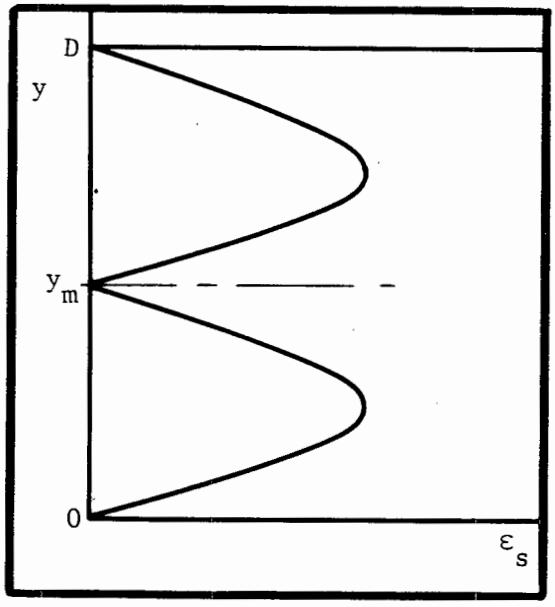

Figure 2.36 : Plot of equn. (2.145), y *versus* ϵ_s .

The value of ϵ_s is in fact not defined at $y = y_m$. This is because the Boussinesq hypothesis is only valid near the walls and does not hold at the point of maximum velocity where both $\tau = 0$ and $\frac{du}{dy} = 0$. From experiments conducted by many researchers it was found that ϵ has a finite value across the pipe centre. ϵ_s must therefore also exist at this point. Ismail (1951) presented a means for defining ϵ_s across the pipe. Figure 2.37 was presented by Ismail (1951) as describing the particle diffusivity. Near the wall the Boussinesq hypothesis holds and the diffusivity is a function of position. Across the pipe centre (the area of maximum velocity) the diffusivity was found to be constant.

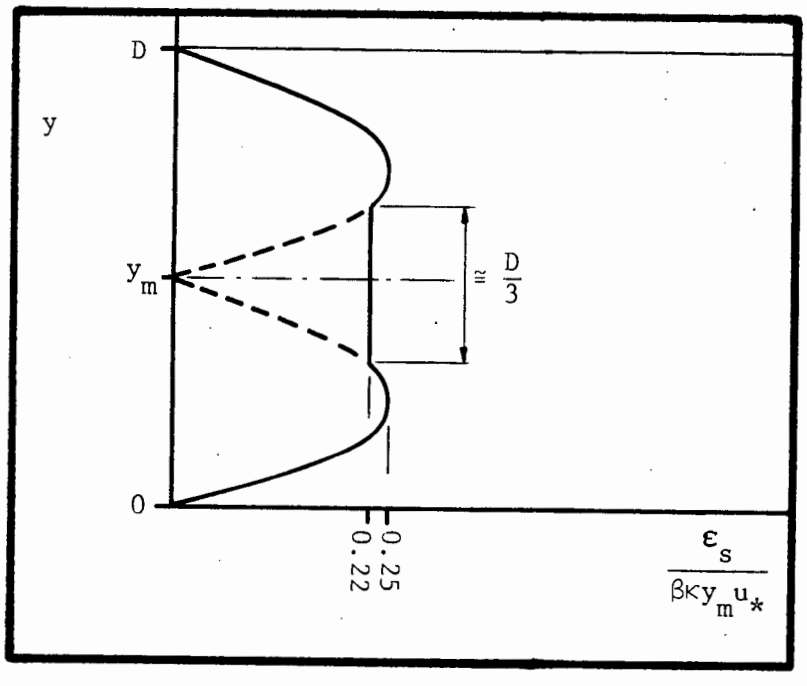

Figure 2.37 : Dimensionless form of ϵ_s plotted against position in the pipe (from Ismail (1951))

Three regions are distinguishable in Figure 2.38. Two outer regions comprising approximately one third of the pipe diameter each where ϵ_s = fn(y) and a centre third where ϵ_s is constant. The concentration profile can now be found for the pipeline from the definition of V_t and ϵ_s .

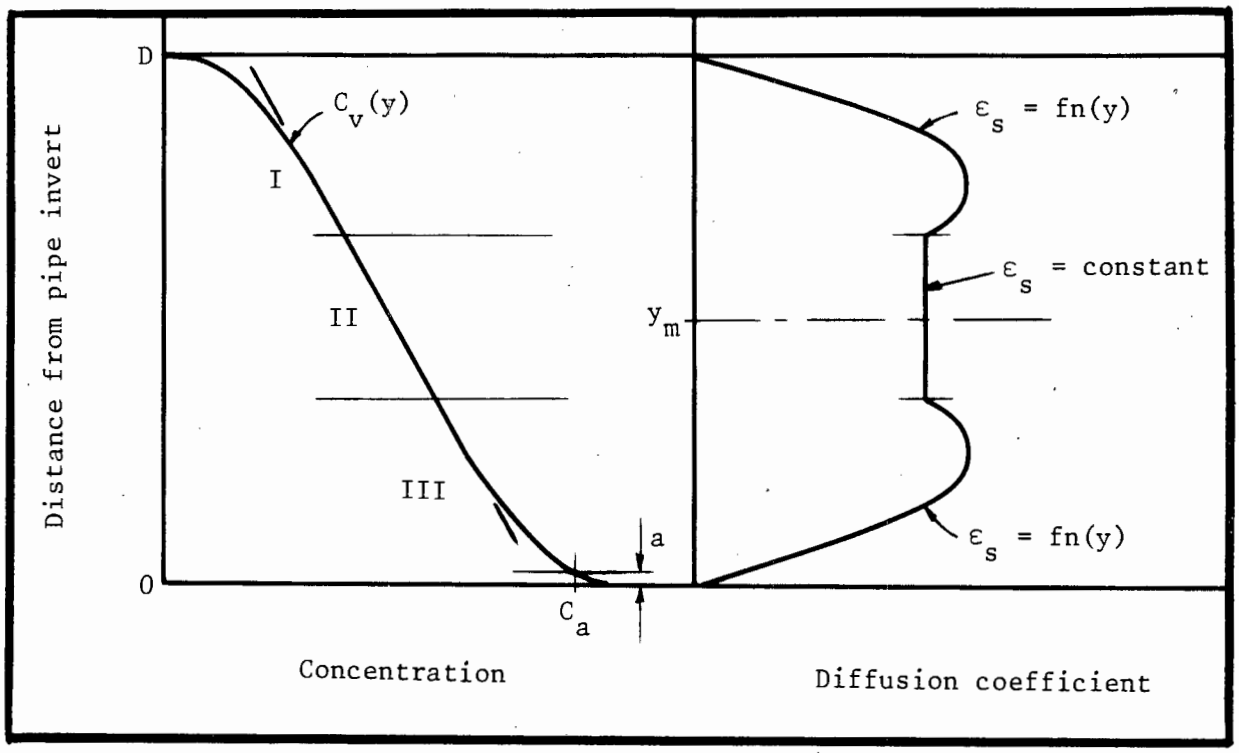

Figure 2.38 : Pipeline divided into the three regions where different definitions of the particle diffusivity ϵ_s apply

In region I and III , ϵ_s = fn(y)

In region II , ϵ_s = constant

Four different concentration profile models are presented :

1. The integration of the diffusion equn. (2.139), if ϵ_s is assumed a function of y , yields $C_v(y)$ throughout this section

$$\frac{C_v(y)}{C_{va}} = \left[\frac{y_a(y_m - y)}{y(y_m - y_a)}\right]^z \qquad (2.146)$$

where $z = \dfrac{V_t}{\beta\kappa u^*}$ (2.147)

and C_{va} is the concentration at reference level y_a .

Carlton *et al.* (1978) found this equation to give a poor fit for the transport of limestone with a particle size of 10mm to 20mm at 4 m/s in a pipe of internal diameter 154mm. Figure 2.39 shows the curve which

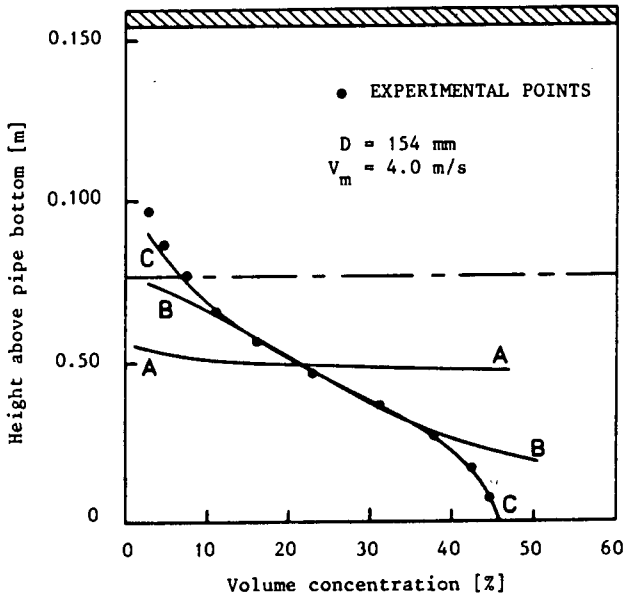

Figure 2.39 : Concentration profile for 10mm to 20mm limestone

was made to fit at y_a = 50mm and C_v = 0.21 (line A). By taking a value of the friction velocity 15 times that of the value given by turbulent theory the curve, line B, was obtained.

2. Carlton *et al.* (1978) presented a method ascribed to Shook for the prediction of concentration gradients.

It is assumed that a large particle falls a short distance (a) before coming into contact with another particle and that this fall time is insufficient for a boundary layer to form. The velocity achieved by the particle is

$$V = \sqrt{2g\left[\frac{S_s - 1}{S_s}\right]a} \quad . \tag{2.148}$$

The mean separation between particles has been found empirically to be

$$a = d\left[\left[\frac{C_b}{C_v}\right]^{1/3} - 1\right] \quad . \tag{2.149}$$

The average "fall" velocity is taken to equal half of the above velocity

$$\bar{V} = 1/2\ V \ .$$

This velocity can be substituted for the settling velocity in the diffusion equation

$$\epsilon_s \frac{dC_v(y)}{dy} + \bar{V} C_v(y) = 0 \qquad (2.139)$$

$$\Rightarrow \quad \frac{dC_v(y)}{dy} = - \frac{C_v(y)}{\epsilon_s} \left[2gd \frac{(S_s - 1)}{S_s} \left[\left[\frac{C_b}{C_v(y)} \right]^{1/3} - 1 \right] \right]^{1/2} . \qquad (2.150)$$

Integrating for $C_v(y)$ with the condition that $C = C_b$ at $y = 0$

$$C_v(y) = C_b \left[\left[\tan \frac{y \left[2gd \frac{(S_s - 1)}{S_s} \right]^{1/2}}{12\epsilon_s} \right]^2 + 1 \right]^{-3} . \qquad (2.151)$$

Curve C in Figure 2.39 for $C_v = .21$ at $y = 50mm$ was plotted using equn. (2.151) and shows good agreement with the data.

3. Newitt *et al.* (1962) presented a concentration profile of the form

$$\frac{1}{C_v(y)} \frac{dC_v(y)}{dy} = - 1.66 \frac{V_t}{u^*} \left[\frac{C_D}{d} \right]^{0.5} \qquad (2.152)$$

where y and d have units in inches

K, β are constants

κ = 0.4 - von Karman's constant.

4. Doron *et al.* (1986) assumed that concentration depends only on its vertical position and that a mean diffusion coefficient and terminal velocity can be applied (i.e. ϵ_s = const.). Integrating equn. (2.140) twice

$$C_v(y) = C_b \exp\left[-\frac{V_t'}{\epsilon_s}(y - y_b)\right] \quad . \tag{2.153}$$

Doron *et al.* (1986) expressed the mean cross flow diffusion coefficient as

$$\epsilon_s = 0.052\, u_* Rh \qquad \text{where } Rh = \frac{D}{4} \quad . \tag{2.154}$$

Integrating the equation across the pipe area yields the mean *in situ* concentration

$$C_{vt} = \frac{1}{A}\int_A C_b \exp\left[-\frac{V_t'}{\epsilon_s}(y - y_b)\right] dA \quad . \tag{2.155}$$

In terms of the bed load angle γ

$$C_{vt} = \frac{2\, C_b\, R^2}{A_\mu} \int_{-\pi/2}^{\pi/2} \exp\left[-\frac{V_t'}{\epsilon_s}(\sin\gamma + 1)\right] \cos^2\gamma\, d\gamma \quad . \qquad (2.156)$$

2.4.4:2 Average *in situ* concentration

The average *in situ* concentration can be obtained by integrating the concentration profile (equn. 2.156). Two empirical equations for *in situ* concentration are :

1. Newitt *et al*. (1962)

The slip velocity $S_v = 3.70 - 0.0397\,(1 - C_{vd})\,\frac{V_m}{V_t}$

where $S_v = |V_s - V_f|$

$$C_{vt} = \left[\frac{V_m + S_v}{2S_v}\right] - \left[\left[\frac{V_m + S_v}{2S_v}\right]^2 - \frac{V_m\, C_{vd}}{S_v}\right]^{1/2} \qquad (2.157)$$

where

S_v - slip velocity

V_s - solid phase velocity

V_f - fluid phase velocity.

2. Wani *et al.* (1983)

Wani *et al.* presented an empirical equation for *in situ* concentration

$$\frac{C_{vt} - C_{vd}}{C_{vd}} = 0.1509 \ (V_t')^N \quad . \tag{2.158}$$

The equation used by Wani *et al.* (1983) for hindererd particle settling is

$$V_t' = V_t \exp(- C_{vt}) \tag{2.159}$$

where V_t is the settling velocity based on a volume surface mean diameter

$$d_v = \frac{\sum_{i=1}^{n} m_i}{\sum_{i=1}^{n} \frac{m_i}{d_i}} \quad . \tag{2.160}$$

The exponent N is given by

$$N = 0.541 \left[\frac{V_t}{V_m}\right] - 0.223 \quad . \tag{2.161}$$

These two empirical models are compared with experimentally determined values in Chapter 6.

2.5 CONCLUSIONS

The literature review serves to outline the main constituents of the analytical model. Some of the equations presented require evaluation using experimental data but conclusions can be drawn from the material presented. Test data will be required for mixtures which constitute only vehicle, a mixture of coarse and fine material and coarse material alone. From flow observations a qualitative model can be produced for the periodic phenomena in slurry flows. Detailed observations will have to be made to evaluate the two-phase model.

A list of conclusions and recommendations can be drawn from the work presented in this chapter :

Particle characteristics

1. Particle size is described as the size of the screen on which the particle is retained.
2. The Rosin-Rammler distribution equation can be made to fit a set of random numbers. Its use is accordingly limited.
3. The graphical representation of particle size distribution is the safest and simplest method.
4. A constant relative density for a particular mixture is not accurate but is realistic and convenient.
5. The maximum particle packing concentration (C_b) for spheres is 63.9% by volume. For real particle mixtures

   $50\% \leq C_b \leq 70\%$.

The vehicle

6. Physico-chemical effects account for the difference between theoretically and experimentally determined rheological parameters. Analysis of fine material can be made by rheological considerations only without the necessity to account for acidity and zeta-potential as long as these remain essentially constant for all tests.
7. Kaolin clay can be described by a yield pseudoplastic rheology.
8. Relative viscosity (η_r) as a function of concentration has a slight slope for well graded particle mixtures but a steep slope for poorly graded mixtures.
9. The equation chosen to represent Newtonian relative viscosity is given by

$$\eta_r = \left[1 - \frac{C_v}{C_b}\right]^{-2.5} . \qquad (2.23)$$

10. Fluid consistency increases with :
    1. increase in particle size up to approximately 16μm .
    2. increase in particle density.
    3. increase in particle roughness.
    4. needle shaped particles as compared to spherical particles.
    5. increase in particle interactions - a consequence of increased concentration.
11. Yield stress is a function of flocculation and floc structure. Increasing floc strength increases yield stress.
12. Floc radius is inversely proportional to strain rate and consequently yield stress.
13. Hindered settling velocity is described by an increased concentration only. The equations for non Newtonian settling are all derived for particles settling in a quiescent vehicle and produce hindered settling velocities much smaller than would occur if the mixture undergoes turbulent flow.
14. The vehicle concentration, if a Newtonian rheology is assumed, is the total suspended solid concentration.
15. The vehicle concentration for a non Newtonian rheology comprises the concentration of all particles smaller than d_{Lmax} .

Particle suspension

16. The mechanism for particle suspension is an adverse pressure gradient which causes a *burst* and subsequent *sweep* process.

17. The threshold velocity for turbulent suspension is given by

$$V_{susp} = 0.6\ V_t \sqrt{\frac{2}{f}} \exp\ (45\ d/D) \quad . \qquad (2.83)$$

18. The interface load is modelled by the Meyer-Peter and Muller (1948) equation modified by three correction factors ascribed to Einstein (1950) for low mixture concentrations.

Sporadic flow

19. Dunes form on the stationary bed interface for Froude numbers less than one and progress downstream at a fraction of the mean flow velocity.

20. A two-fluid model is proposed to describe periodic flow phenomena. The sliding bed material is fluidized to create the heavier fluid with suspended material above the bed.

21. Interfacial shear and the normal forces due to turbulence (*bursts*) cause small ripples to form on the interface. These ripples initiate flow instabilities.

22. Pressure variations in phase with the interface ripples cause them to grow forming interface waves.

23. Pressure variations 180° out of phase with the interface waves cause exponential amplitude growth. This is known as a Kelvin-Helmholtz instability.

24. Slug flow will result from exponential wave growth if sufficient bed material exists.

25. Slugs and waves move downstream at the mean flow velocity.

26. Slug dispersion will lead to heterogeneous flow. The entrainment of the lighter phase mixture into the slug will eventually form a continuous stream resulting in slug *blow through*.

27. Periodic phenomena exist until all particles are maintained in turbulent suspension.

Velocity distribution

28. The universal logarithmic velocity profile with a von Karman constant predicted using the approach of Einstein and Chien (1954) best describes the maximum velocity.
29. The velocity defect law is used to model the velocity profile.

Concentration profile

30. The concentration profile can be modelled using a diffusion equation.
31. The particle diffusivity is a function of distance from the outer thirds of the pipe diameter to the pipe wall and a constant for the middle third.
32. The concentration distribution varies in the plane of the pipe axis but is assumed to remain constant in the transverse direction.

PART 2 : MIXED REGIME INVESTIGATION

CHAPTER 3

A NEW ANALYTICAL APPROACH

INTRODUCTION

The analytical modelling of hydraulic transport systems is a difficult if not elusive problem. The large numbers of variables involved require that some assumptions will have to be made to avoid closure[1] problems in the mathematical description. Even for the simple case of Newtonian flow the concept of the Prandl mixing length had to be included to ensure closure. Roco and Shook (1982) discussed four possible approaches to analytical prediction of slurry flow parameters :

1. Empirical correlations derived from full scale experimentation.
2. Semiempirical dimensional analysis employed to extrapolate experimental results.
3. Mechanistic models of simplified flow conditions satisfactory for the calculation of some parameters.
4. Integration of the governing equations of motion by using computer based numerical methods.

---

[1]Closure occurs when the number of independent descriptive equations equals the number of variables.

The first correlations derived for slurry flow used only the discharge parameters to describe the flow. This led to simplistic models that appeared to work only in the case of the researchers own data. The necessity to investigate *in situ* phenomena led to a significantly better understanding of the flow phenomena. It is in fact due to the work of investigators in open channel flow (Vanoni (1946), Ismail (1951)) that these internal investigations were started. The excellent work of the Saskatchewan Research Council has improved this approach with the development of concentration and velocity profile probes for internal measurements. The starting point for an analytical model is therefore to specify the *in situ* concentration and the mixture flow rate for a particular set of material and pipeline geometries. The final products of the model will be energy consumption and delivered concentration.

3.1 OBSERVATIONS OF MIXED REGIME SLURRY FLOW IN PIPES

An understanding of the complex flow phenomena in hydraulic transportation can only be gained from detailed observations. Purely analytical methods will never be able to include all the intricate dependencies that the many flow variables have on each other. The flow patterns observed determine the type of analytical approach most applicable at a particular concentration and flow rate. In Section 2.1, the visual observations of Boothroyde *et al.* (1979), Thomas (1964a) and Thomas (1964b) are presented. That discussion forms an introduction for this section.

The observations discussed in this section are applicable to a slurry with a narrow or broad particle size distribution that will not flow as a stabilized mixture or dense phase. It is inherent in this investigation that a near planar bed will form at the no flow condition. Figure 3.1 is a block diagram that shows the different flow regimes encountered with increasing mixture flow rate.

3.1.1 Stationary Bed

Two conditions for flow over a stationary bed may exist which, depending on the flow history :

1. Pipeline start up after all solids have settled i.e. after a stoppage duration of several hours.
2. Pipeline start up after only coarse material has settled i.e. after a stoppage duration of minutes.

The first condition will ensure a plane bed interface with clear fluid above while the second condition will be represented by a non Newtonian vehicle over a plane bed of coarse particles. The fine particles which contribute to the vehicle will fill the interstitial gaps between the coarse particles in both cases.

3.1.2 Incipient Particle Motion

As the pipeline flow is initiated the fluid over the bed will begin to move. Particles that protrude through the laminar sublayer will be subject to turbulent bursts and will eventually be dislodged and mobilized. Finer particles will be affected by surface drag due to laminar flow (in the

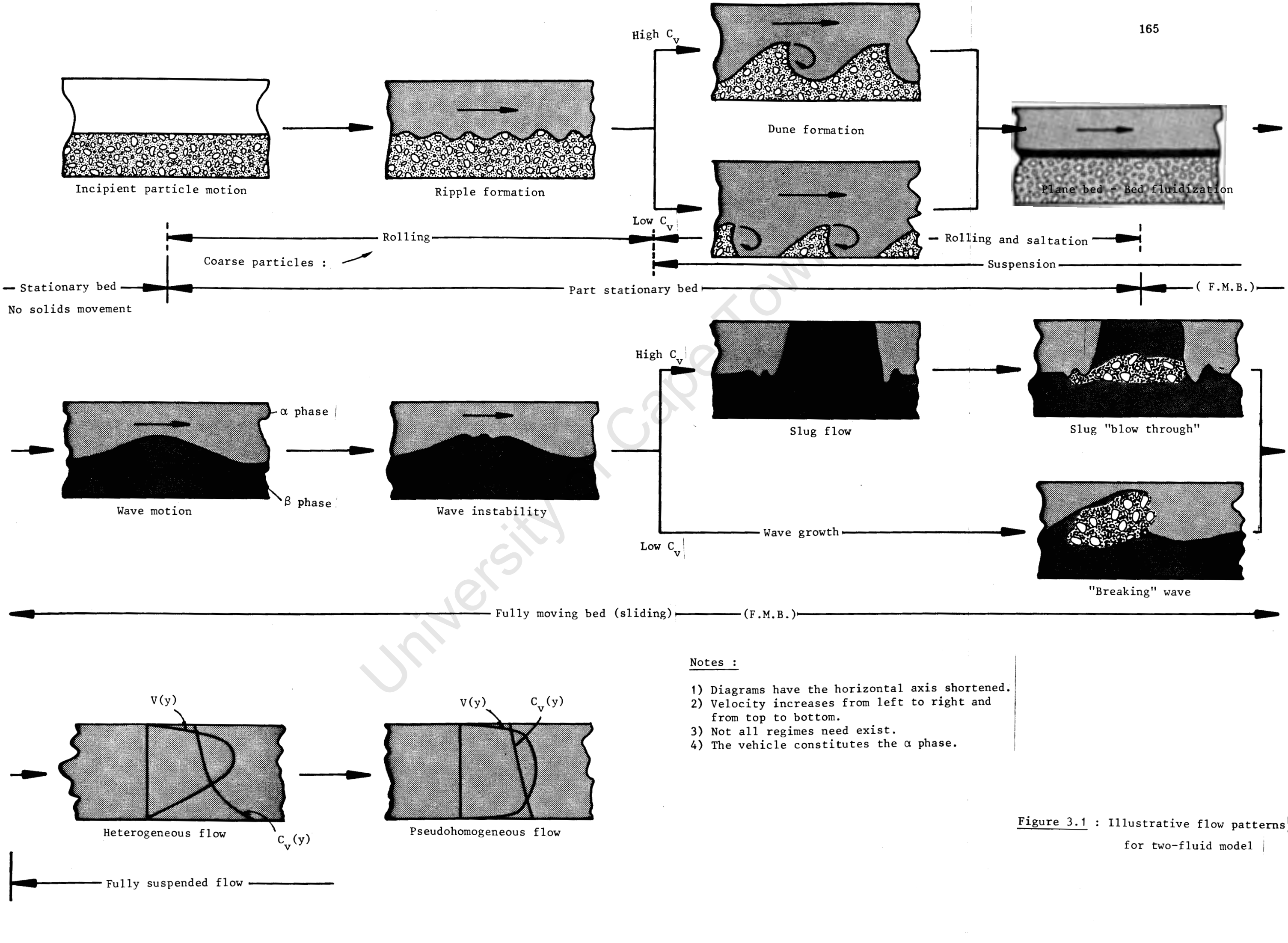

Notes :

1) Diagrams have the horizontal axis shortened.
2) Velocity increases from left to right and from top to bottom.
3) Not all regimes need exist.
4) The vehicle constitutes the α phase.

Figure 3.1 : Illustrative flow patterns for two-fluid model

sublayer) and roll over the bed. It is the particles affected by turbulence that have the most profound affect. Since the turbulent burst process is a deterministic process that occurs randomly in space and time, particles will not be suspended *en mass* but simultaneously at many discrete locations throughout the pipeline.

3.1.3 Dune Formation

An increase in flow rate will produce a bed interface which may form dunes. These dunes move downstream at significantly lower velocity than the overhead fluid. The dune dimensions are dependent on solid mass flow rate (M_s) which is directly related to *in situ* concentration. The dune heights are a fraction of the pipe diameter. The dune length is of the order of 10 pipe diameters. Coarse solid particles are transported by rolling, saltation and occasionally suspension. At low concentration (C_v < 5%) dune formation is almost non existent. At higher concentration dunes will be produced and may grow to dimensions that will produce a trough that coincides with the pipe bottom. Further growth may cause the dunes to separate (called *islands* by Thomas (1964a)). Particle motions will be visible at the bottom of the pipe if this occurs. As the flow rate is further increased the bed will become planar and the dune formation will cease.

3.1.4 Flat Bed Formation

A further increase in flow rate will result in the dunes being *washed out* and a plane bed observed. Material is transported over this bed by rolling, saltation and suspension, as before.

3.1.5 Incipient Bed Fluidization

The plane bed will fluidize with a further increase in flow rate. The bed will then begin to act as a *fluid* of higher density than the overhead vehicle. The exact mechanism of bed fluidization is unknown but can be ascribed to percolation through the bed and the transmitted bed shear causing particles to slide over each other.

3.1.6 Fully Moving Bed

The pipeline will behave as a two-phase mixture comprised of a lighter fluid, the vehicle (α phase) and a heavier fluid, the fluidized bed (β phase). No mass transfer occurs between phases since the migration of a particle from the α phase to the β phase will displace particles back to the α phase. The system is subject to all the instabilities of two-phase, two fluid flow.

3.1.6.1 Interface waves

The interface between the two phases will form a wavy surface with further increases in flow rate. These waves are spaced several pipe diameters apart but have a width of the order of one diameter. The spacing and geometry for the elements are random for an individual, but uniform in the statistical sense. This wave motion is associated with a periodic bed load motion that may be associated with instantaneous bed material stoppages. Boothroyde *et al.* (1979) described this as a 'slip-stick' bed flow condition although they did not describe wave motions in the flow.

3.1.6.2 Wave stability

The condition of wave flow may be stable but a further increase in flow rate will cause wave instability. This will be manifest by secondary small waves located on the peaks of the main formation. Kordyban (1985) interpreted this instability physically 'when the low pressure at the wave crest, resulting from the higher velocity there, overcomes the stabilizing effect of gravity' (Section 2.4.3.4 refers). This instability has two effects that are concentration dependent. At high concentration the unstable wave will grow until the bed material fills the pipe completely. A slug will then develop and slug flow will follow. At low concentrations the resulting wave growth will produce a very steep structure which will be toppled by the fast moving liquid phase α . This will result in the wave returning to stability and may again become unstable resulting in a cyclical process if the flow conditions remain constant.

3.1.6.3 Toppled or breaking waves

The condition where insufficient material exists to cause slug formation will, with an increase in flow rate, produce heterogeneous flow. The toppling waves will disperse the β phase into the vehicle and produce a system where turbulent particle suspension predominates.

3.1.6.4 Slug flow

Slug flow is characterized by a series of large distorted α phase "bubbles" which nearly fill the pipe cross section and which are separated by slugs of β phase which entirely fill the pipe cross section. The α phase may be many

nearest particle size of the actual distribution for mixtures with unknown rheology. This ensures that only whole groups of particles initially constitute the vehicle. Figure 3.4 shows the process diagrammatically.

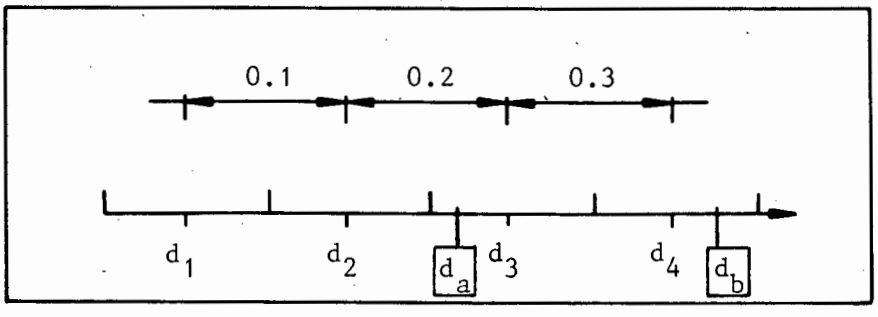

Figure 3.4 : Diagram to explain the initial vehicle ratio value
If $d_{Lmax} = d_a$, vehicle ratio, $R_f = 0.2$
If $d_{Lmax} = d_b$, vehicle ratio, $R_f = 0.4$

For mixtures with known vehicle rheology, the fractional part of the d_{Lmax} split is included. The estimate of vehicle ratio made in this way is considered conservative for two reasons :

1. The viscosity and density of the carrier fluid and not the vehicle are used to find d_{Lmax} .
2. No turbulent suspension due to pipeline flow is included.

This conservative estimate will therefore ensure that all particles ascribed to the vehicle in this way definitely form part of it.

3.2.4.1 Mixtures with vehicle ratio (R_f) equal to unity

Mixtures of this type are considered pseudohomogeneous and various simplifying assumptions can be made :

1. The concentration ratio $C_r = 0$, recalling that $C_r = A_b/A$.

2. The vehicle concentration, $C_{vdf} = C_{vd}$ and from this value the vehicle density and viscosity can be found.
3. Material will be evenly distributed throughout the pipe.
4. The *in situ* and delivered concentrations will be equal (a result of condition 3).

The effect of setting $C_r = 0$ means that the bed area will be set to zero.

3.2.4.2 **Mixtures with vehicle ratio (R_f) different from unity**

Mixtures of this type are analysed in three different stages :

1. Ascertain bed geometry.
2. Calculate forces on pipe wall and bed.
3. Obtain velocity and concentration distribution.

The energy gradient calculations and velocity distribution can be found in the same manner irrespective of the vehicle ratio value.

3.2.5 Bed Load Geometry

The bed load geometry is found by an iterative procedure. An initial quantity of bed material is assumed and a new bed load is calculated until consecutive values of bed load volume are within a prescribed fraction of each other.

The concentration ratio, C_r , is defined from equn. (2.5) as

$$C_r = \frac{C_{vtb}}{C_b} = \frac{A_b}{A} = \frac{\gamma_b}{\gamma_m} \quad . \tag{3.4}$$

The bed load half angle (γ_b) can be calculated from the bed area and the bed geometry can be found in the following way.

Figure 3.5 shows a schematic diagram of a planar bed in stratified pipeline flow.

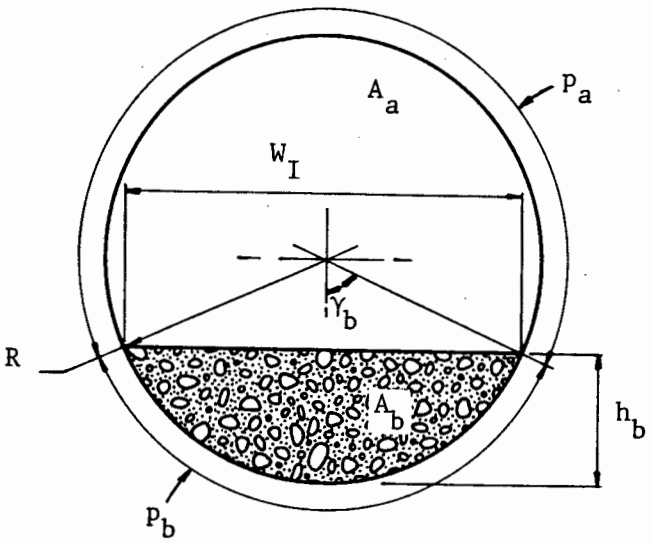

Figure 3.5 : Schematic diagram of pipe cross section

The area of the bed can be calculated from

$$C_r = \frac{A_b}{A} = \frac{1}{2\pi} (2\,\gamma_b - \sin 2\,\gamma_b) \quad . \tag{3.5}$$

This equation can be solved for γ_b by using Newton's method since γ_b is an implicit function of the bed area, A_b .

The geometrical relationship between the bed half angle γ_b and the quantities shown in Figure 3.5 are :

1. The bed height,

$$h_b = R(1 - \cos \gamma_b) \quad . \tag{3.6}$$

2. The interface width,

$$W_I = 2D \sqrt{\frac{h_b}{D} - \left[\frac{h_b}{D}\right]^2} \quad . \tag{3.7}$$

3. The pipe perimeter,

$$p = \pi D \quad . \tag{3.8}$$

4. The pipe perimeter in contact with the suspended material,

$$p_a = p(1 - \gamma_b/\pi) \quad . \tag{3.9}$$

5. The pipe perimeter in contact with the bed,

$$p_b = \frac{p\,\gamma_b}{\pi} \quad . \tag{3.10}$$

6. The area above the bed,

$$A_a = A - A_b \quad . \tag{3.11}$$

The concentration ratio is therefore the only value needed to completely describe the bed geometry.

3.2.6 Initial Bed Volume

The initial estimate of the bed volume is made by assuming that all material not part of the vehicle, as described by the initial vehicle ratio, forms part of the bed load. The bed concentration ratio C_r is therefore

$$C_r = \frac{C_{vt}(1 - R_f)}{C_b} \quad . \tag{3.12}$$

The vehicle concentration can be found from the vehicle ratio

$$C_{vtf} = C_{vt} R_f = \frac{\mathcal{V}_{ss}}{\mathcal{V}_m} \quad . \tag{3.13}$$

The bed concentration then comprises the remaining material

$$C_{vtb} = C_{vt}(1 - R_f) = \frac{\mathcal{V}_{sb}}{\mathcal{V}_m} \quad . \tag{3.14}$$

The vehicle relative density is given by

$$S_{mf} = C_{vtf}(S_s - S_w) + S_w \quad . \tag{3.15}$$

A critical aspect of hydraulic transportation is to be absolutely clear on the definitions used for various volume concentrations. Each concentration is a ratio of volumes. These are shown in eqns. (3.12) to (3.14). The overall concentration values are

$$C_{vt} = \frac{\mathcal{V}_{s\ in\ situ}}{\mathcal{V}_m} \tag{3.16}$$

$$C_{vd} = \frac{Q_s}{Q_m} = \frac{\mathcal{V}_{s\ delivered}}{\mathcal{V}_m} \quad . \tag{3.17}$$

An example of the various concentration relationships is given

for $R_f = 0.3$, $S_s = 2.65$ and $C_{vt} = 0.25$

$C_{vtf} = 0.075$

$C_{vtb} = 0.175$

$S_{mf} = 1.124$.

The vehicle viscosity (assumed Newtonian rheology) is given by

$$\mu_{mf} = \mu_w \left[1 - \frac{C_{vtf}}{C_b}\right]^{-2.5} \quad . \qquad (2.23)$$

Equn. (2.23) should only be used if experimentally determined values are not available for the slurry under investigation.

3.2.7 Calculating the Bed Load Volume

The mixture flow rate above a stationary bed (i.e. in area A_a) is greater than the mean mixture velocity and can be calculated from continuity by

$$V_a = \frac{Q_m}{A_a} \quad . \qquad (3.18)$$

This flow causes a shear stress (τ_I) at the stationary bed interface. The associated turbulence causes bed particles to be entrained into the flow reducing the bed volume. An iterative procedure is needed to find the final bed volume. Two theories are considered to model the entrainment of particles. A combination of the Meyer-Peter and Muller (1948) equation and the Einstein (1950) approach to interface load[1] transport is considered for concentrations at which interparticle interactions can be neglected. At concentrations above 10% by volume the model ascribed to Wilson and Watt (1974) is used.

---

[1]Interface load is the material load that moves at the bed interface and is supported by interparticle contact with the bed. Particles move by rolling and sliding. This term is called "bed load" in open channel flow literature but has been changed to avoid confusion with the "stationary bed load".

3.2.7.1 Low Concentration Determination of Bed Load Volume

1. Determination of interface load

Calculation of the interface load requires a knowledge of the shear velocity at the interface. From the flow velocity in the area above the bed (V_a) the interface friction factor and the shear velocity can be calculated. The fully rough wall equation of Colebrook-White is applicable

$$\frac{1}{\sqrt{f_I}} = -4 \log \left[\frac{k_s}{4\ Rh_a} \right] \tag{3.19}$$

where k_s - sand roughness

$= d_{65}$ after Einstein (1950)

and

Rh_a - hydraulic radius above bed

$$= \frac{A_a}{p_a + W_I} \quad . \tag{3.20}$$

The bed shear velocity

$$u_{*b} = \sqrt{\frac{f_I}{2}}\, V_a \quad . \tag{3.21}$$

The bed shear velocity can be used to find the laminar sublayer thickness. This is required so that an apparent roughness diameter and a characteristic grain size can be found.

The laminar sublayer thickness is

$$\delta = \frac{11.6\ \nu_{mf}}{u_{*I}} \quad . \tag{3.22}$$

The apparent roughness diameter is

$$\Delta = \frac{k_s'}{h} \tag{3.23}$$

where h is a correction factor (Einstein (1950)) derived from the experiments of Nikuradse. The function of h is shown in Figure 2.28.

From Figure 2.28 an empirical equation for h was found.

For

$$\begin{aligned} &\frac{k_s}{\delta} < 0.2 \ ; \ h = 0.1 \\ 0.2 < &\frac{k_s}{\delta} < 10 \ ; \ h = 1.59 - 0.12 \log \frac{k_s}{\delta} - 2.27 \left[\log \frac{k_s}{\delta}\right]^2 \\ 10 < &\frac{k_s}{\delta} \ ; \ h = 1.0 \quad . \end{aligned} \tag{3.24}$$

The characteristic grain size (X) is

$$\begin{aligned} &X = 0.77\ \Delta \quad \text{for} \quad \frac{\Delta}{\delta} \geq 1.8 \\ \text{or} \quad &X = 1.398\ \delta \ \text{for} \ \frac{\Delta}{\delta} < 1.8 \quad . \end{aligned} \tag{3.25}$$

The apparent roughness diameter and the characteristic grain size modify the velocity distribution above the bed. This modification accounts for the presence of solids above the bed.

The shear intensity on each individual particle size group can now be found. For a single particle being suspended in clear fluid the shear intensity is given by

$$\Psi_i = (S_s - S_{mf}) \frac{d_i g}{u_{*I}^2} \quad . \tag{3.26}$$

For the bed particles

$$\Psi_{*i} = \xi \, Y \left[\frac{B}{B_x}\right]^2 \Psi_i \tag{2.115}$$

where $\frac{B}{B_x} = \frac{\log 10.6}{\log \left[\frac{10.6\ X}{\Delta}\right]}$, the velocity distribution correction factor

(3.27)

ξ - hiding factor described in Figure 2.27

Y - pressure correction factor described in Figure 2.29.

An empirical equation was derived for both ξ and Y .

The hiding factor, ξ , is given by Einstein (1950) as a function of $\frac{d_i}{X}$ (see Figure 2.27).

The empirical fit used in the computer program is given by

For

$$\frac{d_i}{X} < 0.01$$

$$\xi = 10^{2.3}$$

For

$$0.01 < \frac{d_i}{X} < 2$$

$$\log \xi = 0.06 - 0.96 \log \left[\frac{d_i}{X}\right] + 2.31 \log^2 \left[\frac{d_i}{X}\right]$$

$$+ 0.40 \log^3 \left[\frac{d_i}{X}\right] - 1.85 \log^4 \left[\frac{d_i}{X}\right] - 1.35 \log^5 \left[\frac{d_i}{X}\right]$$

$$- 0.27 \log^6 \left[\frac{d_i}{X}\right]$$

For

$$\frac{d_i}{X} > 2$$

$$\xi = 1.0 \quad . \tag{3.28}$$

The pressure correction, Y , is given by Einstein (1950) as a function of $\frac{d_{65}}{\delta}$ (see Figure 2.29), where k_s is assumed to be equal to d_{65} .

The empirical fit used in the computer program is given by

$$\text{For } \frac{k_s}{\delta} < 0.2$$

$$Y = 0.1$$

$$\text{For } 0.2 < \frac{k_s}{\delta} < 4$$

$$\log Y = -0.11 + 2.3 \log\left[\frac{k_s}{\delta}\right] - 2.02 \log^2\left[\frac{k_s}{\delta}\right]$$

$$+ 0.26 \log^3\left[\frac{k_s}{\delta}\right] + 2.10 \log^4\left[\frac{k_s}{\delta}\right] - 0.41 \log^5\left[\frac{k_s}{\delta}\right]$$

$$\text{For } \frac{k_s}{\delta} > 4$$

$$Y = 0.504 \; . \qquad (3.29)$$

From the work of Meyer-Peter and Muller (1948)

$$\Phi_{*i} = 8\left[\frac{1}{\Psi_{*i}} - 0.047\right]^{1.5} \; . \qquad (3.30)$$

The interface load rate in weight per unit time and unit width can be calculated from Φ_{*i}

$$q_{sbi} = m_i \, \Phi_{*i} \, \rho_s (g d_i)^{3/2} \sqrt{S_s - S_{mf}} \quad \left[\frac{N}{ms}\right] \; . \qquad (3.31)$$

The interface load volume per metre length is given by

$$\forall_{sbi} = \frac{q_{sbi} \, W_I}{11.6 \, g u_{*I} \, \rho_s} \quad \left[\frac{m^3}{m}\right] \; . \qquad (3.32)$$

2. Determination of suspended load

The concentration distribution equation used in the model should be divided into three regions each occupying approximately one third of the height between the bed interface and the pipe soffit (see Figure 2.38). Figure 3.6 shows the concentration distribution geometry. The concentration distribution assuming ϵ_s is a function of y across the whole pipe is also shown in Figure 3.6. The small difference in the two distributions does not warrent the added complexity of the three region approach and a single function was used.

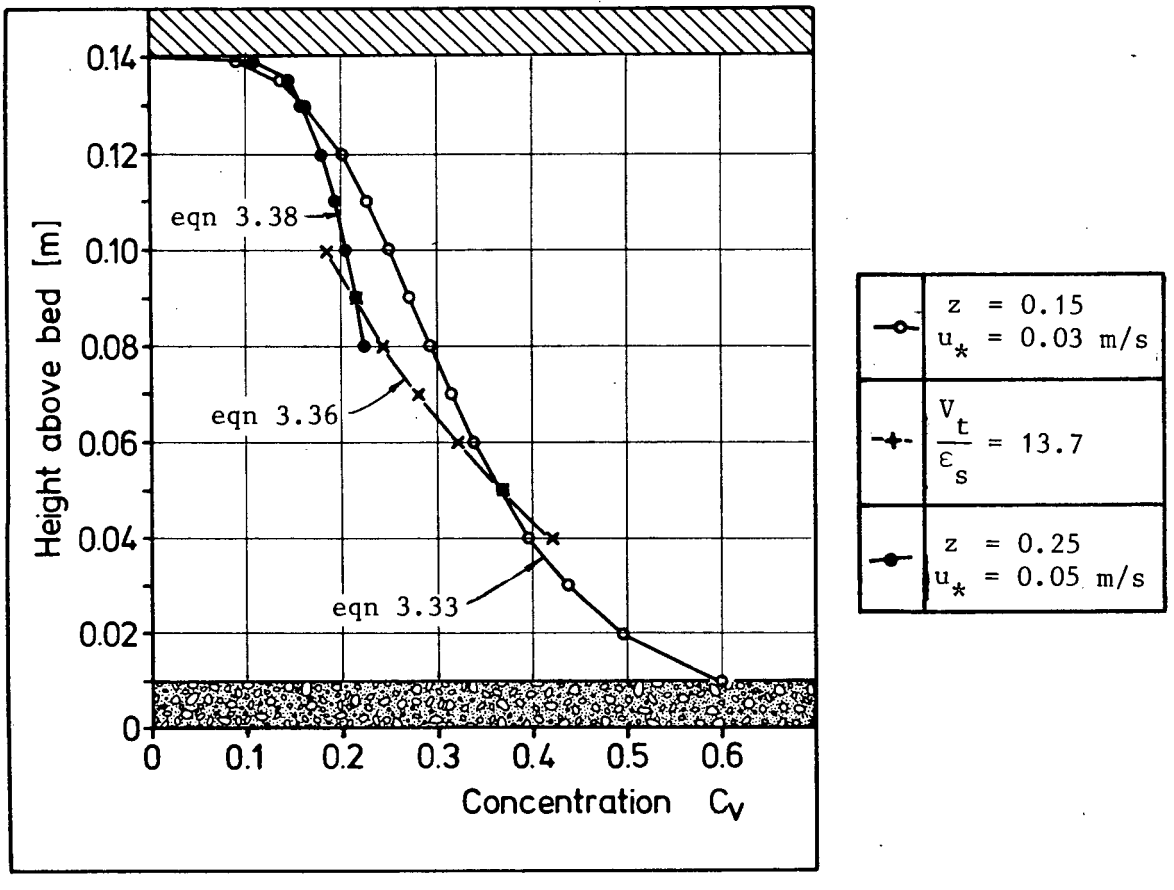

Figure 3.6 : Concentration distribution geometry

In Figure 3.6 the three equations used are given by the following.

In region 1, $y_a < y < 1/3\ h_a$

$$C_v(y) = C_a \left[\frac{D/y - 1}{D/y_a - 1}\right]^{z_1} \tag{3.33}$$

where

$$z_1 = \frac{V_{ti}}{\kappa\ u_{*I}} \quad , \tag{3.34a}$$

u_{*I} is the shear velocity at the bed interface

and

$$y_a = 2\ d_i + h_b \quad . \tag{3.35}$$

This equation is also shown extended throughout the region in Figure 3.6.

In region 2, $\frac{1}{3} h_a < y < \frac{2}{3} h_a$

$$C_v(y) = C_{1/3\ h_a} \exp\left[\frac{V_{ti}'}{\epsilon_s}\left[y - D + \frac{2}{3} h_a\right]\right] \tag{3.36}$$

V_{ti}' - hindered settling velocity of the particle size group i

where ϵ_s - diffusion coefficient

$$= 0.052\ u_{*I}\ D \text{ after Taylor (1954)} \tag{3.37}$$

and $C_{1/3\ h_a}$ can be found from equn. (3.33) at $y = 1/3\ h_a$.

In region 3, $\frac{2}{3} h_a < y < D$

$$C_v(y) = C_{2/3\ h_a} \left[\frac{D/y - 1}{D/(D - 1/3\ h_a) - 1} \right]^{z_2} \qquad (3.38)$$

$$\text{where } z_2 = = \frac{V_{ti}}{\kappa\ u_{*w}} \qquad (3.34b)$$

and $C_{2/3\ h_a}$ can be found from equn. (3.36) at $y = \frac{2}{3} h_a$

u_{*w} - shear velocity at the pipe soffit.

The reference concentration (C_a equn. (3.33)) can be found from the interface load volume since it is from within this layer that the material to be suspended originates.

The reference concentration is given by Einstein (1950) as

$$C_a = \frac{\forall_{sbi}}{2\ d_i\ W_I} \quad . \qquad (3.39)$$

The quantity of material suspended can now be calculated from the integration of the concentration profile over the flow area A_a . The concentration distribution is assumed to be planar with curvature in the vertical plane of the pipe only. The suspended solid volume for each particle size group is

$$\forall_{ssi} = \int_A C_v(y)\ dA_a \qquad \left[\frac{m^3}{m}\right] \quad . . \qquad (3.40)$$

Figure 3.7 shows the region of integration.

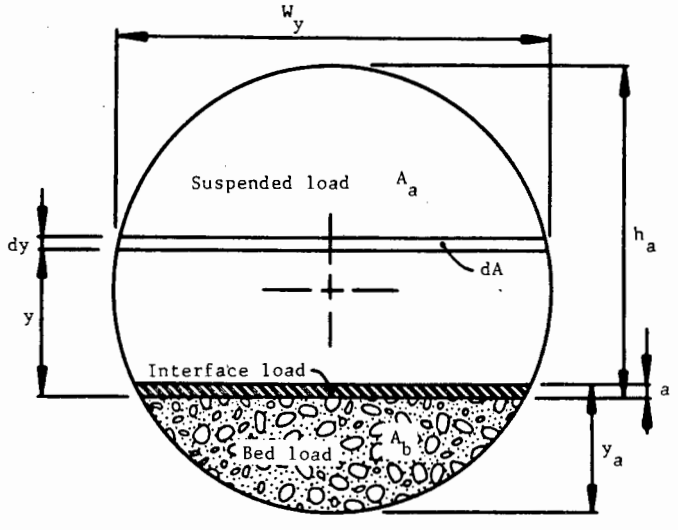

Figure 3.7 : Region of integration for suspended solid volume

$C_v(y)$ is found from the three equations presented (3.33, 3.36 and 3.38).

In equn. (3.40) the integrand can be changed whence

$$dA_a = W_y \, dy \quad . \tag{3.41}$$

The width of the area element is a function of y only where

$$W_y = 2D \sqrt{\frac{y}{D} - \left[\frac{y}{D}\right]^2} \quad . \tag{3.42}$$

$$\text{So} \quad \mathcal{V}_{ssi} = \int_{y_a}^{D} C_v(y)\ 2D \sqrt{\frac{y}{D} - \left[\frac{y}{D}\right]^2}\ dy \qquad \left[\frac{m^3}{m}\right] \quad . \qquad (3.43)$$

This integral is solved numerically using Simpsons 1/3 rule over 30 intervals.

3. Calculating the resultant bed volume

For each size group only a finite quantity of material is available. This must reside in the bed or be part of the interface or suspended load, or a combination of the three. The total volume available for each size group per unit length is given by

$$\mathcal{V}_{si} = m_i\ C_{vt}\ A \qquad [m^3/m] \quad . \qquad (3.44)$$

From the reference concentration (C_{ai}) the volume of each particle size group suspended ($\mathcal{V}_{ssi}$) can be calculated and from the interface load equations the interface load volume ($\mathcal{V}_{sbi}$) can be found. If the sum of the suspended and interface load volume is less than the total solid volume then the remaining solid must reside in the bed.

$$\text{So} \quad \mathcal{V}_{s\ bed\ i} = \mathcal{V}_{si} - (\mathcal{V}_{sbi} + \mathcal{V}_{ssi}) \quad . \qquad (3.45)$$

The limiting condition for material removed from the bed is if

$$\mathcal{V}_{si} = \mathcal{V}_{sbi} + \mathcal{V}_{ssi} \qquad (3.46)$$

and $\mathcal{V}_{s\ bed\ i} = 0$.

A unique relationship exists between γ_{sbi} and γ_{ssi} such that

$$\gamma_{ssi} = fn(C_{ai})$$

and $$C_{ai} = fn\ (\gamma_{sbi})$$

so that $$\gamma_{ssi} = fn\ (\gamma_{sbi}) \quad . \tag{3.47}$$

Use is made of an iterative method for solving the two equns. (3.46) and (3.47) simultaneously. A guess is made of the value of the interface load, the reference concentration is calculated and the suspended solid volume found. The initial guess for γ_{sbi} is zero since all material is assumed to reside in the bed. The sum of the two volumes γ_{ssi} and γ_{sbi} are then compared to the volume of solid available (γ_{si}) until the guessed and calculated values of γ_{sbi} converge.

The total volume of bed load per metre is given by

$$\gamma_{s\ bed} = \sum_{i=n_v+1}^{n} \gamma_{s\ bed\ i} \qquad [m^3/m] \quad . \tag{3.48}$$

The total interface load can be calculated empirically from

$$\gamma_{sb} = \sum_{i=n_v+1}^{n} 11.6\ u_{*I}\ W_I\ 2\ d_i \qquad [m^3/m] \tag{3.49}$$

where n_v - number of particle size groups that constitute the vehicle

and n - total number of particle size groups.

The value of the total bed volume calculated is compared to the volume initially assumed. For any particular flow rate a unique bed volume will exist. This bed volume will be found by successive iterations in which the bed geometry is calculated from the concentration ratio C_r . When successive values of the bed volume are within 1% of each other the iterative procedure is stopped and the current bed volume is taken to be the actual bed volume for the prevailing conditions.

As the bed volume varies so too does the concentration of suspended material. For each iteration new values of vehicle concentration and viscosity must be found. These new values will have an effect on subsequent iterations.

From the new bed volume $\mathcal{V}_{s\ bed}$ the bed concentration can be found

$$C_{vtb} = \frac{\mathcal{V}_{s\ bed}}{A} \quad . \tag{3.50}$$

The vehicle concentration, relative density and viscosity can be found in the conventional way from

$$C_{vtf} = C_{vt} - C_{vtbm} \tag{3.51}$$

$$S_{mf} = C_{vtf}(S_s - S_w) + S_w \tag{3.15}$$

$$\mu_{mf} = \mu_w \left[1 - \frac{C_{vtf}}{C_b}\right]^{-2.5} \quad . \tag{2.23}$$

The bed geometry must be recalculated for the new bed volume. As previously the bed geometry is a function of the ratio C_r only. The new value for this ratio is obtained from

$$C_r = \frac{\gamma_{bed}}{A} \tag{3.4}$$

where

$$\gamma_{bed} = \frac{\gamma_{s\ bed}}{C_b} \quad . \tag{3.52}$$

3.2.7.2 **High concentration determination of bed load volume**

1. **Determination of suspended load**

To account for particle-particle interactions at volumetric concentration above about 10% a semiempirical approach is needed to find the split between bed load and suspended material. The method ascribed to Wilson and Watt (1974) is used. The equations were presented in Chapter 2 as

$$\frac{V_{susp}}{V_t}\sqrt{\frac{f}{2}} = k_1 \exp\,[k_2 d/D] \quad , \tag{2.83}$$

where $k_1 = 0.6$ and $k_2 = 45$

and $$1 - \frac{C_{vt}}{C_v} = \frac{\sum_{i=1}^{n} \left[\frac{V_{susp\ i}}{V_m}\right]^{k_1}}{n} \quad \text{for} \quad \frac{V_{susp\ i}}{V_m} > 1 \quad , \quad \frac{V_{susp\ i}}{V_m} = 1 \tag{2.85}$$

where $k_1 \simeq 2$.

An initial bed load volume is found as described before and the appropriate vehicle viscosity and relative density calculated. The mean velocity is calculated from Q_m and a friction factor based on the vehicle properties is found

$$Re = \frac{\rho_{mf} \, V_m \, D}{\mu_{mf}}$$

$$\sqrt{\frac{1}{f_{mf}}} = -4 \log \left[\frac{k_w}{3.7} + \frac{1.266}{Re\sqrt{f_{mf}}} \right] \quad . \tag{3.53}$$

For each particle size group not included in the vehicle a suspension velocity (V_{susp}) is found

$$V_{susp\ i} = 0.6 \, S_F \, V_{ti} \sqrt{\frac{2}{f_{mf}}} \exp \left[\frac{45 \, d_i}{D} \right] \quad . \tag{3.54}$$

The value is substituted into an equation of the form of equn. (2.85)

$$1 - \frac{C_{vtf}}{C_v} = \frac{\sum_{i=1}^{n} \left[\frac{V_{susp\ i}}{V_a} \right]^2}{n - (n_v + 1)} \quad . \tag{3.55}$$

For those particles d_i that produce a ratio $\frac{V_{susp\ i}}{V_a} > 1$, all particles d_i are suspended so the value of $\frac{V_{susp\ i}}{V_a}$ is set equal to the limiting value of unity.

From the new value of C_{vtf} calculated by equn. (3.55) the value of C_{vtb} can be found along with new values for the viscosity and relative density of the suspended material.

The volume of suspended material per metre length of pipeline is given by

$$\mathcal{V}_{ss} = C_{vtf} * A \qquad [m^3/m] \tag{3.56}$$

where A is the total area.

The concentration distribution is found using equns. (3.33) through (3.38). A characteristic particle diameter is required since the suspended load concentration C_{vtf} in this case is for all suspended particles.

The reference concentration is found by an iterative procedure from the simultaneous solution of the two equations

$$\mathcal{V}_{ss} = fn(C_a) \tag{3.57}$$

and

$$\mathcal{V}_{ss} = C_{vtf} * A \quad . \tag{3.56}$$

This procedure is used irrespective of bed dimension.

2. **Calculating the resultant bed volume**

The total solid volume per metre length of pipeline is given by

$$\mathcal{V}_s = C_{vt} A \qquad [m^3/m] \quad . \tag{3.57}$$

The bed solid volume can be calculated from the difference in the total solid volume and the suspended solid volume

$$\mathscr{V}_{s\ bed} = \mathscr{V}_{s} - \mathscr{V}_{ss} \quad .$$

The value of successive calculations of $\mathscr{V}_{s\ bed}$ are compared until they are within 1% of the pipe area. The vehicle parameters are adjusted for each iteration and the bed geometry is modified by the concentration ratio (C_r) where

$$C_r = \frac{\mathscr{V}_{bed}}{A} \qquad (3.4)$$

and

$$\mathscr{V}_{bed} = \frac{\mathscr{V}_{s\ bed}}{C_b} \quad . \qquad (3.52)$$

3.2.8 Force Balance for Two Component Mixture with Prescribed Bed Geometry

The energy gradient for the calculated bed geometry can be found from a force balance on the mixture flowing over the bed. The bed motion either stationary, sliding or suspended can be found from a force balance on the bed. Figure 3.8 shows the bed geometry and the force balance that exists on a length (L) of the pipeline.

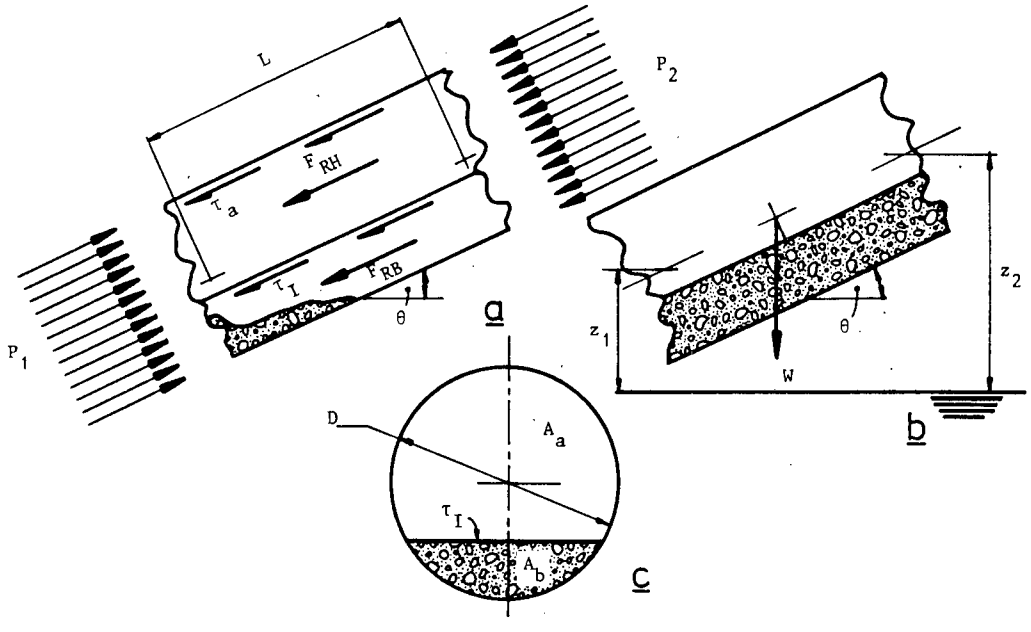

Figure 3.8 : Force balance on two component two-phase flow

3.2.8.1 Wall shear stress

The wall friction factor is calculated by the partially rough wall Colebrook White equation (3.53). The wall shear stress is then found from the equation

$$\tau_a = \frac{1}{2} f_{mf} \rho_{mf} V_a^2 \qquad (3.58)$$

and the wall shear velocity from

$$u_{*b} = \sqrt{\frac{\tau_a}{\rho_{mf}}} \quad . \qquad (3.59)$$

3.2.8.2 Interface shear stress

The interface friction factor is calculated from equn. (2.118) ascribed to Richardson and Simons (1967). This equation accounts for the interface layer in which a higher shear stress will exist than for a solid boundary. The interface shear is calculated from

$$\tau_I = \frac{1}{2} f_I \rho_{mf} V_a^2 \qquad (3.60)$$

and the interface shear velocity from

$$u_{*I} = \sqrt{\frac{\tau_I}{\rho_{mf}}} \quad . \qquad (3.61)$$

Doron *et al.* (1986) suggest that τ_b might be larger than predicted using f_I multiplied by a factor of 2 (Section 2.4.2.3).

3.2.8.3 Forces associated with the pipeline transport of solids

1. The resisting force for pseudohomogeneous flow above the bed is given by

$$F_{RA} = \tau_a p_a \quad . \qquad (3.62)$$

2. The resisting force for pseudohomogeneous flow on the interface is given by

$$F_{RI} = \tau_I W_I \quad . \qquad (3.63)$$

3. The total mixture weight component acting down the slope of an inclined pipeline is shown in Figure 3.8(b). The weight of mixture per unit length is given by

$$W_m = \rho_{mf} g A \quad . \qquad (3.64)$$

The slope of length, L , of pipeline between elevation z_1 and z_2 is given by

$$\theta = \tan^{-1}\left[\frac{z_2 - z_1}{L}\right] \quad . \tag{3.65}$$

The total weight component acting along the pipeline is given by

$$W_{ms} = W_m \sin\theta \quad . \tag{3.66}$$

This is the weight component if all the pipeline material is moving. For the stationary bed condition different components act on the flowing and stationary bed material.

4. The bed resisting force is calculated from the submerged weight of the bed

$$F_{RB} = \mu_s\, g(\rho_s - \rho_m)\, C_B\, A_b \cos\theta \quad . \tag{3.67}$$

It is important that the submerged weight of the bed is calculated from the difference in density between the solid particles and the total mixture relative density. The resisting force on the stationary bed is indeterminate until the incipient sliding condition and once the bed is moving.

The equation presented by Wilson *et al.* (1972) was carefully considered. Although it has been widely used it does not produce good results for mixed regime slurries. The measurement of the coefficient of sliding friction (μ_s equal to the submerged angle of repose of the coarse solids) and a change to the submerged weight term ($S_s - S_w$ changed to $S_s - S_m$) in the present investigation justifies the use of equn. (3.67).

5. The driving force on the bed results from a pressure difference along the pipe, ΔP , and the shear stress at the bed interface

$$F_{DB} = \frac{\Delta P}{L} A_b + \tau_I W_I \quad . \tag{3.68}$$

3.2.8.4 Forces acting under different flow conditions

1. Stationary bed flow .

The driving force for stationary bed flow equals the sum of the resisting forces. The mixture flowing above the bed is assumed to be pseudohomogeneous. The driving force is given by

$$F'_{D_{ST}} = F_{RA} + F_{RI} + A_a \rho_{mf} g \sin \theta \quad . \tag{3.69}$$

2. Transition from stationary to sliding bed flow

At the point of incipient sliding the bed resisting force is given by

$$F'_{RB} = F_{RB} + A_b \rho_{mb} g \tan \theta \tag{3.70}$$

where $\rho_{mb} = C_{vtb}(\rho_s - \rho_w) + \rho_w$. (3.71)

The total driving force on the bed can be found from equn. (3.68) where

$$\frac{\Delta P}{L} = (F_{RA} + F_{RI} + W_{ms})/A \quad . \tag{3.72}$$

Sliding bed flow will occur when

$$F_{DB} \geq F'_{RB} \quad . \tag{3.73}$$

3. Sliding bed flow

The driving force for sliding bed flow is given by

$$F_{D_{SL}} = F_{RA} + F_{RB} + F_{HB} + W_{ms}$$

where F_{HB} - hydrodynamic friction force between the sliding bed and the pipe wall

$$F_{HB} = \tau_b / p_b \qquad (3.74)$$

$$\tau_b = \frac{1}{2} f_b \rho_{mb} V_m^2 \qquad (3.75)$$

and f_b can be found using the Colebrook-White equation.

The mean velocity V_m is used in the calculation of friction factors for F_{RA} and F_{HB} .

4. Fully suspended flow

The driving force for fully suspended flow is given by

$$F_{D_{FS}} = \tau_a \pi D + W_{ms} \quad . \qquad (3.76)$$

5. Transition from sliding bed to fully suspended flow

The transition from sliding to fully suspended flow is dependent on the relative magnitudes of the driving forces associated with the two conditions. The transition is assumed to occur when

$$F_{D_{FS}} \geq F_{D_{SL}} \quad . \qquad (3.77)$$

This transition criterion is justified because the highest driving force active at any time will be the force required to ensure flow at the prescribed flow rate and concentration.

3.2.9 Delivered Concentration Calculation

In order to calculate the delivered concentration for any given flow condition both the concentration and velocity profiles must be modelled.

The delivered volumetric flow of solids can then be found from an integration of the product of the two profiles over the flow area

$$Q_{ss} = \int_A u\, C_v \; dA \tag{3.78}$$

$$Q_m = \int_A u \; dA \quad . \tag{3.79}$$

The delivered concentration can be found from the ratio of the sum of suspended and interface load solids to the sum of suspended and interface load mixture.

For the low concentration approach

$$C_{vd} = \frac{Q_{sb} + Q_{ss}}{Q_{mb} + Q_m} \tag{3.80}$$

where $Q_{sb} = 11.6\ v_{sb}\ u_{*b}$ and the value of Q_{mb} is given by the empirical equation

$$Q_{mb} = 11.6\ u_{*I}\ W_I \sum_{i=n_v+1}^{n} 2\, d_i \quad . \tag{3.81}$$

For the high concentration approach Q_{sb} and Q_{mb} equal zero in equn. (3.80).

3.2.10 Velocity Profile

A logarithmic velocity profile is assumed for the flow. This is justified if no slip occurs between the particles and the transporting fluid. In mixed regime flows the density differential between particles and fluid is small thus minimising the particle slip.

The velocity distribution will be symmetrical about the vertical axis only. The reduced area caused by a bed load and the difference in roughness between the bed interface and pipe wall will cause the maximum velocity to be vertical displaced from the pipe centre.

To ensure that a single maximum velocity point was found for the flow model it was considered best for the maximum velocity, U_{max} , and the location of this maximum to be found and then to model the surrounding velocity distribution using a logarithmic defect law.

3.2.10.1 Eccentricity of maximum velocity point

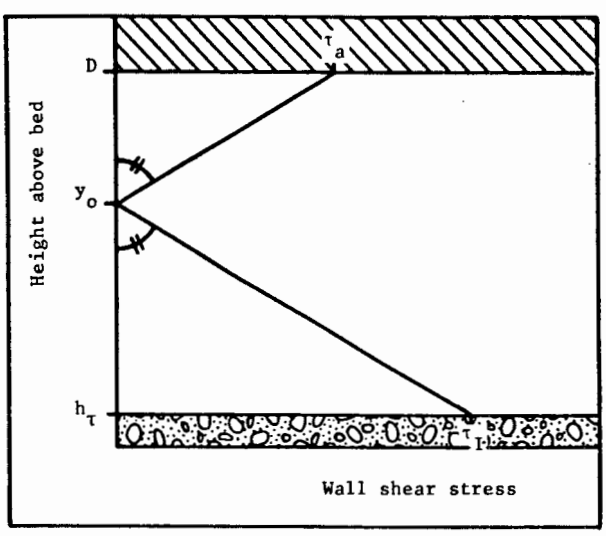

Figure 3.9(a)

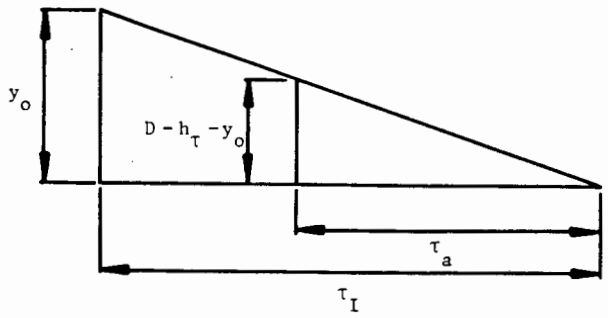

(b)

Figure 3.9 : Geometry for calculating the zero shear position assumed to be the point of maximum velocity

Figure 3.9 shows the shear stress distribution in the flow area above the bed. The wall and bed shear stress are calculated from equns. (3.58) and (3.60) respectively. If a linear shear stress distribution is assumed then the value y_o the point of zero shear can be found by geometry from the equation

$$y_o = \frac{\tau_I (D - h_\tau)}{\tau_a - \tau_I} + h_\tau \quad , \tag{3.82}$$

where h_τ - height above the pipe invert at which τ_I exists,

$h_\tau = h_b$ for stationary bed flow,

$h_\tau = 0$ for sliding or suspended bed flow.

The eccentricity of the point of zero shear is given by

$$e = y_o - R \quad , \tag{3.83}$$

where R = D/2 the pipe radius.

The maximum velocity is found from the universal velocity profile given by

$$u^+ = y^+ \qquad \text{for } y^+ < 5 \quad , \tag{2.88}$$

$$u^+ = \frac{2.0}{\kappa} \ell n\, y^+ - 3.05 \qquad \text{for } 5 < y^+ < 30 \tag{2.89}$$

and

$$u^+ = \frac{1}{\kappa} \ell n\, y^+ + 5.5 \qquad \text{for } y^+ > 30 \quad . \tag{2.90}$$

For the velocity profile equations

$$u^+ = \frac{U_{max}}{u_*}$$

and

$$y^+ = \frac{u_* \rho_{mf} y}{\mu_{mf}}$$

where y is measured from the surface at which u_* exists.

The maximum velocity is calculated from a profile associated with the pipe soffit as shown in Figure 3.10.

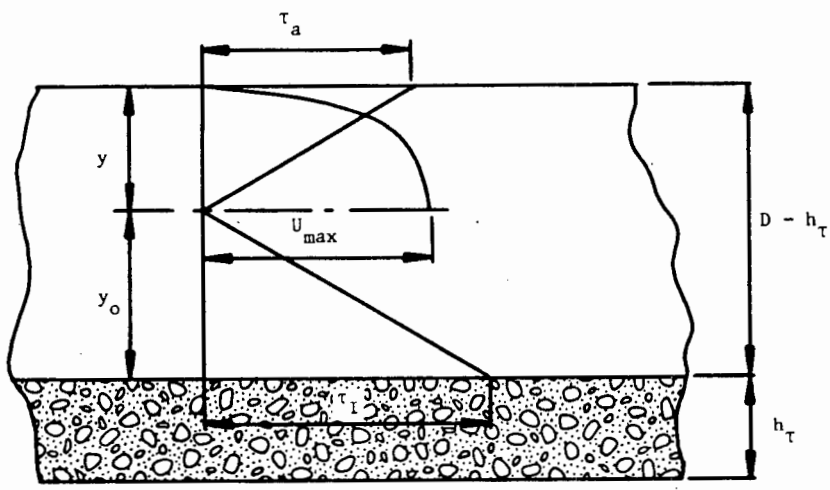

Figure 3.10 : Calculation of U_{max} from the universal velocity distribution associated with the pipe soffit

3.2.10.2 Evaluation of the von Karman constant

The von Karman constant for slurry flow is lower than that for clear fluid. The approach of Einstein and Chien (1954) is used to obtain the value of κ to be used to calculate the maximum velocity (Figure 2.24).

An empirical fit of the graph presented by Einstein and Chien is shown in Figure 2.24, Chapter 2. The function evaluation was interpreted for low concentration mixtures to be

$$fn(\kappa) = \sum_{i=n+1}^{n} \frac{C_{vtf}\, V_{ti}(S_s - S_m)\, g\, Rh_a}{S_s\, V_a\, u_*^2} \quad . \tag{3.84}$$

For high concentration calculations V_t is found for the characteristic particle diameter and no summation is necessary.

A simple empirical fit of the data in Figure 2.24 can be given by the following

if $fn(\kappa) < 0.002$ then $\kappa = 0.38$ otherwise

$$\kappa = 0.1689 - 0.0782 \log (fn(\kappa)) \quad . \tag{3.85}$$

The maximum velocity is calculated from the pipe soffit since the roughness size is known at that point. The shear velocity value used in equn. (3.84) is consequently u_{*_w} the wall value.

3.2.10.3 Velocity at any point in the flow

The velocity defect law is used to calculate the velocity at any point in the flow. This type of profile ensures the integrity of the maximum velocity point.

The velocity at a point y' from the flow boundary located on a line, length R', drawn from the maximum velocity point through the point y' and intersecting the flow boundary is given by

$$u = U_{max} + \frac{u_*}{k_1} \ell n \frac{y'}{R'} \quad . \tag{3.86}$$

u_* is the shear velocity value at the point of intersection of line R' with the flow boundary.

k_1 is the von Karman constant in clear fluid flow but is a velocity profile shape factor for slurry flows. The value of k_1 is found by an iterative procedure such that the value of mean mixture flow rate input to the model (Q_m) equals the calculated mean mixture flow given by equn. (3.79). Figure 3.11 shows a plot of equn. (3.86) for various values of k_1 showing that a decrease in k_1 for fixed U_{max} results in a decrease of the total discharge.

3.2.11 Concentric Computational Net

The integration of the concentration and velocity profile over the flow area can be achieved numerically. This may be done in any systematic way that will involve the summation of the product of concentration and velocity over a defined area.

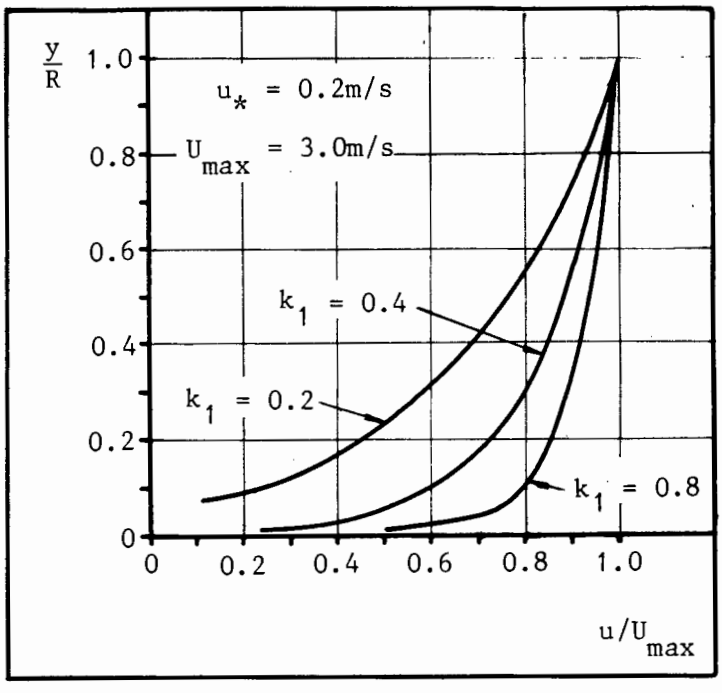

Figure 3.11 : Defect logarithmic velocity profile showing the constant k_1 as parameter

A concentric computational grid is used for this purpose. Figure 3.12 shows the computational grid. The system is concentric to simplify the calculation of each elemental area. The vertical flow symmetry is utilised and the elemental areas on either side of this symmetrical axis are accounted for by doubling the area of the right hand half.

The elemental area can be calculated from

$$A_{ij} = R_j \, \Delta H \, \Delta\gamma \tag{3.87}$$

where

$$\Delta H = \frac{R}{n} \quad , \quad n = 1,2,\ldots,10 \tag{3.88}$$

$$\Delta\gamma = \frac{\pi}{m - 1} \quad , \quad m = 1,2,\ldots,9 \quad . \tag{3.89}$$

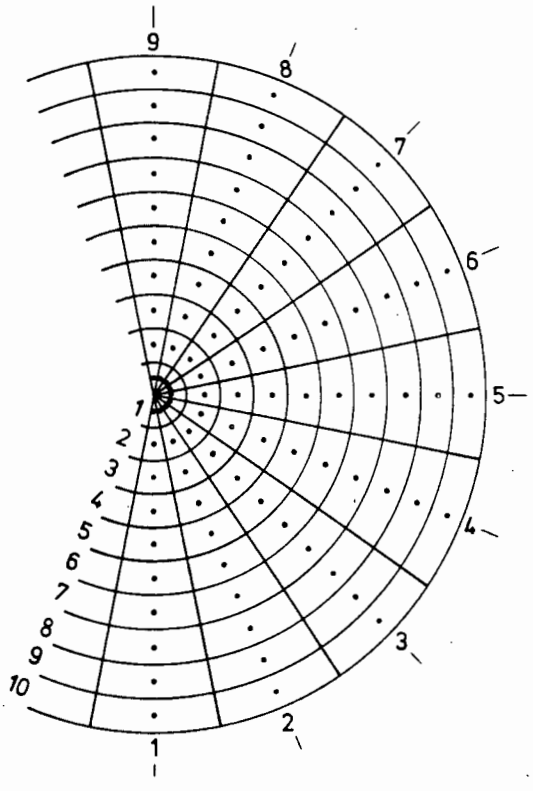

Figure 3.12 : Concentric computational flow net used to integrate the concentration and velocity profiles

For radials R_2 to R_8

$$A'_{ij} = 2\, A_{ij} \tag{3.90}$$

and for radials R_1 and R_9

$$A'_{ij} = A_{ij} \tag{3.91}$$

where A'_{ij} - total flow area for each element.

3.2.12 Computational Net Calculation Geometry

For each of the 190 points on the computational net (Figure 3.12) a concentration and velocity value must be found. These values are then assumed to occur across the calculated area A'_{ij} .

To define the concentration at any point in the pipeline requires a knowledge of the height of that point above the bed. This height value is then used in a linear interpolation of the two proximate points from the 30 points at which $C_v(y)$ is known (see Section 3.2.7.1, page 192).

The velocity at any point can be found from the velocity defect law centred on the point of maximum velocity and terminating with the "no wall slip" condition at either the pipe wall or the bed interface.

Figure 3.13 shows the notation associated with a point on the computational net. The point , i , is defined by R_i and γ_i on the computational net. The velocity profile is defined by a line at an angle θ_i to the vertical. The distance from the point of maximum velocity to the pipe wall (or bed as shown in Figure 3.16, point R_i , C_1) is given by R' . The distance from the pipe wall to the point of interest is given by the distance y' . The point is located at a distance h_i above the bed interface.

Figure 3.14 defines the angle (θ_b) between the bed interface-wall intersection and the point of maximum velocity. The bed load half angle γ_b is calculated from the bed geometry as described by equn. (3.5).

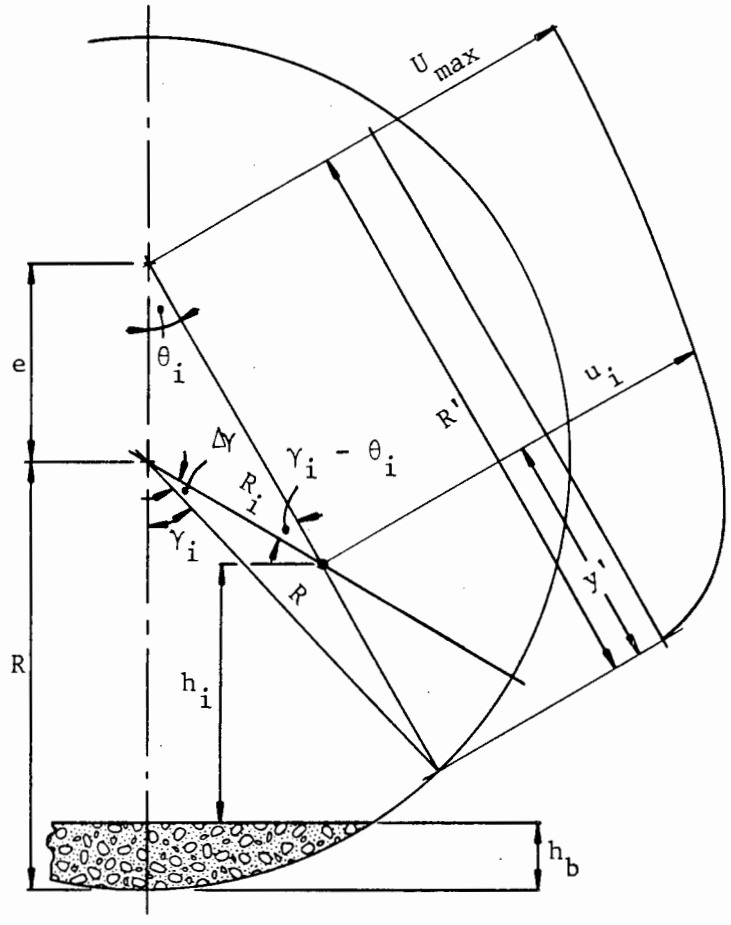

Figure 3.13 : Notation associated with a point on the computational net

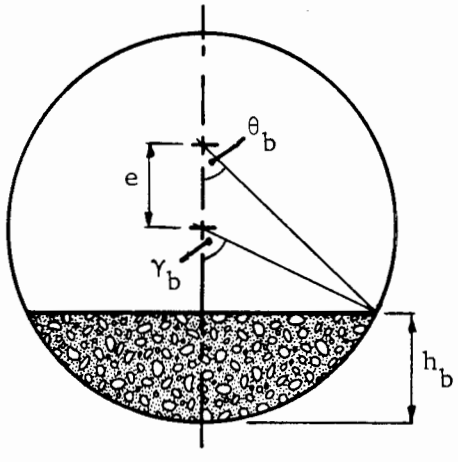

Figure 3.14 : Definition diagram for bedload half angles γ_b and θ_b

From the geometry of Figure 3.14

$$\theta_b = \tan^{-1}\left[\frac{R_i \sin \gamma_i}{e + R_i \cos \gamma_i}\right] \quad . \tag{3.92}$$

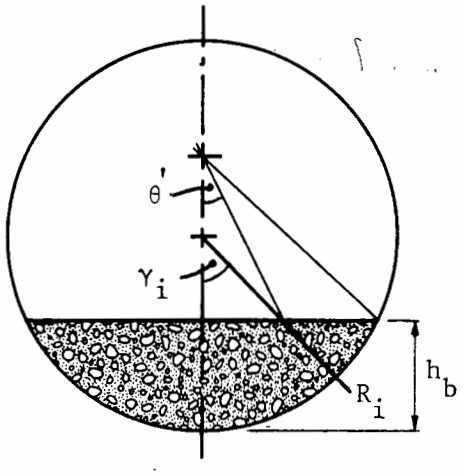

Figure 3.15 : Definition diagram for radial-bed intersection angle θ'

Figure 3.15 defines the value θ' where

$$\theta' = \tan^{-1}\left[\frac{R - h_\tau \tan \gamma_i}{R - h_\tau + e}\right] \tag{3.93}$$

where $h_\tau = h_b$ for stationary bed flow

and $h_\tau = 0$ for sliding or fully suspended flow.

Four different bed geometries exist depending on the values of γ_i and θ_i in relation to the value γ_b, θ_b and θ' . Each geometry will be dealt with separately.

3.2.12.1 $\gamma_i > \gamma_b$

The radials associated with this condition all intersect the pipe wall above the bed thus ensuring that no calculation points on them will be located in the bed. For a radial of this type a further condition exists :

1. $\theta_i \leq \theta_b$

The velocity distribution for a point of this type will intersect the bed interface. For condition where $h_\tau \neq 0$, the shear velocity is calculated at the bed interface where as for $h_\tau = 0$, the shear velocity is calculated at the pipe wall. The points R_i C_1 in Figure 3.16(a) and 3.16(b) are of the type described. The following equations apply

$$y' = \frac{R - (R_i \cos \gamma_i + h_\tau)}{\cos \theta_i} \qquad (3.94)$$

$$R' = \frac{e + R - h_\tau}{\cos \theta_i} \quad . \qquad (3.95)$$

For points above the bed, i.e. $h_i > 0$, the concentration is calculated at the height

$$h_i = R - R_i \cos \gamma_i \quad . \qquad (3.96)$$

For points located in the bed, i.e. $h_i \leq 0$, the concentration is equal to the maximum packing concentration C_b .

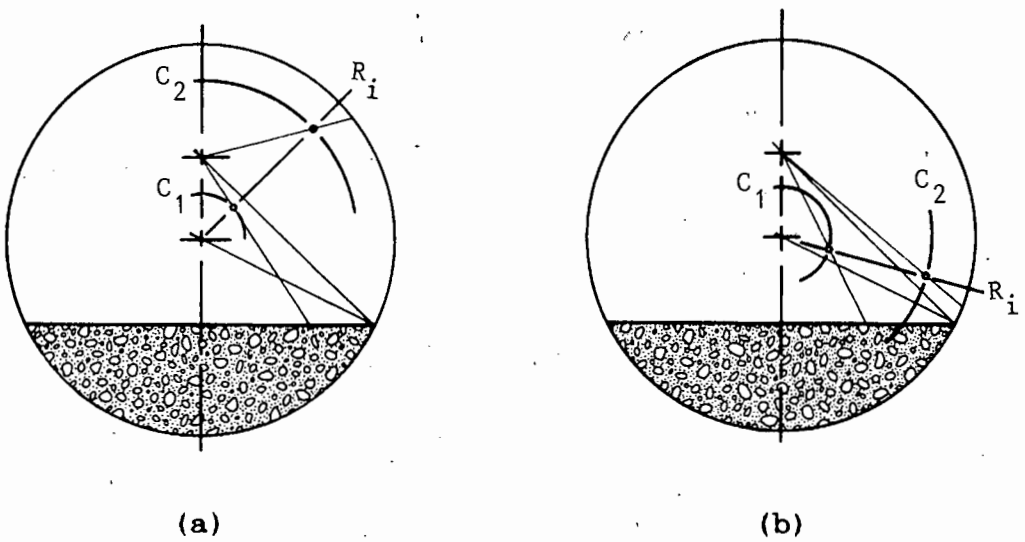

(a) (b)

Figure 3.16 : Calculation geometry for $\gamma_i > \gamma_b$

In both diagrams for $R_i\ C_1$; $\theta \leq \theta_b$

and for $R_i\ C_2$; $\theta > \theta_b$

2. $\theta_i > \theta_b$

The velocity distribution for a point of this type will intersect the pipe wall and the shear velocity will be that associated with the pipe wall. Points $R_i\ C_2$ in Figure 3.16 are of this type. The following equations apply

$$y' = \sqrt{R^2 + R_i^2 - 2\,R\,R_i \cos \Delta\gamma} \qquad (3.97)$$

$$R' = \sqrt{R^2 + e^2 - 2\,R\,e\,\cos\,(\pi - \gamma_i + \Delta\gamma)} \qquad (3.98)$$

$$\text{where } \Delta\gamma = \gamma_i - \left[\theta_i + \sin^{-1}\left(\frac{e \sin \theta_i}{R}\right)\right] \quad . \qquad (3.99)$$

Figures 3.13 and 3.17 show the detailed geometry associated with equations (3.97) to (3.99).

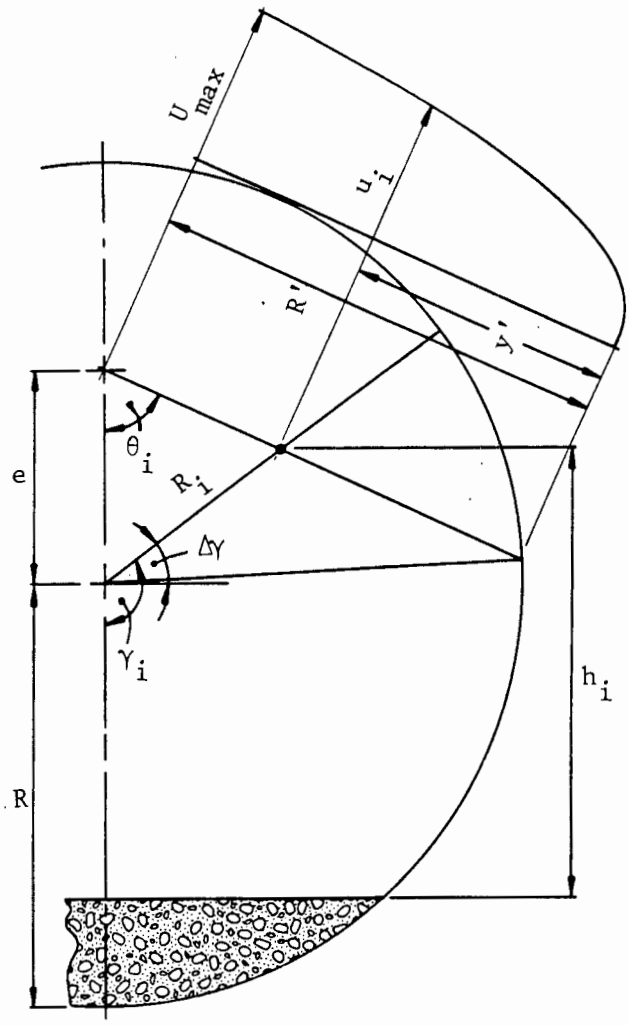

Figure 3.17 : Identical geometry exists for all points with $\gamma_i > \gamma_b$ and $\theta_i > \theta_b$ (see Figure 3.13)

3.2.12.2 $\gamma \leq \gamma_b$

The radials associated with this condition may result in points being located in the flow area above the bed or in the bed. Points of this type always have $\theta_i \leq \theta_b$. For radials of this type a further condition exists

1. $\theta > \theta'$

   Points that fulfill this condition will be located in the bed. Figure 3.18(a) shows a point that is of this type (R_i , C_2) . If stationary bed flow exists all points of this type will have zero velocity and concentration equal to the maximum packing concentration C_b . If sliding or fully suspended flow exists then equns. (3.97), (3.98) and (3.99) apply.

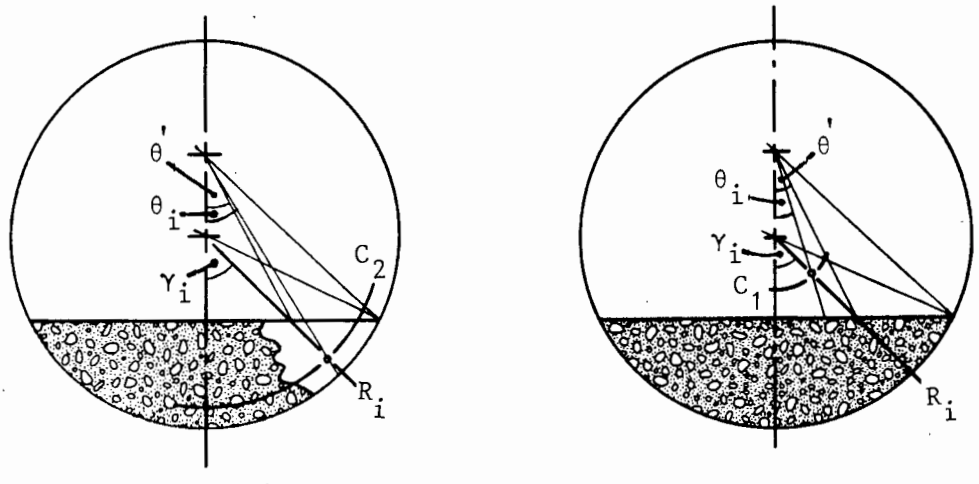

(a) (b)

Figure 3.18 : Calculation geometry for (a) $\theta > \theta'$, (b) $\theta \leq \theta'$

2. $\theta \leq \theta'$

Figure 3.18(b) has a point (R_i , C_1) that fulfills this conditions. The point will be located above the bed. The velocity distribution will intersect the bed interface if $h_\tau = h_b$ or the pipe wall for $h_\tau = 0$. The equations of condition 3.2.12.1, point 1, will apply if $h_\tau = h_b$ while those of condition 3.2.12.1, point 2, will apply for $h_\tau = 0$. The concentration can be found at a height h_i above the bed.

The concentration is calculated using the equations (3.33) to (3.38) at 30 points vertically across the flow area. The concentration at a height h above the bed or pipe invert, depending on prevailing conditions, is calculated from a linear interpolation of the two proximate concentration values around h_i .

The velocity defect law is used under all conditions to calculate the velocity of the point under consideration using the values of y' and R' given.

3.2.13 Calculation of the Delivered Concentration

The delivered concentration is found from the ratio of solids volume flow rate to mixture volume flow rate

$$C_{vd} = \frac{Q_s}{Q_m} \quad . \tag{3.80}$$

From the computational net

$$Q_s = \sum_{i=1}^{9} \sum_{j=1}^{10} u_{ij} C_{vij} A'_{ij} \qquad (3.100)$$

and

$$Q_m = \sum_{i=1}^{9} \sum_{j=1}^{10} u_{ij} A'_{ij} \quad . \qquad (3.101)$$

3.2.14 Iterative Procedure to Ensure Correct Concentration Values

The solution procedure described has mixture flow rate and delivered concentration as input. The *in situ* concentration is required to find the correct bed geometry and *in situ* flow parameters. The model assumes that no slip occurs between the suspended particles and the vehicle so a difference in *in situ* and delivered concentration can only exist if a bed exists. An iterative procedure is used to solve for *in situ* and delivered concentration.

For the first iteration the *in situ* and delivered concentration are assumed to be equal. A new value of delivered concentration is calculated and compared to the input value. If the new value is below the input value by more than 1% then the *in situ* and delivered concentration differ and a new and higher value for the *in situ* concentration must be input to the model until the actual and calculated delivered concentration values are within 1% of each other.

The method used to solve this procedure is a modified linear interpolation or *reguli falsi*. The two equations that must be solved simultaneously are

1. $C_{vd} = C_{vd\ input}$
2. $C_{vd} = fn(C_{vt})$.

The function evaluated for the linear interpolation is the error in the calculated value of the delivered concentration

$$\text{Error function} = \frac{C_{vd\ calculated} - C_{vd\ input}}{C_{vd\ input}} \quad . \qquad (3.102)$$

The iterations will continue until the error function is below 1%. The two start values for the procedure must ensure that the error function is of opposite sign. This is achieved by using the input value of C_{vd} as one of the start values and $C_{vt} = C_b$ the maximum packing concentration as the other value. C_b is the highest possible concentration that can exist in the pipeline and will ensure a positive error function (equn. 3.102).

Appendix 7 contains the mathematical routines of the Bisection method or the modified linear interpolation used.

3.3 CONCLUSIONS

This chapter presents two models :

1. A qualitative model of the flow phenomena including periodic flow.

2. An analytical model for slurry flow of materials with broad particle size distribution.

The qualitative model proposes a two-fluid approach for periodic flow phenomena. The wave and slug flow can be explained by instabilities associated with pressure variations along the pipeline. The concept of a stationary deposit velocity is not required since a transition occurs from stationary bed to heterogeneous flow through a succession of regimes associated with periodic flow. The analytical model predicts the velocity range over which periodic flow occurs without modelling the phenomenon explicitly. The model is therefore applicable for all flow regimes including stationary bed, sliding bed and fully suspended flow.

The inputs to the analytical model are mean mixture flow rate, delivered concentration and the particle and pipeline characteristics. Use is made of the Meyer-Peter and Muller (1948) or Wilson and Watt (1974) equation, for low and high mixture concentration respectively, to calculate the suspended material load. The concentration distribution is found using a diffusion model with a diffusion coefficient that is a function of the height above the bed. A logarithmic velocity distribution is used to ascribe velocity values to volume elements in a concentric computational grid. Calculated values of mean mixture flow rate and delivered concentration are compared to the input values and an iterative proceudre is employed to ensure equality with a result being the computation of *in situ* concentration.

CHAPTER 4

EXPERIMENTAL INVESTIGATION

INTRODUCTION

This chapter describes the experimental investigation undertaken. A description of the measured variables is followed by a summary of the equipment and the experimental procedure. A detailed description of the experimental equipment is contained in Appendix 2. The experimental procedures and equipment calibration techniques are also contained in Appendix 2 which should be studied in conjunction with this chapter. The measurement philosophy adopted in this experimental investigation is discussed and a detailed analysis is presented.

4.1 INDEPENDENT VARIABLES

Figure 4.1 shows the relationship between *independent* variables and *response* variables. Errors can be ascribed to *unknown* variables. Both independent and response variables must be carefully chosen according to the nature of the physical system under investigation.

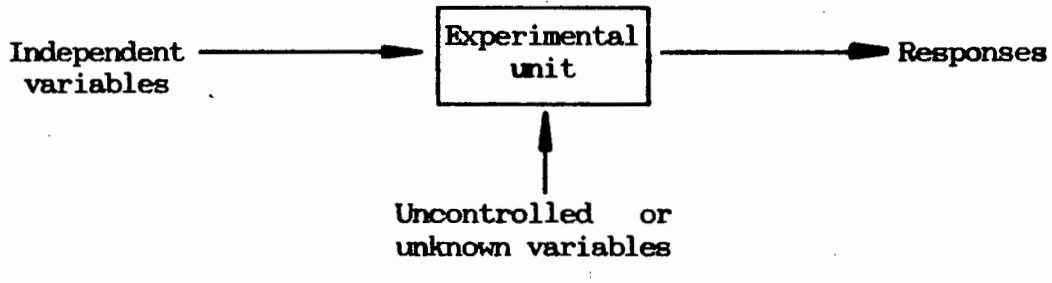

Figure 4.1 : Representation of an experimental run (after Murphy (1977))

The delivered volumetric concentration is defined as the ratio of solids volume flow rate to total mixture volume flow rate

$$C_{vd} = \frac{Q_s}{Q_m} \tag{3.80}$$

$$= \frac{4\ M_s}{V_m\ \pi\ D^2\ \rho_s}$$

$$\text{i.e. } C_{vd} = fn(M_s\ ;\ V_m\ ;\ D\ ;\ \rho_s) \quad . \tag{4.1}$$

Equation 4.1 is a form of the continuity equation. Any four of the variables presented must be known to find the fifth. These five variables were chosen as the independent variables.

It was found impractical to maintain a constant mass flow rate (M_s) while varying the mean mixture velocity (V_m) for a system containing a large slurry volume. This would require continuous adjustment of the slurry concentration. Consequently a decision was taken to maintain a constant concentration (C_{vd}) while the mass flow rate varied. It was considered important to measure all the independent variables during a test. This means that each data point can be considered a unique measurement independent of the test during which it was made. The independent variables are :

1. Pipe geometry.
2. Solid properties.
3. Mean mixture velocity or more correctly mean mixture flow rate.
4. Delivered volumetric concentration.

4.2 DEPENDENT OR RESPONSE VARIABLES

The analytical method described in Chapter 3 is particularly concerned with *in situ* parameters and an endeavour must therefore be made to measure *in situ* response variables. Table 4.1 presents the response variables considered for measurement. Thomas Murphy (1977) suggested that response variables 'can be classified, according to measurement scale, into three main types : quantitative, qualitative or quantal[1]'. Table 4.1 uses this classification of variables.

4.3 DESCRIPTION OF THE HYDRAULIC TRANSPORT TEST FACILITY

(see also Appendix 2 for a detailed description of the test facility and operating procedures)

Figure 4.2 reproduced from Appendix 2 shows an overall view of the hydraulic transport test facility. The test facility comprises an East System with two pipelines of 90mm and 160mm nominal diameter and a West System with two pipelines of 50mm and 63mm nominal diameter. Each system has its own feed hopper and centrifugal pump. A weigh tank, manometer control board, and data acquisition facility are common to both systems.

---

[1]Relating to a sensitivity response marked by the presence or absence of a definite reaction.

Table 4.1 : Experimental investigation variable list

Response variables	Independent variables
Quantitative	
1. *In situ* concentration 2. Vertical flow energy gradient 2.1 Upward 2.2 Downward 3. Horizontal flow energy gradient 4. Bed material velocity 5. Temperature	1. Volumetric flow 2. Delivered concentration 3. Solid characteristics 4. System geometry
Qualitative	
1. Flow visualization 2. Periodic phenomenon	
Quantal	
1. Bed movement condition	

SYSTEM COMPONENTS

4.3.1 Centrifugal pumps

The East System is supplied by a 200 x 150mm pump with a Ni-hard impeller and powered by a 75kW variable speed hydraulic drive. The West System is supplied by a 100 x 75mm rubber lined pump powered by a 15kW electric motor at constant speed. Both pumps are specifically designed by their respective manufacturers to pump particulate solid slurries.

4.3.2 Pipeline

The pipeline is constructed of Polyvinyl Chloride (PVC).

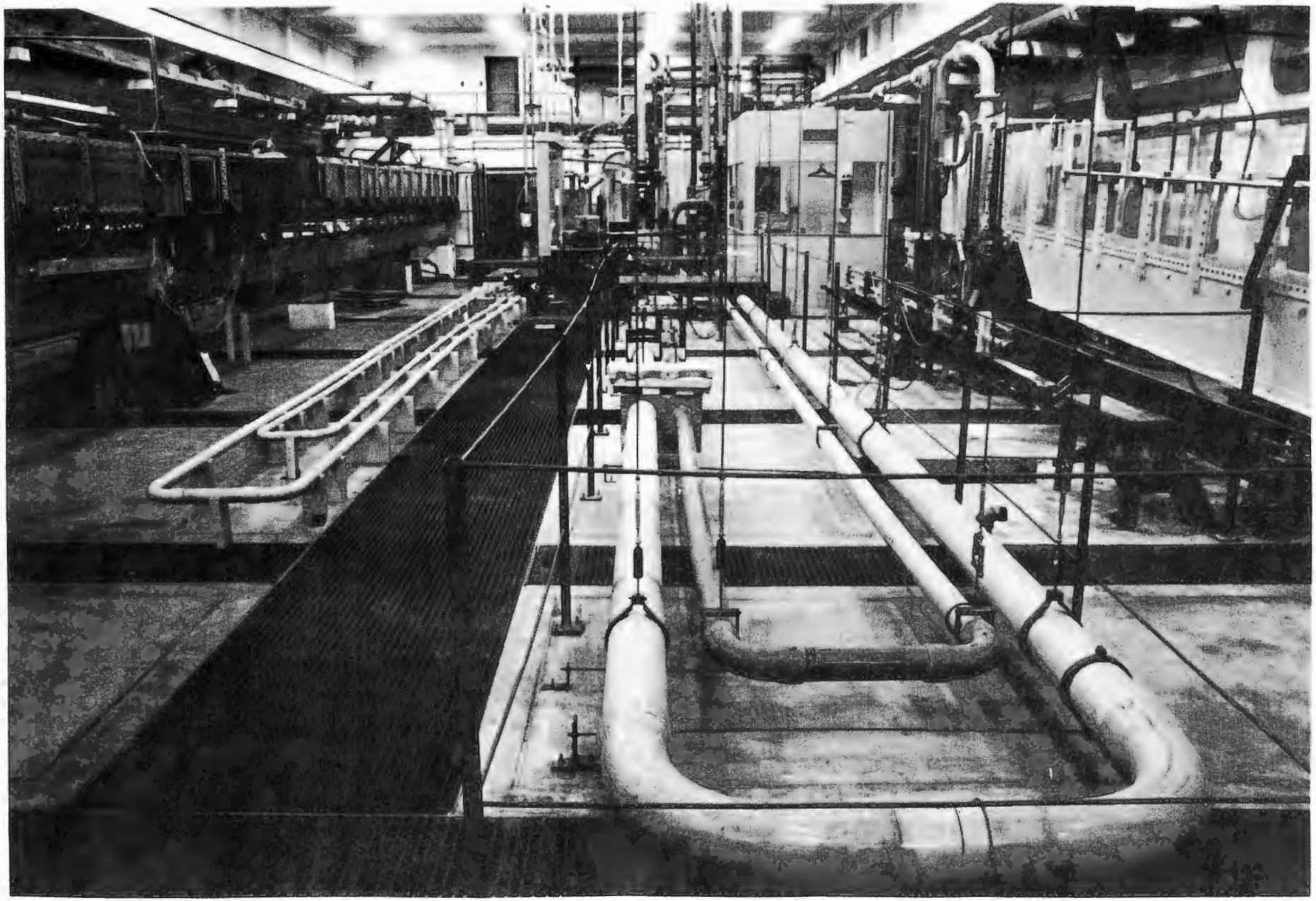

Figure 4.2 : Overall view of Hydraulic Transport Test Facility (l to r) West System, manometer control board, East System and computer control room. Note the suspending wires for the *in situ* concentration measurement.

4.3.3 Pressure Tappings

Pressures along the pipeline are measured by static pressure tappings located in the pipeline wall. Each pressure tapping is provided with a solids trap to ensure that the mixture under test is isolated from the clear water in the manometers and manometer supply lines.

4.3.4 Manometer Board

The manometer board serves as a centralised point for measuring pressure and flow. The pressure transducers and flow meter signal processors are located on the manometer board and electrical signals generated here are fed to the data acquisition unit. Flushing water and air pressure is supplied by the water main (400 kPa) and a compressor (800 kPa).

4.3.5 Pressure Transducers

Three pressure transducers measuring differential water pressure are used. The transducers are common to both systems.

4.3.6 Counter Flow Meters

A counter flow meter is provided on each pipeline for measurement of delivered concentration. Two of the differential pressure transducers are used to measure the energy gradient in the vertical upward and downward flowing pipelines to determine the delivered volumetric concentration. Appendix 2 contains a sub-appendix with a detailed account of a counter-flow meter.

4.3.7 Magnetic Flow Meters

The magnetic flow meters which consist of a detection head and a signal processor provide a direct current output which is proportional to the mean volumetric flow (Q_m) .

4.3.8 *In situ* Concentration Meters

In situ concentration can only be measured in the pipelines of the East System (90mm and 160mm nominal diameter). Three methods are employed.

4.3.8.1 Suspended pipe

A 20 metre section of both East System pipelines is suspended by equidistantly spaced tie wires. Load cells are located on the central three tie wires. The tie wires are approximately 5m long and attach to the laboratory roof. The load cells are calibrated for the zero load case when the pipeline contains clear water only. Any increase in pipeline weight after calibration represents an *in situ* concentration.

4.3.8.2 Articulated pipeline

An articulated joint section of pipe is provided as an alternative method for measuring *in situ* concentration. Three rubber joints between two 2 metre lengths of pipe result in a weighing system with bending moment relief at the joints. A load cell is located at the central joint. Any increase in pipeline weight after calibration represents an *in situ* concentration.

4.3.8.3 Gamma ray densitometer

A gamma ray densitometer is located in the 160mm nominal diameter pipe in a horizontal orientation. This measures *in situ* concentration.

4.3.9 Clear Viewing Section

Flow patterns must be noted for each flow rate at which a slurry is tested. Clear viewing sections are provided in both horizontal and vertical sections of each pipeline.

4.3.10 Probe Test Section for Deposition Velocity

Brown *et al.* (1983) and Brown and Shook (1982) presented a method of measuring particle velocity that has been adapted for measuring the bed material velocity.

When a particle agglomeration moves past a conductivity probe a random noise wave signal is generated. As long as the particle agglomeration remains essentially coherent this noise signal can be repeated at a second probe a short distance downstream of the first probe. The noise signals generated by the two probes can be cross-correlated and the time shift ascertained. With this information and the probe spacing the particle agglomeration velocity can be determined. The particle velocity probe is specifically used to determine the bed velocity.

4.3.11 Weigh Test Equipment

This equipment in the form of a weight and volume measuring tank is used to verify both mean mixture flow rate and delivered concentration. A pneumatic actuator diverts flow from the feed hopper to the sampling tank triggering a timer. The timer is stopped when the actuator returns the flow to the feed hopper. The weigh tank is circular, has a 1.5m^3 volume and is located on a 1750 kg mass scale.

4.4 EXPERIMENTAL PROCEDURE

Table 4.2 is extracted from Appendix 2 and presents an outline of the experimental procedure. For a detailed explanation of the physical test procedure Appendix 2 refers. This section is concerned exclusively with the measurement philosophy adopted. All measurements were made using

PIPELINE TEST SYSTEM DATA LOGGING COMPUTER PROGRAM

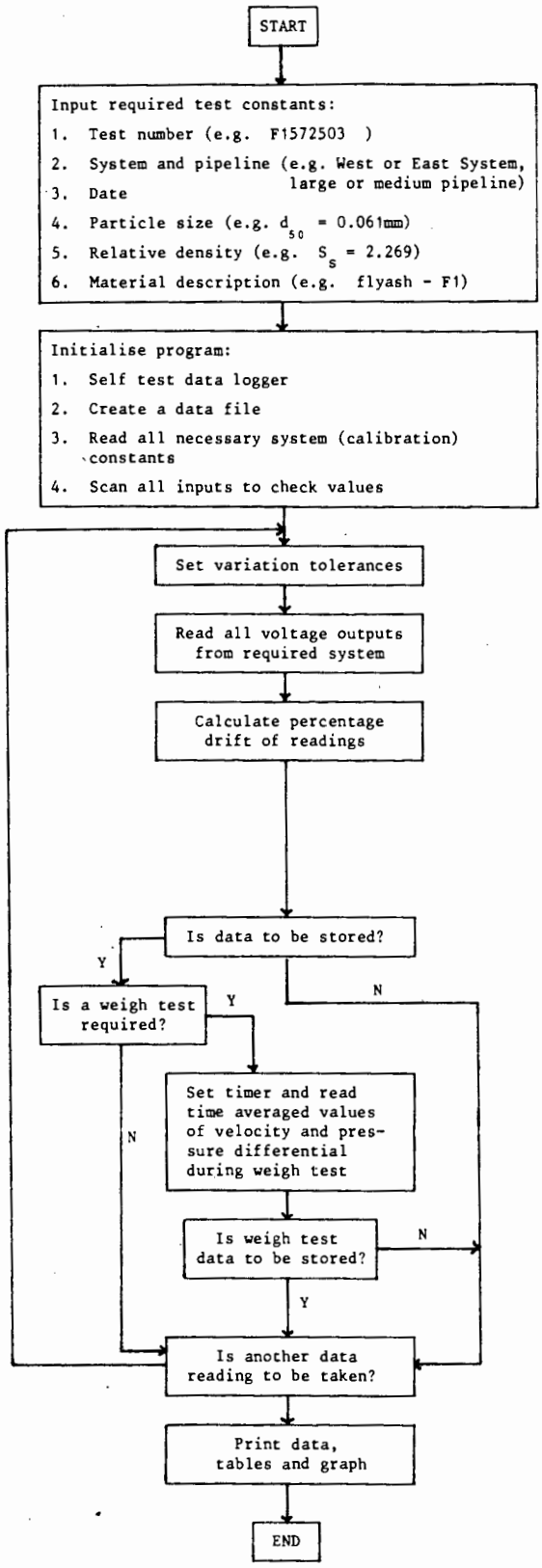

OPERATOR'S EXPERIMENTAL PROCEDURE

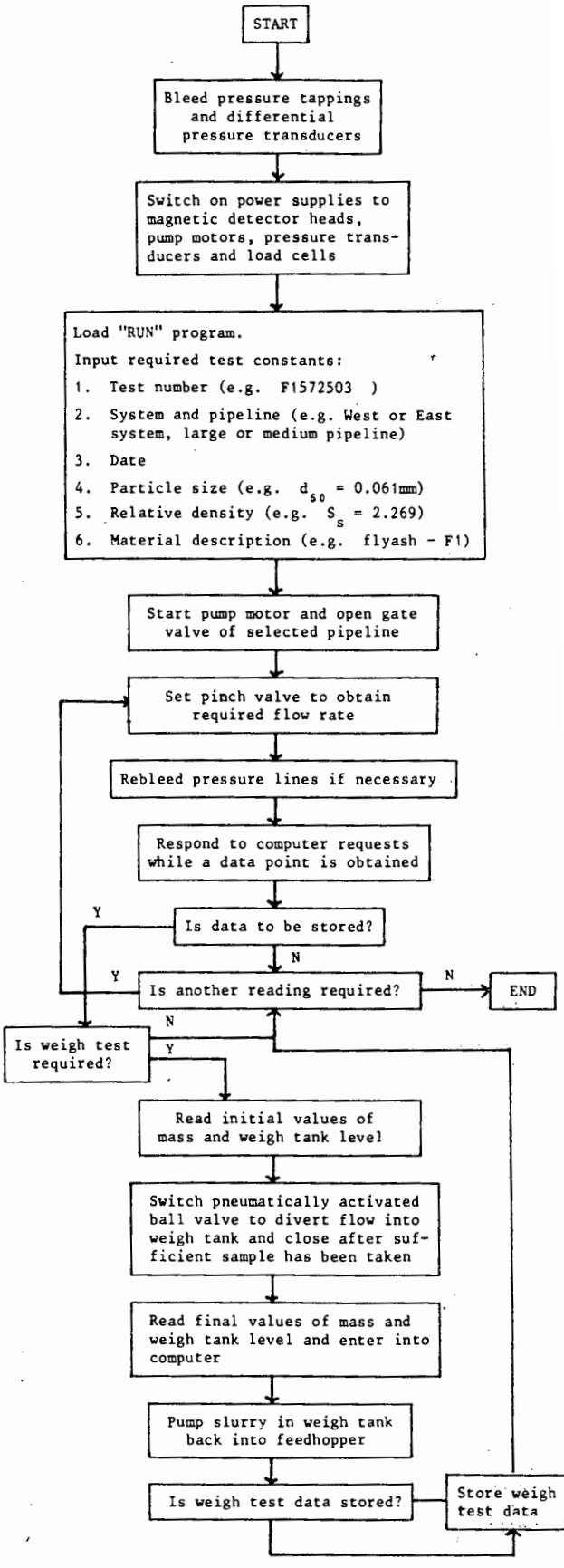

Table 4.2 : Major sequence flow charts for conducting a test on the Hydrotransport Research Unit Facility

transducers connected to a data acquisition unit. The computer program written to control the data acquisition unit is presented as Appendix 3.

Observations made of slurry pipeline flow show two distinct measurement regimes, time averaged and periodic. These two measurement regimes require different instrumentation for data capture. A decision was taken to measure time averaged values quantitatively while periodic phenomena were investigated qualitatively. Reasons for measuring time averaged values are:

1. A reliable data bank for mixed regime slurry flow was required to augment existing slurry flow data of time averaged values.
2. The number of parameters to be measured was large and high speed data acquisition equipment, at great expense, would have been required
3. The objective of the analytical work was to obtain a general understanding of mixed regime flow and the experimental work should reflect this.
4. The objective of the analytical model produced is to design a slurry pipeline system. The experimental test facility would be required to give prototype results that would be of an acceptable industrial standard.

The decision to investigate only time averaged values of the experimental parameters required that the periodic phenomena present did not affect the values measured.

Table 4.3 lists the possible ways of taking a measurement of a typical parameter with the data acquisition unit. The measurement technique is a statistical evaluation of readings taken over a period of time.

Table 4.3 : Measurement techniques

Number of readings	Comments
1. Single reading	Subject to periodic phenomenon
2. Average of two readings	Worst case gives one value positive and the other equal in magnitude but negative so the mean value is zero
3. Reading over long periods (many minutes)	1. Uneconomical 2. System variable (i.e. temp.) may change over long periods of time
4. Reading at high rates	1. Uneconomical 2. Require special equipment 3. Subject to periodic phenomenon
5. Physical instrumentation damping (i.e. clamping pressure lines)	Response might change with temperature and time
6. Electronic damping	Might overshadow system changes and result in incorrect interpretation by operator (also applies to 5 above)
7. Statistical evaluation	1. Statistical parameters available to operator to accept or reject reading 2. Approach is consistent since the same set of mathematical formulae are applied to every point

4.4.1 Stabilization of Data Output Signals from Transducers

Before a time averaged value can be obtained a check must be made to ensure that the pipeline is operating in a stable condition. This is the first check to ensure that the physical system will not change during an accumulation of values. Four voltage outputs are checked for stability.

These voltages are output from the following transducers :

1. Flow rate.
2. Vertical upward flowing energy gradient.
3. Vertical downward flowing energy gradient.
4. Horizontal energy gradient.

The Data Acquisition Unit collects a *set* of voltages from the four instruments and passes them to the computer where a *local average value* is obtained. The set of voltages measured is comprised of readings taken in quick succession for each of the four instruments. The actual number of readings is discussed in Section 4.5.1 of this chapter. Another set is taken a short time later, again averaged and compared to the initial set. If the two consecutive averaged sets are within a preselected tolerance of each other, the data reading procedure can continue. The computer program used for data acquisition is designed to perform this comparison test three times after which operator action is required if the percentage deviation remains above the preselected tolerance. The tolerance value is discussed in Section 4.5.1.

4.4.2 Data Collection

Most test institutions accept the stabilization procedure described above as necessary and sufficient for data collection. The second data point reading, if it is within the required percentage of the first, would be accepted as representative of the actual data. Figure 4.3 shows that this can lead to recording erroneous data.

The two points (1 and 2) shown in Figure 4.3 are within a small percentage of each other but are both below the time averaged value.

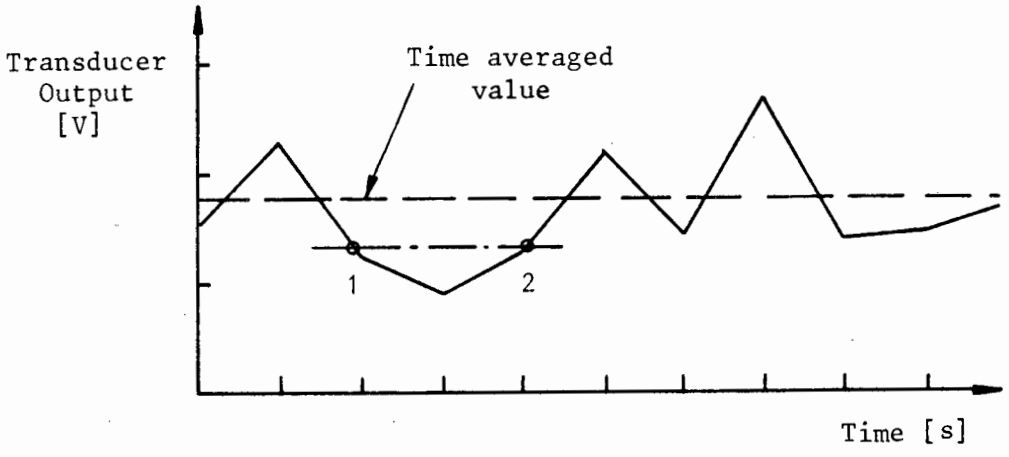

Figure 4.3 : Idealized output of a single transducer

This problem can be overcome by taking a *global time average value* over a number of cycles of the *local average* (e.g. points 1 and 2 in Figure 4.3) comprised of *sets* of readings. Figure 4.4 shows a typical output from a test. The data point voltage outputs include the two vertical differential pressures, the horizontal differential pressure, the load cells and the magnetic flow meter. All other parameters although not represented on the graph are read in exactly the same way.

The real time monitoring of *local average values*, on the computer screen in an analogue format, allows an immediate response from the operator if any changes or instabilities in the systems are detected during a test.

In Figure 4.4, "Loop Number" represents the record of *local average* values plotted against time. The number of times this procedure of obtaining a *local average* occurs, corresponds to the number of "data read loops".

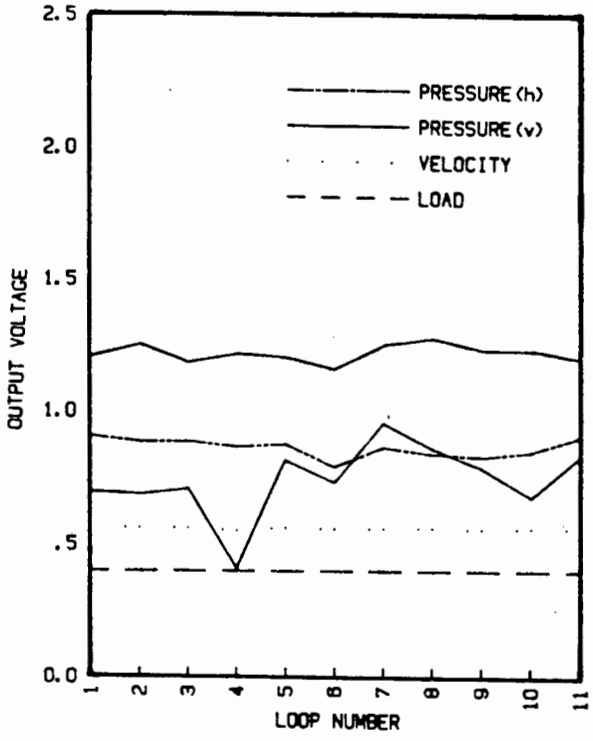

Figure 4.4 : Example of transducer output voltages during a data point reading

When the required number of loops or local averages have been collected, the global average is obtained. Various data acceptance criteria are now applied. A linear least squares fit shown in Figure 4.5, of the local average value, is calculated for the flow meter and horizontal energy gradient transducer outputs. The global average value is compared with the least squares values at the graph extremity. This gives a percentage drift of the voltage during the data acquisition period. If a maximum percentage drift criteria is met the complete set of *global average values* is transformed to physical units by the calibration transformation equations and stored on computer disk. The maximum percentage drift value is discussed in Section 4.5.1.

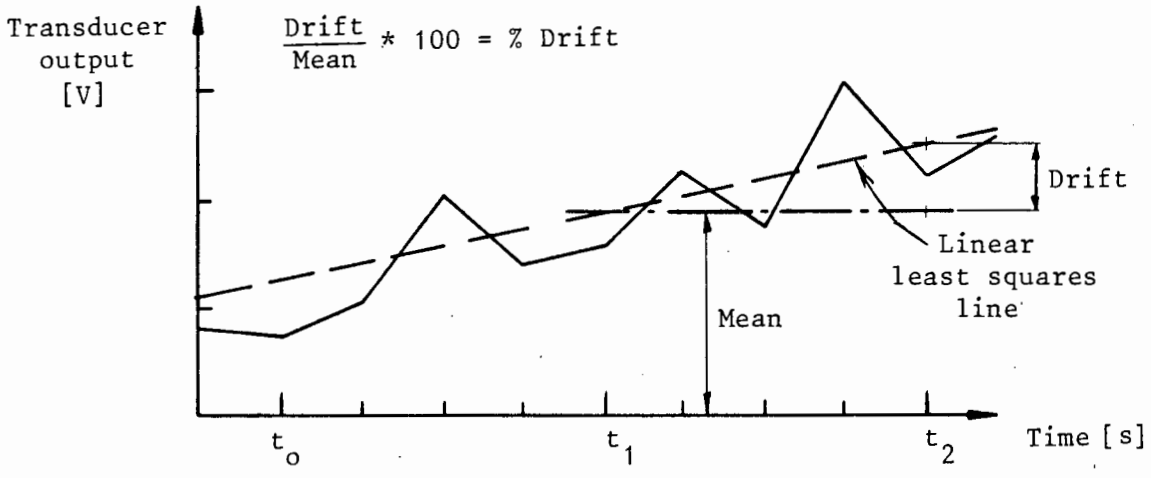

Figure 4.5 : Voltage as a function of time for a typical transducer showing drift selection criterion

From the description of the procedure used to read a *global time averaged value*, the following tolerances need to be defined :

1. Stability check tolerance

$$\frac{|\text{Last reading - This reading}|}{\text{This reading}} < \text{Maximum stabilization tolerance} \qquad (4.2)$$

Points 1 and 2 in Figure 4.3 would comprise such a set of readings.

2. Global average drift tolerance

$$\frac{|\bar{V}(t_2) - \bar{V}(t_1)|}{\bar{V}(t_1)} < \text{Maximum drift tolerance} \qquad (4.3)$$

t_1 and t_2 are defined in Figure 4.5.

Figure 4.6 serves as a definition sketch for the terms *local average* and *global average*. The time taken to acquire the values for a local average is of the order of a few seconds. The time taken to acquire the global average value for a particular data point is of the order of minutes.

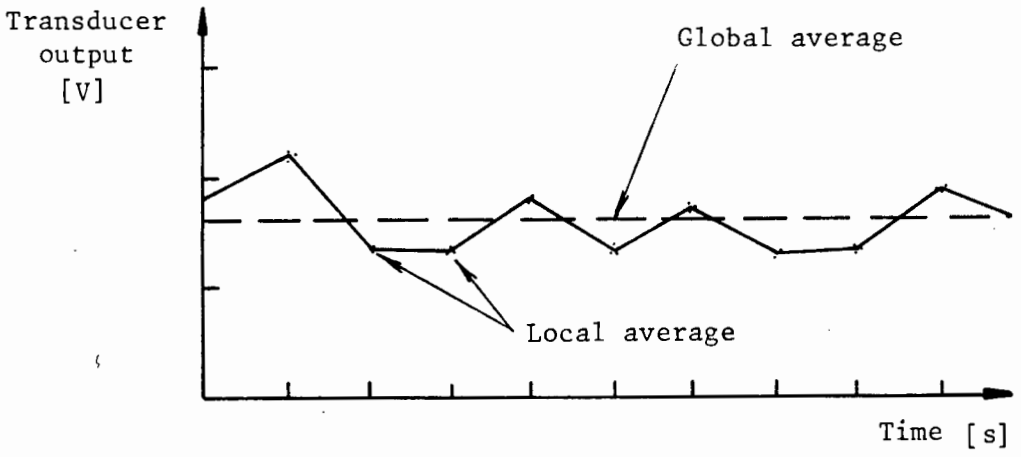

Figure 4.6 : Typical transducer output with time showing applicable terminology

Local average value = average of M transducer voltage values
Global average value = average of N local average values

4.4.3 Weigh Test Sampling and Sample Analysis

Appendix 2 contains a detailed description of the method used to conduct a weigh test. A pneumatic actuator diverts flow from the return line into the sampling tank triggering a timer in the data acquisition unit. When the sample tank is full the flow is returned to the feed hopper switching off the timer. The weigh tank weight and volume are ascertained and typed into the computer. The mean velocity and delivered concentration calculated for the weigh test are compared to the measured values.

4.5. EXPERIMENTAL ERROR

This section is divided into two subsections. The first deals with the statistical analysis required to ensure the best possible global average values while maintaining an economy of measurement. The second deals with instrument error.

4.5.1 Data Acquisition Tolerances

Observation of the analogue output of all the transducer signals from the pipeline system showed small variations with time. These fluctuations exist in any measurement system and can be ascribed to a large number of factors. The fluctuations in transducer signals when converted to digital signals by the data acquisition unit may be in error since the data acquisition unit may read the value at a time when the variation is at some extreme position. The error caused by these fluctuations are accountable and can be handled by statistical techniques.

Accountable errors are of five possible forms :

1. Scale error.
2. Static response error.
3. Dynamic response error.
4. Interference.
5. Personal error.

Unaccountable errors can be of two main types :

1. Mistakes.
2. Random error.

If a large number of experimental measurements are made the sample error may be distributed according to a normal or Gaussian distribution. If this is the case then the statistical techniques applicable to normally distributed systems can be applied.

It is not possible to assess if the data is normally distributed by inspection. The most reliable test for normality is to plot the output of a transducer on probability graph paper. Appendix 4 contains plots of the transducer outputs on probability graph paper as well as a worked example on testing for normality.

In Section 4.4 two types of average value were discussed :

1. Local average.
2. Global average.

The local average value was chosen to be the average of 3 readings taken at the maximum read rate of the data acquisition unit. These readings are taken within 2 seconds of each other. The statistical data presented in Appendix 4 shows that an average of only 3 readings is insufficient to ensure accuracy. The *global average* was taken to be the average of 11 *local average* values. A total of 33 readings from each transducer was found necessary to obtain a reliable global average value. The local average is obtained in less than 2 seconds. A wait period of 10 seconds is then introduced before the next local average is taken. The time taken to measure a global average is therefore of the order of 130 seconds.

The two tolerance values discussed in Section 4.4 were ascertained from experiments with clear water. It was found that the *maximum stabilization*

tolerance that would ensure good quality readings was 15%. The *maximum percentage drift tolerance* was found to be 10%. The maximum percentage drift tolerance of 10% was only necessary at low mixture flow rates where the energy gradient was of the order of a few millimetres head of water per meter length of pipe. For most data readings the actual drift tolerance was below 1%.

The test facility operator is required to accept each global average by typing an acceptance to a request by the computer's interactive program. Acceptance is judged on the basis of the system stabilization, the analogue output that was monitored during the accumulation of a global average, the drift tolerance and an assessment of the system equipment condition. During a reading pressure lines, solids traps and associated equipment are continually checked to ensure that no blockages occur. If any doubt existed in the quality of the data point or it falls outside the maximum allowable tolerance values, the data point is rejected. Table 4.4 presents an outline of the data reading philosophy.

4.5.2 Test Facility Calibration Methodology

Frequent accurate calibration of all measurements ensured reliable results. For this reason all transducers are equipped with calibration devices that could be easily used and intepreted. The overall system calibration is checked by running clear water tests and comparing the data thus derived to theoretical predictions.

Appendix 2 contains the physical procedures used when calibrating the test facility instrumentation. An abbreviated description is included here.

Table 4.4 : Data acquisition procedure. The measured parameters are converted to a digital signal and then back to an analogue graph on the computer screen for operator interpretation during a measurement.

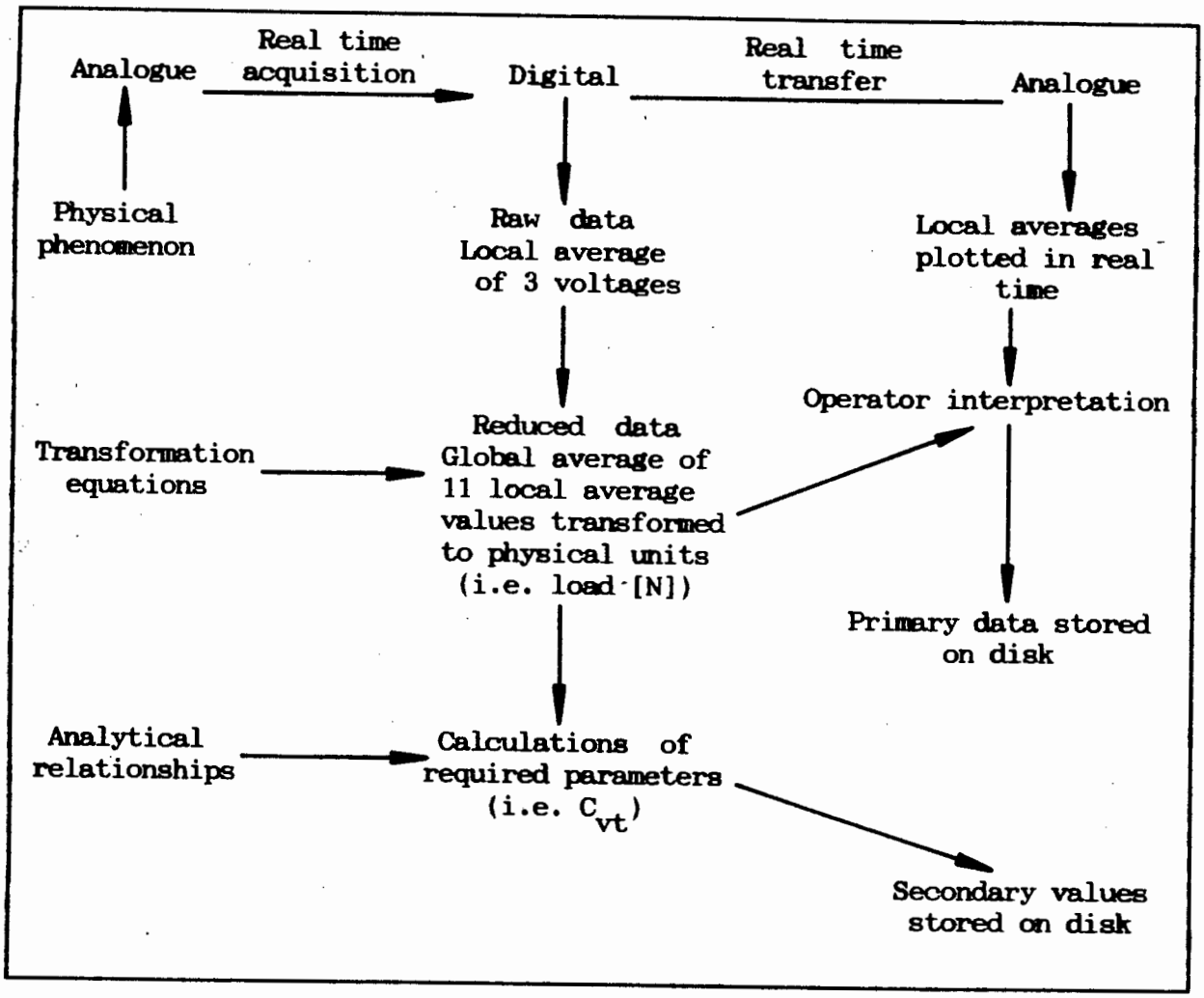

4.5.2.1 Pipeline

1. Diameter

The pipeline diameter is measured by weighing a known length of pipeline filled with water at a measured temperature. The weight of the pipeline is subtracted from the total and the volume of water calculated. From the water volume the pipe area and hence its diameter can be found.

2. Pipe wall roughness

The pipeline wall roughness is calculated from the velocity and headloss measurements taken during clear water tests.

For partially rough wall turbulent flow from the Colebrook-White equation

$$\frac{1}{\sqrt{f}} = -4 \log \left[\frac{k}{3.7D} + \frac{1.26}{Re\sqrt{f}} \right] \qquad (3.53)$$

where

$$f = \frac{\Delta HgD}{2L V_m^2} \qquad (4.4)$$

so

$$k = 3.7D \left[10^{(1/4\sqrt{f})} - \frac{1.26}{Re\sqrt{f}} \right] \qquad (4.5)$$

4.5.2.2 Differential pressure transducer

The differential pressure transducers are calibrated using air over water manometers. The manometers are 1.5m long which corresponds to the range setting of the transducer. The air in the manometer tubes in pressurized to 200 kPa which is the average working pressure (gauge) of the transducers. A differential head is created across the transducer and the corresponding electrical output is measured using the data acquisition unit. A linear calibration equation is found from the output electrical signals and the measured differential head.

4.5.2.3 Temperature

The temperature of the mixture in the delivery hopper is measured by a thermistor (temperature dependent resistor) supplied with a constant

current. The thermistor is calibrated by immersing it in a variable temperature water bath. The data acquisition unit is used to measure the voltage output from the thermistor over the expected temperature range, and calibrated against the actual temperature. The thermistors used produced a logarithmic calibration equation.

4.5.2.4 Counter flow meter

The delivered concentration measured by the counter flow meter is dependent on the accuracy of the pressure transducers. The calculated concentration is, however, compared to weigh test measured values during both clear water and slurry tests in the pipeline.

4.5.2.5 Magnetic flow meter

The magnetic flow meters are calibrated by taking timed mass samples using the weigh tank equipment. During a weigh test the delivery hopper level decreases changing the suction conditions of the pump and hence the flow delivered by the pump. The magnetic flow meter electrical output is read at 1/2 second intervals by the data logger during the weigh test and the readings taken are averaged. This yields the time average voltage during the weigh test and corresponds to the time averaged mass sample taken.

The calibration equation calculated for clear water is checked during slurry testing by taking weigh samples of the mixture.

4.5.2.6 *In situ* concentration

1. Suspended pipeline

Figure 4.7 shows a schematic of the pipeline weighing system. Three of the tie wires are instrumented by load cells. The load cells are calibrated on the pipeline. The suspended pipe is treated as a complete measuring system.

The load cells which support three of the pipeline brackets are zero set when the pipeline is filled with water only. Two different techniques were used to calibrate this system :

(a) Calibration weights placed at 1/4 points between the wires.

(b) Calibration weights placed uniformly along the pipeline not in sympathy with the load cell positions.

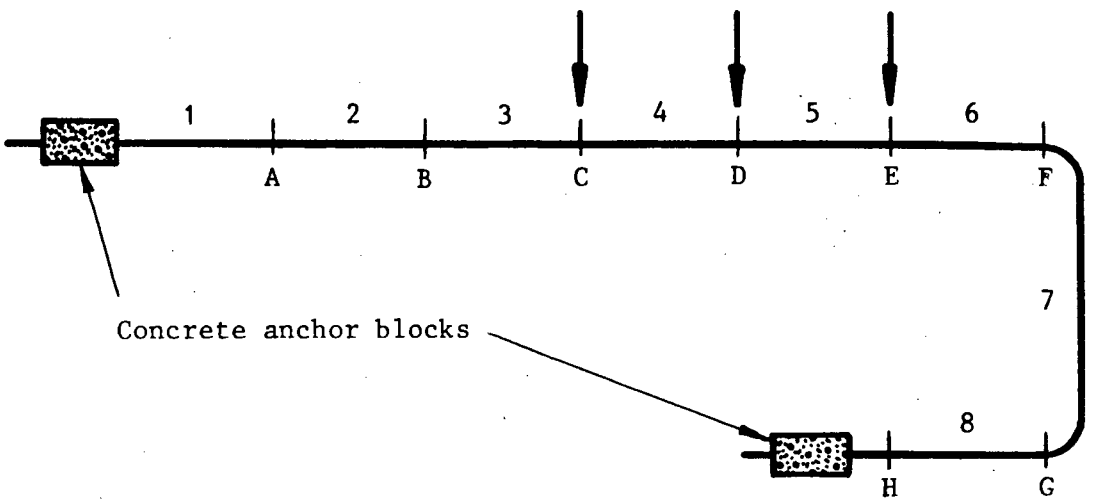

Figure 4.7 : Notation for tie wires and load cells of pipe weighing sections (on 90mm and 160mm nominal diameter pipelines)

The load cells are located at positions C, D and E (Figure 4.7). For method (a), only spans 3 to 6 were loaded at their quarter points. For method (b) loads were placed at intervals of 0.9m along the full length of the pipe centre line including the bends. The 0.9m spacing was determined by the number of weights available and the total suspended length. Method (b) was adopted as the more successful.

2. Articulated section

The articulated section can be modelled as a two member system with bending moment relief (and a small capability for temperature compensation). Since

the members are considered rigid, loads placed at the 1/4 points will approximate a uniformly distributed load. Figure 4.8 shows the articulated section and loading positions.

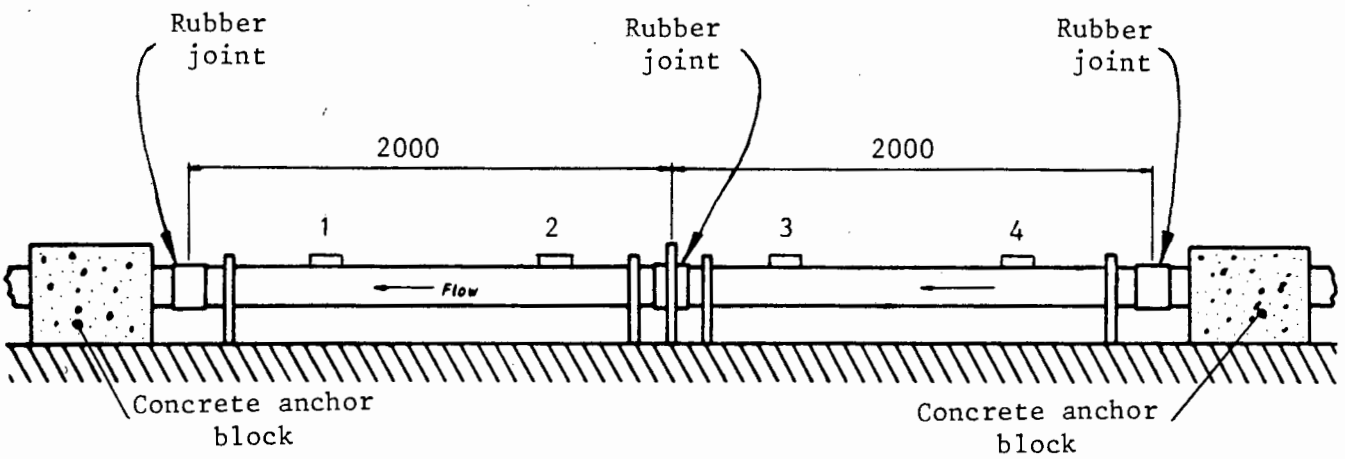

Figure 4.8 : Side view of articulated *in situ* concentration meter showing calibration loading position numbered 1 to 4 (not to scale)

A single load cell is located above the centre rubber joint. The single load cell output is read by the data acquisition unit and a calibration curve set up with these values and the load applied. The load cell can be considered a zero deflection device (deflection is in fact of the order of 10μm) and therefore almost complete bending moment relief can be achieved at the rubber joints. Any inaccuracy in this assumption would be accounted for by the calibration procedure adopted (i.e. load cell is calibrated *in situ*).

4.5.2.7 Particle velocity probe

The particle velocity probe requires no calibration. Two measurements are required for the calculation of particle velocity. These are the *time* taken to traverse the *distance* between the probes. The time is measured by a cross correlation analyser. This instrument has an inherent electronic timer with a predefined accuracy. The distance between the probes is measured on a milling machine bed to ensure accuracy.

4.5.2.8 **Weigh test equipment**

The timer used during a weigh test is built into the data acquisition unit and, as for the cross correlation analyser, has an inherent accuracy.

1. Weigh scale

The weigh scale is factory calibrated but was checked by placing known weights on the scale bed and comparing these to the registered scale output.

2. Weigh tank

The weigh tank, located on the weigh scale, has an acrylic window located on the side of the tank (full depth). A measuring rule is affixed to the window and a depth of mixture can be measured and related to the measured mass. The weigh tank volume versus rule reading is calibrated using quantities of water at a measured temperature. The water mass is converted to a volume and plotted against scale reading to produce the desired calibration curve.

Calibration equations are presented in Appendix 5 for each of the transducers used. The calibration graph, calibration equation and correlation coefficient are presented. Calculated residuals between actual and calculated y-axis values are also presented.

4.5.3 Instrument Measurement Error

4.5.3.1 **Maximum and expected error** (after Brinkworth (1968))

The expected error for a particular measurement can be determined if the functional relationship which defines the measurement is known.

In general for a given quantity X which is a function of several variables (measurements)

$$X = fn\ (a, b, c, \ldots, n) \quad . \tag{4.6}$$

The error in X due to measurement n (i.e. $(\Delta X)_n$) can be found by

$$\frac{(\Delta X)_n}{X} = \left[\frac{\partial X}{\partial n}\right] \frac{\Delta n}{X} \tag{4.7}$$

or expanding

$$\frac{(\Delta X)_n}{X} = \left[\frac{\partial X}{\partial n}\right] \cdot \frac{n}{X} \cdot \frac{\Delta n}{n} \quad . \tag{4.8}$$

The maximum possible error in X is given by the sum of errors of the n contributory measured quantities

$$\left[\frac{(\Delta X)}{X}\right]_{max} = \Sigma \left[\frac{\partial X}{\partial n} \cdot \frac{n}{X} \cdot \frac{\Delta n}{n}\right] \quad . \tag{4.9}$$

The expected highest error is given by the square root of the sum of the squared values of each term which ensures that all contributions will be positive.

So

$$\left[\frac{(\Delta X)}{X}\right]^2_{exp} = \Sigma \left[\frac{\partial X}{\partial n}\right]^2 \left[\frac{n}{X}\right]^2 \left[\frac{\Delta n}{n}\right]^2 \tag{4.10}$$

where X - overall result

ΔX - error in the overall result

n - quantity measured (e.g. flow, weight, etc.)

Δn - error in the quantity measured in units of the measurement.

4.5.3.2 **Linear regression analysis** (after Lipson and Sheth (1973))

The calibration equations for the various transducers is derived from a regression analysis. This is either linear or logarithmic.

For the linear regression the method of least squares is employed. The sum of the squares of the deviations (ϵ) is minimized in the y-direction. This is done since the random variation exists in the y values while the x values are held constant (see Figure 4.9).

The resulting equation is

$$y = m\,x + C + \epsilon \qquad (4.11)$$

where ϵ is the measure of deviation of the data points in the y-direction (Figure 4.10).

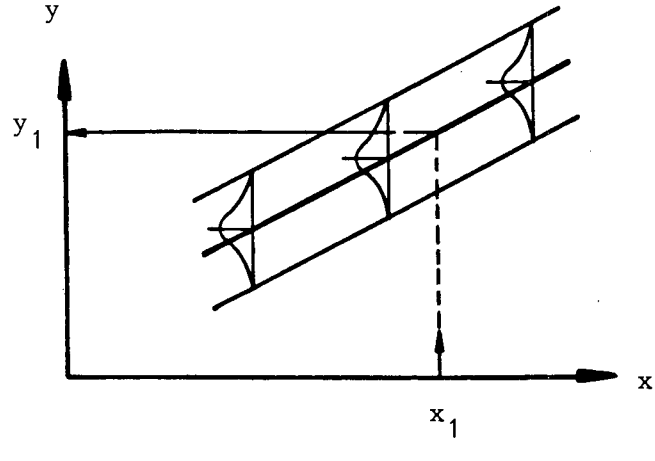

Figure 4.9 : Variance distributed normally on y
Regression of y on x , y = f(x)

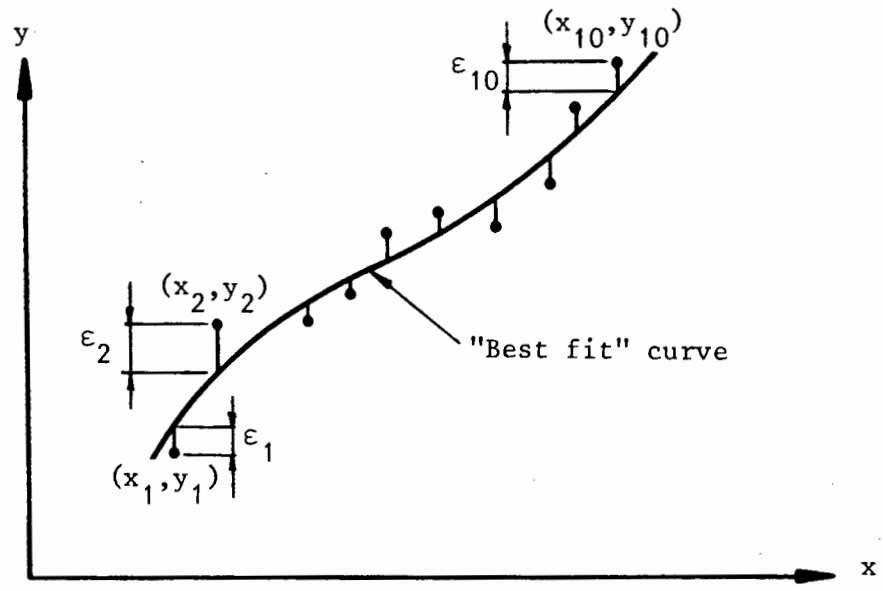

Figure 4.10 : Sum of squares of deviations in y direction for least squares approximation

4.5.3.3 Correlation analysis

The correlation coefficient (r) is defined as the quantitative measure of association between two variables x and y

$r = \pm 1$, perfect correlation.

$r = 0$, no correlation.

$$r = \pm \sqrt{\frac{\text{explained variation}}{\text{total variation}}} \quad . \tag{4.12}$$

In terms of variables

$$r = \pm \sqrt{\frac{\Sigma(y_{est} - \bar{y})^2}{\Sigma(y - \bar{y})^2}} \tag{4.13}$$

where y - actual measurement

$\bar{y}$ - mean value of y

$y_{est.}$ - correlation estimate of y .

Expanding

$$r = \frac{n \Sigma xy - \Sigma x \Sigma y}{\{[n \Sigma x^2 - (\Sigma x)^2] [n \Sigma y^2 - (\Sigma y)^2]\}^{1/2}} \quad . \qquad (4.14)$$

The value of r is significant in that r^2 of the total variation in y can be accounted for by the least squares line, and $(1 - r^2)$ is unaccountable. Therefore, physical (explained) variation is r^2 while random (unexplained) variation is $(1 - r^2)$.

4.5.4 Errors in Measured Parameters

Systematic errors will appear in the mean value of any measurement and statistical methods will not disclose them. These errors are accountable and are of the following forms;

1. Scale errors
2. Static response errors
3. Dynamic response errors
4. Interference
5. Personal error.

Clear water tests, in which experimental results and theoretical predictions could be compared, were performed in each pipeline to ensure that systematic errors were minimized.

4.5.4.1 Pipeline diameter

The pipe diameter is calculated by the equation;

$$D = \sqrt{\frac{4 M_w}{\rho_w \pi L}} \quad . \qquad (4.15)$$

Possible errors exist in the measurement of L and M_w where

L - length of pipe

M_w - mass of water contained in the pipe.

Calculating the expected highest error as discussed in Section 4.5.3.1 of this chapter. The expected highest error in the pipe diameter is therefore

$$\left[\frac{\Delta D}{D}\right]^2 = \left[\frac{\partial D}{\partial M_w}\right]^2 \left[\frac{M_w}{D}\right]^2 \left[\frac{\Delta M_w}{M_w}\right]^2 + \left[\frac{\partial D}{\partial L}\right]^2 \left[\frac{L}{D}\right]^2 \left[\frac{\Delta L}{L}\right]^2$$

where

$$\frac{\partial D}{\partial M_w} = \frac{1}{2}\sqrt{\frac{4}{\rho_w M_w \pi L}} \qquad \frac{\partial D}{\partial L} = -\frac{1}{2}\sqrt{\frac{4 M_w}{\rho_w \pi L^3}}$$

so

$$\left[\frac{\Delta D}{D}\right]^2 = \left[\frac{1}{2}\sqrt{\frac{4}{\rho_w M_w \pi L}}\right]^2 \left[\frac{M_w}{D}\right]^2 \left[\frac{\Delta M_w}{M_w}\right]^2 + \left[-\frac{1}{2}\sqrt{\frac{4 M_w}{\rho_w \pi L^3}}\right]^2 \left[\frac{L}{D}\right]^2 \left[\frac{\Delta L}{L}\right]^2 . \tag{4.16}$$

For the 50mm nominal diameter pipe the following data was obtained

Nominal size	Pipe mass	Total mass	Length	Volume	Diameter
50mm	0.611kg	2.385kg	1095.0mm	1.779ℓ	45.418mm

$$\frac{M_w}{D} = \frac{2.385}{0.045418} = 52.51$$

$$\frac{\Delta M_w}{M_w} = \frac{0.01}{2.385} = 0.00042$$

$$\frac{L}{D} = \frac{1.095}{0.045418} = 24.11$$

$$\frac{\Delta L}{L} = \frac{0.001}{1.095} = 0.0009$$

$$\frac{1}{2}\sqrt{\frac{4}{\rho_w M_w \pi L}} = 0.0128$$

where ρ_w = 998.68 kg/m³

$$\frac{1}{2}\sqrt{\frac{4 M_w}{\rho_w \pi L^3}} = 0.0208$$

$$\left[\frac{\Delta D}{D}\right]^2 = 1.638.10^{-4} * 2.757.10^{3} * 1.764.10^{-5} + 4.326.10^{-4} * 5.813.10^{2} * 8.1.10^{-7}$$

$$= 8.170.10^{-6}$$

$$\Delta D = 2.858.10^{-3} * D$$

So $$\Delta D = 1.298.10^{-4} \text{ m}$$

$$= 0.286 \% \quad .$$

Table 4.5 shows the expected highest error values for the four pipelines used.

Table 4.5 : Expected highest error for a chosen diameter

Nominal Diameter [mm]	L[m] ±0.001	M_w [kg]	Actual Diameter [mm]	Error in Diameter [mm]	% Error
50	1.095	1.77±0.01	45.418	±0.130	0.286
63	1.217	3.13±0.01	57.206	±0.252	0.441
90	1.419	7.07±0.01	79.715	±0.084	0.106
160	1.538	23.41±0.01	139.300	±0.077	0.054

Water temperature : 18°C Water density : 998.68 kg/m^3

4.5.4.2 **Differential pressure transducers**

The error in differential head is given by the accuracy of the pressure transducers and the accuracy with which the calibration manometers can be read.

The calibration equation is of the form

$$H = aV + B$$

H - differential head output

V - transducer output voltage.

The maximum expected error for this equation is

$$\left[\frac{\Delta H}{H}\right]^2 = \left[\frac{\partial H}{\partial V}\right]^2 \left[\frac{V}{H}\right]^2 \left[\frac{\Delta V}{V}\right]^2 \quad . \tag{4.17a}$$

The error term for the voltage output $\Delta V/V$ can be found from the calibration manometer reading error

$$\left[\frac{\Delta V}{V}\right]^2 = \left[\frac{\partial V}{\partial L}\right]^2 \left[\frac{L}{V}\right]^2 \left[\frac{\Delta L}{L}\right]^2 \tag{4.17b}$$

L - measured differential head, input.

The manufactured accuracy of the pressure transducers is given in Table 4.6.

Table 4.6 : Differential pressure transducer accuracy

Transducer	Orientation	Accuracy
A	Vertical upward flow	±0.1%
B	Vertical downward flow	±0.1%
C	Horizontal flow	±0.25%

The calibrated range for the pressure transducers is 1.5m . The error in measurement is therefore expected to be

ΔH = 1.5mm for Transducer A and B

ΔH = 3.75mm for Transducer C .

Combining equations (4.15a) and (4.15b)

$$\left[\frac{\Delta H}{H}\right]^2 = \left[\frac{\partial H}{\partial V}\ \frac{\partial V}{\partial L}\ \frac{V}{H}\ \frac{L}{V}\ \frac{\Delta L}{L}\right]^2$$

$$\left[\frac{\Delta H}{H}\right]^2 = \left[\frac{\partial H}{\partial L}\right]^2 \left[\frac{L}{H}\right]^2 \left[\frac{\Delta L}{L}\right]^2 \quad . \qquad (4.18)$$

For Transducer A , $\frac{\partial H}{\partial L}$ is the slope of a graph of measured head versus actual head.

So $\frac{\partial H}{\partial L}$ = 1.0002

assuming $\partial H \simeq \Delta L$

where

ΔL - accuracy with which the calibration manometer can be read,

ΔL = $\pm$1.0mm .

For Transducer B and C

$$\left[\frac{\partial H}{\partial L}\right]_B = 1.0004 \quad \text{and} \quad \left[\frac{\partial H}{\partial L}\right]_C = 1.00063 \quad .$$

$$\text{So} \quad \left[\frac{\Delta H}{H}\right]_A^2 = (1.0002)^2 \left[\frac{1.10^{-3}}{H}\right]^2$$

similarly for B and C .

Figure 4.11 shows a plot of expected highest error for the three differential pressure transducers.

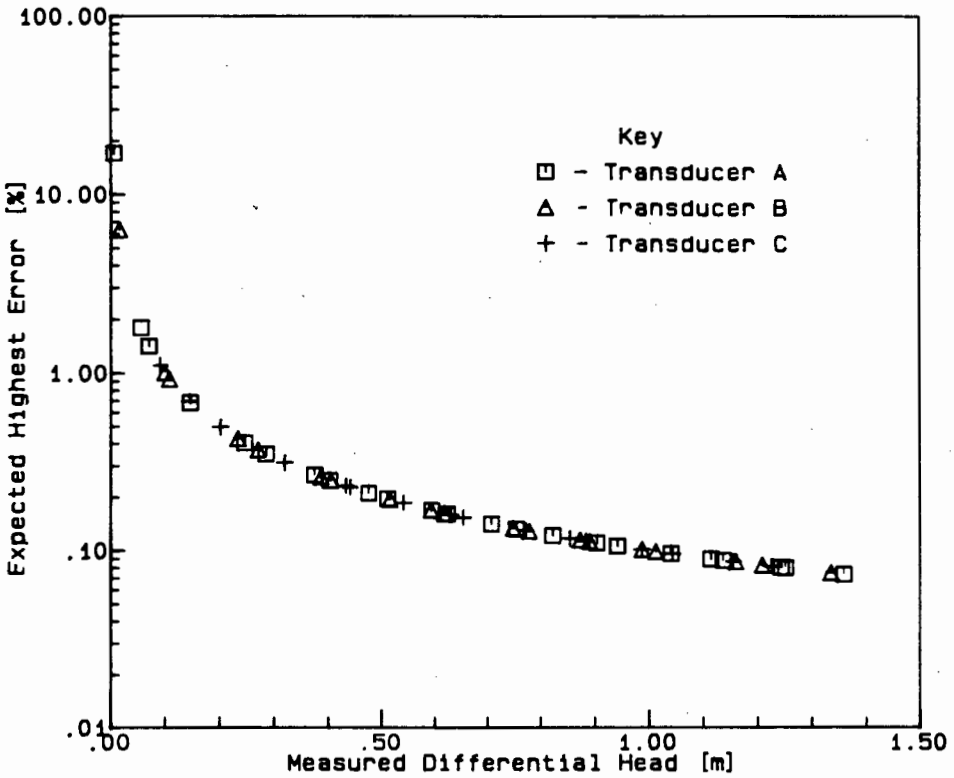

Figure 4.11 : Error graph for differential pressure transducers

4.5.4.3 **Temperature**

Figure 4.12 shows the error graphs for the two thermistor calibration equations. The curves are calculated from the equation

$$\left[\frac{\Delta T}{T}\right]_{out}^2 = \left[\frac{\partial T_{out}}{\partial T_{in}}\right]^2 \left[\frac{T_{in}}{T_{out}}\right]^2 \left[\frac{\Delta T}{T}\right]_{in}^2 \qquad (4.19)$$

T_{in} - actual temperature [°C]

T_{out} - measured temperature [°C] .

From the thermometer used to measure the actual temperature $\Delta T = \pm 1°C$. The slope of the curve of actual temperature versus measured temperature yields the value of $\frac{\partial T_{out}}{\partial T_{in}}$.

For the East System $\frac{\partial T_{out}}{\partial T_{in}} = 0.99953$

West System $\frac{\partial T_{out}}{\partial T_{in}} = 0.99838$.

For the East System

$$\left[\frac{\Delta T}{T}\right]^2_{out} = (0.99953)^2 \left[\frac{\Delta T_{in}}{T_{out}}\right]^2$$

and similarly for the West System.

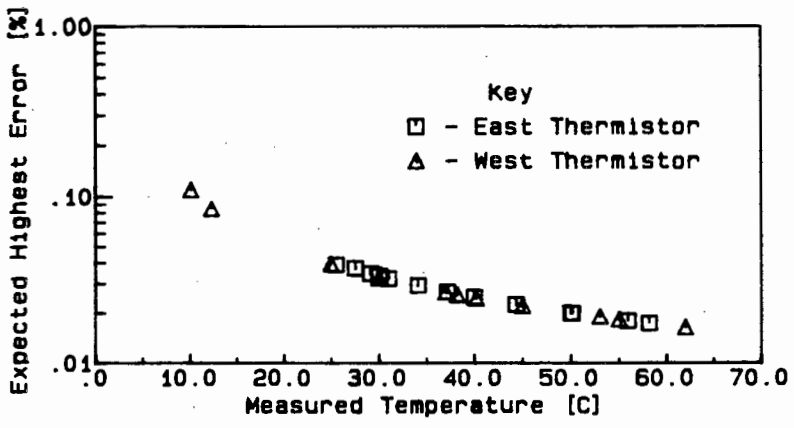

Figure 4.12 : Error graph for thermistors

4.5.4.4 Magnetic flow meter

The equation used to determine the mean velocity (V_m) is

$$V_m = \frac{4\ M_m}{\rho_m\ t\ \pi\ D^2} \qquad (4.20)$$

$$= \frac{\mathcal{V}_m}{t\ \pi\ D^2}$$

where

M_m - sample mass [kg]

$\mathcal{V}_m$ - sample volume (in weigh tank) [m³]

ρ_m - sample density [kg/m³]

t - time taken to collect sample [sec.]

D - pipe diameter [m] .

The error in the given variables are listed in Table 4.7.

Table 4.7 : Error in variables used to measure mean velocity

Variable	Error
ΔM_m	±250 g
Δt	±0.001 sec
ΔD	See Table 4.5
$\Delta \mathcal{V}_m$	$3.8.10^{-3}$ m³

The maximum expected error in V_m is given by

$$\left[\frac{\Delta V_m}{V_m}\right]^2 = \left[\frac{4}{t\ \pi\ D^2}\right]^2 \left[\frac{V_m}{V_m}\right]^2 \left[\frac{\Delta V_m}{V_m}\right]^2 + \left[\frac{-\ 4\ V_m}{t^2\ \pi\ D^2}\right]^2 \left[\frac{t}{V_m}\right]^2 \left[\frac{\Delta t}{t}\right]^2$$

$$+ \left[\frac{-\ 8\ V_w}{t\ \pi\ D^3}\right]^2 \left[\frac{D}{V_m}\right]^2 \left[\frac{\Delta D}{D}\right]^2 \quad . \qquad (4.21)$$

Figure 4.13 shows the experimental error for the flow meters in the test facility.

4.5.4.5 Delivered concentration

The equation used to calculate the delivered concentration (C_{vd}) is given by

$$C_{vt} = \frac{S_m - S_w}{S_s - S_w} \qquad (4.22)$$

and for S_m the delivered relative density by

$$S_m = S_w\left[\frac{\Delta H_{up} - \Delta H_{down}}{2\ L}\right] + 1 \qquad (4.23)$$

where L - distance between differential pressure measuring tappings.

The relative density (S_m) is checked using the weigh tank where

$$S_m = \frac{M_m}{\nu_m 1000} \quad . \qquad (4.24)$$

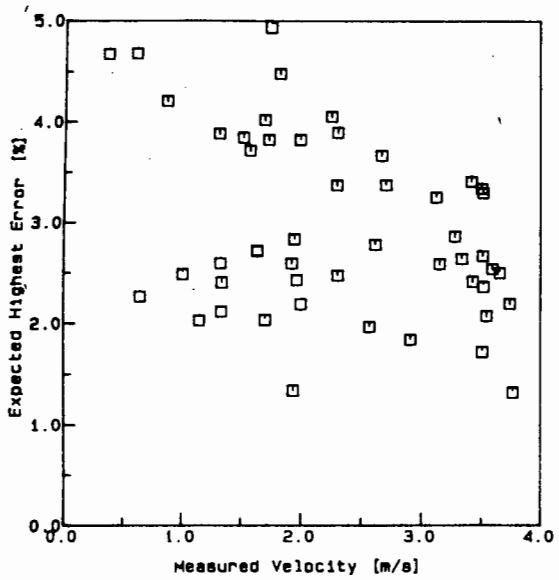

Figure 4.13(a)

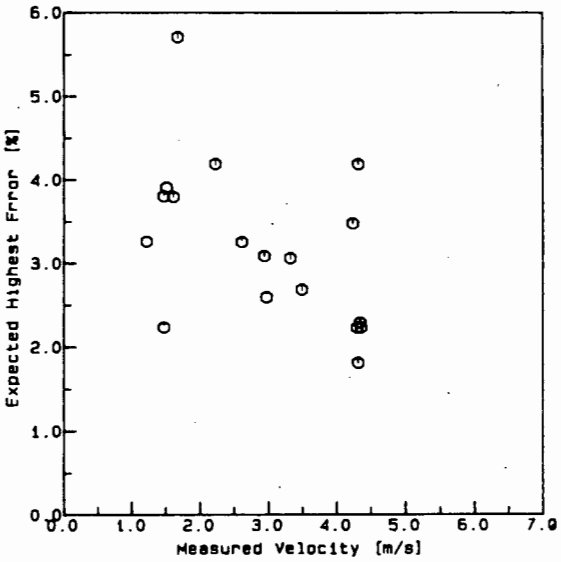

Figure 4.13(b)

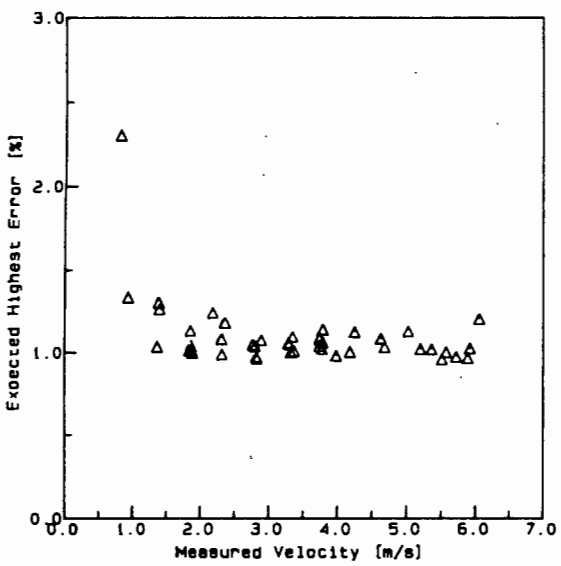

Figure 4.13(c)

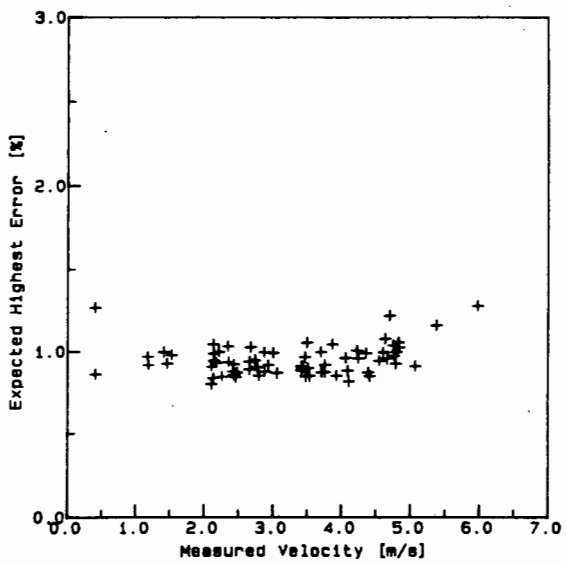

Figure 4.13(d)

Key

□ - Nom. Diameter : 50 mm

⊙ - Nom. Diameter : 63 mm

△ - Nom. Diameter : 90 mm

\+ - Nom. Diameter : 160 mm

Figure 4.13 : Error graph for velocity measurement

$$\text{So} \quad \left[\frac{\Delta S_m}{S_m}\right]^2 = \left[\frac{1}{\gamma_m 1000}\right]^2 \left[\frac{M_m}{S_m}\right]^2 \left[\frac{\Delta M_m}{M_m}\right]^2 + \left[\frac{-M_m}{\gamma_m^2 1000}\right]^2 \left[\frac{V_m}{S_m}\right]^2 \left[\frac{\Delta V_m}{V_m}\right]^2 . \tag{4.25}$$

Figure 4.14 shows the experimental error for the counter flow meters in the test facility.

4.5.4.6 *In situ* concentration

The error in the load cell calibration equations can be calculated from

$$\left[\frac{\Delta L}{L}\right]^2_{out} = \left[\frac{\partial L_{out}}{\partial L_{in}}\right]^2 \left[\frac{L_{in}}{L_{out}}\right]^2 \left[\frac{\Delta L}{L}\right]^2_{in} . \tag{4.26}$$

This equation is represented in Figures 4.15 and Figure 4.16 for the 160mm nominal diameter pipeline and the 90mm nominal diameter pipeline respectively. The graphs are produced in the same way as that for the thermistors (Section 4.5.4.3).

The equation used to calculate the *in situ* concentration from the load values is given by

$$C_{vt} = \frac{L}{9.81(\rho_s - \rho_w)A} \tag{4.27}$$

where

L - pipeline weight per metre length

A - pipe area.

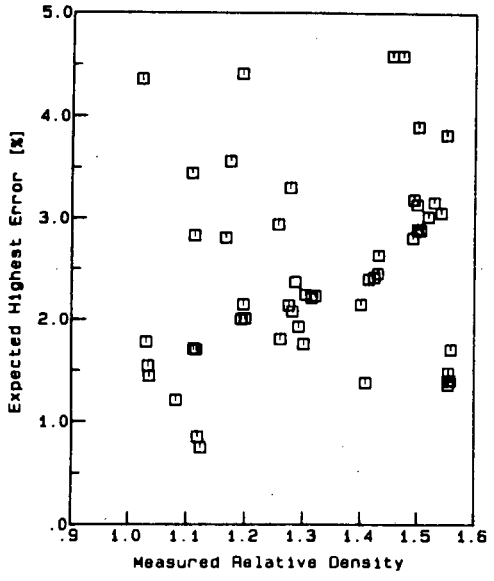

Figure 4.14(a)

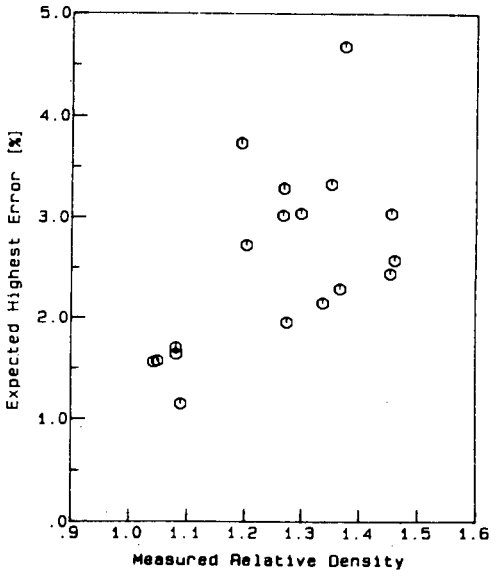

Figure 4.14(b)

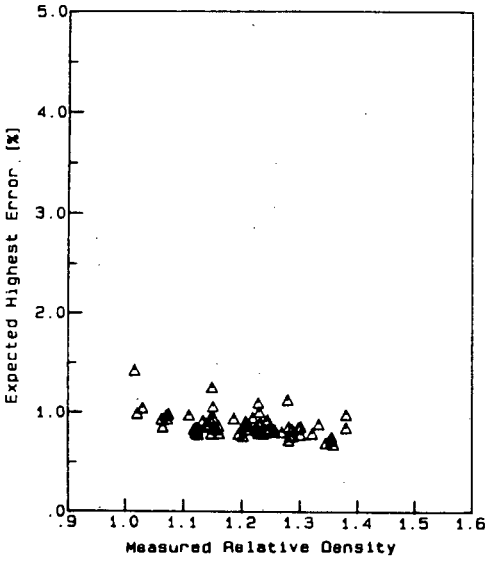

Figure 4.14(c)

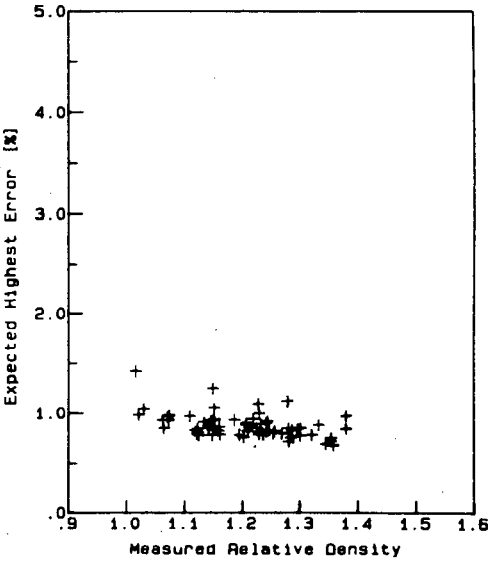

Figure 4.14(d)

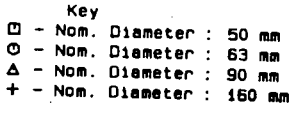

Figure 4.14 : Error graph for delivered mixture relative density.

CHAPTER 5

EXPERIMENTAL RESULTS

INTRODUCTION

An important aspect in the verification of an analytical model is the availability of a large, reliable data base for comparison with analytical predictions. Data used for this verification were derived from two sources:

1. Local data, presented in Volume 3 and produced at the University of Cape Town.
2. Imported data, presented in Appendix 6 and assembled from a survey of data produced at other test institutions.

The local data serves to provide the exact requirements to best verify the analytical model. The imported data serves to broaden and verify the available local data base.

This chapter is divided into the following sections :

5.1 Materials tested

5.2 Clear water tests

5.3 Test observations and discussion

5.4 Secondary measurements

5.5 Conclusions.

The data base of Volume 3 should be used as a reference to actual tests discussed.

5.1 MATERIALS TESTED

5.1.1 Coal Fired Power Station Ash

Coal fired power stations produce ash as a by-product of the combustion process. Two types of ash are produced by the boiler furnaces :

1. Clinker ash commonly referred to as bottom ash.
2. Fly ash.

Bottom ash is that portion of the coal ash that falls to the bottom of the boiler furnace. A high velocity, and vertically upward flowing, gas draught exists in the furnace. Consequently only large ash particles (with a top size of up to 25mm) which overcome this high velocity draught will fall to the bottom of the furnace. This ash constitutes 20% of the total ash production. Power stations have a grinding facility to process this ash prior to transportation.

Fly ash (constituting the remaining 80% of the production) is that portion that is fine enough to be taken with the high velocity gases leaving the furnace. This ash is extracted from the flue gases by mechanical or electrostatic precipitators denoted ash *fields*. Four ash fields exist collecting increasingly finer product.

Table 5.1 shows the average production quantities of a typical coal fired power station boiler. Fly ash derived from the precipitator of fields 1 and 3 as well as bottom ash was tested.

Table 5.1 : Average production quantities of ash and typical particle size for a coal fired power station boiler

	Clinker	Field 1	Field 2	Field 3	Field 4
%	20	64	12.8	2.6	0.4
Tonnes of ash per 100 tonne of coal	5	16	3.2	0.64	0.13
d_{50} (μm)	380	45	35	20	15

J M Galvin (1982) describes the ash used in tests at the University of Cape Town. The fly ash tested was obtained from the electrostatic precipitators of boiler units 3 and 5 at the Grootvlei Power Station[1].

Galvin (1982) reported a relative density of 2.2 for all fly ash samples. More accurate values have been used for calculation purposes. A close inspection of dry fly ash reveals particles ranging in colour from white to black. This could indicate a change in particle relative density, the black particles being unburned coal which has a relative density of 1.4 and the white particles being silica in the form of SiO_2 (quartzite) with a relative density of 2.65. The concept of a global relative density is therefore an approximation. The variation in particle relative densities can be taken into account by a careful investigation of particle size distribution only.

Bottom ash consists of pitted conglomerates of burnt ash and silica and, when dry, is loosely bonded and granular. Grains of "glass" form during the

[1]Located in the southern Transvaal coal fields of South Africa.

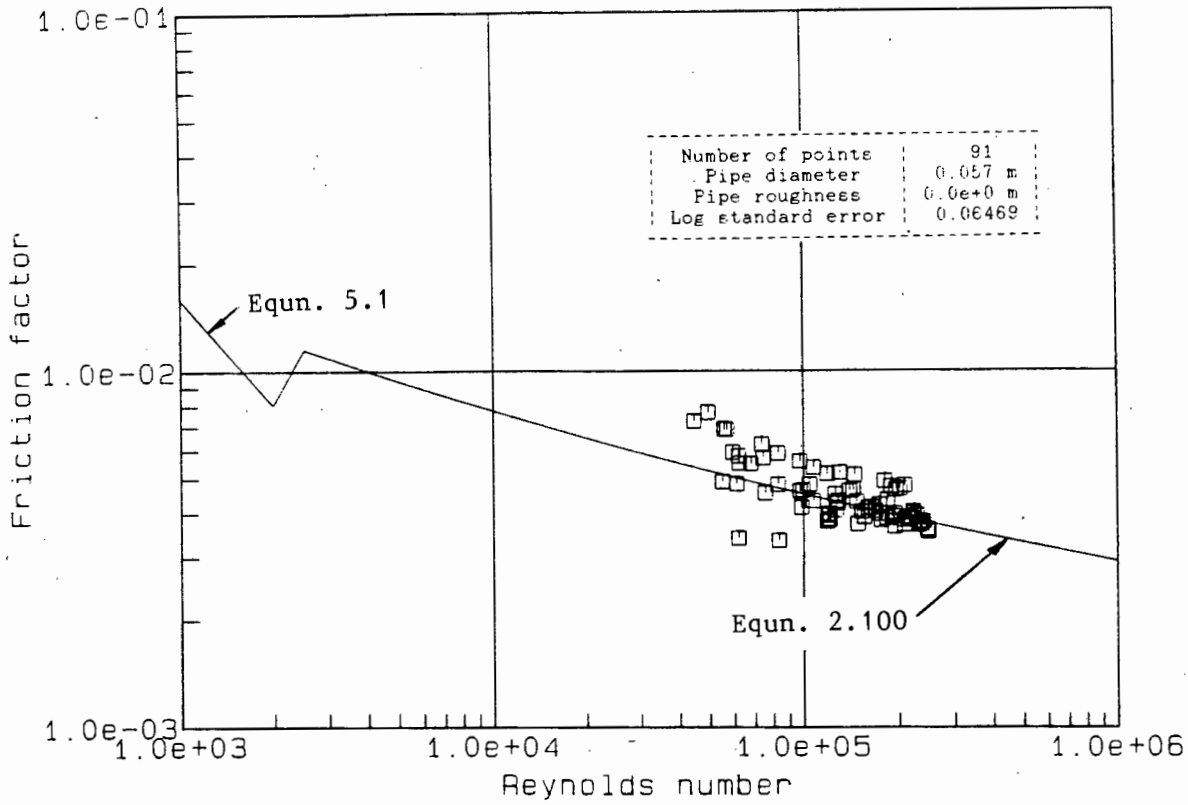

Figure 5.2 : Clear water test for 0.057 m diameter pipeline

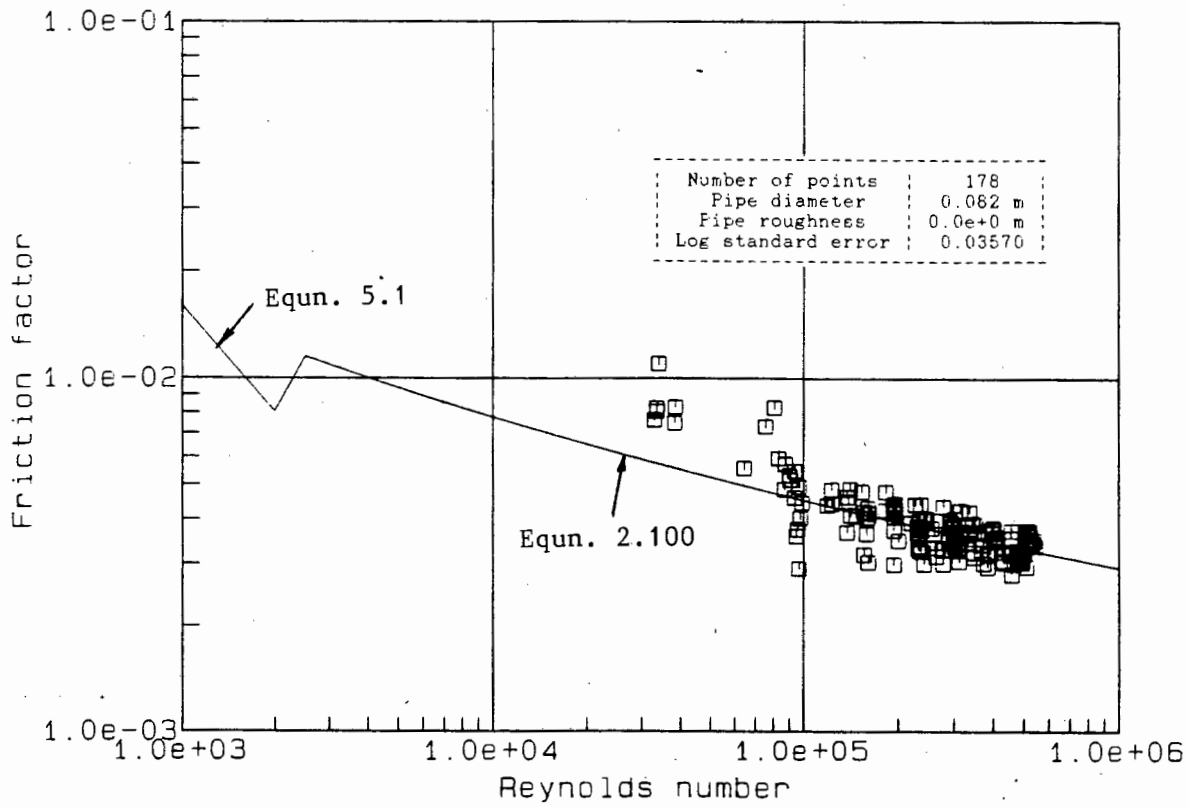

Figure 5.3 : Clear water test for 0.082 m diameter pipeline

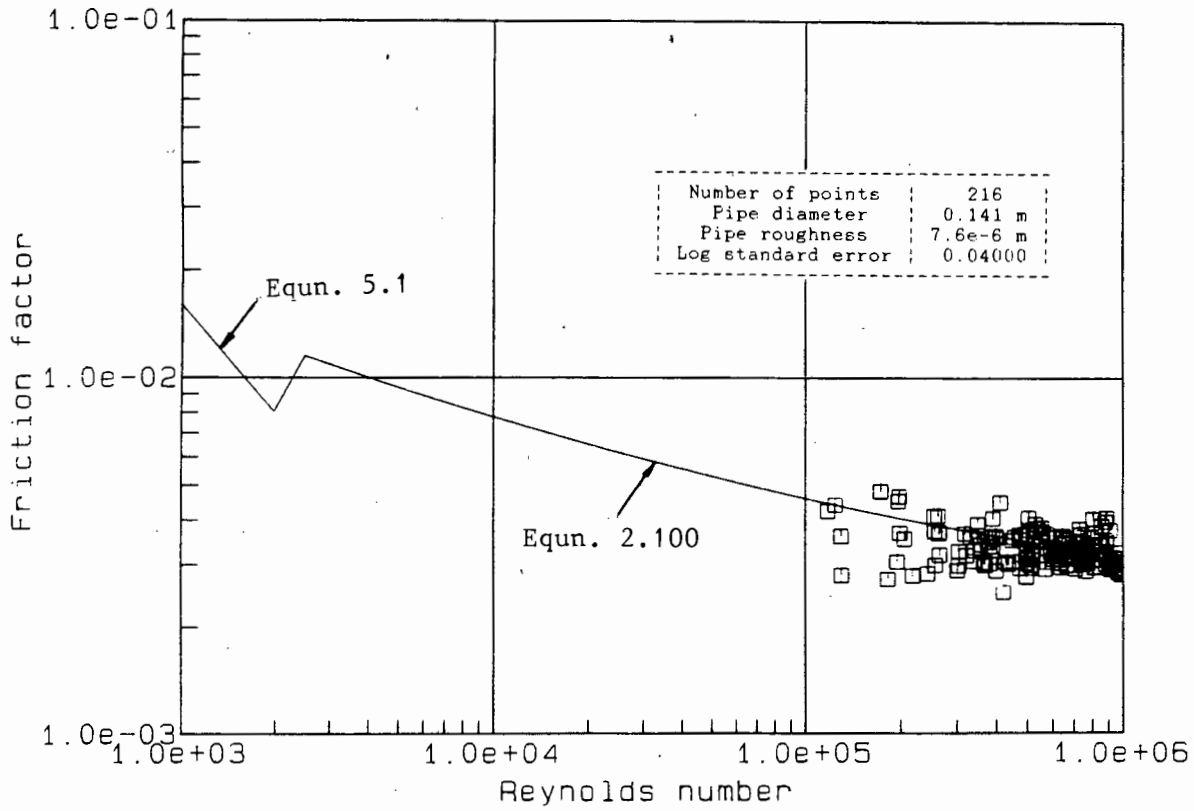

Figure 5.4 : Clear water test for 0.141 m diameter pipeline

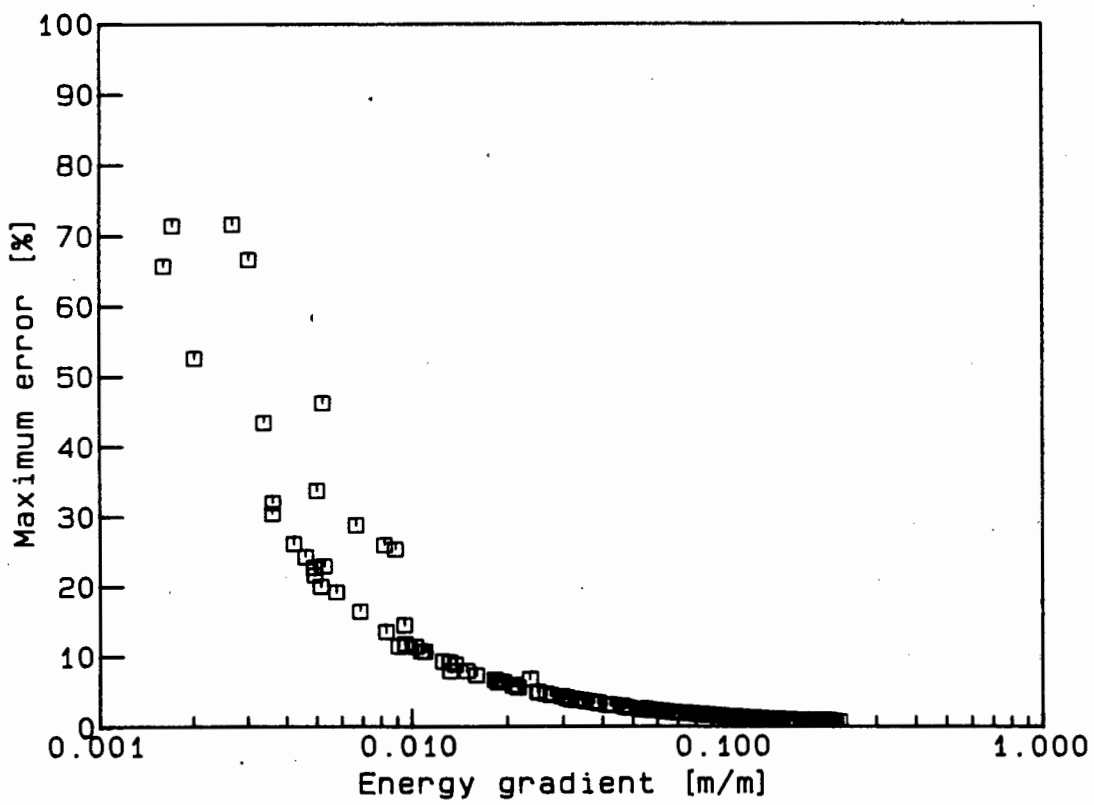

Figure 5.5 : Expected highest error for the clear water friction factor in the 0.1393m diameter pipe

The dark colour of the slurry made observations difficult but stationary bed flow was investigated for each test conducted. Periodic flow was apparent for all low velocity points although the flow features could not easily be seen.

5.3.1.2 Field 1 fly ash

Slurries of field 1 fly ash are considered to be mixed regime. Small lumps exist in the material due to its pozzolanic activity. The material had to be broken up prior to testing but some lumps persisted throughout the test program. The slurry is a two phase mixture made up of a heavy medium (vehicle) supporting suspended coarse particles. The rheologically active part of field 1 ash can be considered to be as field 3 ash.

Figure 5.6 shows energy gradient versus velocity graphs with delivered concentration as parameter. The graphs were generated from a concentration contour plot of the field 1 fly ash data. The data points have not been plotted for better clarity. The incipient stationary bed velocity decreases with decreasing concentration. No strong periodic flow was experienced in any test although weak, high frequency fluctuations were visible at high concentrations (above C_{vd} = 20%). The ash lumps could be seen settled on the pipe invert at the lowest velocities tested. These lumps may have caused a reduction in the flow area with an increase in the measured energy gradient at these low velocities.

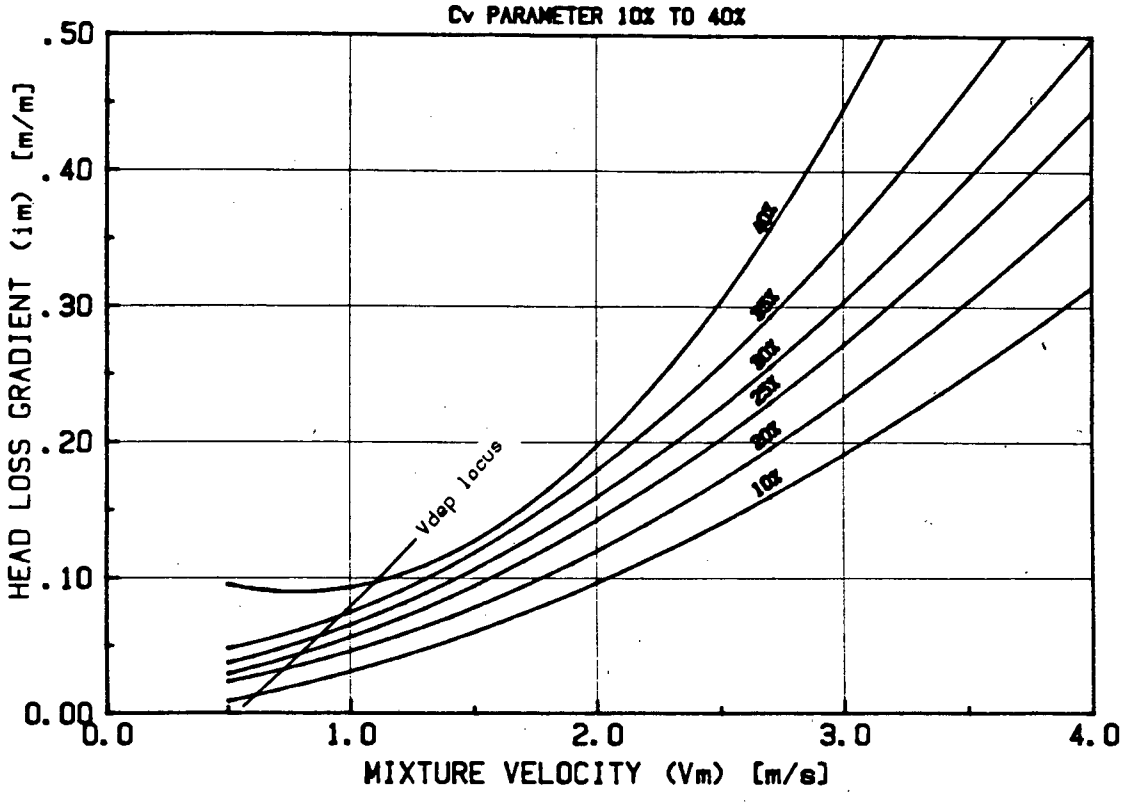

Figure 5.6(a) : Field 1 fly ash, 45.4mm diameter

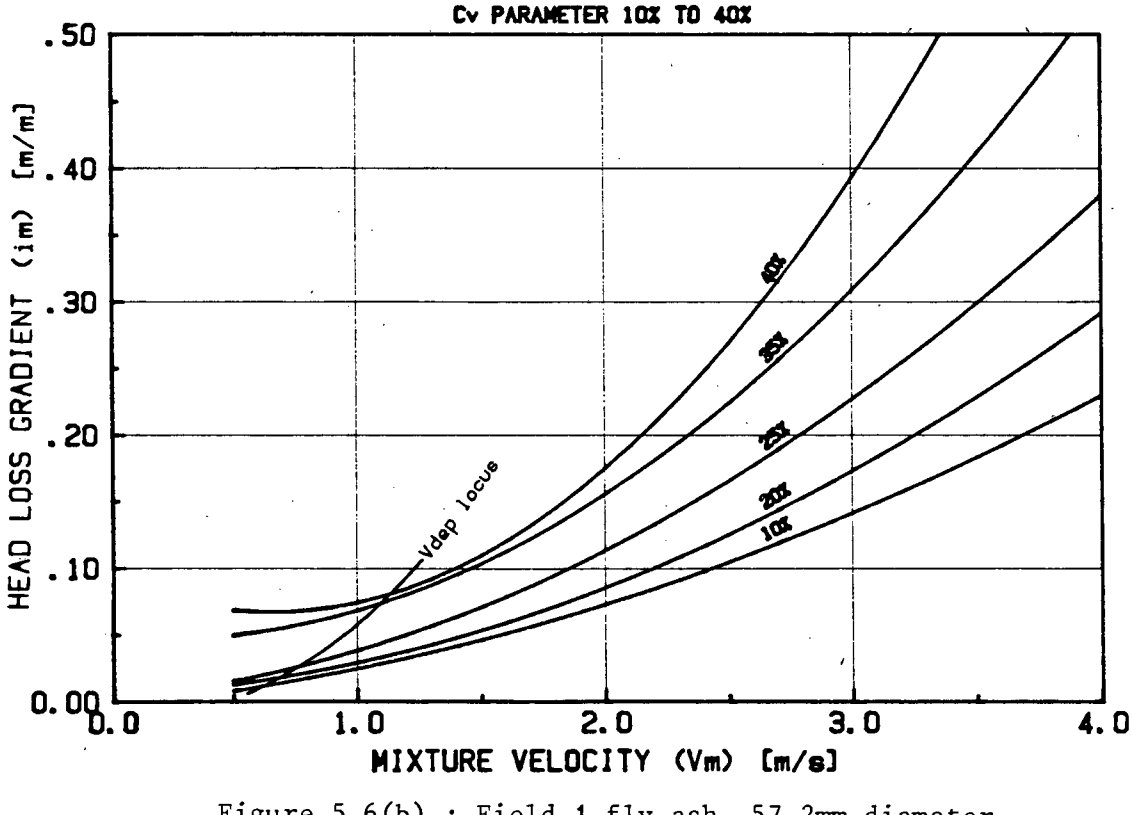

Figure 5.6(b) : Field 1 fly ash, 57.2mm diameter

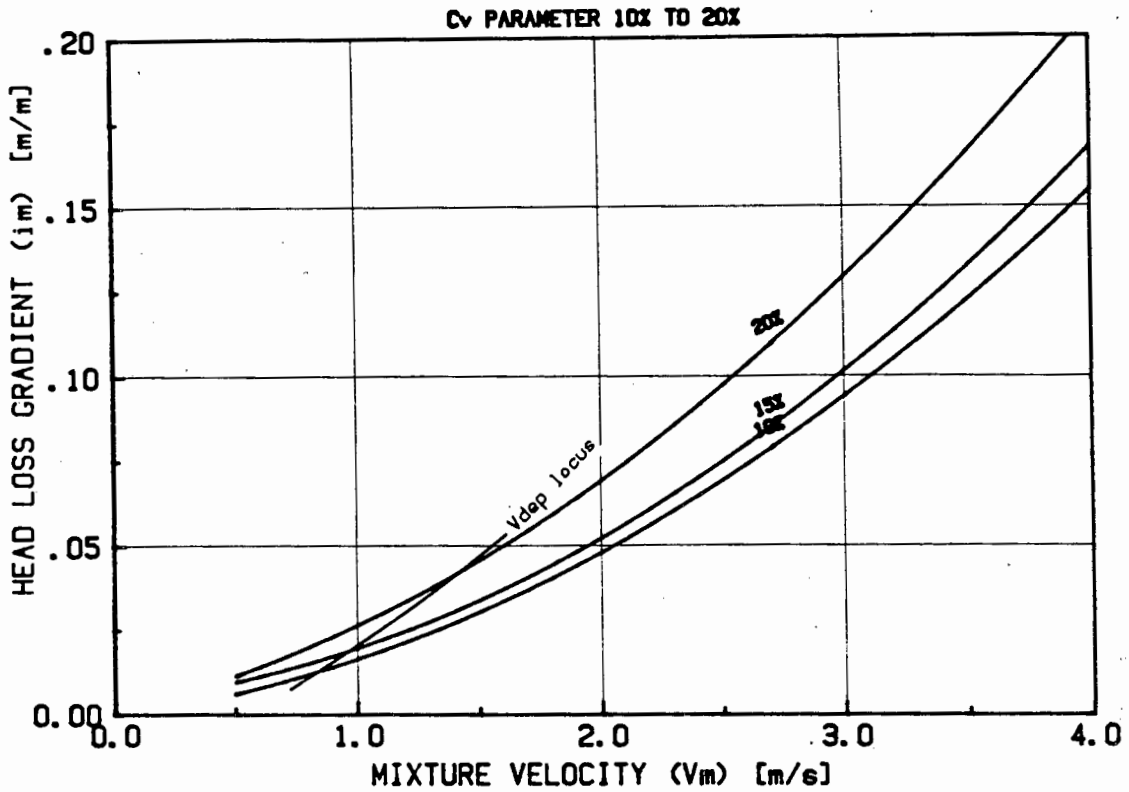

Figure 5.6(c) : Field 1 fly ash, 81.5mm diameter

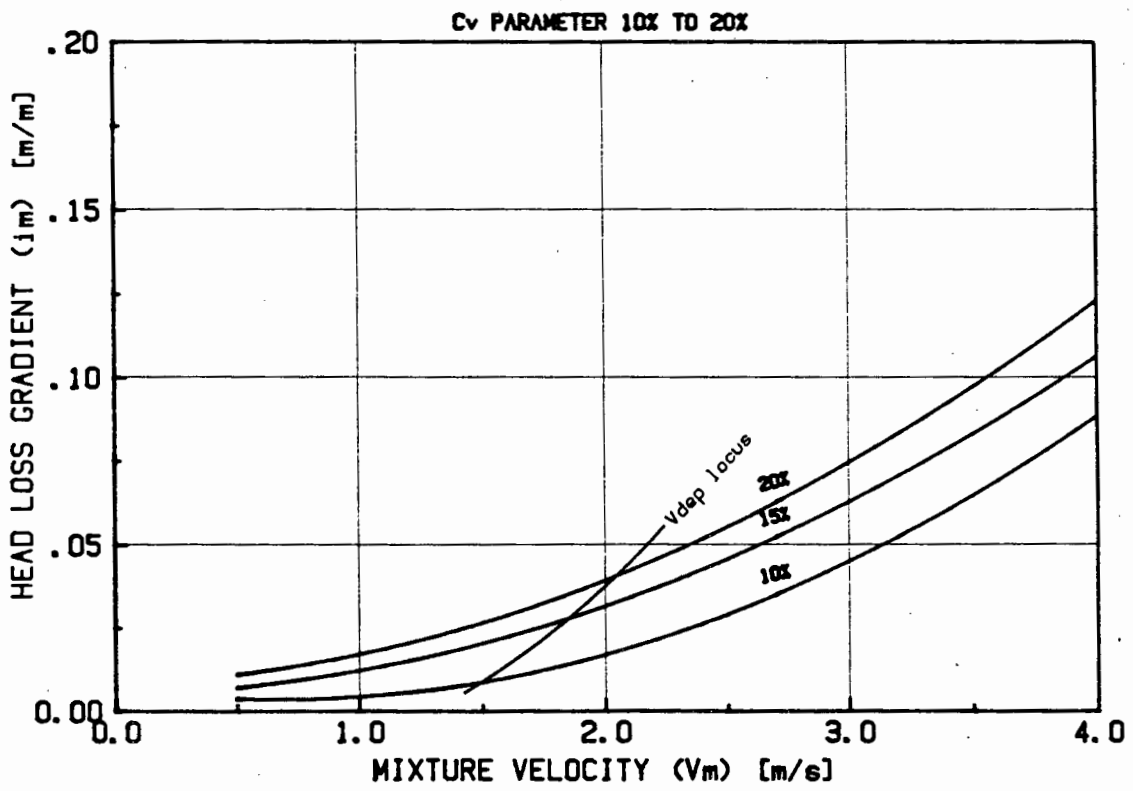

Figure 5.6(d) : Field 1 fly ash, 141.7mm diameter

5.3.1.3 **Field 3 fly ash**

Slurries of field 3 fly ash are considered non settling and pseudo-homogeneous. Small lumps did exist in the material due to its pozzolanic activity as for the field 1 ash. The material had to be broken up prior to testing and some lumps persisted throughout the test program.

Figure 5.7 shows energy gradient versus mean mixture velocity with delivered concentration as parameter. The graphs were generated from a concentration contour plot of the field 3 fly ash data. The data points have not been plotted for better clarity. Fly ash slurries characteristically have a low yield stress and so the energy gradient should approach zero as the velocity is reduced. The apparent increase shown in energy gradient at velocities of 0.5 m/s in Figure 5.7, is therefore ascribed to the reduction in flow area due to the lumps. Any analytical analysis of this fly ash slurry will therefore underpredict at low velocities because no information on the lump size could be obtained and therefore no information is contained in the particle size distribution. For the field 3 ash no periodic phenomena were apparent.

5.3.2 <u>Ocean Bed Material</u>

The ocean bed material tested comprised rounded pebbles and shell material. The shell material was rapidly ground to form a fine 'clay'. All tests were conducted once the shell had been ground to fines, to ensure a constant particle size distribution during the tests. A slurry concentration of around 12% by volume (delivered) was tested because this is representative of the commercial pipeline application envisaged.

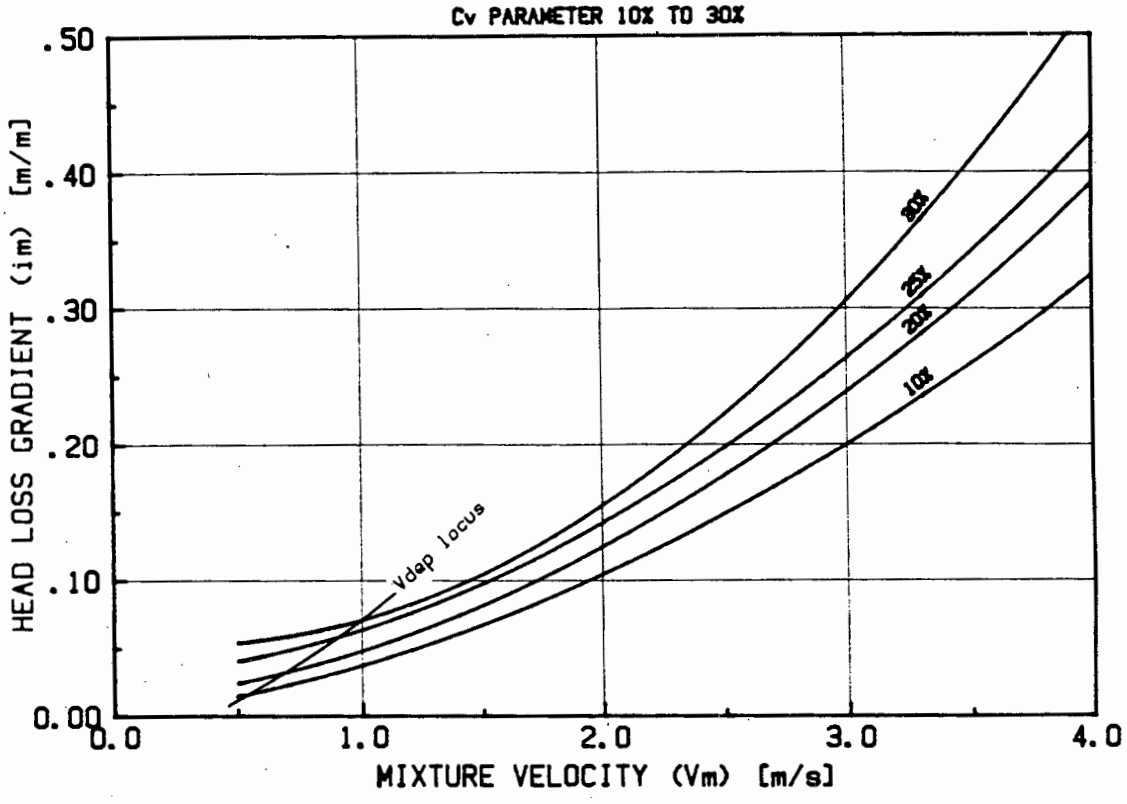

Figure 5.7(a) : Field 3 fly ash, 45.4mm diameter

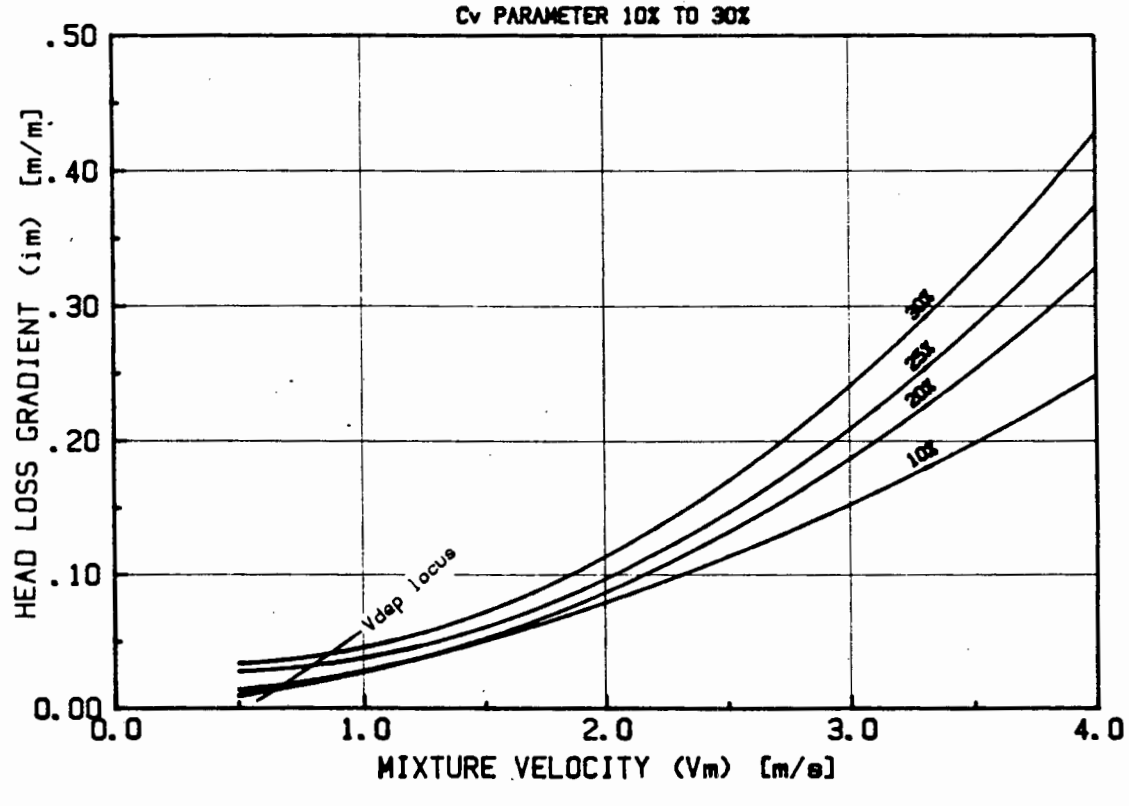

Figure 5.7(b) : Field 3 fly ash, 57.2mm diameter

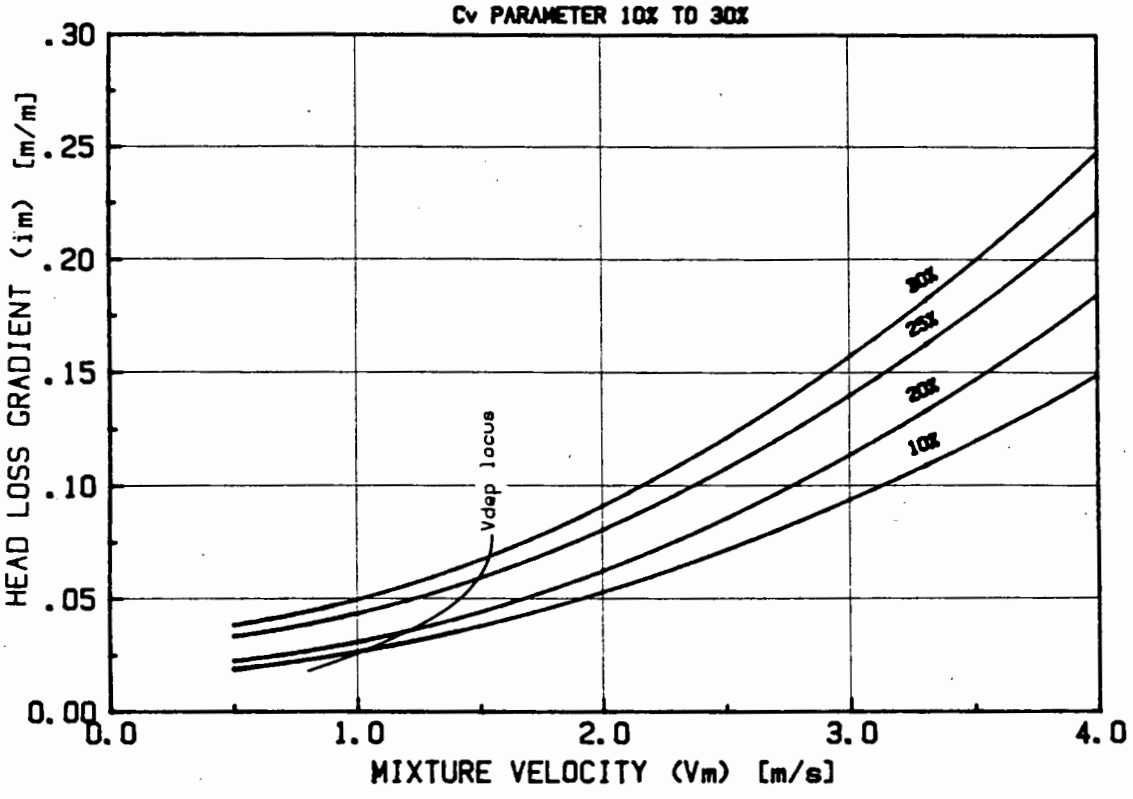

Figure 5.7(c) : Field 3 fly ash, 81.8mm diameter

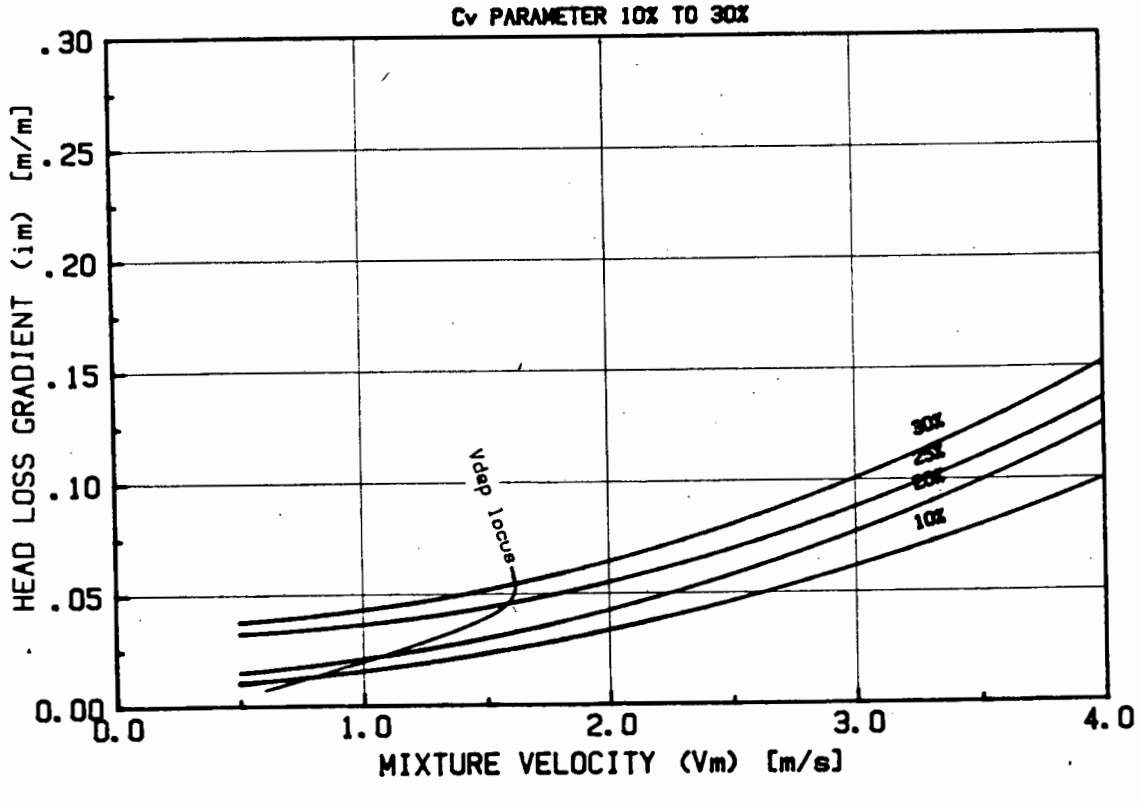

Figure 5.7(d) : Field 3 fly ash, 141.7mm diameter

The slurry is highly heterogeneous with a sliding bed existing up to the highest velocity tested ($\simeq$ 6 m/s). The energy gradient is approximately constant for the velocity range 2 m/s to 5 m/s after which it becomes parallel to the clear water curve and approximates the pseudofluid curve.

5.3.3 Uranium Mine Tailings

Uranium mine tailings slurries with three different particle size distribution were tested. All slurries were considered to be of the mixed regime type. At delivered volumetric concentrations of above 30% the energy gradient, velocity curve is relatively flat showing no change in energy gradient between 0.5 m/s and 2.5 m/s. Flow observations were made difficult by the opacity of the high concentration mixtures tested. No stationary bed deposit was evident since a bed deposit probe registered movement at all velocities tested. Highly periodic flow was experienced which on several occasions resulted in pipeline blockages. The blockages were probably caused by a mismatch in the pump and pipeline characteristics. The periodic phenomenon was considered to be slug flow.

5.3.4 Kaolin Clay

Kaolin clay slurries show highly non Newtonian flow characteristics in laminar flow (Slatter, (1986)). The slurries tested all showed characteristic floc structures[4] in the delivery hopper prior to starting the pump. The concentrations tested were the highest achievable for two reasons :

1. the kaolin was received as a filter cake and had a high moisture content.

---

[4]The interface between the settled clay and supernatent liquid showed a 'cracked' surface with agglomerations of particles.

2. the high yield stress made mixing in the tank difficult and limited the stirring action of the return line.

All tests were conducted for turbulent flow. The floc structure may have been broken down by the turbulent action of the flow. At the lowest velocities tested (< 0.5 m/s) a sliding bed of impurities was visible (≃ 15mm wide, comprising fine black and grey particles).

5.3.5 Beach Sands

Flow regime maps for the two sand types tested are shown in Figures 5.8(a) and 5.8(b) for sand type 1 and in Figures 5.9(a) and 5.9(b) for sand type 2. Table 5.3 presents a description of the flow regime present in each region of Figures 5.8 and 5.9. These graphs were produced by plotting the experimental data on the required axes and ascribing a number, which corresponds to the prevalent flow condition, at the location of the data point. Lines are then drawn demarcating the areas in which a particular flow condition predominates. Figure 5.8 for sand type 1 shows the data plotted on the graphs. For the other graphs the data points have not been plotted to ensure better clarity.

Condition 4, described in Table 5.3, is a transition condition and was not clearly defined for type 2 sand. Velocities below 1 m/s were not tested so no flow descriptions are shown for this region. Figures 5.8 and 5.9 show clearly the relatively large areas in which periodic phenomena are prevalent (Regions 1b to 4 inclusive). An increase in concentration has the effect of stabilizing the mixture, reducing the periodic flow region and decreasing the velocity of transition to fully suspended flow. The transition from heterogeneous flow to pseudohomogeneous flow is a gradual

one that cannot be visualised. For this reason no transition line is shown in Figures 5.8 and 5.9.

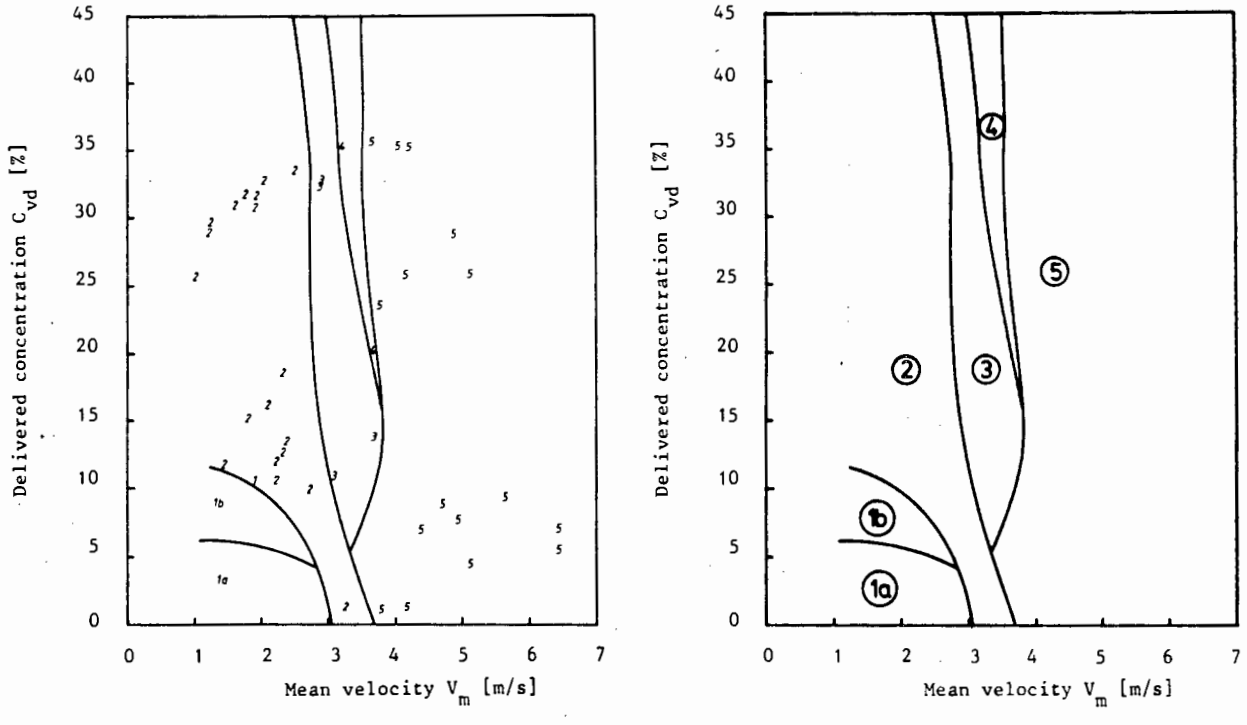

Figure 5.8(a) : Flow pattern map for sand type 1 in 90mm nominal diameter pipeline

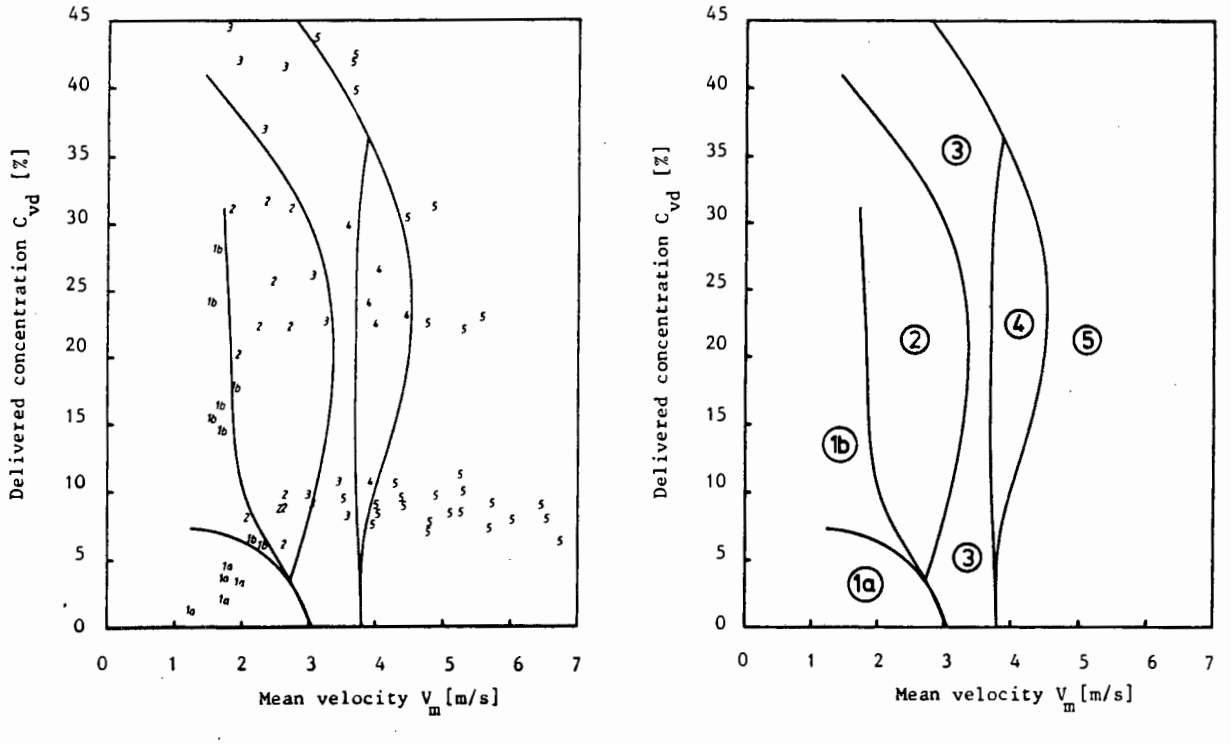

Figure 5.8(b) : Flow pattern map for sand type 1 in 160mm nominal diameter pipeline

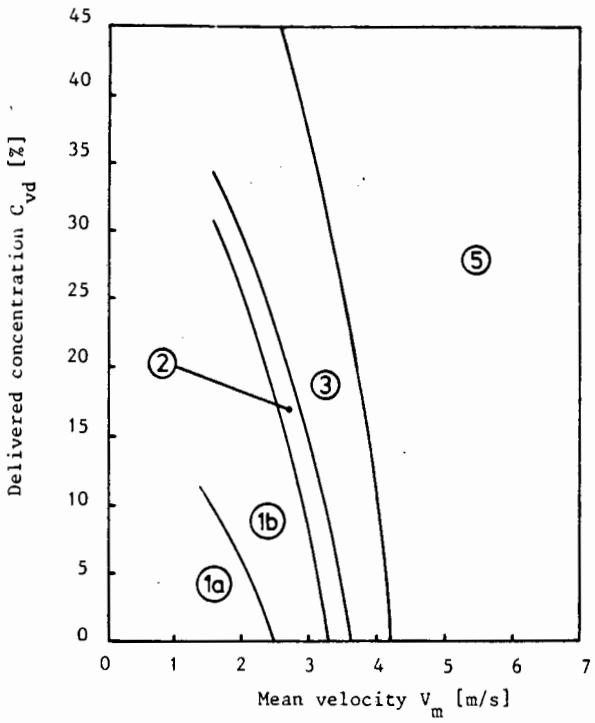

Figure 5.9(a) : Flow pattern map for sand type 2 in 90mm nominal diameter pipeline

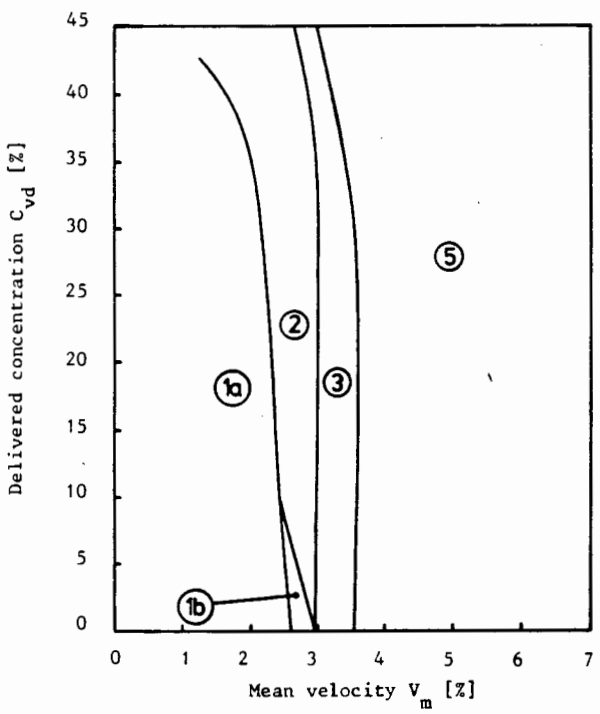

Figure 5.9(b) : Flow pattern map for sand type 2 in 160mm nominal diameter pipeline

Table 5.3 : Flow conditions for sand type 1 and 2 shown in Figures 5.8 and 5.9

Region Number	Condition description
1a	Stationary bed with slow variation in bed height caused by rolling and saltating particles. Dune lengths are of the order of several pipe diameters.
1b	As for 1a but bed slides as bed height reaches maximum then reforms as stationary bed and slides again as bed height reaches maximum.
2	Sliding bed flow with instantaneous stoppages occurring just after a wave or slug. The pulses (wave or slug) are of the order of one diameter long and are spaced several diameters apart.
3	Rhythmic periodic flow with no periods of stationary bed. May be waves or slugs.
4	Irregular fluctuations causing waves or slugs with interspersed heterogeneous flow.
5	Fully suspended smooth flow - heterogeneous or pseudo-homogeneous.

5.3.6 Kaolin-Sand Mixtures Prepared in the Laboratory

Kaolin clay was added to the beach sands tested to evaluate the following effects :

1. Increase in the maximum concentration pumpable.
2. Reduction in the strength and range of periodic phenomena.
3. Increase in the solid mass flow rate for the equivalent specific power consumption.
4. Reduction in the slip velocity of the coarse components.

The grading coefficient (d_{90}/d_{10}) calculated for each test is a measure of the fines content of a particular mixture. For low grading coefficients

($G_d \simeq 5$) the fines content is low and high ($G_d \simeq 300$) for high fines content. This value is limited in its application as demonstrated by the following example :

From Table 5.4 it can be seen that the two tests have similar average particle sizes (d_{50}) and grading coefficients (G_d) . The minimum particle sizes are significantly different. The effect of this on the mass flow of solids at equal head loss values is shown in Table 5.5.

Table 5.4 : Comparison of average particle size (d_{50}) and grading coefficient (G_d) for two tests

Test number	Material type	Grading coefficient	d_{50}	Particle size	
				Minimum	Maximum
KS31021A	Kaolin-sand	2.8	970µm	≃ 1 µm	≃ 2 mm
S1303317	Sand type 1	3.0	851µm	≃ 280 µm	≃ 2 mm

Table 5.5 : Mass flow rate values (M_s) for similar energy gradients for two different tests

KS31021A			S1303317		
i_m [m/m]	M_s [kg/s]	SEC $\left[\frac{Ws}{kg\ m}\right]$	i_m [m/m]	M_s [kg/s]	SEC $\left[\frac{Ws}{kg\ m}\right]$
0.400	10.0	12.51	0.380	6.09	19.58
0.134	2.2	5.48	0.136	1.6	5.60
0.130	3.6	4.50	0.131	2.7	4.47
0.113	1.2	4.88	0.108	0.53	32.57

The specific energy consumption was given in Chapter 1 by

$$SEC = \frac{i_m \, g}{C_{vd} \, S_s} \qquad [Ws/kgm] \quad . \qquad (1.1)$$

The sand type 1 results consistently show lower solid mass flow rates for similar or higher specific energy consumption values when compared to the kaolin-sand results. The only difference between the two tests is the finest size component, described in Table 5.4. The values of d_{50} and G_d are therefore limited in their application.

A second example comparing the solid mass flow rate and specific energy consumption for high concentration mixtures is shown in Tables 5.6 and 5.7.

Table 5.6 : Comparison of average particle size (d_{50}) and grading coefficient (G_d) for two tests

Test Number	Material type	Grading coefficient	d_{50} size
KS43619C	Kaolin-sand	5.4	490μm
S243012C	Sand type 2	6.1	425μm

Table 5.7 : Mass flow rate values (M_s) for similar energy gradient values with specific energy consumption as parameter

KS43619C			S243012C		
i_m [m/m]	M_s [kg/s]	SEC $\left[\frac{Ws}{kg\ m}\right]$	i_m [m/m]	M_s [kg/s]	SEC $\left[\frac{Ws}{kg\ m}\right]$
0.195	76.0	1.91	0.195	64.5	2.64
0.158	65.5	1.51	0.158	61.3	1.89
0.127	56.8	1.22	0.125	45.8	1.28

This second example confirms that the fine component, produced by the addition of kaolin, increases the carrying capacity of a particular mixture. The coarse fraction (Sand type 2) considered was similar in both tests as confirmed by the d_{50} particle size in Table 5.6.

Figures 5.10 and 5.11 show flow pattern maps for the kaolin-sand tests conducted in the 90mm nominal diameter pipeline and the 160mm nominal diameter pipeline respectively. These graphs were generated in the same way as those for sand types 1 and 2. The data points have not been plotted to ensure better clarity. These figures are presented only to show general trends since the average particle size changed for each test. Table 5.8 presents a description of the conditions encountered in each region. The condition 2 presented in Table 5.3 for Sand types 1 and 2 is divided into two separate regions 2a and 2b in Figure 5.10 and 5.11. This is as a result of the stabilizing effect of the fine component on the periodic flow phenomenon. At delivered concentrations of above 30% the sliding bed condition becomes a stable phenomenon. This is a distinct change from the type 1 and 2 sand tests which always demonstrated fluctuations.

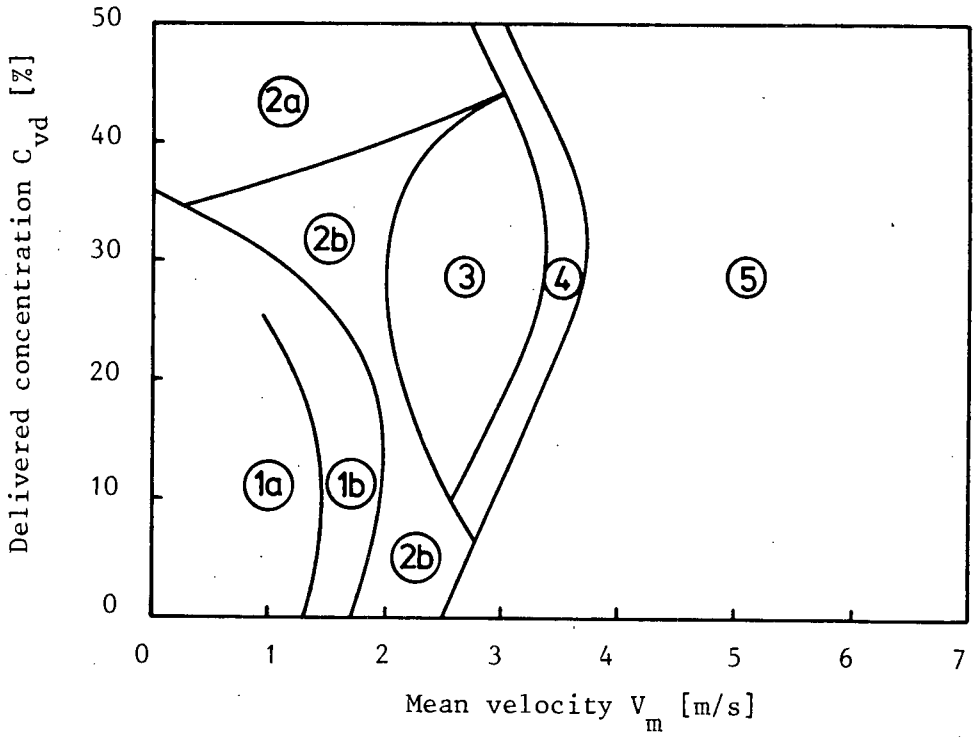

Figure 5.10 : Flow pattern map for kaolin-sand mixtures in 90mm nominal diameter pipeline derived from experimental data

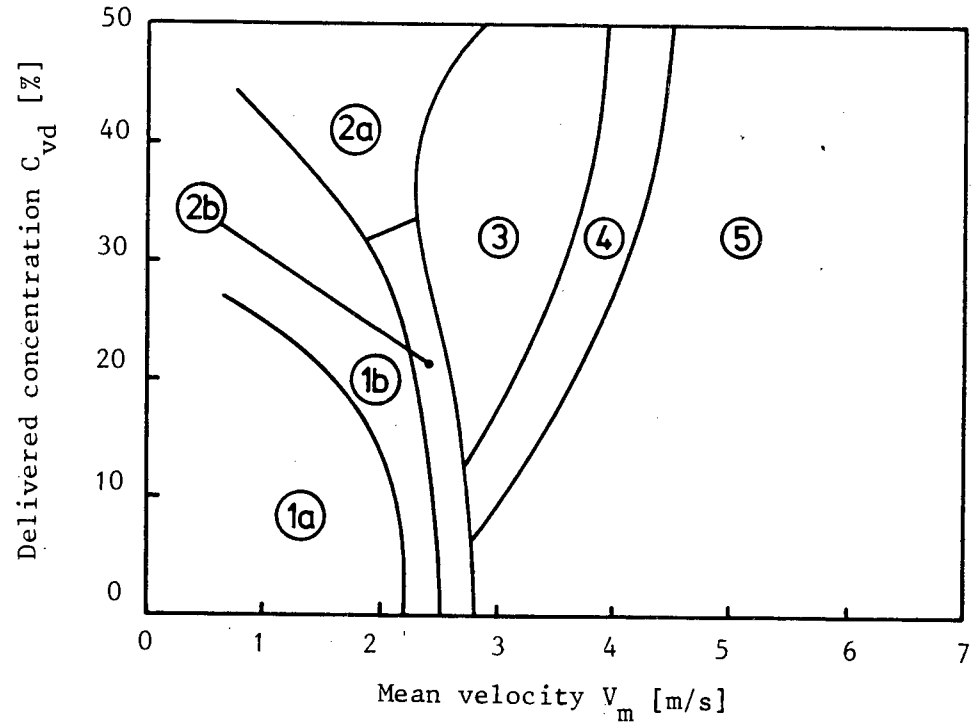

Figure 5.11 : Flow pattern map for kaolin-sand mixtures in 160mm nominal diameter pipeline derived from experimental data

Table 5.8 : Flow condition descriptions for kaolin-sand tests

Region No.	Condition description
1a	As for condition 1a in Table 5.3
1b	As for condition 1b in Table 5.3
2a	Smooth sliding bed flow
2b	As for condition 2 in Table 5.3
3	As for condition 3 in Table 5.3
4	As for condition 4 in Table 5.3
5	As for condition 5 in Table 5.3

5.4 SECONDARY MEASUREMENTS

Various secondary measurements were made for each test conducted. These include

1. Pump characteristics.
2. Bed particle velocity.
3. Gamma ray density measurements in horizontal orientation.

The pump characteristic results are outside the scope of this thesis and therefore not included but the other two topics fulfil important roles in understanding the flow conditions encountered.

5.4.1 Bed Particle Velocity

The bed particle velocity was measured for the beach sand and the kaolin-sand mixtures only. The cross correlation technique used to measure the bed velocity (refer Appendix 2, Section 2.9.2) required several seconds

to make a single velocity measurement. For this reason only steady state flow conditions could be analysed. Figure 5.12 shows typical cross correlation output for test S1430068. Three correlations for decreasing mean velocity are shown. Figures 5.13 and 5.14 show some of the results obtained for kaolin-sand mixtures in the 160mm nominal diameter pipeline. Figure 5.15 show results obtained for the Sand type 2.

The bed velocity is directly related to the velocity profile. Figure 5.16 shows three velocity profiles based on the mixture concentration. All velocity profiles are for turbulent flow.

The trends in Figures 5.13 to 5.15 can be explained in the following way :

1. Figures 5.13, Low concentration kaolin-sand mixture

   For a low fines content the velocity profile for low concentration mixtures will approximate the turbulent logarithmic velocity profile shown in Figure 5.16(a). For a high fines content the von Karman constant would be reduced resulting in a more conical velocity profile (Figure 5.16(b)) with an increase in the difference in the mean and bed velocity.

2. Figure 5.14, High concentration mixtures

   For high concentration mixtures of kaolin-sand the particle slip will be negligible so that the velocity profile experienced will be that shown in Figure 5.16(c). For the Sand types 1 and 2 the bed concentration will decrease with increasing velocity resulting in increasing particle slip. The larger particles (Sand type 1) will have a greater slip component.

3. Figure 5.15, Sand type 2 mixtures

Figure 5.15 shows a decrease in the slip value for increasing concentration and velocity. For low concentration mixtures the slip remains constant at all velocities. The velocity effect is largest for the highest concentration tested. The velocity distribution is of the type shown in Figure 5.16(a).

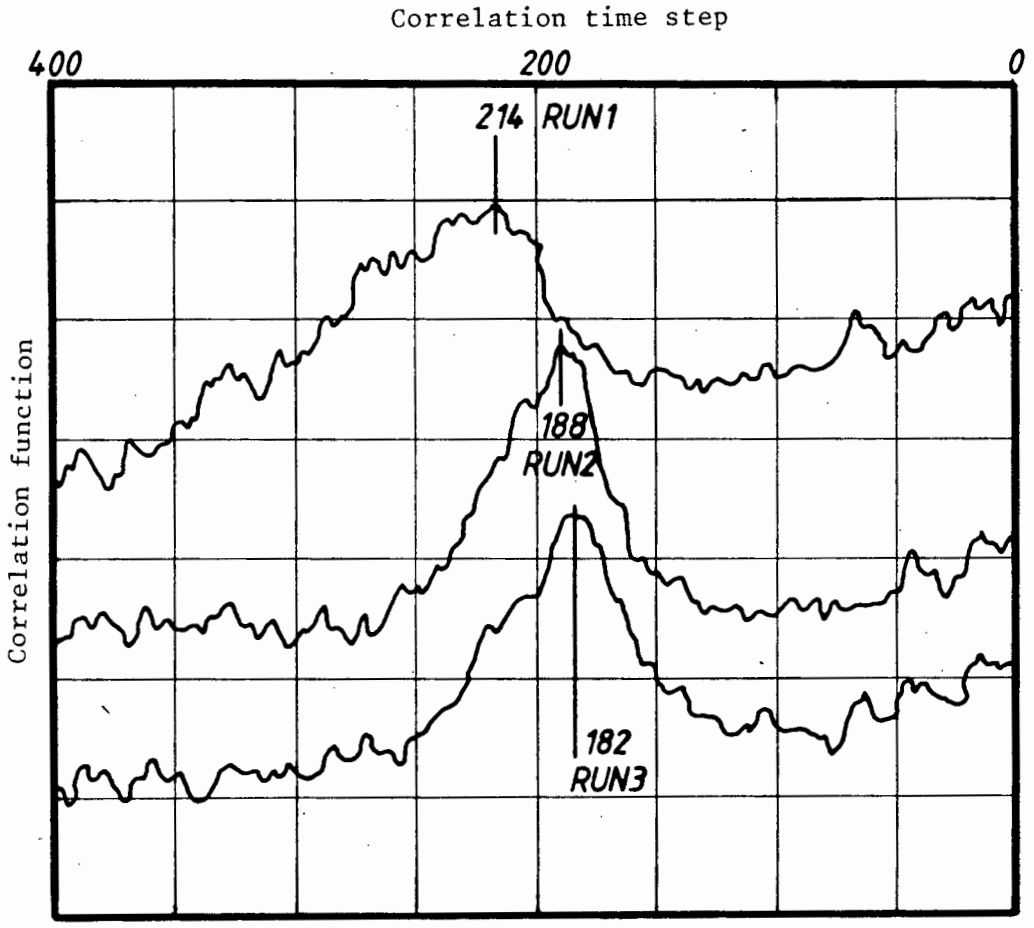

Figure 5.12 :
Cross correlation output for test S1430068. The horizontal axis is divided into 400 points. The numbers shown (i.e. 214 for RUN1) is the point at which maximum correlation occurred. The step length was set at 50μs so the delay between the two noise signals is 214*50 = 0.0107 sec.
The distance travelled (between probes) is 19.65mm so V_b = 1.84 m/s.

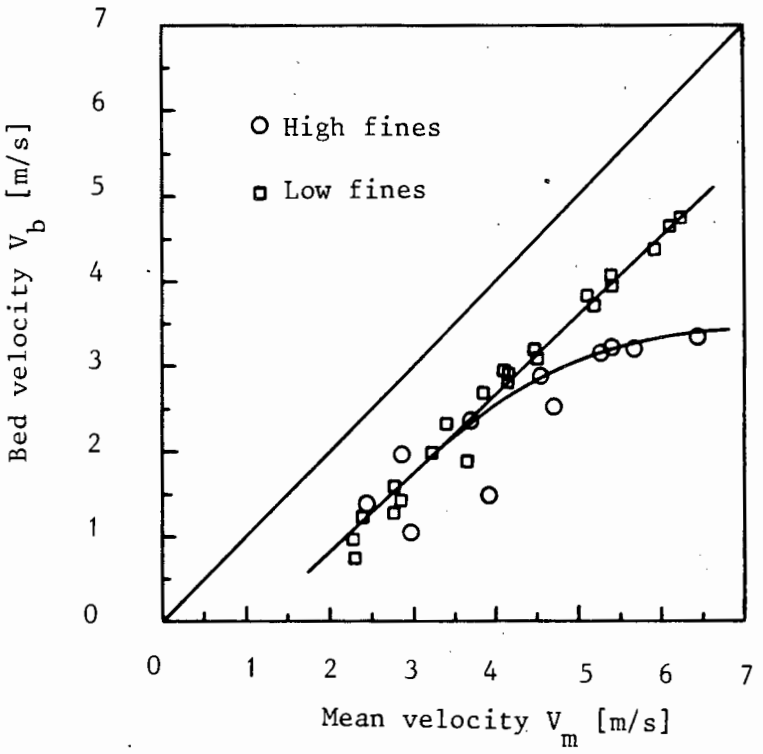

Figure 5.13 : Low concentration (C_{vd} < 10%) kaolin-sand mixture bed velocity versus mean velocity

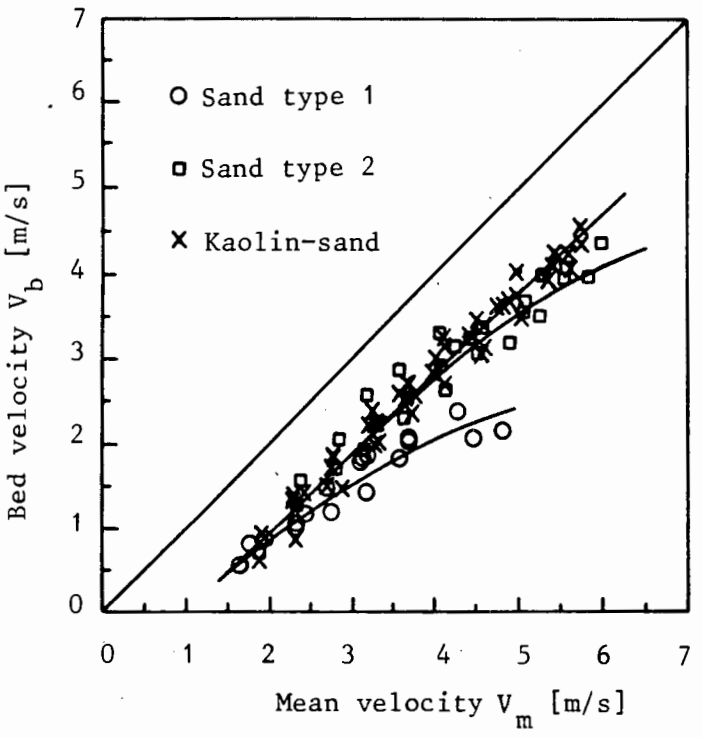

Figure 5.14 : Bed velocity versus mean velocity for high concentration mixtures (C_{vd} > 30%)

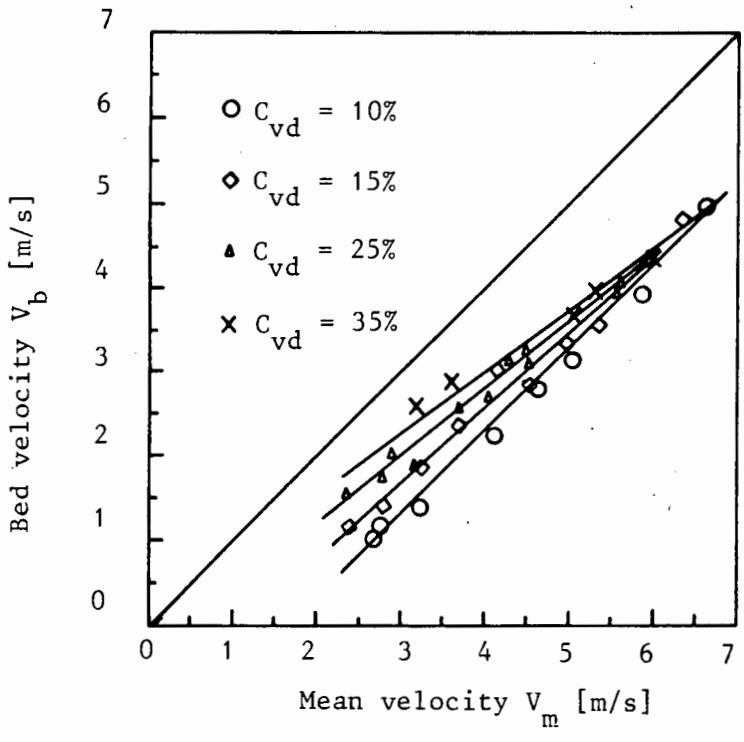

Figure 5.15 : Bed velocity versus mean velocity for Sand type 2 mixtures with concentration as parameter

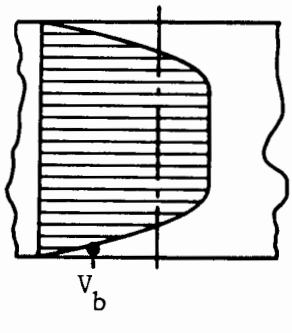

Figure 5.16(a) : Logarithmic velocity distribution $\kappa \simeq 0.4$

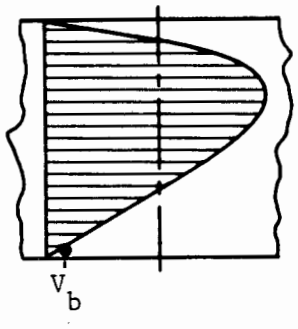

Figure 5.16(b) : Logarithmic velocity distribution $\kappa \simeq 0.25$ with asymmetric concentration distribution

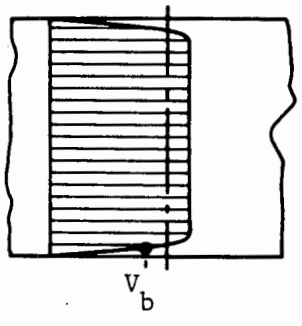

Figure 5.16(c) : *Plug* flow velocity distribution associated with high concentration mixtures

Figure 5.16 : Idealised velocity profiles based on mixture concentration

5.4.2 Horizontally Oriented Gamma Ray Densitometer

Manufacturers of gamma ray densitometer equipment specify in their applications brochure that gamma ray equipment should only be installed in vertical pipelines where no stratification occurs. This limitation can be used to advantage if stratification and the conditions under which it occur are sought. Figure 5.17 shows a layout sketch for the gamma ray densitometer used.

Figure 5.18 and Table 5.9 present some of the gamma ray densitometer results produced. The *in situ* concentration measured by the suspended pipeline is

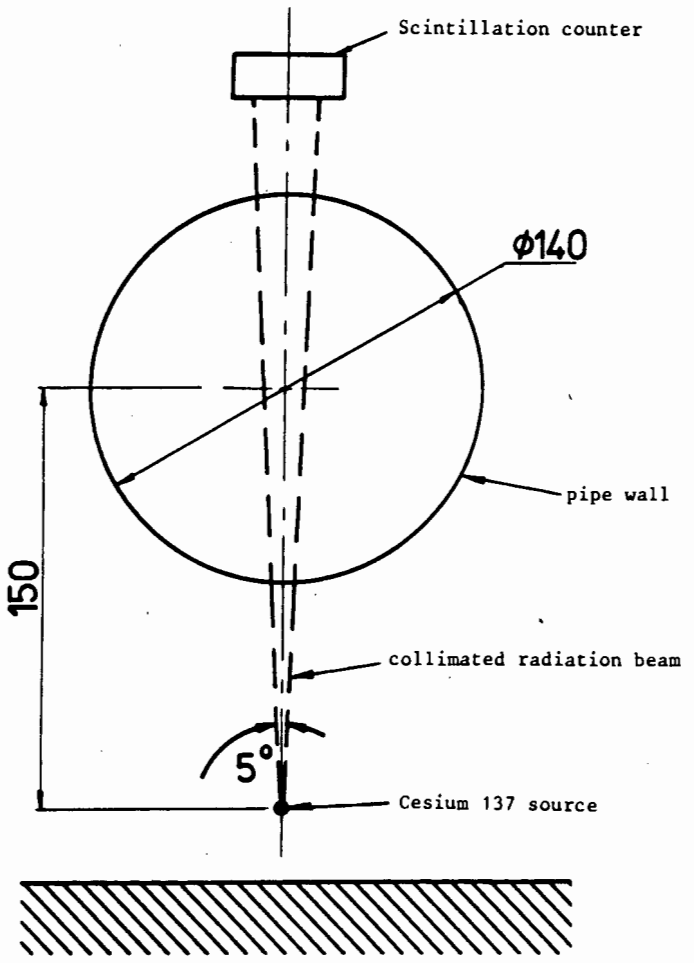

Figure 5.17 : Layout sketch of gamma ray densitometer

used for comparison. Any deviation of the gamma ray measurements from the suspended pipeline measurements can be ascribed to either stratification or experimental error. The deviations presented in Figure 5.18 are considered too large to be accountable to error alone. Stratification of the transported mixture would account for the deviation.

Figure 5.19 shows two possible flow conditions. For Figure 5.19(a) the two *in situ* concentration values would be equal but for Figure 5.19(b) the gamma ray density measurement would always be greater than the suspended pipeline measurement. Figure 5.18 confirms this since all points lie above or on the line of equal concentration.

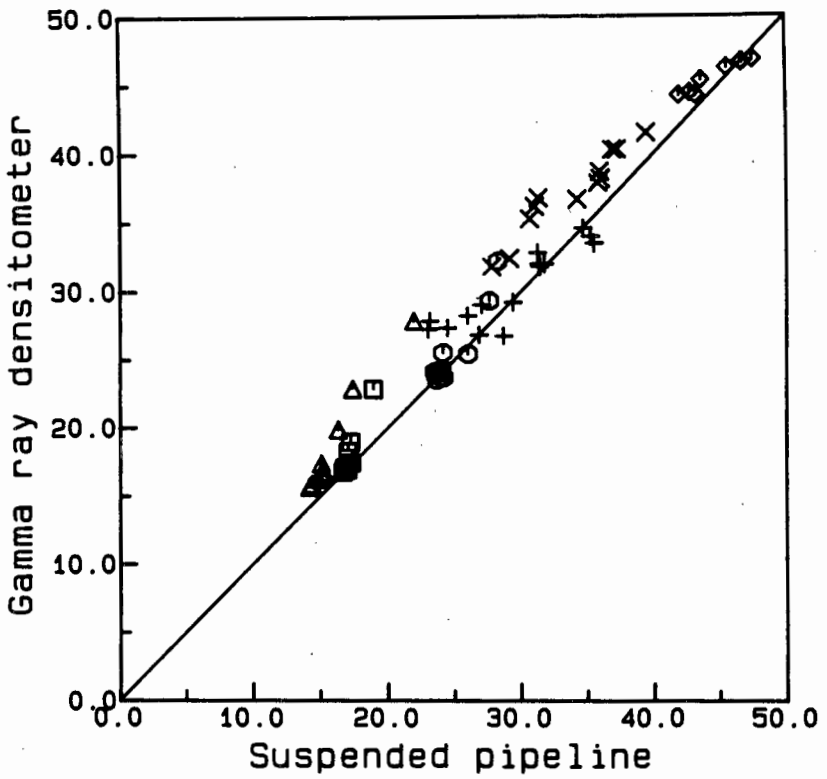

Figure 5.18 : *In situ* concentration for gamma ray densitometer versus suspended pipeline (C_{vt} given as a percentage)

Table 5.9 : *In situ* concentration results for gamma ray densitometer and suspended pipeline (160mm nominal diameter)

□ TEST NUMBER : KS42003A

Vm m/s	Cvt %	Cvt-Gamma %
1.837	18.90	22.85
2.439	17.20	18.95
2.733	17.02	18.25
3.340	16.81	17.05
3.580	16.75	17.05
3.933	17.26	17.45
4.107	16.71	16.95
4.490	16.97	17.15
4.881	16.63	16.75
5.486	16.96	16.95
6.289	16.95	16.95

○ TEST NUMBER : KS42106A

Vm m/s	Cvt %	Cvt-Gamma %
1.443	28.25	32.25
1.971	27.62	29.35
2.336	24.12	25.55
2.872	26.02	25.45
3.184	23.57	23.95
3.769	24.18	23.75
4.441	24.03	24.35
4.556	23.98	23.75
5.131	23.49	24.15
5.493	23.66	23.55
5.887	23.78	24.15

△ TEST NUMBER : KS415309

Vm m/s	Cvt %	Cvt-Gamma %
1.423	21.93	27.85
1.873	17.35	22.85
2.320	16.27	19.85
2.791	15.03	17.35
3.217	15.01	16.65
3.651	14.80	16.25
4.113	15.08	16.45
4.483	14.34	15.85
5.129	15.12	16.45
5.413	14.16	15.65
5.956	15.31	16.55
6.338	15.09	16.55

+ TEST NUMBER : S1415018

Vm m/s	Cvt %	Cvt-Gamma %
1.527	34.69	34.65
1.654	35.25	34.05
1.699	35.50	33.55
1.850	31.26	32.85
1.927	31.79	32.05
2.257	31.42	31.85
2.274	31.36	32.05
2.595	27.03	29.05
3.162	29.42	29.25
3.847	26.83	26.85
4.001	28.66	26.75
4.461	24.46	27.35
4.784	26.00	28.25
5.300	23.13	27.85
5.524	23.01	27.25

× TEST NUMBER : S1430068

Vm m/s	Cvt %	Cvt-Gamma %
1.530	39.47	41.55
1.657	36.90	40.35
1.874	37.26	40.35
2.332	35.96	38.75
2.336	36.02	38.25
2.437	35.83	37.95
2.754	34.28	36.75
3.190	29.17	32.45
3.576	31.35	36.85
4.047	27.81	31.85
4.475	31.07	36.25
4.832	30.69	35.35

◇ TEST NUMBER : S1435148

Vm m/s	Cvt %	Cvt-Gamma %
1.786	47.53	46.85
1.963	46.74	46.65
2.301	46.66	46.65
2.689	45.57	46.25
3.117	43.64	45.35
3.659	42.79	44.45
3.673	41.96	44.25
3.679	43.25	44.25

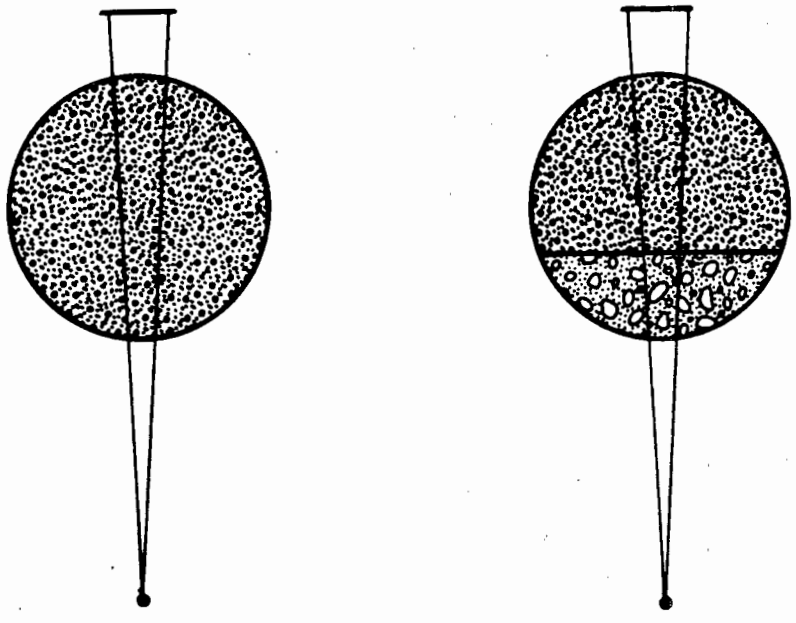

(a) homogeneous flow

(b) bed load flow either sliding or stationary

Figure 5.19 : Possible flow scenarios for gamma ray densitometer results presented in Figure 5.18 and Table 5.9

1. Sand Type 2

For the beach sand tests stratification would disappear both with increasing velocity and concentration. Although some scatter exists in the data shown in Figure 5.18 these general trends are discernible. The scatter can be ascribed to the highly periodic flow that exists for much of the range of the results shown. The gamma ray densitometer employs integrating circuitry that would *smooth* the output from the device. The suspended pipeline output was read over a period of time to develop an average value. These two ways of generating *in situ* concentration values could account for the scatter. Figure 5.19(b) would be considered applicable to the flow of Sand type 2 slurries.

2. Kaolin-Sand Mixtures

The kaolin-sand results show very clear trends in Figure 5.18. The fines in the slurry tend to stabilize the periodic flow phenomenon. At low velocities the gamma ray densitometer results are higher than the suspended pipeline values. This condition is shown in Figure 5.19(b) as before.

The gamma ray densitometer operates by measuring a reduction in radiation due to attenuation of the collimated beam as it passes through the mixture. For stratified flow the concentration of the mixture contained in the region of the beam is higher than the overall concentration. Duckworth *et al.* (1985) presented a mathematical method for correcting the concentration measurements made using gamma ray densitometers in stratified flow. Appendix 8 contains an extract from Duckworth *et al.* (1985) presenting this method.

5.5 CONCLUSIONS

This chapter presents a comprehensive data base of the industrial and laboratory fabricated slurries tested. The following conclusions can be drawn :

1. The polyvinyl chloride pipes used can be considered essentially smooth walled.

2. The clear water tests conducted at intervals during the test program are consistent with expected theory confirming the operation of transducers.

3. Bottom ash slurries are generally stratified and demonstrate periodic flow for most velocities tested.

4. An inspection of the percentage retained curves show that the PSD for the fly ash tested is generally bimodal in character (Volume 3, p.13 and 84). The fly ash PSD is therefore well graded and will yield particles of widely varying settling velocity. This phenomenon will have a marked effect on the hydraulic characteristics of fly ash slurries and must be carefully considered.

5. The field 3 ash is considered non settling. 100% of the sample is rheologically active and will be analysed as such. Although particles exist up to 200 μm in size, those above 40 μm constitute a small proportion of the total sample and can be neglected in the analysis. Tests conducted in the viscometer confirm the non settling character of field 3 ash (Sive and Lazarus (1985)). The field 3 ash has an average particle size of 17 μm and a relative density of 2.233.

6. The field 1 ash is well graded. This ash forms a slurry which is considered to be in the mixed regime. Viscous as well as mechanistic effects prevail. The slurry is considered a two phase mixture made up of a heavy medium or *vehicle* supporting suspended coarse particles. The field 1 ash has an average particle size of 61 μm and a relative density of 2.269. The rheologically active part of the field 1 ash can be considered as field 3 ash. Field 1 ash slurries demonstrated periodic flow over a limited range at low velocity.

7. The ocean bed material was tested as a slurry with a volume concentration of 12%. The slurry remained in the sliding bed flow

regime up to the highest velocity tested ($\simeq$ 6 m/s). No periodic flow was evident.

8. Uranium mine tailings slurries were tested at high concentrations (C_{vd} = 35%). Highly periodic flow existed causing pipe blockages on several occasions. A stationary bed was never evident. The slurry is highly abrasive causing pipeline failures at bends and pipe joints.

9. The flocculated kaolin slurries tested produced a homogeneous mixture with impurities visible as a small sliding bed at velocities below 0.5 m/s.

10. Sand-water slurries demonstrate periodic flow over the velocity range in which particles form a bed, be it stationary or sliding.

11. Transition criteria (from one flow regime to another) occur at higher velocities for larger diameter pipelines. The effect is reduced with a decrease in particle diameter.

12. An increase in the fines content of a slurry has a stabilizing effect on periodic flow phenomena.

13. The minimum particle size is an important factor in determining slurry behaviour.

14. The addition of fine particles to a coarse particle slurry reduces the specific energy consumption (SEC) for an equivalent mass flow of solids.

15. At high concentration (above 30%), kaolin-sand slurries produce a stable sliding bed down to velocities below 0.5 m/s. This was not true for the beach sand slurries tested.

16. The bed velocity probe proved a successful instrument for use in the sliding and suspended flow regimes.

17. The bed velocity results show trends that can be predicted from an understanding of the velocity profile that exists in a pipeline.

18. A gamma ray densitometer mounted in a horizontal pipeline, with the beam passing vertically through the pipe, will overpredict the *in situ* concentration for stratified flow mixtures and can be used to determine the point at which stratification occurs.

PART 3 : EVALUATION

CHAPTER 6

COMPARISON OF EXISTING AND PROPOSED ANALYTICAL APPROACHES USING EXPERIMENTAL DATA

INTRODUCTION

The analytical component of this thesis, presented in Chapters 1 to 3, and the experimental component, presented in Chapters 4 and 5, can be used to complete the analysis of mixed regime slurries by comparing the results of the two components. Important aspects to consider are :

1. Energy gradient calculation.
2. Bed condition prediction be it stationary, sliding with interfacial wave phenomena, or suspended flow.
3. *In situ* concentration.
4. Concentration and velocity profiles.

In Chapter 2 various models were proposed for the vehicle of a mixed regime slurry. Evaluation of the vehicle prediction equations can now be achieved. Topics to be considered are :

1. Newtonian and yield pseudoplastic rheologies.
2. Colebrook-White and Torrence friction factor correlations for the vehicle.
3. Particle suspension models.

These different approaches can now be compared and a choice made as to the most successful, based on the correlation of experimental data.

The chapter concludes with system designs using the proposed analytical model for two flow conditions :

1. Constant mass flow of solids.
2. Constant delivered concentration.

6.1 COMPARISON OF CORRELATION ERRORS

A graphical and an analytical technique are used to compare the errors between experimentally determined and analytically derived values.

A graphical presentation is shown in Figure 6.1 for observed energy gradient versus calculated energy gradient. The calculated energy gradient is derived from a pseudofluid approximation which is used for example only.

The most meaningful analytical comparison was considered by Lazarus and Nielson (1978) to be a log standard error rather than a correlation coefficient. The equation used is given by

$$S = \sqrt{\frac{\sum_{i=1}^{n} [\log(\text{observed}) - \log(\text{calculated})]^2}{(n - 1)}} \qquad (6.1)$$

where S is the root mean square deviation of the log of observed points from the log of calculated points.

Figure 6.2 shows the value of S in the logarithmic domain and its transformation into the linear domain. The value ϵ is the expected average error above (positive) and below (negative) the actual value.

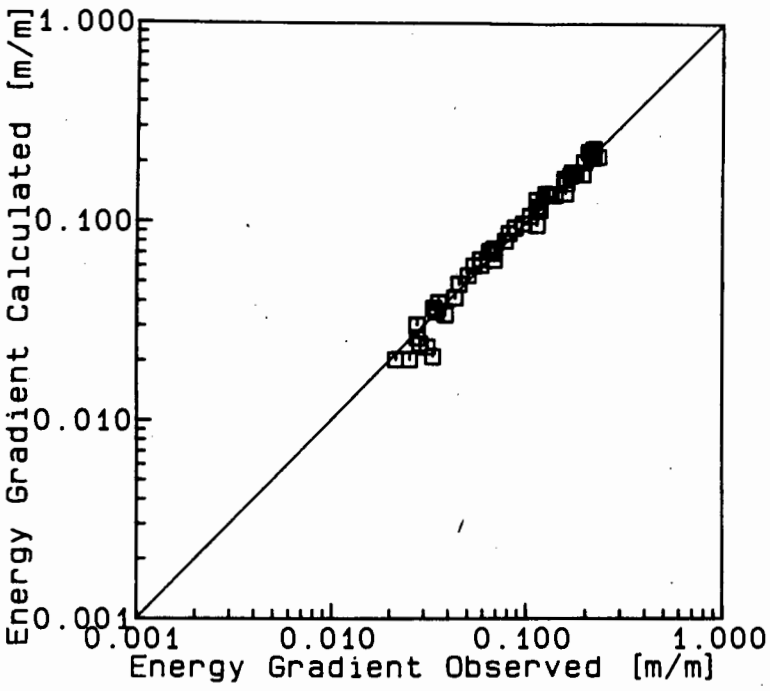

Figure 6.1(a) : Bottom ash

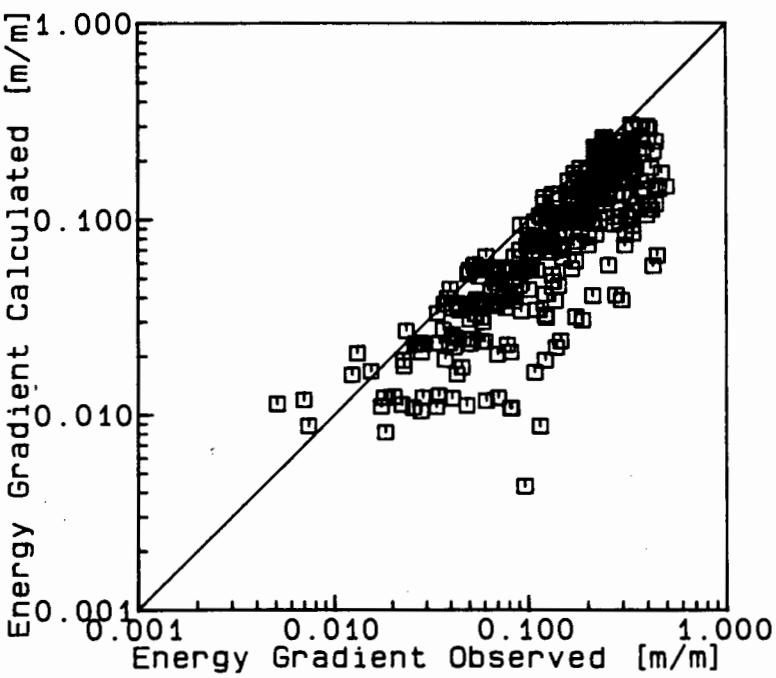

Figure 6.1(b) : Field 1 ash

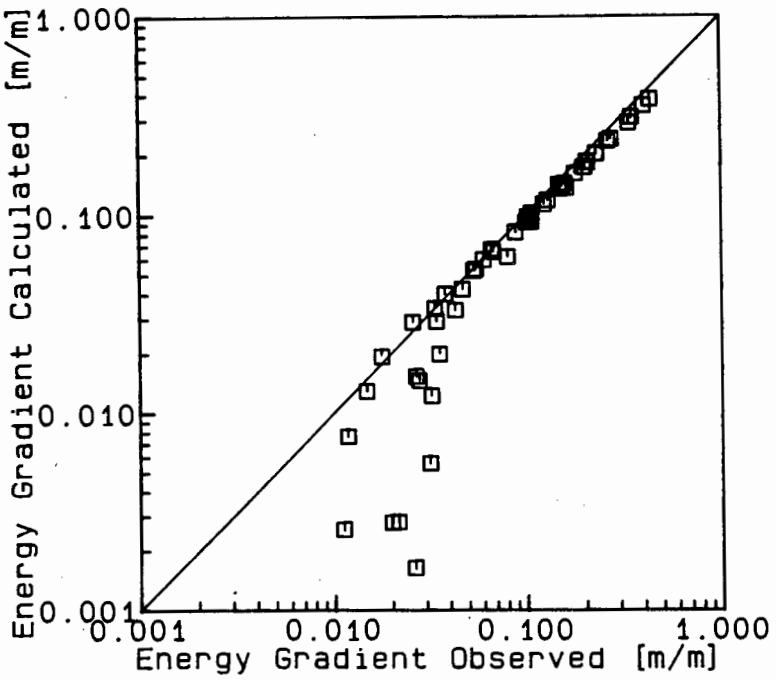

Figure 6.1(c) : Kaolin clay

Figure 6.1 : Calculated energy gradient (pseudofluid) versus observed energy gradient for three of the slurries tested

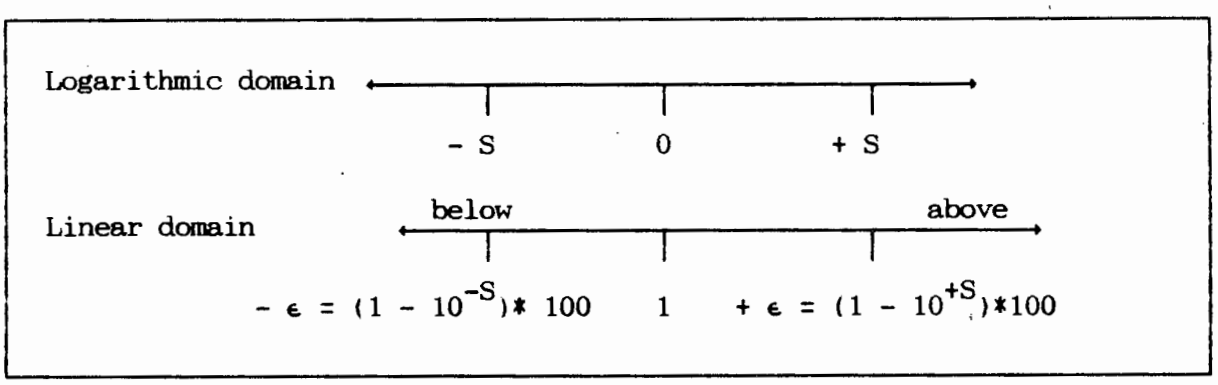

Figure 6.2 : Definition diagram for log standard error

The log standard error values for the graphs shown in Figure 6.1 are presented in Table 6.1.

Table 6.1 : Log standard error and percentage error values for the graphs shown in Figure 6.1

Figure number	Material description	Log standard error	Average error above [%]	Average error below [%]	No. of data points
6.1(a)	Bottom ash	0.00786	1.83	1.79	49
6.1(b)	Field 1 ash	0.01709	4.01	3.86	383
6.1(c)	Kaolin clay	0.05937	14.65	12.78	51

A comparison of the graphs of Figure 6.1 and the error values shown in Table 6.1 suggest that the log standard error should be used with some care since the error values are average values and not maximum expected values. Average error values of below 2% should be considered the upper limit for a good correlation of the data.

The kaolin clay results show the highest error and on the graph (Figure 6.1(c)) the data points confirm this. For the Field 1 ash a large scatter is apparent from Figure 6.1(b) but an expected average error of 4% is found. From the large number of data points tested only a small percentage (± 15%) show error values larger than 4%. The log standard error is therefore weighted by the number of data points in a particular region.

6.2 EXPERIMENTALLY DERIVED DATA REQUIRED BY THE MODEL

Samples of the material to be hydraulically transported must be available before any system design can be initiated. The simplest hydraulic transport

models require only a knowledge of the average particle size and relative density. The models presented in Chapters 1 and 3 require various values from the following list :

1. Particle size distribution and material constants.
2. Coefficient of sliding friction.
3. Loose packed bed concentration.
4. Particle shape factor.

A small quantity of material is required to ascertain the values listed. It is the ultimate objective of any analytical model that from this small sample a complete, accurate design can be achieved without the need for expensive prototype or laboratory testing.

6.2.1 Particle Size Distribution and Material Constants

The particle size distribution used for each test was achieved by wet screening material down to 400μm. All material less than 400μm was then analysed using a Malvern 2600/3600 Particle Sizer VF.6. As a calibration check, standard latex calibration particles were analysed using the Malvern particle size analyser. Table 6.2 shows the actual and measured particle sizes (Slatter (1986)) which compare very well.

Table 6.2 : Check calibration on Malvern Particle Size Analyser

	d_{10} [μm]	d_{50} [μm]	d_{90} [μm]
Actual	64.43	75.21	87.70
Measured	66.93	76.09	92.70

The particle size distribution data is input into the computer programs, as required, in the form of percentage retained values and the screen size on which the material was retained in micrometers. The particle size distribution is divided into 5 or 10 particle size groups depending on the grading coefficient.

The particle relative density is found by displacement of a measured volume of de-aired, distilled water at a known temperature. Air was removed from the sample by applying a vacuum to below the vapour pressure of the water.

6.2.2 Coefficient of Sliding Friction

Brisco *et al.* (1983) conducted tests to measure the coefficient of sliding friction. Experiments were conducted on two types of sand with mean particle diameters of 0.68mm and 1.7mm. The following coefficients were proposed :

Static friction, $\mu_s = 0.65 \pm 0.25$

Dynamic friction, $\mu_s = 0.22 \pm 0.05$.

Televantos *et al.* (1979) found,

μ_s for gravel $\simeq 0.32$

μ_s for coal $\simeq 0.4$.

For the materials tested at the University of Cape Town the coefficient of sliding friction was determined by finding the angle that a pipe, of similar roughness to the actual pipelines used, needed to be tilted to achieve sliding motion. The coefficient of sliding friction was then found from

$$\mu_s = \tan \theta \qquad (6.2)$$

θ - the angle defining pipe slope.

The coefficient of sliding friction was determined for different particle size distributions but was found to be affected by many other factors including particle shape, bed packing concentration, bed dilatancy and the mixture flow rate. A simple desk top test was considered the best way to measure an apparent value for this coefficient. The particle size

distribution of the observed stationary bed deposit in the actual flow situation, which contained only traces of kaolin, was used to measure the coefficient of sliding friction. Floc structures which exist for mixtures in a quiescent state do not exist in the pipeline due to the turbulent nature of the flow. Inclusion of the fine component in a tilting tube test, in a quiescent state, would therefore have given erroneous results. The coefficient of sliding friction obtained in this way is equal to the submerged angle of repose of the coarse component.

Analysis of the imported data is achieved by assuming values for sliding friction based on available literature.

Sliding friction values used are presented in Tables 6.11 and 6.12.

6.2.3. Loose Packed Bed Concentration

The loose packed bed concentration (C_b) was found in Chapter 2 (Literature Review) to vary between 0.5 and 0.7. Measurement of this value in a quiescent state by bench top tests is difficult because the value required is a function of the flow conditions. Two complicating factors are :

1. **Shearing of the vehicle with a consequent breakdown in the floc structure**

For the kaolin-sand mixtures with concentration (C_{vt}) above about 10%, stabilized mixtures were obtained for quiescent samples. If these samples were subject to vibration the coarse fraction settled until the vibration stopped. This effect demonstrates the difficulty in measuring C_b since the point at which sufficient settlement has occurred is subjective.

During a pipeline test in which a stationary bed occurs, a clear distinction exists between the bed and the suspended mixture indicating that the bed is composed primarily of the coarse material. Some fine material may be trapped in the interstitial spaces between coarse particles. The removal of the fine component to measure C_b is therefore also subject to error.

2. **Dilatancy of the bed due to percolation and applied shear stress**

The effect of dilatancy on the value of C_b can only be inferred but not measured. The only way of measuring C_b would be by sampling the actual bed material in a prototype pipeline. The concept of deriving constants for an

analytical model from simple bench top tests alone is therefore not possible unless a constant value of C_b can be chosen. Table 6.3 shows a sensitivity analysis for C_b varying from 0.5 to 0.7 for a type 1 sand mixture using the Lazarus model (Section 1.4.4). For the same material the change in average error is different for different concentrations. This highlights the problem of measuring C_b using a bench top test. A value of C_b = 0.67 was chosen as being representative of the mixtures investigated. By using a constant for all calculations no subjective bias is included in the analysis.

Table 6.3 : Variations in log standard error values for two type 1 sand tests for different values of C_b

Test Number	Maximum bed concentration			Change in average error
	C_b = 0.5	C_b = 0.6	C_b = 0.7	
S142023A	0.00979	0.01057	0.01123	0.34%
S1430068	0.06831	0.05899	0.05371	3.87%

6.2.4 Particle Shape Factor

The particle shape factor (S_F) can be measured by allowing particles to settle in water and comparing the measured settling velocity to the settling velocity calculated for spheres of a diameter equal to the mean of the particles tested. This can be achieved for each particle size group found between successive screens when doing a particle size analysis. The particle size is considered to be the screen size on which the particles are retained.

The following observations can be made from shape factor experiments conducted :

1. Shape factor is inversely proportional to particle diameter.
2. Shape factor is invariably less than unity for naturally occurring materials.
3. A shape factor of unity is suggested herein if no other information is available.

Figure 6.3 shows the shape factors for the uranium tailings as an example of the tests done.

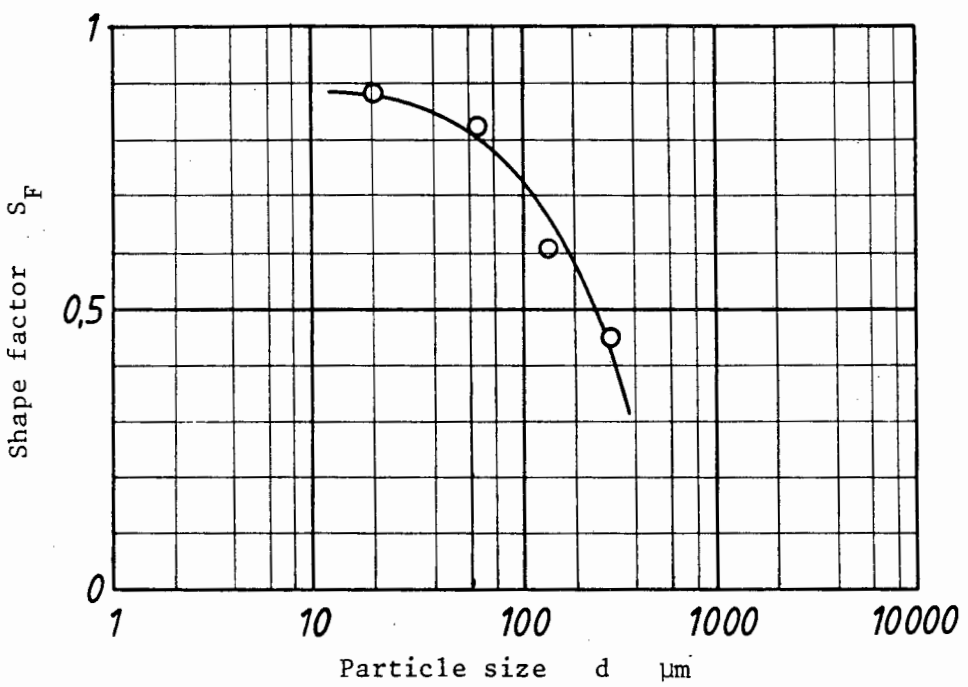

Figure 6.3 : Particle shape factor as a function of particle diameter for uranium tailings

6.3 PREDICTION OF VEHICLE FRICTION FACTORS

6.3.1 Rheological Equations

Figure 6.4 shows a plot of two rheograms :

1. A Newtonian fluid with viscosity determined by

$$\mu_m = \mu_w \left[1 - \frac{C_v}{C_b}\right] \quad . \tag{2.23}$$

2. A yield pseudoplastic (kaolin clay) with constants derived from Table 2.12 for C_v = 14.88%. If the two rheograms intersect at a strain rate similar to that expected in the pipeline flow then the two rheograms will have similar wall shear stress values and no further investigation is necessary.

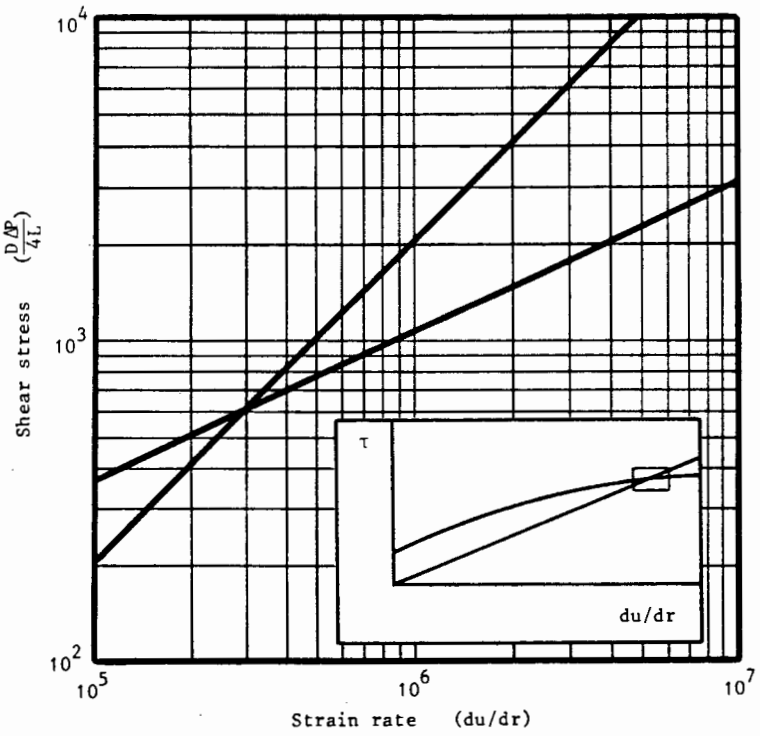

Figure 6.4 : Rheogram for Newtonian and yield pseudoplastic showing point at which rheograms intersect

Table 6.4 shows the data represented in Figure 6.4.

Table 6.4 : Shear stress as a function of strain rate for two rheologies

Strain rate $[s^{-1}]$	Newtonian shear stress [Pa]	Yield pseudoplastic shear stress [Pa]
1.10^{-1}	$2.04.10^{-4}$	44.38
1.10^{0}	$2.04.10^{-3}$	45.17
1.10^{1}	$2.04.10^{-2}$	47.62
1.10^{2}	$2.04.10^{-1}$	55.17
1.10^{3}	2.04	78.59
1.10^{4}	20.43	150.71
1.10^{5}	$2.04.10^{2}$	373.75
1.10^{6}	$2.04.10^{3}$	1063.03
1.10^{7}	$2.04.10^{4}$	3192.10

The two lines intersect at a strain rate of 3.10^{5} per second. For turbulent flow in a pipe of 150mm inside diameter the mean velocity required to produce this strain rate at the wall can be calculated.

For the laminar sublayer

$$\frac{u}{u_*} = \frac{u_* \rho y}{\mu} \quad . \tag{2.88}$$

Differentiating, $\frac{du}{dy} = \frac{u_*^2}{\nu}$

$$= \frac{\tau}{\rho\nu} \quad .$$

By definition $\tau = \frac{1}{2} f \rho V^2$. (3.58)

So $\frac{du}{dy} = \frac{f V_m^2}{2\nu}$. (6.3)

For the kaolin slurry; $\mu = 2.04.10^{-3}$ Pas

$\rho = 1214$ kg/m^3

so $\nu = 1.68.10^{-6}$ m^2/s .

For smooth wall flow after Colebrook-White, (i.e. k = 0)

$$\frac{1}{\sqrt{f}} = 4 \log \frac{Re \sqrt{f}}{1.26} \qquad (6.4)$$

where $Re = \frac{V_m D}{\nu}$.

Equations (6.3) and (6.4) can be solved simultaneously to find $V_m = 19.49$ m/s . This velocity is significantly higher than the maximum velocity value of interest. The maximum strain rate expected at $V_m = 6.5$ m/s is

$$\frac{du}{dy} \simeq 4.10^4 \quad .$$

Over the velocity range tested the two rheological equations will produce significantly different results. The turbulent flow data for kaolin clay slurries should now be investigated.

6.3.2 Analytical Description of the Vehicle

In Chapters 2 and 3 equations were given for predicting the wall friction factor of the vehicle :

1. Blasius type.
2. Colebrook-White equation.
3. Torrence equation.

Figure 6.5 shows a comparison of the Colebrook-White and Torrence equations for a Newtonian fluid (i.e. $\tau_y = 0$, $n = 1$) . These equations produce similar results over the Reynolds number range of interest.

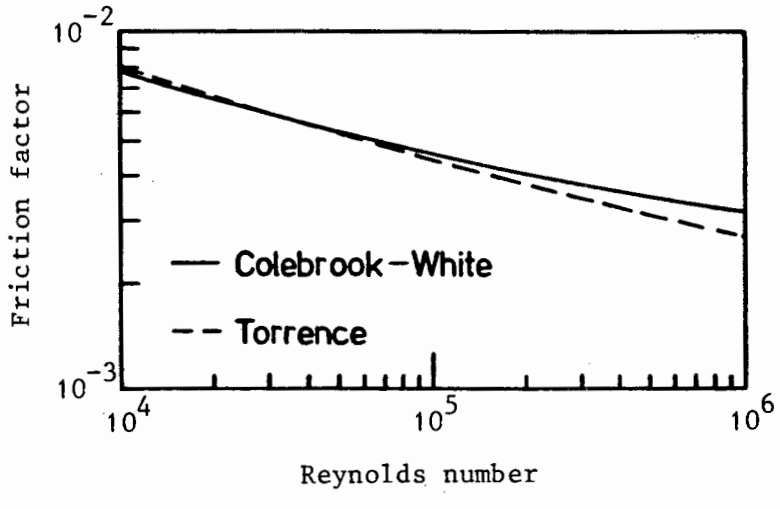

Figure 6.5 : Comparison of Colebrook-White and Torrence equations for a Newtonian fluid

Using a Newtonian rheology with viscosity predicted by equn. (2.23), the Colebrook-White equation is compared to the kaolin clay data in Figure 6.6.

For Reynolds number values greater than 2.10^5 the prediction is good. Below this Reynolds number the data varies sharply from the prediction.

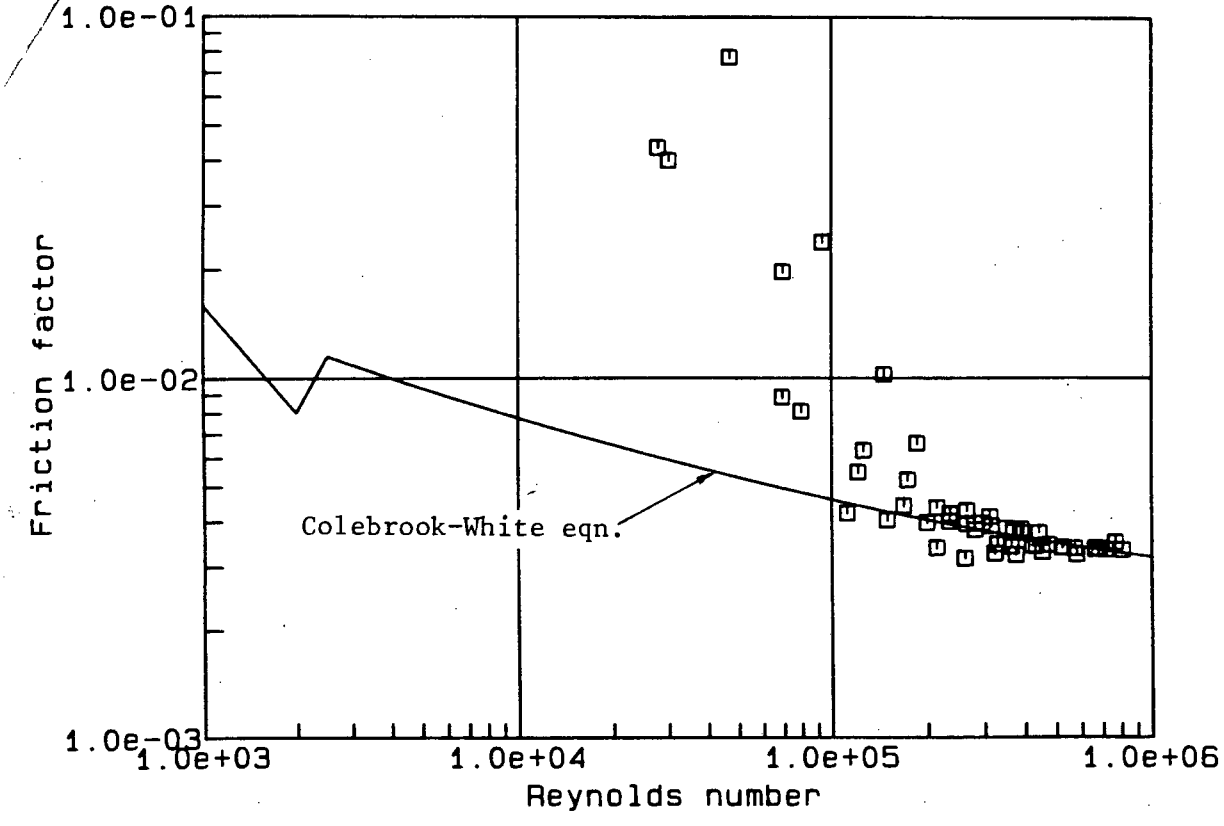

Figure 6.6 : Kaolin clay data and Colebrook-White prediction (equn. 2.100)

From the discussion on rheological equations (Section 6.3.1) the close agreement for Re > 2.10^5 in Figure 6.6 cannot be ascribed to a convergence in the rheological equations at high shear rate and hence the laminar sublayer effect on the wall shear stress. A possible explanation is that a Newtonian rheology best describes the mixture at Re > 2.10^5 while non Newtonian effects occur for Re < 2.10^5 . This is only possible if a physical change occurs in the mixture.

The kaolin slurries tested were always flocculated when at rest. In Chapter 2 the effect of strain rate on floc size was discussed. The two equations presented are

$$C_{FP} = fn\left[\frac{du}{dr}\right] \qquad (2.30)$$

and

$$r_F = \left[\frac{du}{dr}\right]^{-B} \qquad (2.36)$$

$0 \leq B \leq 1$.

The floc structure that exists in the slurry will therefore break up with increasing strain rate. The break up of the floc structure appears to be completed for $Re = 2.10^5$. It is important in this argument that the maximum concentration of kaolin tested in the pipeline was only $C_{vd} \simeq 6\%$. The viscosity used to calculate R_e is predicted by equn. (2.23) as before.

Figure 6.7 shows field 3 fly ash data for the 50mm and 160mm diameter pipelines for concentration up to $C_{vd} = 35\%$. Good agreement is again apparent for $Re > 2.10^5$ although no significance can be attached to this particular value. The data points vary, both above and below the prediction, below this value of Reynold number. The viscosity used to calculate R_e is predicted by equn. (2.23) as before.

Viscometer tests conducted on field 3 fly ash by Lazarus and Sive (1984) show no yield stress for $C_{vd} \simeq 16\%$. At $C_{vd} = 28\%$, the yield stress $\tau_y \simeq 2.5$ Pa . Yield stress and the existence of floc structures are synonymous and so the explanation for the discrepancy in friction factor below $Re = 2.10^5$ cannot be ascribed to floc destruction alone for the field 3 fly ash.

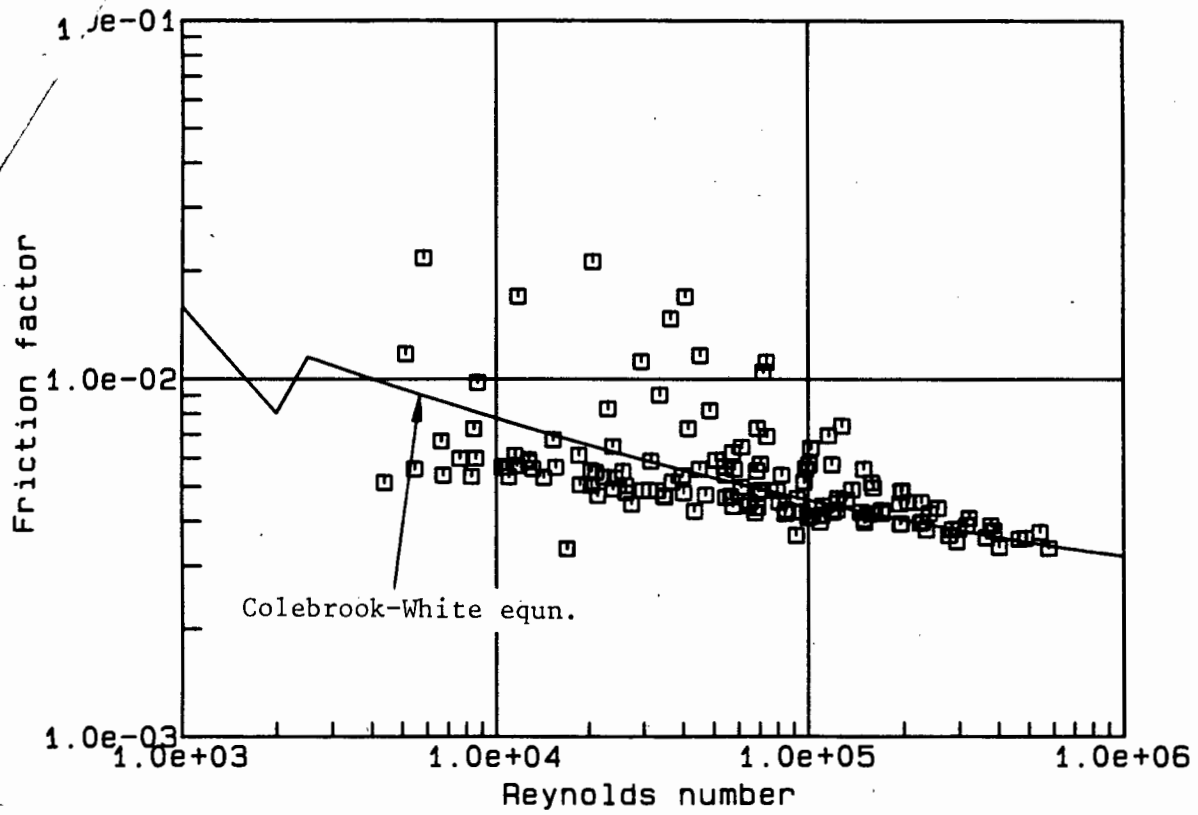

Figure 6.7 : Field 3 fly ash data and Colebrook-White prediction

Shook (1985) suggest that particle migration away from the pipe wall can account for the reduction in friction factor for the field 3 ash for low and moderate concentrations. "For particles of diameter greater than 50μm floc formation becomes less likely and particle migration more likely to occur (Shook 1985)". Different mechanisms therefore exist for the two mixtures. The kaolin is comprised of particles with a maximum size of approximately 50μm (d_{50} = 9 μm) . High yield stress exists at low concentration (see Table 2.12) and floc destruction is the governing mechanism.

More than 20% of the particles in field 3 ash slurries are greater than 50μm. The particle migration hypothesis is therefore considered applicable and the friction factor reduction can be accounted for. The mechanism of particle migration can only occur for relatively low concentrations. This is borne out by the field 3 ash data which show a friction factor reduction only for mixtures with delivered concentration less than about 28% (Sive and Lazarus 1985).

Shook (1985) rejected the particle migration hypothesis for high concentration slurries because no such segregation was measured by isokinetic sampling for C_v = 35% . At concentrations greater than 35%, Shook (1985) suggested that the particles would be even more uniformly distributed.

Shook (1985) suggested that heterogeneity would only occur in the space between the pipe wall and the first layer of particles for high concentration mixtures and that these particles would penetrate the viscous sublayer. The local concentration in the "penetrated layer is determined by the balance of repulsive effects (Shook 1985)". From lubrication theory, Shook (1985) points out that this repulsive effect is associated with an increase in local wall shear stress.

From lubrication theory Shook (1985) derives an equation for the friction factor of high concentration mixtures

$$f = (1 - x)\, f_f + k_3\, \lambda x \left[\frac{d}{D}\right]^{m-0.5} Re^{-0.5} \qquad (6.5)$$

where x - fraction of pipe wall area with increased boundary stress due to particles

λ - linear concentration parameter = $\left[\left[\frac{C_b}{C_v}\right]^{1/3} - 1\right]^{-1}$

κ_3, m - constants .

Making a simplifying assumption for high concentration where the distance between particles and the pipe wall will be small, for a particular diameter ratio (d/D) , Shook (1985) gives the following equation

$$f = (1 - C_v)\, f_f + k_4\, \lambda\, C_v\, Re^{-0.5} \quad . \tag{6.6}$$

Figure 6.8 shows a plot of field 3 data for $C_v > 28\%$ and equn. (6.6). The value of $k_4 = 3$ was empirically chosen from the field 3 ash data. Equation (6.6) predicts the friction factor for the field 3 ash data. The accuracy of equn. (6.6) is dependent on a choice of the value of k_4 . The viscosity used to calculate R_e (equn. 6.6) is that for clear water.

Figure 6.9 presents a plot of the kaolin data and predictions based on the Torrence equation for

$$Re = Re_{plc} = \frac{D^n\, V_m^{2-n}\, \rho_{mf}}{K\, 8^{n-1}} \quad . \tag{2.101b}$$

The values of the rheological parameters are based on the data of Slatter (1987). The prediction shows good agreement with the data for $Re_{plc} < 3.10^4$. The Reynolds number values (equn. 2.101) for this prediction are lower by an order of magnitude then for those of Figures 6.6,

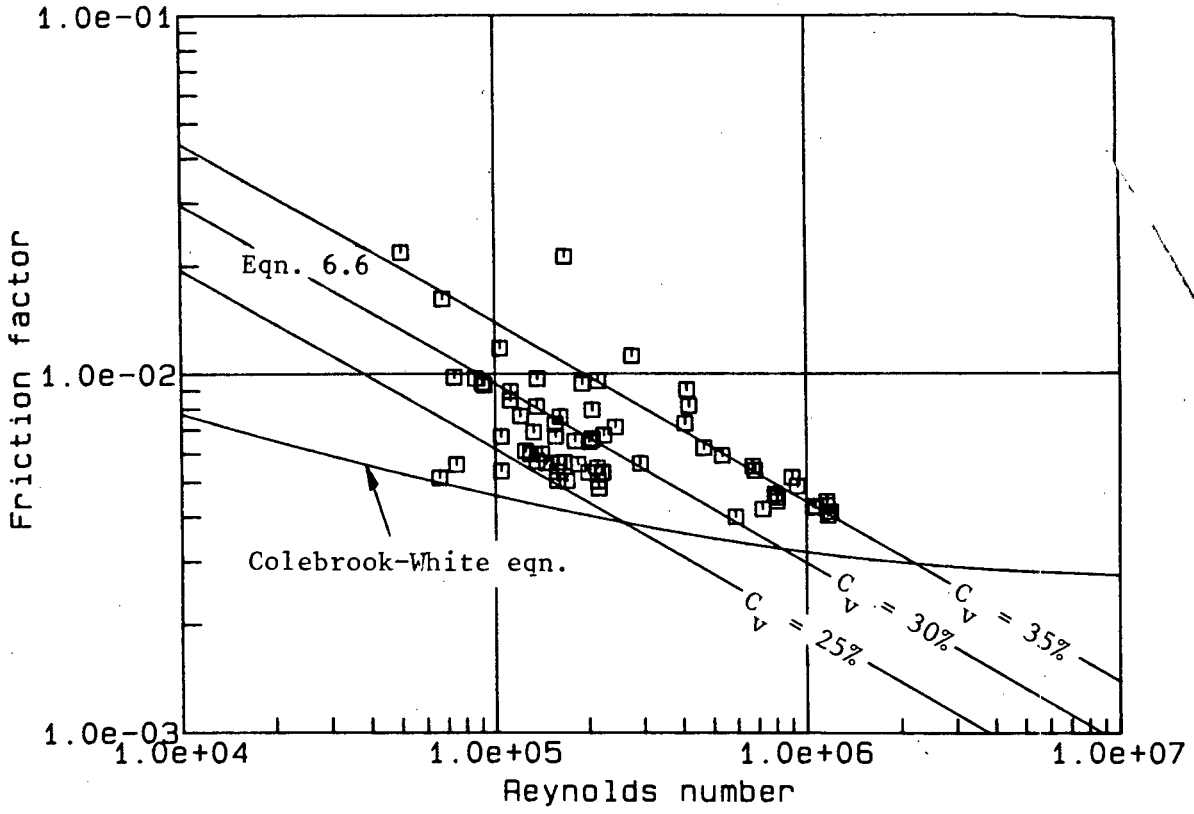

Figure 6.8 : Field 3 ash data for C_v > 28% showing Colebrook-White and equn. (6.6) prediction

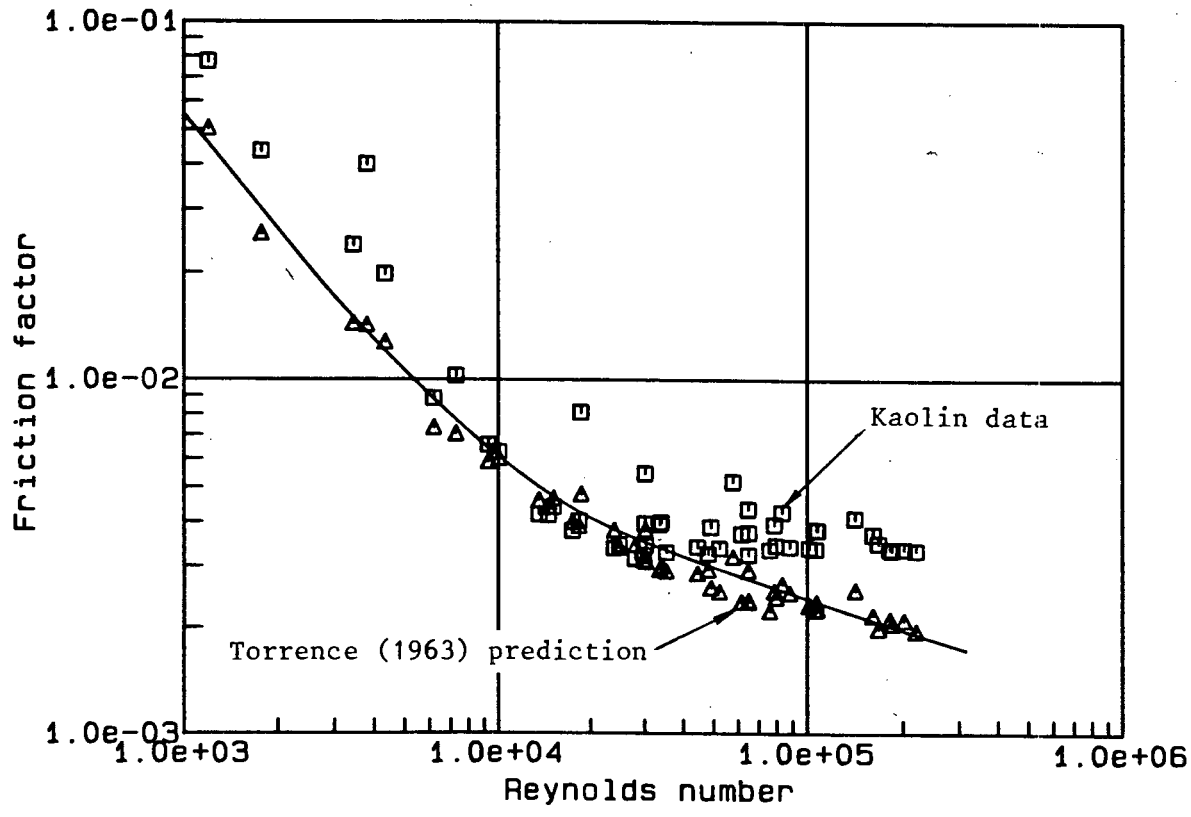

Figure 6.9 : Kaolin clay data and Torrence prediction

6.7 and 6.8. The Torrence (1963) prediction is low for $Re_{plc} > 3.10^4$. The Colebrook-White equation prediction was better for the higher Reynolds numbers. A mixture of these two equations might be considered to achieve the best fit.

Figure 6.10 shows a plot of Eckalite clay data from the M.D. Research Company (see Appendix 6, pg. 7) with the Torrence equation. The rheological parameters presented by Slatter (1987) were used. The same trends shown in Figure 6.9 are apparent in Figure 6.10.

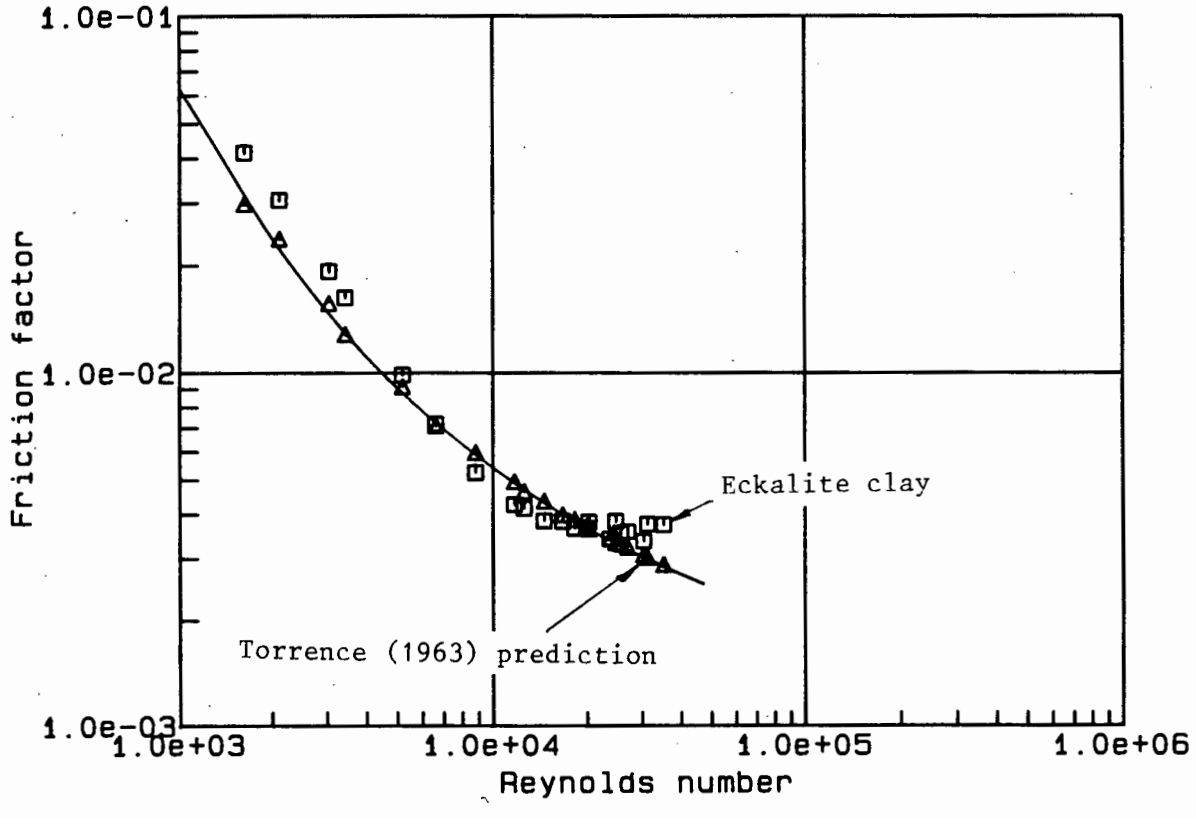

Figure 6.10 : Eckalite clay data and Torrence prediction

Table 6.5 presents the log standard error values for the predictive approaches to the kaolin clay slurries.

Table 6.5 : Log standard errors for the prediction of energy gradient values using four models for kaolin clay slurry

No.	Predictive model	Log standard error
1	Colebrook-White	0.04902
2	Torrence	0.02186
3	The greater i_m prediction from Colebrook-White or Torrence	0.01355
4	Pseudofluid	0.07350

Table 6.6 shows log standard error values for field 3 fly ash. The rheological parameters used were derived from Sive and Lazarus (1985). Slatter (1986) suggested that these values might be incorrect due to viscometer entrance effects that were not accounted for. For all the mixtures tested which did not have a kaolin vehicle the prediction of Colebrook-White is used for the vehicle friction factor. This would ensure acceptable results as long as the mixtures being investigated do not show high yield stresses.

For field 3 ash data the Colebrook-White equation produces the best results. The empirical choice of constant in equn. (6.6) and the exclusion of the ratio (d/D) adversely affects this approach. The Colebrook-White equation will therefore be used in the analysis of high concentration mixtures of field 3 ash although the use of equn. (6.6) with the correct constants appears advantageous.

Table 6.6 : Log standard error for the prediction of energy gradient values using three models for field 3 fly ash slurry

Predictive model	Log standard error	Reynolds number
Colebrook-White	0.00817	$Re = \rho_m V_m D/\mu_{mf}$
Torrence	0.01512	Re_{plc} (equn. 2.101b)
Colebrook-White for $C_v < 28\%$	0.01064	$Re = \rho_m V_m D/\mu_{mf}$ for $C_v < 0.28$ else
Equn. (6.6) for $C_v \geq 28\%$		$Re = \rho_m V_m D/\mu_w$

Different predictive approaches need to be used in the analysis of mixed regime slurries depending on the nature of the slurry vehicle. For kaolin clays, non Newtonian behaviour is apparent at low velocities due to the formation of floc structures which break up with increasing shear rate.

For mixtures with particles greater than 50μm particle migration away from the wall will occur for low and moderate concentration mixtures causing a reduction in the mixture friction factor below that the for the fluid alone with increased density. At high concentration, particle-wall effects predominate and an approach suggested by Shook (1985) based on lubrication theory will model an increase in the mixture friction factor above that for the fluid alone.

6.4 PROPOSED ANALYTICAL MODELS

6.4.1 Particle Suspension and *in situ* concentration

In Chapter 2 two approaches to the suspension of bed load particles is presented. The particle suspension equations of Einstein (1950) and Meyer-Peter and Muller (1948) based on the shear intensity of the flow are essentially similar but for the calculation of the shear intensity parameter on individual particles. In Chapter 3 an alternative method based on the velocity required for turbulent suspension (Wilson and Watt, 1974) is proposed. These models can be compared using experimental data for which *in situ* concentration measurements have been made.

Recapping, the proposed models are :

1. Einstein's approach (1950)

   The analytical expression relating the shear intensity on individual particle sizes to the intensity of bed load transport for the individual size is given in Chapter 2 as

$$1 - \frac{1}{\sqrt{\pi}} \int_{-B_* \Psi_* - 1/k_1}^{+B_* \Psi_* - 1/k_1} e^{-t^2} \, dt = \frac{A_* \Phi_*}{1 + A_* \Phi_*} \qquad (2.114)$$

   where $A_* = 43.5$

   $B_* = 0.143$

   $k_1 = 0.5$.

   The integral in equn. (2.114) was solved using third order Gauss quadrature over 10 intervals.

2. Meyer-Peter and Muller approach (1948)

The Meyer-Peter and Muller (1948) equation that relates shear intensity to the intensity of bed load transport is given in Chapter 2 as

$$\Phi_* = \left[\frac{4}{\Psi_*} - 0.188\right]^{3/2} \quad . \tag{2.117}$$

3. Present approach based on turbulent suspension velocity

Wilson (1972) and Wilson and Watt (1974) presented a semi empirical model for the turbulent support of solids in pipeline flow where the velocity for turbulent suspension is given by

$$V_{susp} = 0.6\ V_t \sqrt{\frac{2}{f_w}}\ \exp\ (45d/D) \quad . \tag{2.83}$$

This equation was implemented as

$$V_{susp} = 0.6\ S_F\ V_t'\ \sqrt{\frac{2}{f_I}}\ \exp\ (45_i d/D) \quad . \tag{6.7}$$

For the purpose of comparing the three methods presented, two sand type 1 tests are used. The complete tables produced for tests S142023A and S1430068 are presented in Appendix 9. Table 6.7 and Figure 6.11 present the measured and predicted *in situ* concentration values for test S142023A. Table 6.8 and Figure 6.12 present those for test S1430068.

Table 6.7 : *In situ* concentration value predictions for test number S142023A

C_{vt} [%]				V_m [m/s]
Measured	Einstein	Meyer-Peter	Present	
11.77	16.47	13.05	10.45	1.78
14.36	20.72	14.63	8.22	2.20
7.94	11.76	8.52	6.09	2.40
7.45	9.84	6.80	5.47	2.52
7.31	9.00	6.52	5.14	2.56
11.36	14.71	20.40	9.15	2.65
10.72	12.16	16.78	8.74	2.87
5.81	4.61	4.61	4.67	3.14
5.22	4.50	4.50	4.43	3.51
7.44	8.90	8.90	9.59	3.69
6.11	9.51	9.51	10.23	3.78
6.90	5.74	5.74	7.88	4.47
5.09	4.99	4.99	6.69	4.74
6.65	7.03	7.03	8.77	5.50

Table 6.8 : *In situ* concentration value predictions for test number S1430068

C_{vt} [%]				V_m [m/s]
Measured	Einstein	Meyer-Peter	Present	
39.47	43.14	46.26	35.37	1.53
36.90	42.84	48.51	37.04	1.66
37.26	42.63	43.59	41.25	1.87
35.96	44.12	46.54	35.39	2.33
36.02	44.06	46.02	34.46	2.34
35.83	42.64	45.30	34.19	2.44
34.28	43.07	43.07	33.86	2.75
29.17	37.75	37.75	28.46	3.19
31.35	35.11	35.11	30.95	3.58
27.81	31.15	31.15	27.57	4.05
31.07	30.56	30.56	34.96	4.48
30.69	31.47	31.47	35.20	4.83

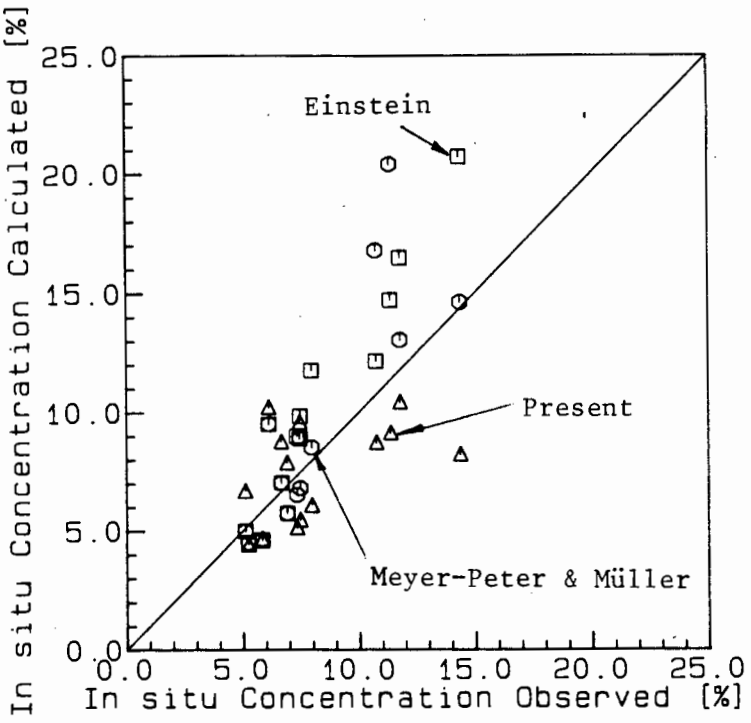

Figure 6.11 : Observed *in situ* concentration versus calculated *in situ* concentration for the three predictive methods presented on the data of test S142023A

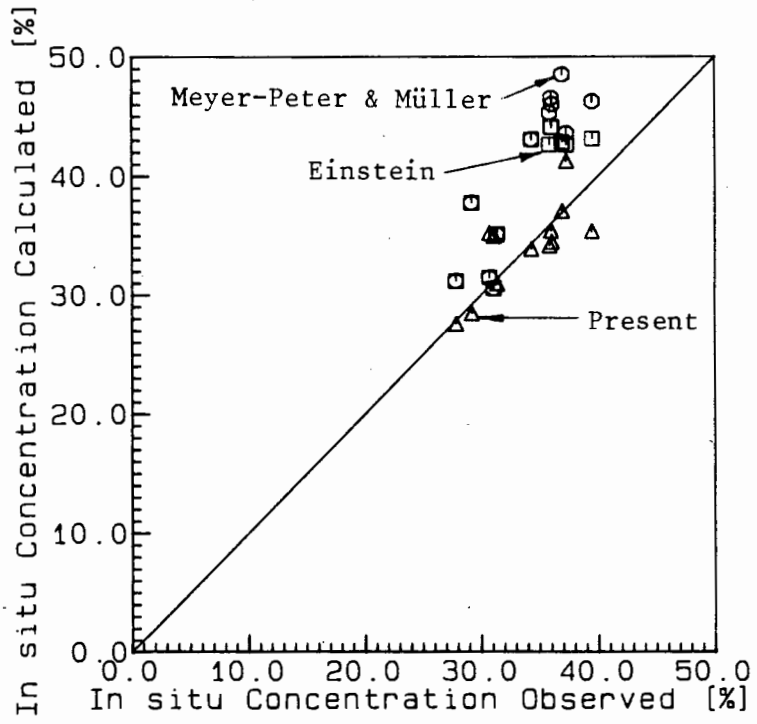

Figure 6.12 : Observed *in situ* concentration versus calculated *in situ* concentration for the three predictive methods presented on the data of test S1430068

The log standard error between the measured and calculated values of *in situ* concentation are presented in Table 6.9.

Table 6.9 : Log standard error values for *in situ* concentration predictions

Test Number	Diameter [mm]	Nominal C_{vd} [%]	Log standard error of C_{vt}		
			Einstein	Meyer-Peter	Present
S142023A	139.3	5.0	0.03249	**0.03207**	0.03776
S1430068	139.3	25.0	0.02653	0.02653	**0.00972**

For the low concentration test, all three models predict with the same order of accuracy, the Meyer-Peter and Muller approach (1948) being most successful. From Table 6.7 it can be seen that the shear intensity equations overpredict the *in situ* concentration at low velocities. This can be interpreted as an underprediction in the suspended load flow rate. An increase in the *in situ* concentration causes an increase in the bed height (stationary bed) with a consequent decrease in the flow area. This causes an increase in mean velocity above the bed. This increased velocity causes an increase in the solid flow rate. The models presented predict *in situ* concentration as a consequence of ensuring that the calculated and actual delivered concentration are equal. An overprediction in C_{vt} is therefore a result of an underprediction in the quantity of solid suspended. The present model predicts *in situ* concentration values lower than those measured. An overprediction in solid flow therefore exists.

For the data of Table 6.8 the shear intensity equations still underpredict the solid flow rate but by a smaller margin as borne out by a decrease in the log standard error values (Table 6.9). The present model successfully predicts the *in situ* concentration for this test. The log standard error value is less than half of the other predictions.

The poor results at high concentration for the shear intensity approach can be ascribed to the fact that both these models were developed for open channel flow where delivered concentration values in excess of 5% by volume are rarely encountered. The effect of interparticle interaction is neglected resulting in errors for flows where these interactions predominate. The equation of Wilson and Watt (1974) is semi-empirical and was derived for mixtures with concentration similar to test S1430068.

Two empirical correlations for the prediction of *in situ* concentration are presented in Section 2.4.4.2. Figure 6.13 shows a comparison of observed and calculated *in situ* concentration values. Table 6.10 presents the log standard error values for the predictions.

Table 6.10 : Log standard error values for empirical *in situ* concentration prediction

Test	Newitt *et al.* (1962)	Wani *et al.* (1983)
S142023A	0.13303	0.05812
S1430068	0.11554	0.02334

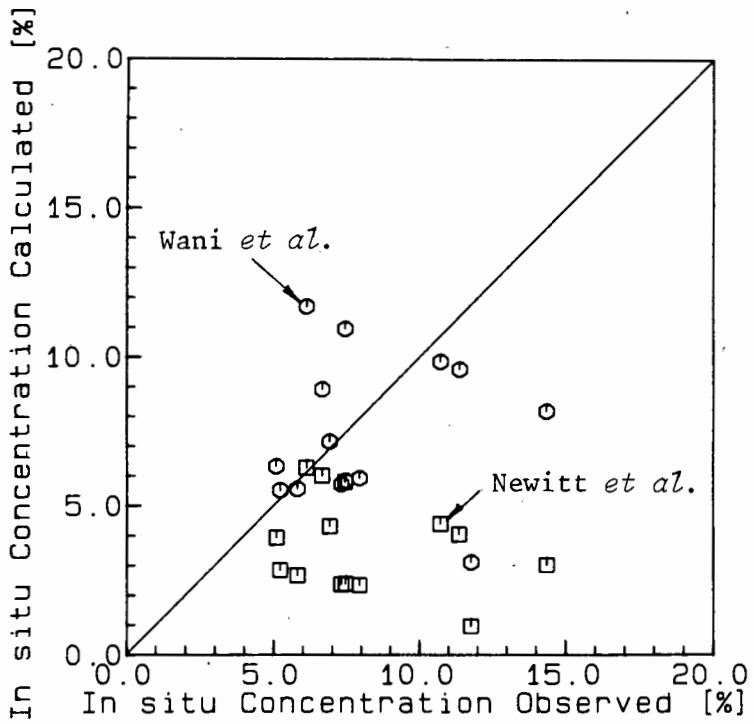

(a) Test number S142023A

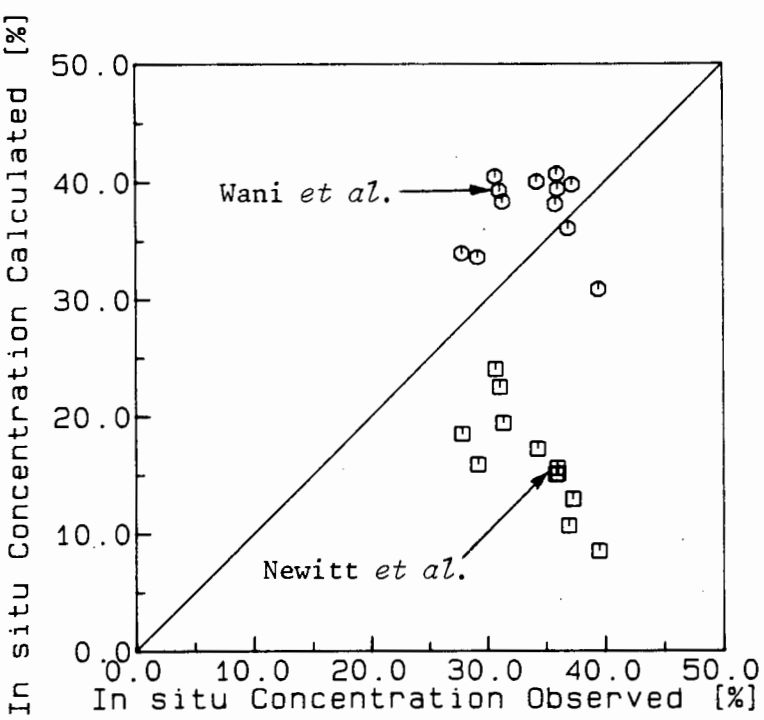

(b) Test number S1430068

Figure 6.13 : Empirical correlations of Newitt *et al.* (1962) and Wani *et al.* (1983) for *in situ* concentration

For the low concentration test the empirical prediction is poor but for the high concentration test the prediction of Wani *et al.* (1983) is of the same order as that for the Einstein (1950) or Meyer-Peter and Muller (1948) prediction (see Table 6.9). Newitt *et al.* derived their correlation for coarse gravel in a 25mm nominal diameter pipeline. It is therefore unlikely that this correlation would be applicable for much larger pipe diameters. The correlation of Wani *et al.* has a much broader data base and predicts accordingly better.

6.4.2 Energy Gradient Comparison

The prediction of energy gradients for a particular set of physical conditions is the fundamental requirement of any correlation. For this purpose a data base of 2975 individual data points derived from five different test institutions was assembled. The results will be discussed in two sections, namely those results produced at the University of Cape Town (local data) and those produced elsewhere (imported data).

The computer programs used to generate the energy gradient results are presented in Appendices 12 to 16. Appendix 12 contains the computer code for the Wasp model, Appendix 13 for the Wilson model, Appendix 14 the Lazarus model and Appendix 15 the Meyer-Peter and Muller model. Appendix 16 contains the computer code for the present analytical model.

6.4.2.1 Local data

Table 6.11 presents log standard error values for the prediction of energy gradient using the correlations investigated. The pesudofluid correlation is included for comparison. The log standard error values are for each

Table 6.11 : Energy gradient log standard error values for local data

Source of data	Fluid phase	Material description	ρ_s [kg/m^3]	μ_s	Shape factor	d_{50} [mm]	G_d	Number of data points	D [mm]	k [mm]	E Q U A T I O N				
											Pseudofluid	Wasp *et al.*	Wilson	Lazarus	Present
HYDROTRANSPORT RESEARCH UNIT UNIVERSITY OF CAPE TOWN	WATER	Bottom ash	≃ 2000	0.47	0.80	0.087-0.338	34.4-108	49	139.30	0.0019	0.00786	0.01511	0.02381	*0.00781*	0.01447
		Field 1 ash	2320	0.42	0.90	0.068	15.0	116	45.42	0	0.01999	*0.00919*	0.01962	0.01131	0.01258
								134	57.21	0.0004	0.02384	*0.01283*	0.02253	0.01632	0.01728
								62	81.49	0	0.01096	0.01386	0.01096	0.01018	*0.01000*
								71	141.70	0.0076	0.01355	0.01180	0.01188	0.01181	*0.01170*
		Field 3 ash	2233	-	-	0.017	50.0	65	45.42	0	0.01711	*0.01147*	0.01697	0.01254	0.01379
								57	57.21	0.0004	0.02893	*0.01837*	0.02428	0.02017	0.02261
								60	81.49	0	0.01777	*0.01413*	0.01650	0.01589	0.01641
								80	141.70	0.0076	0.02380	*0.01553*	0.02127	0.01922	0.02100
		Kaolin clay	2440	-	-	0.009	11.9	22	79.72	0	0.08937	0.08159	0.08516	0.08855	*0.02687*
								29	139.30	0.0019	0.05762	0.05532	0.05416	0.05693	*0.01339*
		Kaolin-sand	≃ 2650	0.49	0.95	0.277-0.970	2.4-440	99	79.72	0	0.06111	0.02431	0.02845	*0.01089*	0.01349
								188	139.30	0.0019	0.01791	0.01168	0.01587	*0.00801*	0.00947
		Ocean bed	2450	0.39	0.80	8.280	4.96	17	141.70	0.0076	0.08006	*0.02014*	0.10628	0.03329	0.02535
		Sand type 1	2650	0.49	0.95	0.851	3.0	58	79.72	0	0.06930	0.02610	0.03169	*0.01898*	0.02915
								90	139.30	0.0019	0.04969	*00.1192*	0.02104	0.01815	0.01768
		Sand type 2	2650	0.49	0.95	0.425	6.1	40	79.72	0	0.04540	0.02750	0.03371	0.02938	*0.02567*
								61	139.30	0.0019	0.04892	*0.01182*	0.03228	0.03037	0.03910
	RETURN DAM SOLUTION (pH 1.9)	Tailings 1	2958	0.53	0.90	0.010	44.8	9	45.42	0	0.18346	*0.08855*	0.12754	0.15233	0.16078
								10	57.21	0.0037	0.09938	*0.04051*	0.07859	0.08249	0.08464
		Tailings 2	2852	0.53	0.75	0.099	95.7	14	45.42	0	0.06407	0.04113	*0.03565*	0.04590	0.04131
								8	57.21	0.0037	0.16294	*0.07291*	0.10696	0.11606	0.10552
		Tailings 3	2742	0.53	0.45	0.592	92.0	5	57.21	0.0037	0.21715	0.13811	*0.06012*	0.15394	0.11693
							TOTAL	1345	OVERALL		0.00858	0.00422	0.00591	0.00435	0.00442

material in each pipe diameter for which results were obtained. Information relating to each test is also presented. The sliding friction coefficient (μ_s) and shape factor (S_F) values were obtained from bench top tests as described in Section 6.2.

The minimum log standard error value for each test group is shown italicised in Tables 6.11 and 6.12. In Table 6.11 the model ascribed to Wasp *et al.* produced the lowest overall log standard error value. The present correlation and that of Lazarus have overall error values comparable to that for Wasp *et al.*

The Wasp *et al.* correlation was developed specifically for the heterogeneous flow of mixed regime slurries. The field 1 ash and the uranium tailings fall into this category. The semi-empirical approach of Wasp *et al.* is therefore ideally suited to these mixtures. The present correlation and that of Lazarus are generalised approaches and considered applicable for all slurry flows.

6.4.2.2 Imported data

Table 6.12 presents log standard error values for the energy gradient predictions for the imported data. The sliding friction coefficients (μ_s) presented in Table 6.12 were chosen from a review of relevant literature. The choice is considered convenient rather than absolute. This is justified since all correlations presented used identical values and so are useful for comparative purposes. The shape factor (S_F) was taken to be unity for all materials. This again is convenient for comparison and is justified in that any deviation from unity would be arbitrary and may bias a particular model unfavourably.

Source of data	Fluid phase	Material description	ρ_s [kg/m^3]	μ_s	Shape factor	d_{50} [mm]	G_d	Number of data points	D [mm]	k [mm]	E Q U A T I O N				
											Pseudofluid	Wasp *et al.*	Wilson	Lazarus	Present
C. S. I. R. SOUTH AFRICA	WATER	Coal GC	1457	0.4	UNITY	0.203	16.5	12	104.9	0.0367	0.02723	0.01857	0.02418	*0.01674*	0.02151
								12	206.6	0.0372	0.02296	0.02485	0.02072	*0.01614*	0.02097
								12	261.0	0.0365	0.02625	0.07907	0.01814	*0.01099*	0.01654
		Coal PC	1560	0.4		0.135	25.3	18	206.6	0.0372	0.03233	0.01400	0.02807	0.01620	*0.01043*
								18	261.0	0.0365	0.03703	0.05362	0.02482	0.01650	*0.01176*
		Slimes G1	2740	0.5		0.057	13.5	22	104.6	0.0367	0.01894	0.02939	0.01248	0.01027	*0.00726*
								20	206.6	0.0370	0.00835	0.03262	0.00876	*0.00556*	0.00848
								23	261.0	0.0365	0.01412	0.10427	0.02147	0.00925	*0.00516*
		Slimes G2	2725	0.5		0.049	14.1	23	104.6	0.0367	0.01623	0.00670	0.01454	0.00839	*0.00560*
								26	206.6	0.0372	0.00761	0.02553	0.00714	*0.00344*	0.00532
								21	261.0	0.0367	0.01483	0.08957	0.01454	0.00691	*0.00600*
		Slimes S1	2650	0.5		0.113	8.0	30	206.6	0.0372	0.00845	0.05382	0.00615	*0.00388*	0.00575
								26	261.0	0.0367	0.01599	0.11463	0.01260	0.00738	*0.00638*
		Slimes S2	2650	0.5		0.194	5.4	29	206.6	0.0372	0.02143	0.05692	*0.00918*	0.01328	0.01497
								21	261.0	0.0367	0.01070	0.11082	0.01274	*0.00518*	0.00804
M. D. RESEARCH CO. AUSTRALIA		Eckalite EC	2370	-		0.009	11.9	25	105.0		0.21011	0.10906	0.12754	0.13604	*0.01457*
		Eckalite ES	2440	0.5		0.854	2.2	11	105.0		0.10662	0.02758	0.15195	0.03876	*0.02736*
		Ilmenite IL	4470	0.5		0.127-0.170	1.23-1.73	35	53.0		0.02423	0.02513	*0.01707*	0.02473	0.02381
								25	105.0		0.05800	*0.04977*	0.05061	0.05962	0.05851
		Coal RW	1400	0.4		0.180-0.187	15.3-17.7	51	105.0		0.07251	0.03881	0.03758	*0.03323*	0.05296
		Loam WL	2540	0.5		0.348	19.2	70	105.0		0.07361	0.03529	0.03298	*0.02103*	0.04334
SASKATCHEWAN RESEARCH COUNCIL CANADA		Coal CC	1416	0.4		1.538-5.332	81.8-287	39	107.57		0.06702	0.02111	0.07827	*0.01196*	0.01484
		Coal CN	1340	0.4		0.275-0.308	31.3-36.6	10	107.57		0.08300	0.05448	0.05865	*0.03888*	0.04132
	WATER /NaOCl							55	209.32	ASSUMED ZERO	0.02675	0.01706	0.02618	*0.00845*	0.01137
								37	315.21		0.02488	*0.03586*	0.02267	*0.00799*	0.01272
	WATER	Coal FC	1531	0.4		0.382-2.688	14.3-309	16	52.22		0.05054	0.04326	0.04439	0.04123	*0.03815*
								54	107.57		0.04067	0.00670	0.06015	0.00897	*0.00701*
		Iron Con. IC	5245	0.5		0.037	14.6	44	107.57	-	0.01612	0.04986	0.01742	0.00946	*0.00652*
								40	158.5		0.00928	0.05762	0.01675	0.01070	*0.00555*
								33	209.3		0.01256	0.09791	0.02649	0.01687	*0.00497*
								37	263.14		0.01260	0.08758	0.02740	0.01923	*0.01246*
								30	315.21		*0.00896*	0.13224	0.04445	0.03087	0.01239
	WATER /NaOCl	Coal KC	1370	0.4		1.85-0.207	43.4-49.4	34	158.5	UNKNOWN	0.03862	0.01816	0.03631	*0.00649*	0.00963
								29	209.3		0.03990	0.02413	0.03822	*0.00379*	0.00924
								22	263.14		0.03941	0.04289	0.03486	*0.00542*	0.01005
								33	315.21		0.04354	0.04124	0.03980	*0.00563*	0.00609
	WATER	Sand SA	2658	0.5		0.174	2.1	30	52.22		0.03806	*0.01817*	0.03021	0.02958	0.02797
								25	107.57		0.02970	*0.01109*	0.02459	0.02019	0.01624
								27	158.5		0.02349	0.01514	0.01841	0.01707	*0.01279*
								20	209.3		0.02231	0.04353	0.01439	0.01359	*0.00876*
								29	263.14		0.02100	0.03442	0.01630	0.01219	*0.00871*
								25	315.21		0.01588	0.05413	0.00824	0.00798	*0.00531*
		Coal SC	1512	0.4		1.231-2.611	4.27-438	138	107.57		0.04654	*0.01441*	0.03126	0.01551	0.02077
								32	158.5		0.10295	*0.01749*	0.06396	0.02351	0.03355
		Sand SM	2650	0.5		0.168-0.265	33.1-43.3	78	107.57		0.01508	0.00852	0.00796	0.00643	*0.00547*
								58	158.5		0.01788	0.01527	0.00987	*0.00545*	0.01052
								42	263.14		0.01374	0.02141	0.00717	0.00699	*0.00530*
WITS		Fly ash FW	2200	-		0.027	16.3	83	101.7	0.0076	0.00900	0.00738	0.00891	0.00737	*0.00655*
							TOTAL	1630	OVERALL		0.00749	0.00644	0.00550	0.00333	0.00351

Table 6.12 : Energy gradient log standard error values for imported data

For the broad set of conditions represented by tests in Table 6.12 the correlation of Lazarus produces the lowest overall log standard error value. The present correlation produced an error value comparable to that of Lazarus and predicted better in more than half of the tests (55%). The correlation of Wasp *et al.* shows an overall log standard error of 1.6 times greater than the minimum.

6.4.2.3 Detailed investigation of selected tests

Table 6.13 presents the tests used for a detailed investigation of the present correlation. These tests were selected on the basis of increasing concentration. A mix of pipe diameters was included to ensure that no diameter dependence was overlooked.

Table 6.13 : List of tests used for detailed investigation

Test number	D [mm]	Nominal C_{vd} [%]	L.S.E.	Figure number
KS410299	139.3	12.4	0.01520	6.14
KS316269	79.7	13.9	0.01141	6.15
KS43014A	139.3	29.6	0.02232	6.16
KS34022C	79.7	39.2	0.03430	6.17
KS44522C	139.3	43.4	0.02815	6.18
S142023A	139.3	5.9	0.01544	6.19
S1430068	139.3	29.4	0.07320	6.20

For the low concentration tests (C_{vd} < 15%) the correlation is good for both poorly and well graded mixtures. For the highest concentrations the

correlation performs less well. For the sand type 1 test (S1430068) this reduction in performance of the correlation can be explained by the following effects :

1. Energy is expended by the particle-particle interactions within a stationary or sliding bed that undergoes a shearing process.
2. Energy is expended in the wave or slug action in the flow.
3. Particle-wall interactions discussed in Section 6.3.2 and represented by equns. (6.5) and (6.6) after Shook (1985) are not taken into account.

In a recirculating slurry test facility the rate of heat generation in the slurry can be related to the internal friction in the slurry since no other work is done on the system (e.g. a change in potential energy). For a test such as S1430068 (C_{vd} = 29%) the particles have pure water as an interstitial fluid. The rate of heat generation was found to be much higher for this test than for tests at an equivalent concentration (KS42613A, C_{vd} = 27%) that contain kaolin-water mixtures as an interstitial fluid. The difference in the rate of heat generation cannot be ascribed to the difference in wall friction alone. A reduction in heat generation rate for the kaolin-sand tests (and consequently energy gradient) can be partly ascribed to a lubrication effect as discussed in Section 2.3.2.1. At low concentrations, interparticle interactions are reduced and this effect is therefore less intense.

For the case of kaolin-sand mixtures the kaolin acts as a lubricant when mixed with the interstitial water. For this reason only a small quantity of kaolin is needed to produce this effect. This fact was presented in Section

1.3.6 (Kazanskij *et al.*, 1974 and Smoldyrev, 1982). For test KS44522C the lubricating effect of the kaolin is insufficient and an increase in the actual energy gradient over the predicted energy gradient is apparent.

Shook (1985) suggests that equns. (6.5) and (6.6) are equally applicable for coarse as well as fine high concentration mixtures. The lubricating effect of kaolin will have an effect on the liquid film between the coarse particles and the pipe wall since the kaolin particles will be of the same order of magnitude as the laminar sublayer. The increased heating could also be accounted for by this approach since particle migration away from the wall is said to occur at low to moderate concentrations with a reversal, with particles penetrating the laminar sublayer, for high concentrations.

Slug and wave flow would result in a further dissipation of energy particularly in the transition to heterogeneous flow where slug *blow through* and dispersion occurs. This mechanism would enhance the energy loss due to shearing of the bed particles.

An empirical method for the measurement of internal mechanisms in the pipeline would destroy the purely mechanistic character of the present correlation. For this reason it was decided not to include an empirical energy loss term to account for the particle interactions. Newitt *et al.* (1955) later confirmed by Babcock (1970) presented a semi-empirical correlation for sliding bed flow

$$\frac{i_m - i_w}{C_{vd}\, i_w} = k_1 (S_s - S_w) \frac{gD}{V_m^2} \qquad (6.8)$$

where k_1 = 66 after Newitt *et al.* (1955)

k_1 = 60.6 after Babcock (1970).

This correlation was developed for fully developed sliding bed flow. Babcock (1970) suggests that this equation represents the maximum energy gradient for sliding bed flow. For the condition of transition between sliding bed flow and homogeneous flow "the head loss may or may not be proportional to the volumetric concentration depending on the particle size and on the concentration and velocity (Babcock, 1970)". There is no simple transition from equn. (6.8) to the mechanistic approach of the present model. An understanding of the internal mechanisms of this transition type flow is therefore required to model the condition. Figure 6.21 shows the data of test S1430068 compared with the correlation of Newitt *et al.* (1955) (equn. (6.8)). Test S1435148 is shown in Figure 6.22. This test is included because it is the only test for which fully developed sliding bed flow occurred. The prediction of equn. (6.8) is accordingly good. Table 6.14 shows the log standard error values for these two figures (Figures 6.21 and 6.22).

Table 6.14 : Log standard error values for energy gradient predicted by equn. (6.8)

Test number	D [mm]	Nominal C_{vd} [%]	L.S.E.	Figure number
S1430068	139.3	29.4	0.02931	6.21
S1435148	139.3	42.1	0.01172	6.22

Figure 6.23 shows the data of test S1435148 compared to equn. (6.6) for $k_4 = 5$. The slope of the correlation appears to be in error. This is because the definition for the Reynolds number may be incorrect. The concept of high concentration mixtures causing a penetration of the sublayer by particles with lubrication occurring over the contact distance appears attractive and should be investigated further. For mixed regime slurries (with fine material producing a vehicle) the present correlation is a consistent mechanistic approach which produces accurate energy gradient prediction over a broad range of materials.

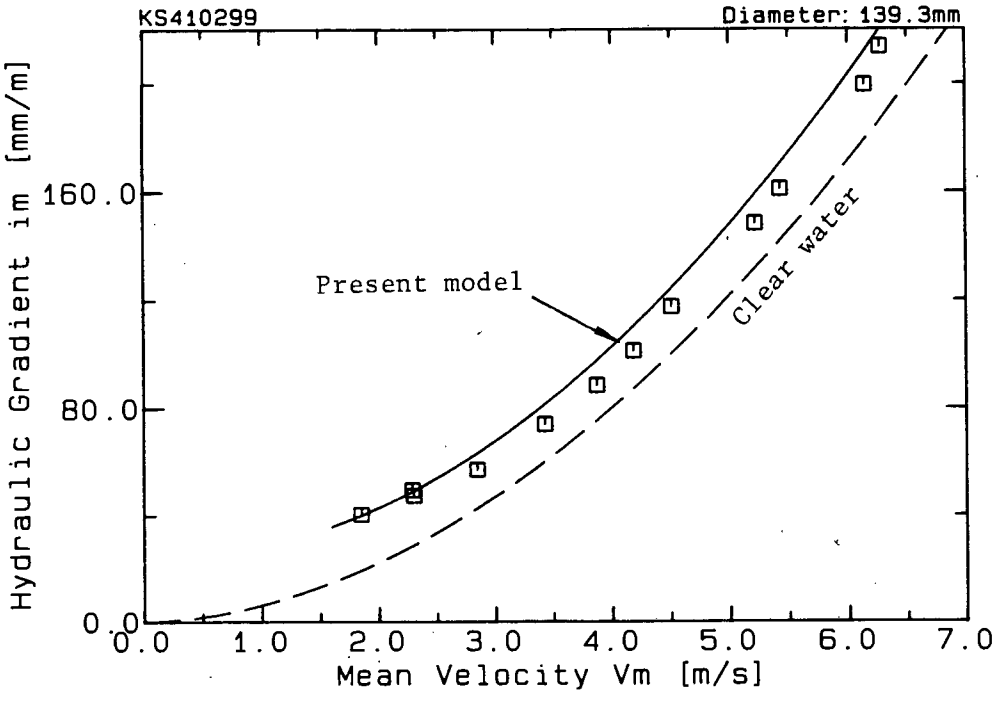

Figure 6.14 : Kaolin-sand test, nominal concentration C_{vd} = 12.4%

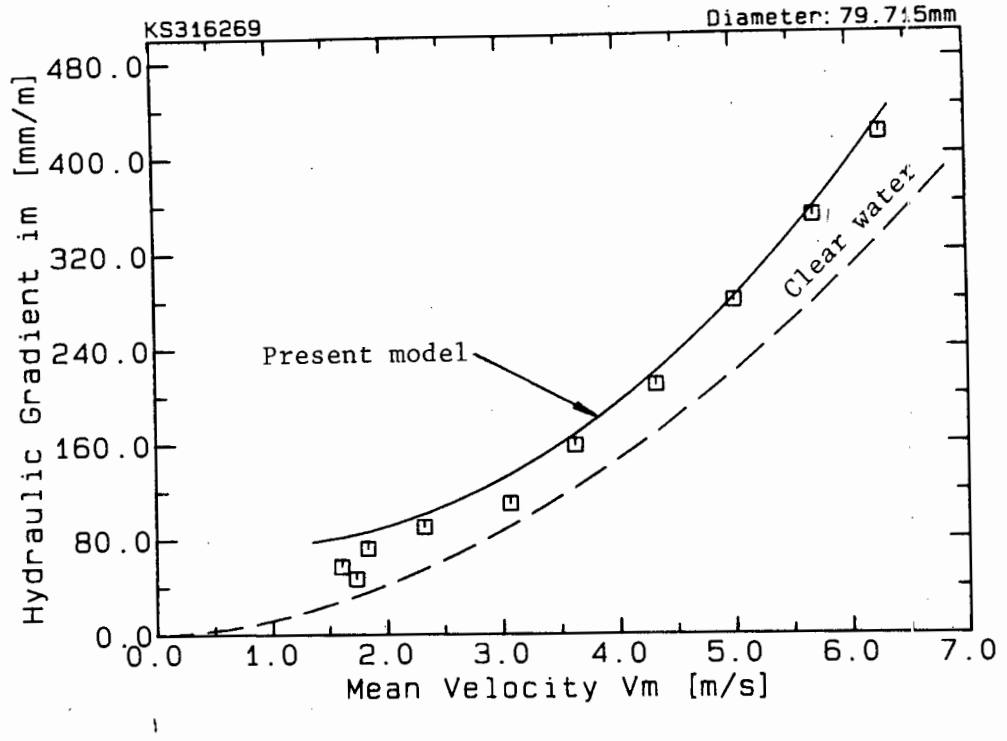

Figure 6.15 : Kaolin-sand test, nominal concentration C_{vd} = 13.9%

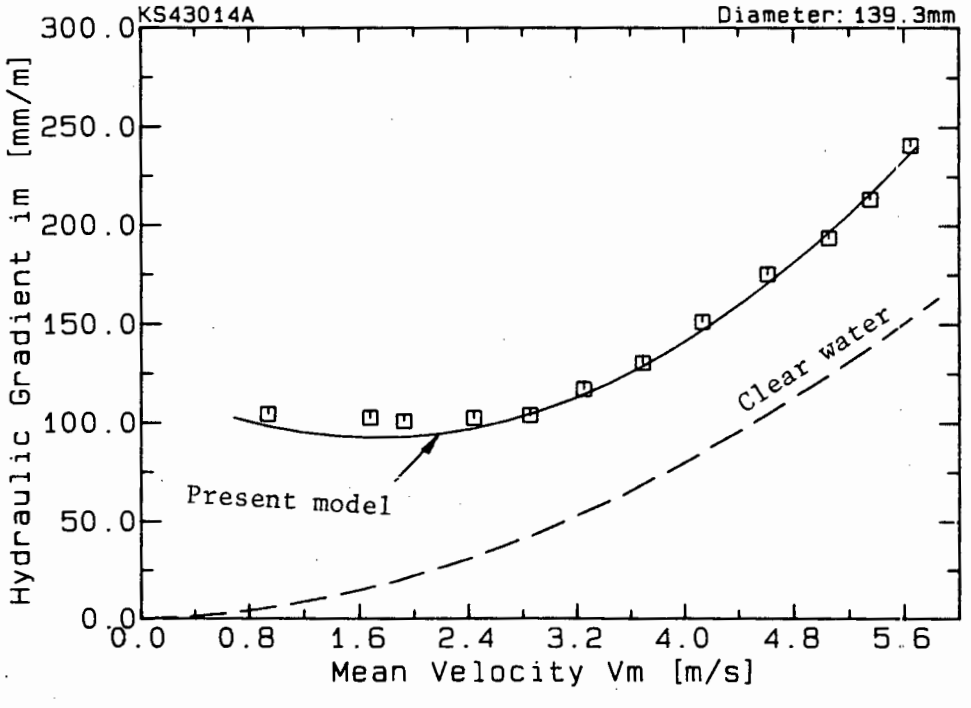

Figure 6.16 : Kaolin-sand test, nominal concentration C_{vd} = 29.6%

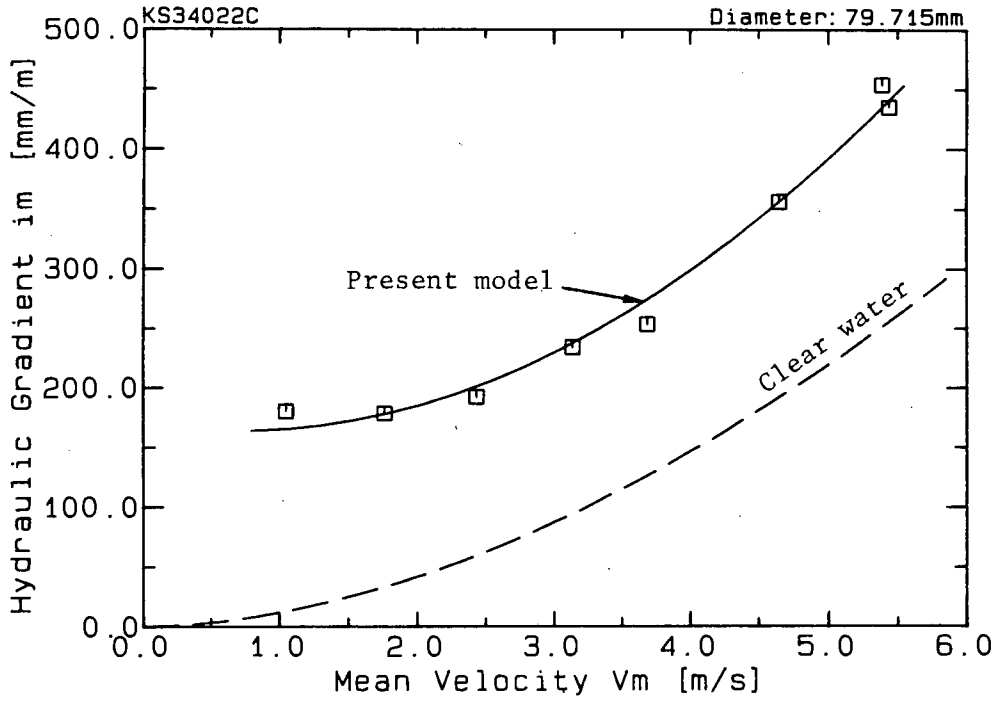

Figure 6.17 : Kaolin-sand test, nominal concentration C_{vd} = 39.2%

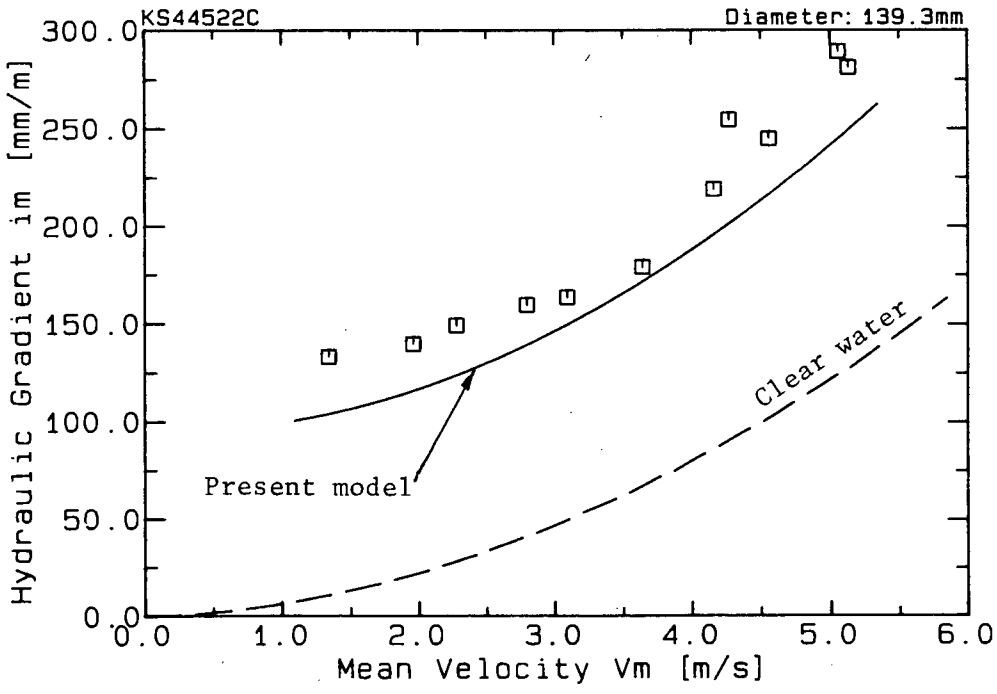

Figure 6.18 : Kaolin-sand test, nominal concentration C_{vd} = 43.4%

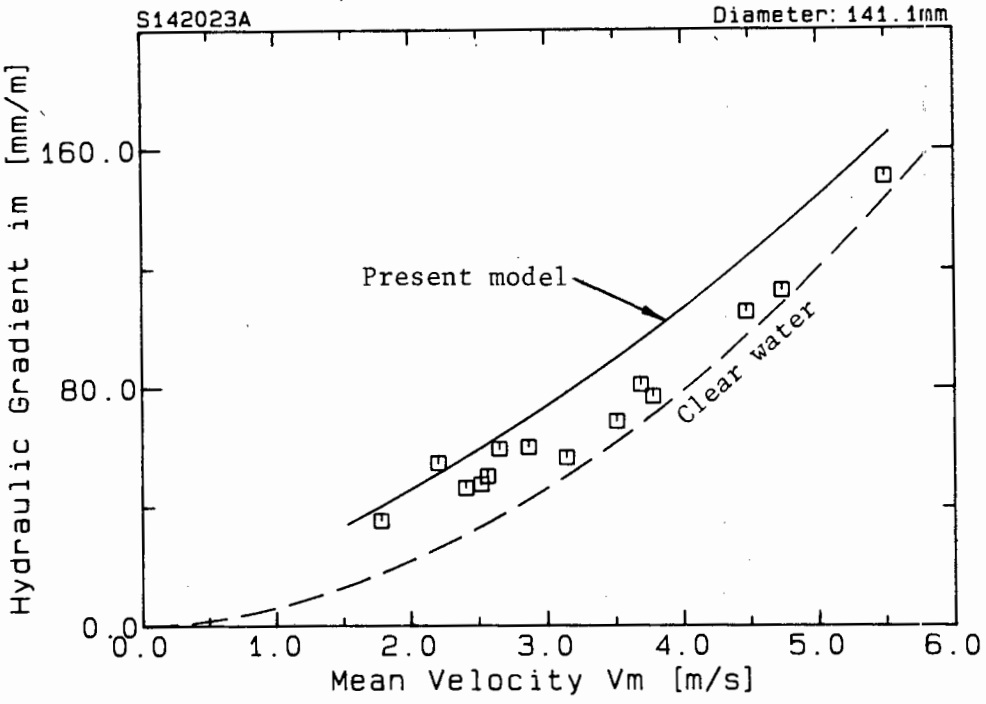

Figure 6.19 : Sand type 1 test, nominal concentration C_{vd} = 5.9%

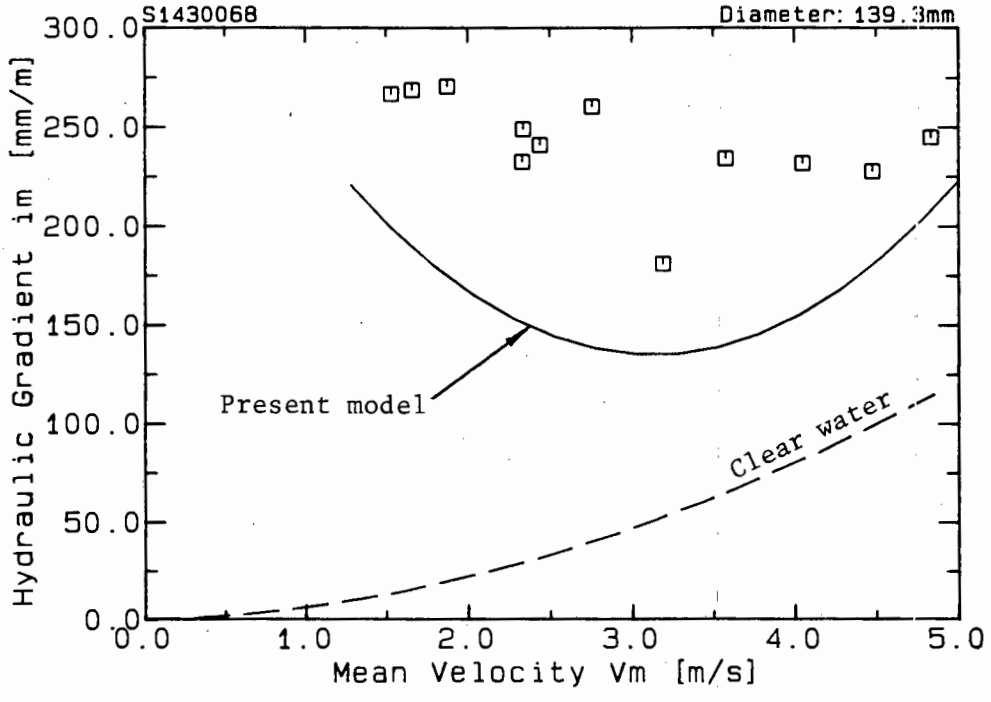

Figure 6.20 : Sand type 1 test, nominal concentration C_{vd} = 29.4%

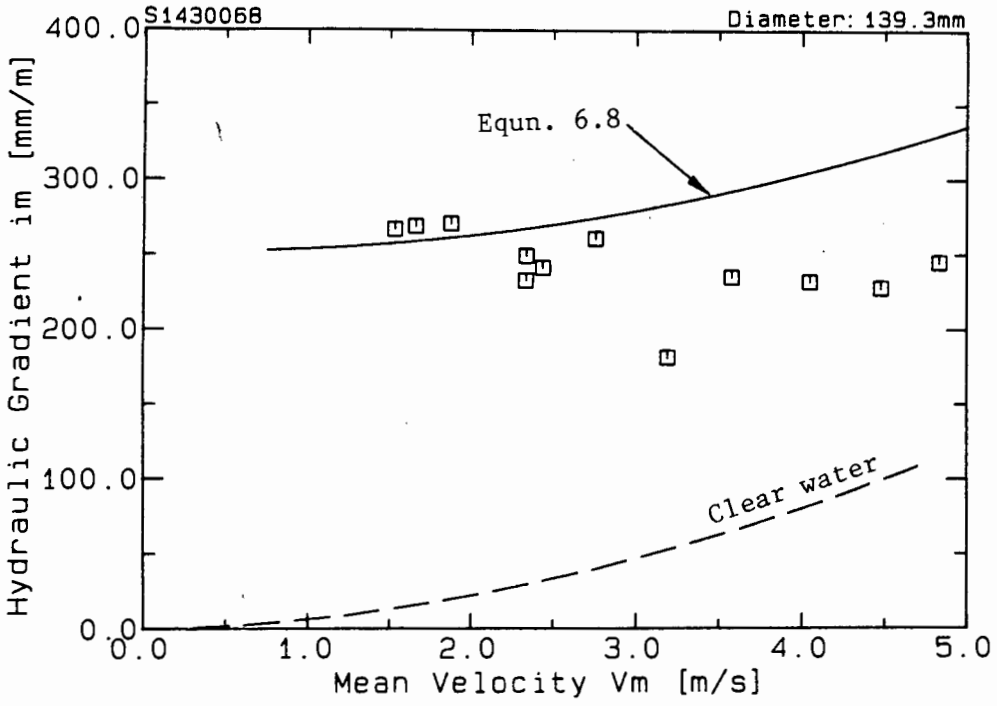

Figure 6.21 : Sand type 1 test, nominal concentration C_{vd} = 29.4%

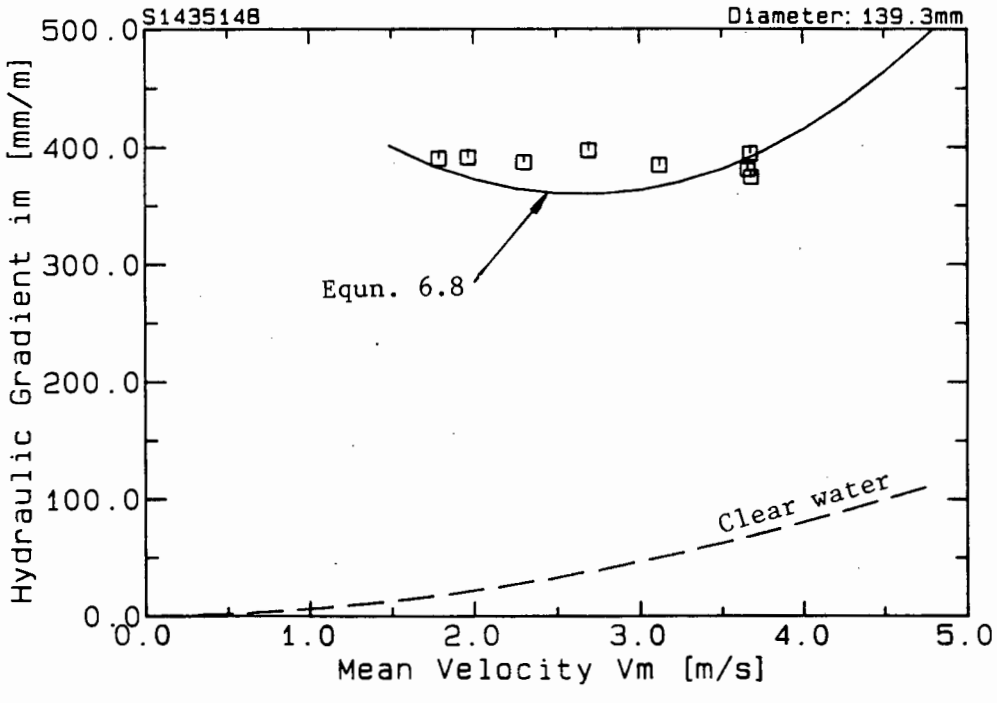

Figure 6.22 : Sand type 1 test, nominal concentration C_{vd} = 42.1%

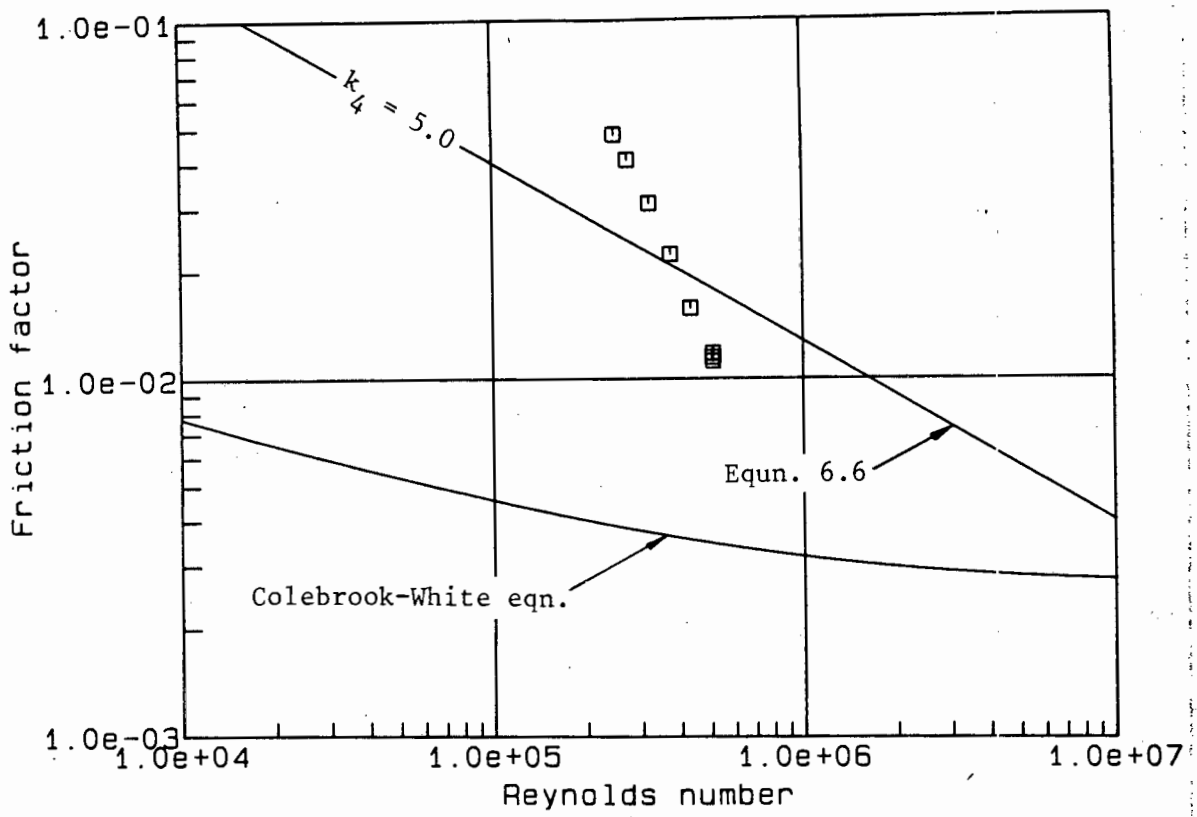

Figure 6.23 : Friction factor versus Reynolds number for test S1435148 with equn. (6.6)

6.4.3 Bed Condition Prediction

A clear distinction between stationary and sliding bed flow and sliding bed and fully suspended flow does not exist. For a slurry flow system to be modelled mechanistically a distinction must be made so that the correct force balance on a pipeline of unit length is used. Table 6.15 details the transition criteria for each of the correlations presented. Table 6.16 presents a set of results comparing the percentage of correct predictions for the complete data base (imported and local) for the flow conditions existing at any particular point.

Table 6.15 : Transition criteria for stationary, sliding and fully suspended flow for the correlations investigated

Correlation	Stationary to sliding bed flow	Sliding to fully suspended flow
Wasp *et al.* (1970)	For $C_{vd} \leq 5\%$ $F_L = 3.67\ C_{vd} + 1.1633$ For $C_{vd} > 5\%$ $F_L = 3$ $V_d = F_L \left[\frac{d_{50}}{D}\right]^{1/6} \sqrt{2gD(S_s-S_w)}$ (1.11)	None
Wilson	If $X < X_S$ then bed is stationary where : $X = \frac{i_{susp}}{i_p}$ (1.23) $X_S = \frac{(\sin\gamma - \gamma\cos\gamma)(1-a_{bed})^2}{\xi \sin\gamma}$ (1.25)	None
Lazarus	Bed is stationary if $\frac{\Delta P}{L} A_b + \tau_I D \sin\gamma$ $< F_{RB} + W_b \sin\theta$ (1.43)	Fully suspended flow if $A_b \leq 0.01A$
Present	Bed is stationary if $F_{DB} < F_{RB}$ (3.73)	Fully suspended flow if $F_{D_{FS}} \geq F_{D_{SL}}$ (3.77)

Table 6.16(a) : Prediction of three transition flow conditions. The results are presented as a percentage of the total number of predictions that are correct. The 3 conditions are stationary bed, sliding bed and fully suspended flow.

Correlation	Local data	Imported data
Wasp *et al.*	77.31%	70.32%
Wilson	77.70%	74.23%
Lazarus	14.72%	15.66%
Present	62.16%	43.17%
Number of points	1345	1304

Table 6.16(b) : Prediction of two transition flow conditions. The 2 conditions are stationary bed and non stationary bed.

Correlation	Local data	Imported data
Wasp *et al.*	93.30%	83.67%
Wilson	95.32%	90.41%
Lazarus	89.29%	81.50%
Present	94.42%	90.57%
Number of points	1345	1304

In many cases periodic phenomena exist in the flow down to very low velocities. The predictions of stationary bed, shown in Table 6.15, should not be over emphasized because of the subjective nature of their measurement.

The correlation of Wilson and Wasp *et al.* have only one transition criterion from stationary to fully suspended flow. The Lazarus model, although having two transition criteria never predicts fully suspended flow. The criterion set by Lazarus (Table 6.15) is therefore in error. For the imported data the sum of the number of points in each flow category is less than the total number of data points. This is because some of the data had no given flow condition so none was ascribed. For the single transition criterion the present correlation predicts with the same order of accuracy as the best correlation (Table 6.16(b)). For the two transition criterion the present model predicts better than the Lazarus model.

The present model predicts sliding bed flow for a large number of the points where suspended flow was recorded. This is why the error shown in Table 6.16(a) is large. The distinction between sliding bed and fully suspended flow is subjective. In Table 6.16(b) where this transition (sliding to suspended) is suppressed, and only the transition from stationary to non stationary bed is included, the present correlation performs as well as the best presented.

6.4.4 Velocity and Concentration Profiles

Figures 6.24 to 6.26 show velocity and concentration profiles for the flow of a slurry from stationary bed (Figure 6.24) to pseudohomogeneous flow (Figure 6.26). These profiles are generated from a concentric grid with nine radials on 10 circumferential elements (190 points in total). The data used is presented in Appendix 11. The profiles presented are a consequence of the calculation of *in situ* and delivered concentration. Profiles are therefore available automatically for every point processed using the

present model. Table 6.17 shows the good agreement between measured and calculated concentration values obtained from integrating the profiles shown in Figure 6.24.

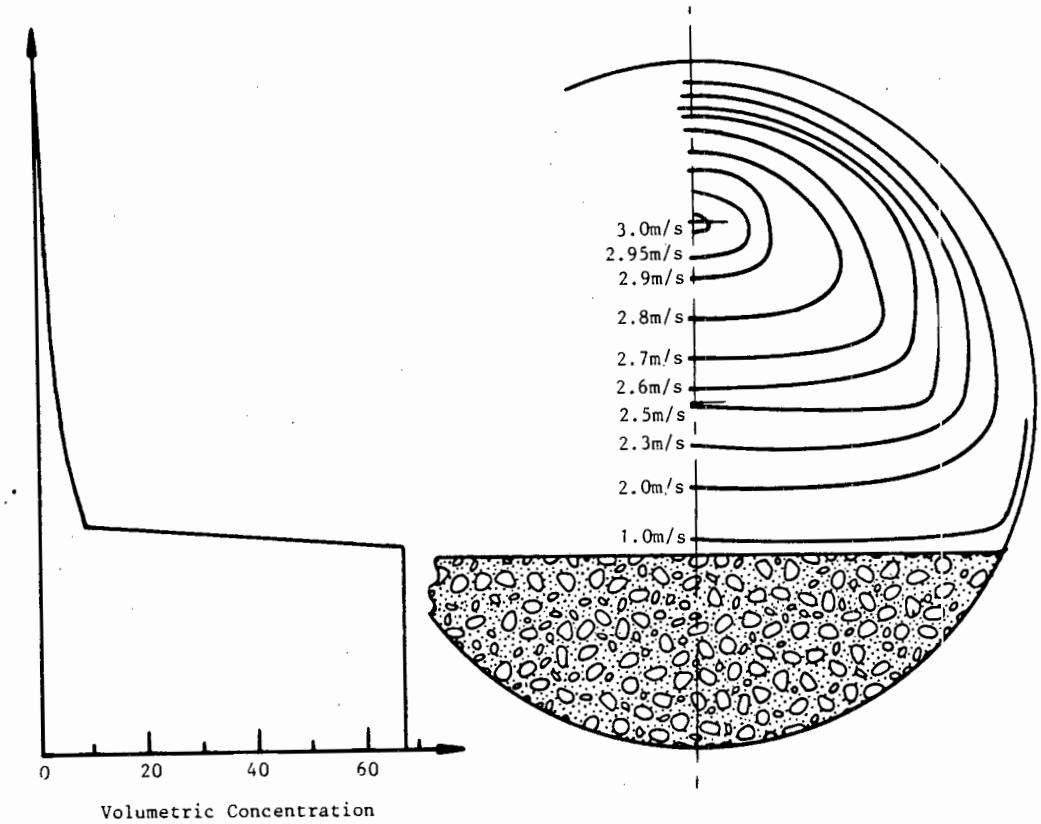

Figure 6.24 : Concentration and velocity profile for stationary bed flow. Test S142023A, V_m = 1.78 m/s.

Table 6.17 : Measured and calculated concentration values for the flow conditions shown in Figure 6.24

	Measured	Calculated
C_{vt}	11.77%	10.45%
C_{vd}	2.49%	2.48%

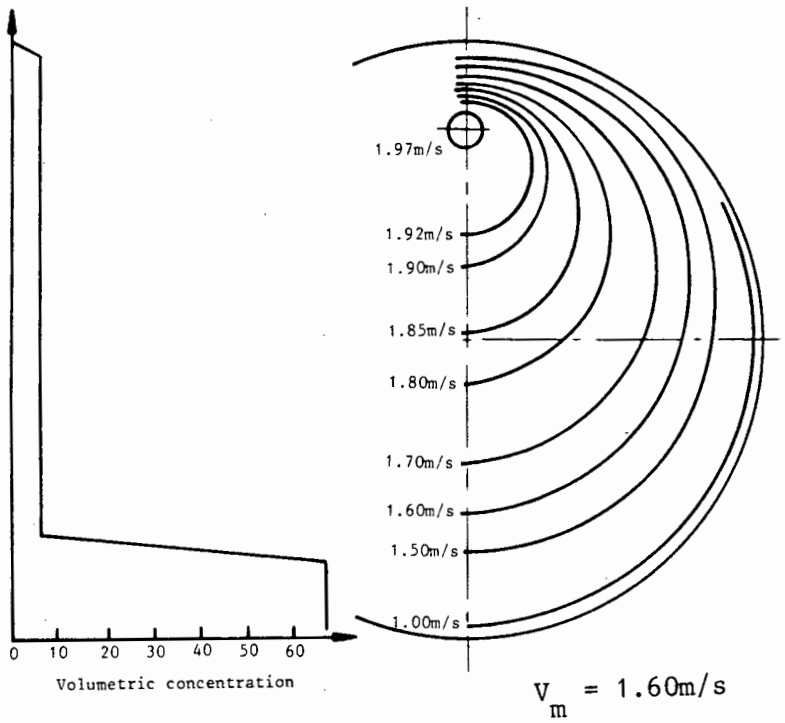

(a)

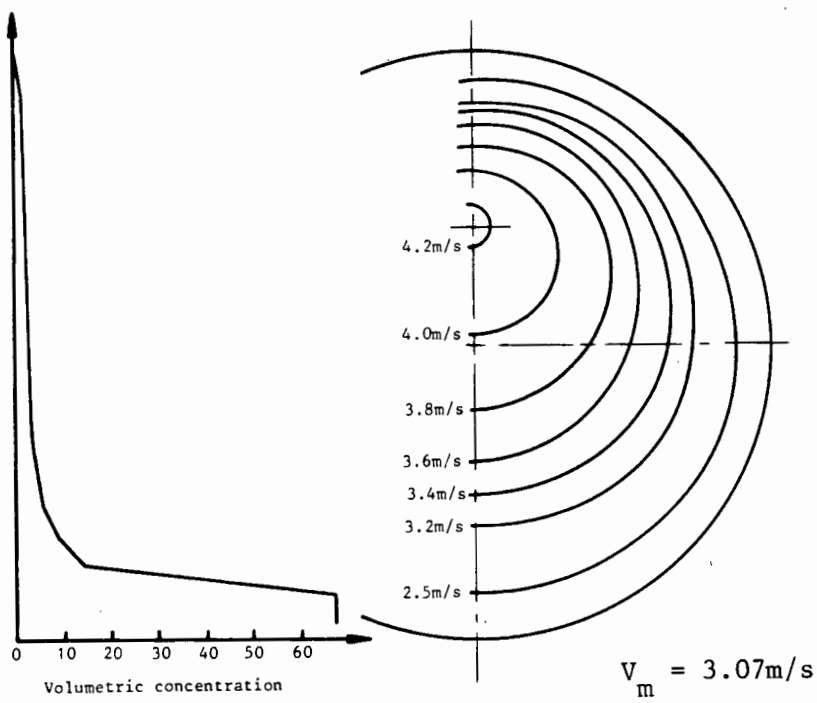

(b)

Figure 6.25 : Concentration and velocity profile from sliding bed flow

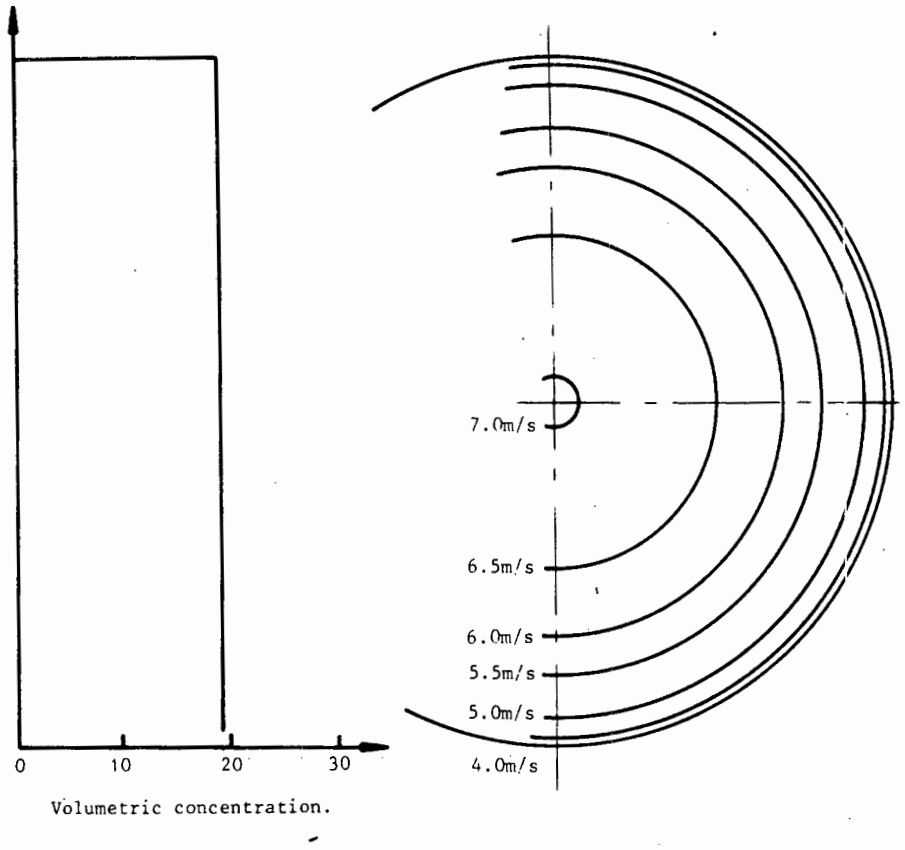

Figure 6.26 : Concentration and velocity profile for fully suspended flow (pseudohomogeneous)

6.5 HYDROTRANSPORT SYSTEM DESIGN

The ultimate objective of any predictive model is its use as a system design tool. The computer programs used for this purpose are presented in Appendix 16. Two design conditions are considered, one for constant mass flow of solid and the other for constant delivered concentration. These quantities can be related by a form of the continuity equation

$$C_{vd} = \frac{Q_s}{Q_m} = \frac{4\ M_s}{V_m\ \pi\ D^2\ \rho_s} \quad . \tag{4.1}$$

Examples of the two design conditions would be the transport of mine tailings where a specified mass of ore is processed which results in a fixed mass flow of solids. A constant concentration is required if a mine tailings slurry is used to backfill the underground works for strata control. The quality of this placed material is critical and is directly related to the slurry concentration.

For a fixed diameter pipeline a series of design graphs can be drawn to show some general trends. Figure 6.27 presents the particle size distribution for the material considered in the sample calculations. This mixture produces a typical mixed regime slurry.

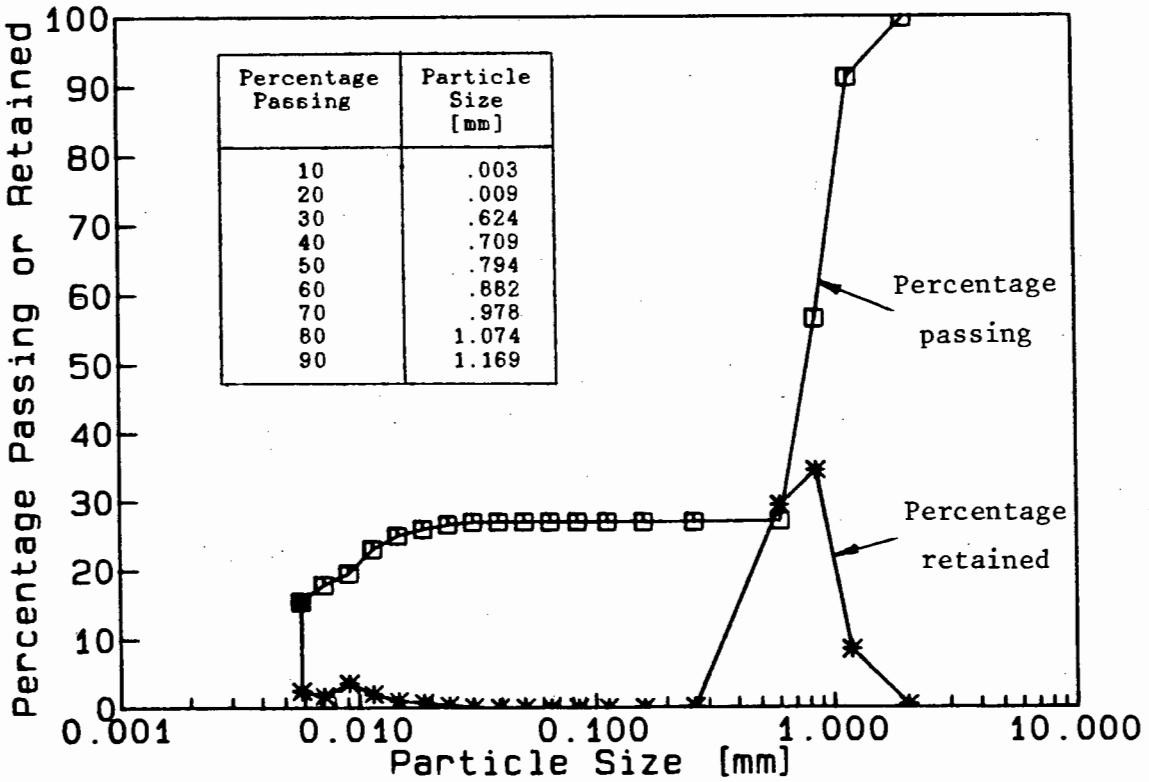

Percentage Passing	Particle Size [mm]
10	.003
20	.009
30	.624
40	.709
50	.794
60	.882
70	.978
80	1.074
90	1.169

Figure 6.27 : Particle size distribution of the material considered in the sample calculations

Figures 6.28 and 6.30 show delivered concentration as parameter for graphs of mean velocity versus energy gradient and specific power consumption respectively. Figures 6.31 and 6.32 show the same ordinate and abscissa but with mass flow of solids as parameter. In Figure 6.28 the expected trend for the energy gradient to increase with increasing concentration fails at mean velocity around 2 m/s for concentration between 20% and 30%. This is because the bed condition that exists is different for the two concentrations. At

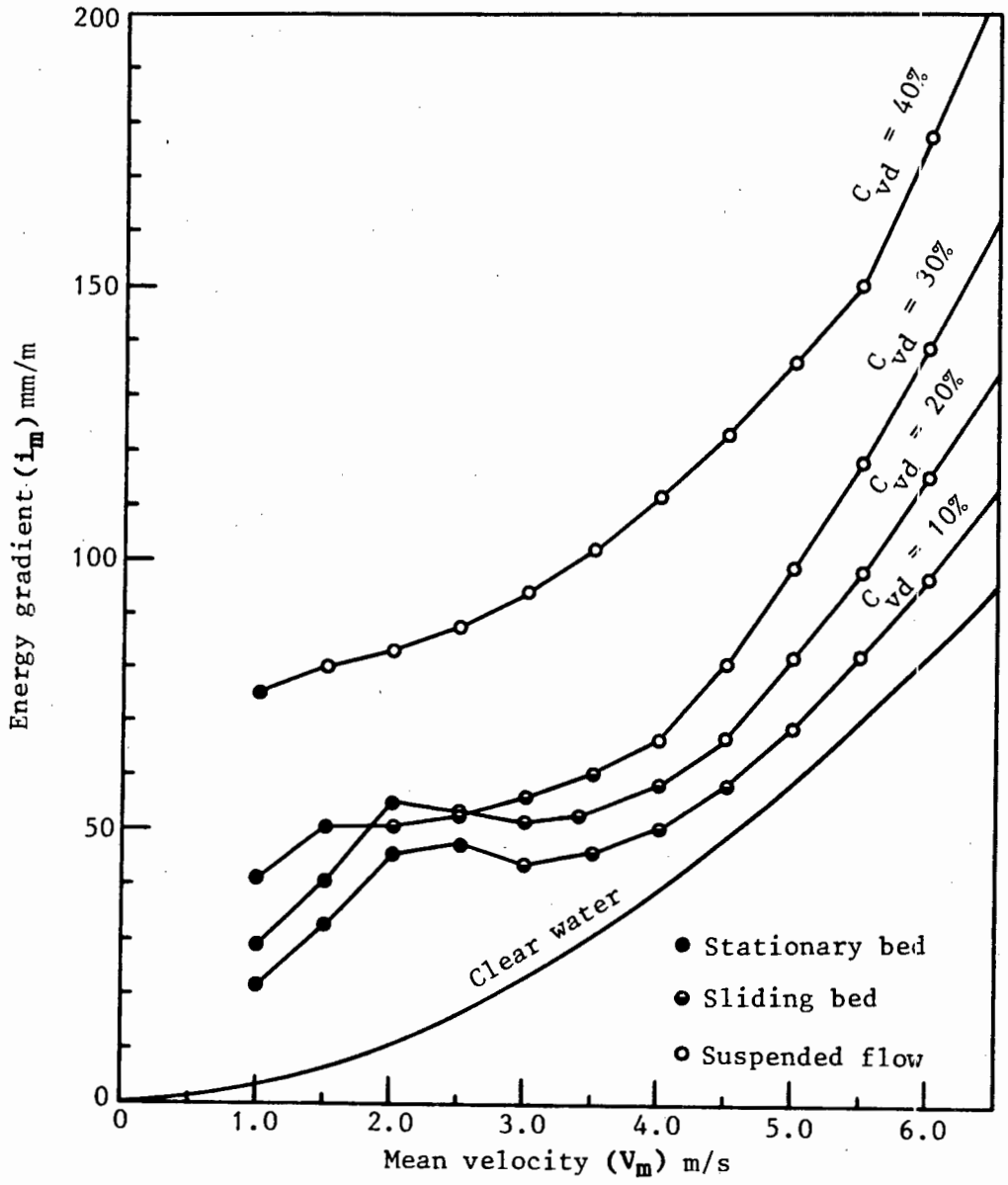

Figure 6.28 : Energy gradient versus mean mixture velocity with delivered concentration as parameter. D = 250mm, $k_w = 7.6.10^{-6}$ m . Points shown designate the flow regime for the prevailing flow conditions.

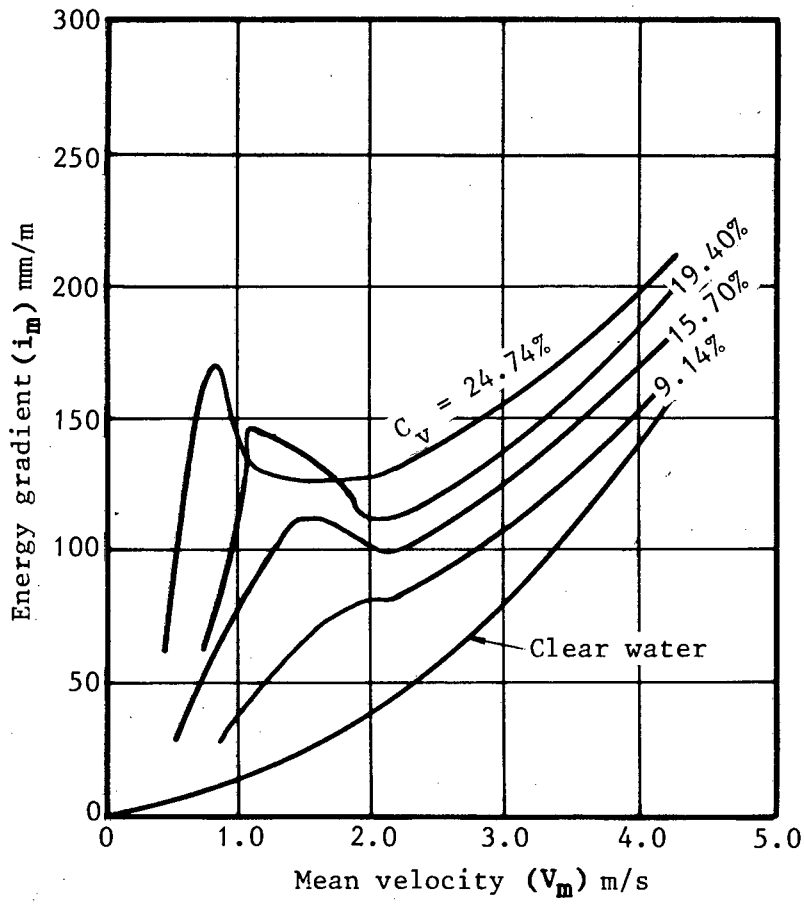

Figure 6.29 : Energy gradient versus mean mixture velocity with delivered concentration as parameter from Kazanskij *et al.* (1974) D = 100mm

V_m = 2.0 m/s for a concentration of 20%, a stationary bed exists. At a concentration of 30% the bed is sliding, the flow area is increased with a resultant decrease in velocity and a drop in energy gradient. This crossover is not unique to the mixture used here but is a common phenomenon for most mixtures in which stationary beds will form at low velocity. Figure 6.29 shows a similar graph to Figure 6.28 extracted from the work of Kazanskij *et al.* (1974). A crossover is also demonstrated by this sand-water mixture.

Figure 6.30 shows a graph with the same parameter as Figure 6.28, plotted against specific power consumption

$$SPC = \frac{i_m}{C_{vd}\, S_s} \qquad \left[\frac{Ws}{Nm}\right] \quad . \tag{6.9}$$

An optimum specific power consumption is evident near C_{vd} = 30%. It is usual for a fixed diameter to find that the maximum obtainable concentration produces the minimum specific power consumption. In this example the non Newtonian character of the vehicle results in an optimum concentration lower than the maximum pumpable.

Figure 6.31 and 6.32 are produced by changing the subject of the continuity equn. (4.1) to mass flow of solids. In Figure 6.32 for a mass flow rate of 25 kg/s the specific power consumption is 0.0582 Ws/Nm . This point appears to be the optimum. The flow condition at any point on the graph is important in selecting the optimum specific power consumption. At M_s = 25 kg/s stationary bed flow exists up to a mean velocity of 2.5 m/s. The stationary bed flow condition would need further investigation as to its stability in terms of pipe blockage and in the case of a centrifugal pump application whether the pump characteristic might not result in a pump-system mismatch and pipe blockage.

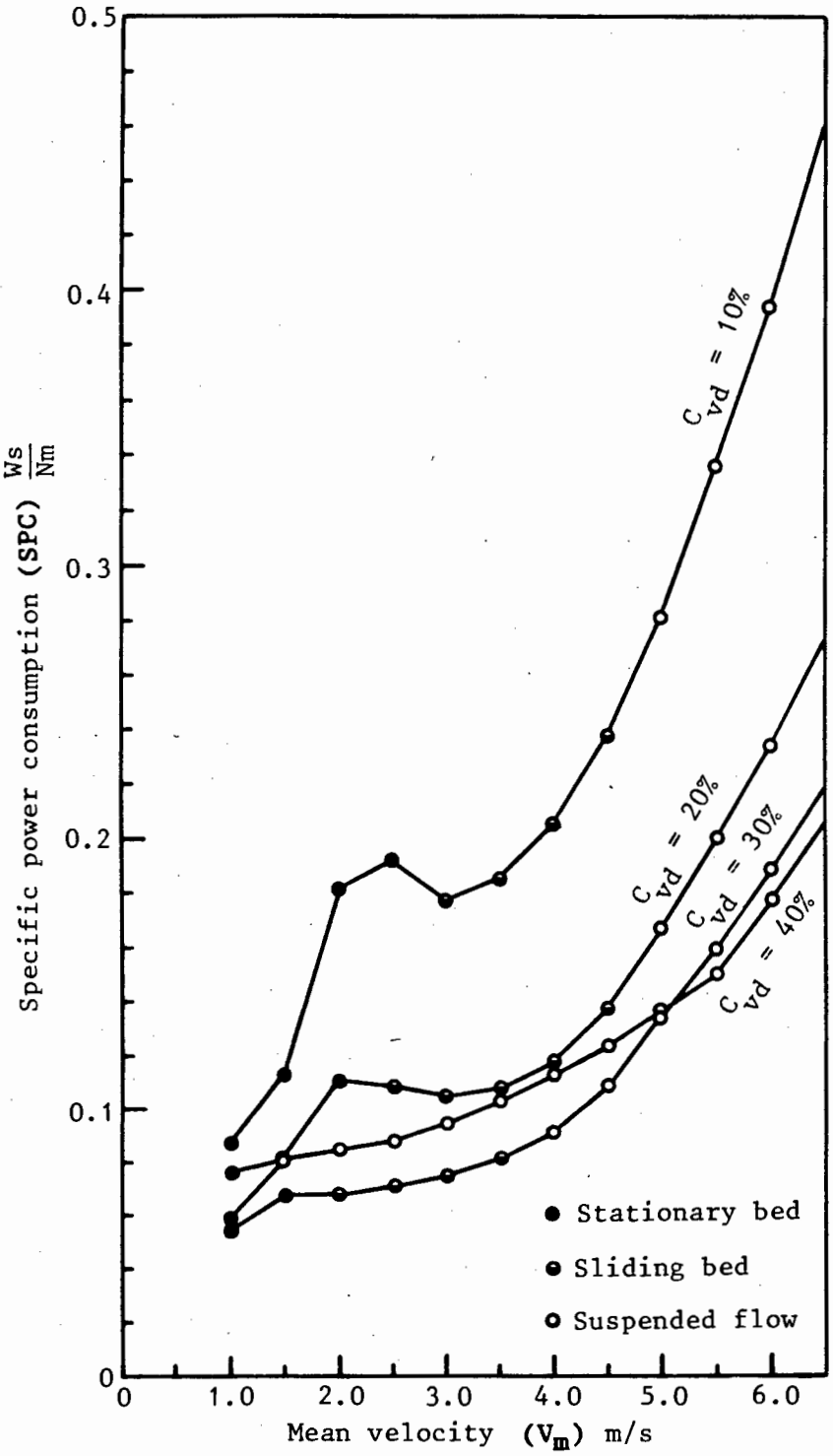

Figure 6.30 : Specific power consumption versus mean mixture velocity with delivered concentration as parameter D = 250mm, $k_w = 7.6.16^{-6}$ m. Points shown designate the flow regime for the prevailing flow conditions.

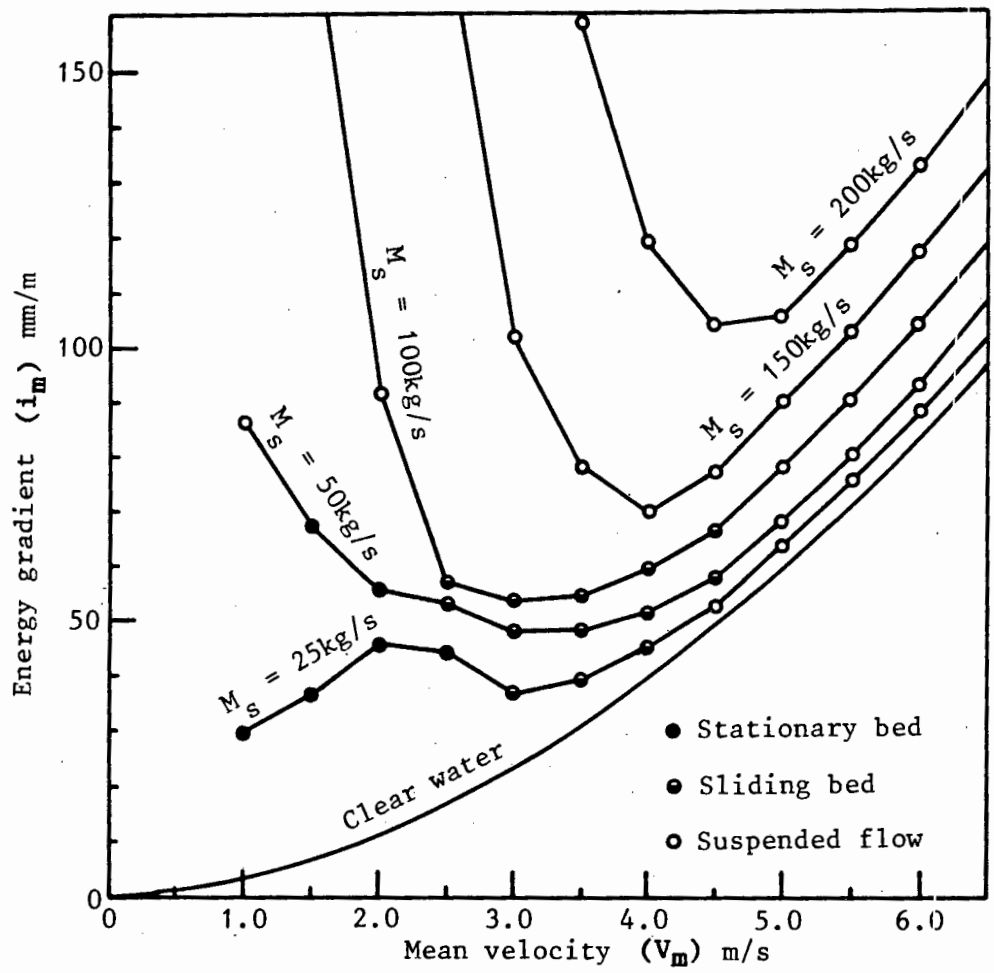

Figure 6.31 : Energy gradient versus mean mixture velocity with solid mass flow rate as parameter D = 250mm, $k_w = 7.6.16^{-6}$ m . Points shown designate the flow regime for the prevailing flow conditions.

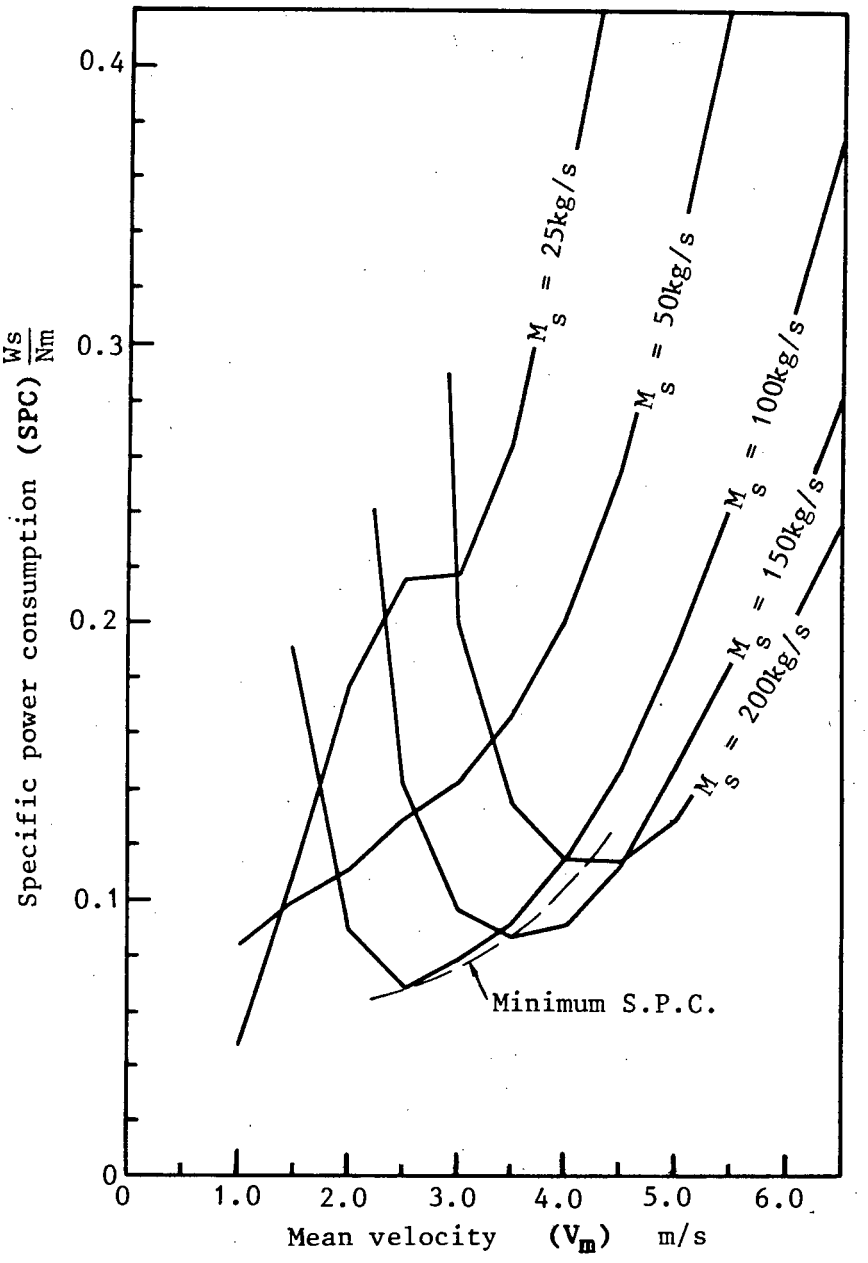

Figure 6.32 : Specific power consumption versus mean mixture velocity with mass flow rate of solids as parameter D = 250mm, $k_w = 7.6.16^{-6}$ m

6.5.1 Constant Mass Flow of Solids

Figure 6.33 shows a design graph for a fixed mass flow rate of solids. To avoid the problem of pipe blockage a shaded area is shown in which all points have stationary bed flow and should be considered only if the

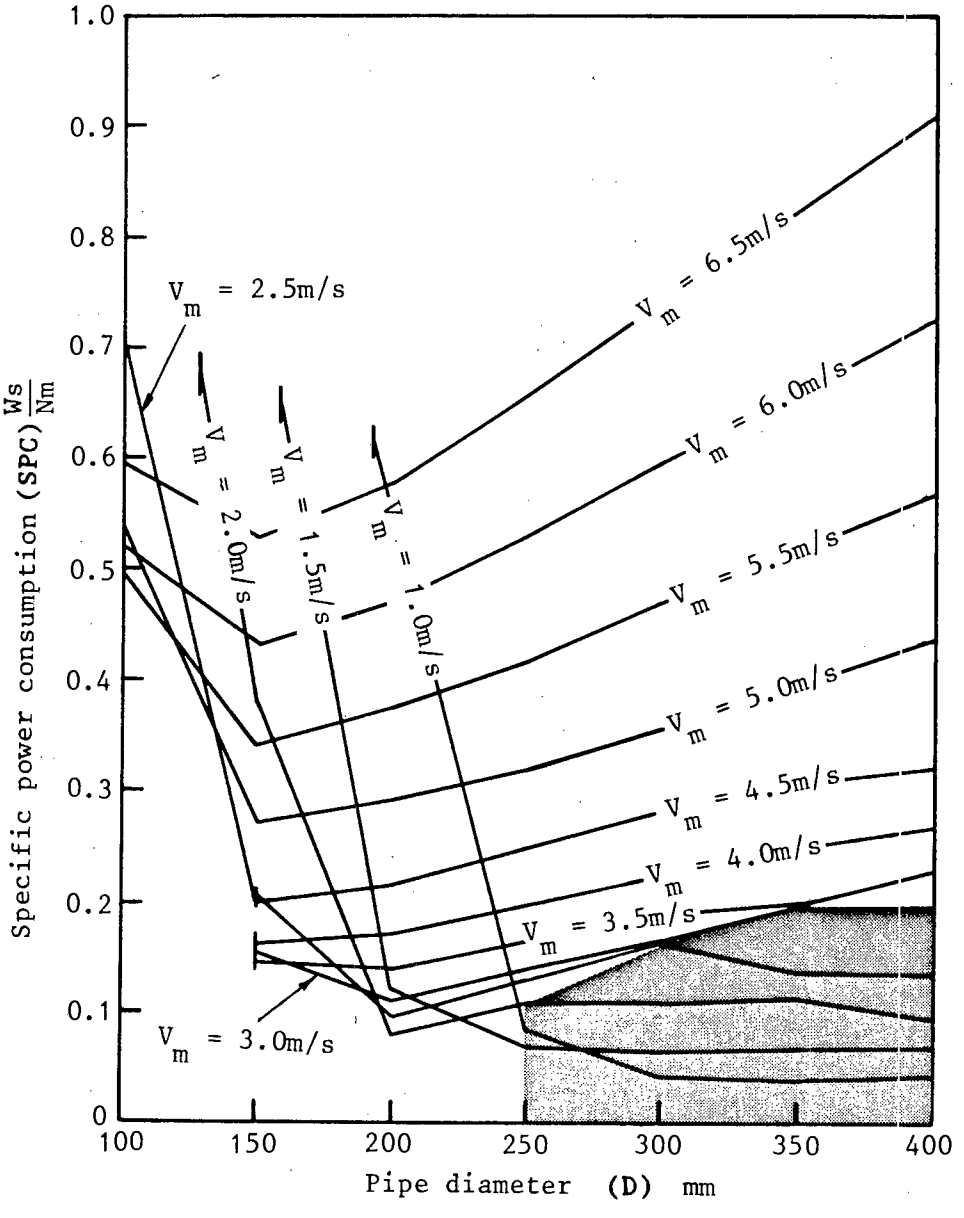

Figure 6.33 : Specific power consumption versus pipe diameter with mean mixture velocity as parameter M_s = 50 kg/s , k_w = 0

problems connected with pipe blockage can be accounted for. Two candidate points exist for minimum specific power consumption :

1. V_m = 1.5 m/s in a 250mm diameter pipeline.
2. V_m = 2.0 m/s in a 200mm diameter pipeline.

Streicher (1984) points out that minimum specific power consumption is only one of the many variables that must be accounted for in the complete economic optimisation of a hydrotransport system. The study of hydrotransport design optimisation is at present in its infancy and may eventually result in designs where the operating point is well away from the minimum specific power consumption. For this study it is expedient to present specific power consumption to show the general trends predicted by the present correlation.

6.5.2 Constant Delivered Concentration

Figure 6.34 shows a design graph for a fixed delivered concentration. A shaded region in which stationary bed flow occurs is shown. From this graph the minimum specific power consumption occurs at the maximum pipe diameter and mass flow rate of solids. Specific power consumption decreases with increasing pipe diameter. For diameters ranging between 200mm and 400mm specific power consumption varies between 0.09 Ws/Nm and 0.05 Ws/Nm . If care is taken an operating point in the shaded region may be selected.

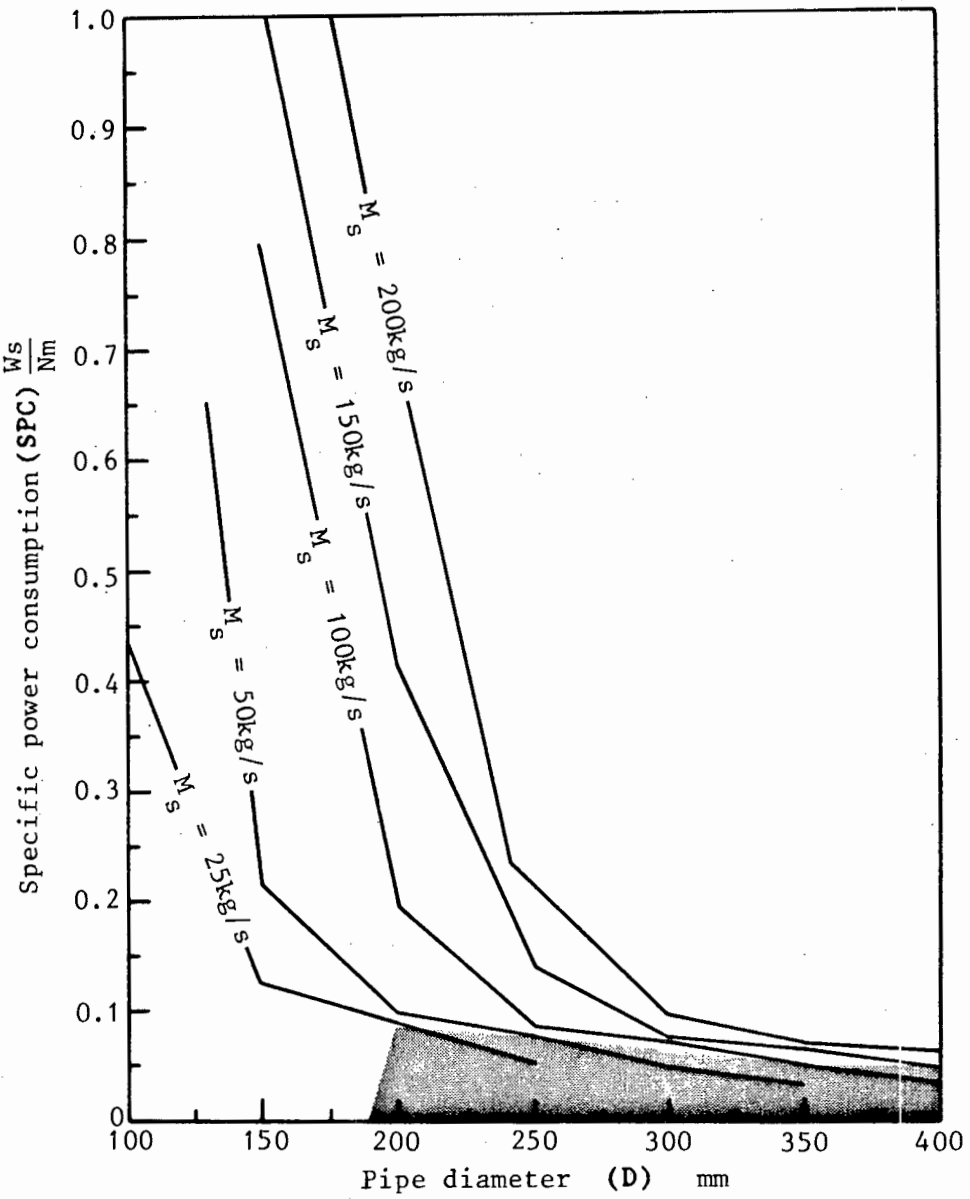

Figure 6.34 : Specific power consumption versus pipe diameter with delivered concentration as parameter C_{vd} = 25% , k_w = 0

6.6 CONCLUSIONS

The level of sophistication of energy gradient prediction has in recent years improved significantly. The problem of overall design and optimisation of hydraulic transport systems needs to be addressed in order that the improvement in energy gradient prediction can best be utilised.

From this chapter on comparisons between the analytical and experimental results the following conclusions can be drawn :

1. Log standard error is a successful technique for comparing observed and predicted quantities.
2. The Malvern 2600/3600 Particle Sizer VF.6 is an accurate instrument for measuring particle size less than 400μm .
3. The coefficient of sliding friction was measured for the tests conducted. Table 6.18 presents the results. For the imported data the value of the coefficient of sliding friction was assumed to be 0.4 for coal and 0.5 for all other tests.

Table 6.18 : Measured values of the coefficient of sliding friction

Material	μ_s
Bottom ash	0.47
Fly ash	0.42
Sand and kaolin-sand	0.49
Ocean bed	0.39
Uranium tailings	0.53

4. The maximum bed concentration (C_b) was assumed to be constant and assigned a value of $C_b = 0.67$.
5. A sensitivity analysis on the variation of the maximum packing concentration showed that this value has a complex relationship to mixture concentration, vehicle floc structure and dilatancy of the bed caused by shear stress. A measurement of the actual value of C_b is not

possible at present and so the use of a constant value although not accurate is found to be realistic for comparative purposes and convenient for design purposes.

6. Particle shape factors are presented in Table 6.19 for those materials for which it was measured. Although constant values have been assigned the shape factor usually varies in inverse proportion to the particle size. A shape factor of unity should be assumed if a value is not measured.

Table 6.19 : Particle shape factors for the material for which it was measured

Material	S_F
Bottom ash	0.80
Fly ash	0.90
Sand	0.95
Ocean bed	0.80
Uranium tailings	0.45 → 0.90

7. A Newtonian and a non Newtonian rheogram for kaolin clay will intersect (giving the same shear stress for the given strain rate) at a strain rate significantly in excess of the strain rate encountered in pipeline flow.

For example, a kaolin clay slurry for C_v = 14.88% the two rheograms intersect at $\frac{du}{dr} = 3.10.^{5}s^{-1}$. This is equivalent to a mean mixture velocity of 19.49 m/s in a 150mm inside diameter pipeline.

8. The Colebrook-White and Torrence equations produce similar predictions for Newtonian fluids.

9. For kaolin clay the Colebrook-White equation prediction is satisfactory for Reynolds numbers greater than 2.10^5 . Below this value the prediction is too low by an order of magnitude.

10. Kaolin slurries are flocculated at rest. With increasing strain rate the floc structure is broken down until at a Reynolds number of 2.10^5 the flocs are completely destroyed and the flow becomes Newtonian.

11. Field 3 ash slurries deviate above and below the Colebrook-White prediction for Reynolds numbers less than approximately 2.10^5 .

12. The yield stress and hence floc formation for field 3 ash is weak (at C_v = 28%, $\tau_y \simeq$ 2.5 Pa) . Field 3 ash data points below the Colebrook-White prediction have low and moderate concentrations (C_v < 28%). For these concentrations particle migration away from the pipe wall occurs reducing the friction factor. At concentrations above 28%, particles are forced against the pipe wall and a thin film lubrication friction component between particles and the pipe wall must be added to the hydrodynamic friction already present. This mechanism accounts for data points above the Colebrook-White prediction.

13. Kaolin clay can best be described by a combination of the Colebrook-White and Torrence friction factor predictions. Both should be calculated for any point and the higher value assumed.

14. The prediction of suspended flow concentrations was tested using three equations :

    1. Einstein (1950) interface load model.
    2. Meyer-Peter and Muller (1948) model.
    3. Wilson and Watt (1974) model.

The first two approaches overpredict the *in situ* concentration and hence underpredicted the suspended flow concentration at low delivered concentrations. The third model underpredicts *in situ* concentration and hence overpredicts the suspended concentration at low delivered concentrations.

At high delivered concentration values the first two approaches still overpredict *in situ* concentration. The third model successfully predicts *in situ* concentration for intermediate and high delivered concentrations.

15. Two empirical correlations for *in situ* concentration are tested :

    1. Newitt *et al.* (1962).
    2. Wani *et al.* (1983).

The correlation of Newitt *et al.* (1962) underpredicts the *in situ* concentration at all values of delivered concentration. The correlation of Wani *et al.* (1983) predicts *in situ* concentrations within the correct order of magnitude of the actual values but shows large scatter.

16. For the local data base the energy gradient log standard error values for the correlations selected are shown in Table 6.20.

Table 6.20 : Log standard error for all local data points

Equation	L.S.E.
Pseudofluid	0.00858
Wasp *et al.*	0.00422
Wilson	0.00591
Lazarus	0.00435
Present	0.00442

17. For the imported data base the energy gradient log standard error values for the correlations selected are shown in Table 6.21.

Table 6.21 : Log standard error for all imported data points

Equation	L.S.E.
Pseudofluid	0.00749
Wasp *et al.*	0.00644
Wilson	0.00550
Lazarus	0.00333
Present	0.00351

18. Tables 6.20 and 6.21 show that the present correlation predicts energy gradient values with a log standard error approximately equal to the minimum obtained. The correlation therefore fulfills the requirement that it should predict at least as well as any existing correlation. The present correlation predicts better over a broader range of tests as shown by the percentage of the number of tests for which it predicted a minimum log standard error (Table 6.22).

Table 6.22 : Percentage value for which each correlation predicted a minimum log standard error

Equation	Percentage of total of 71 tests
Pseudofluid	1.5%
Wasp *et al.*	24.0%
Wilson	4.0%
Lazarus	32.5%
Present	38.0%
TOTAL	100.0%

19. The present correlation predicts better at low and intermediate concentration than at high concentrations.

20. Two energy terms may be required to improve the present accuracy of the model :

    1. A shear stress exists between the sliding bed and suspended material that depends on the difference in mean velocity between these components.

    2. At high concentrations particles are forced against the pipe wall and a thin film lubrication friction loss must be added to the hydrodynamic and sliding friction loss terms.

    The exact nature of these two terms is at present unknown.

21. The sliding bed flow equation of Newitt *et al* (1955) predicts the energy gradient for a mixture where pure sliding bed flow occurs. One such test was conducted (S1435148) and an accurate prediction found.

22. The present correlation is the only correlation that predicts the range of velocities in which periodic flow phenomena are expected to occur.

23. Table 6.23 shows the percentage of correct predictions out of the total number of points for a particular flow regime.

Table 6.23 : Number of correct predictions for each particular flow regime as a percentage

Equation	Stationary	Sliding	Suspended
Wasp *et al.*	41%	0	94%
Wilson	30%	0	98%
Lazarus	72%	56%	0
Present	28%	77%	48%

24. Concentration and velocity profiles can be produced from the present correlation. The accuracy with which these are predicted will require further investigation.

25. The present correlation can be used as a design tool by selecting the input conditions based on the continuity equation given in the form

$$C_{vd} = \frac{4\ M_s}{V_m\ \pi\ D^2\ \rho_s} \quad . \tag{4.1}$$

CHAPTER 7

CONCLUSIONS AND RECOMMENDATIONS

INTRODUCTION

The study of mixed regime flow is important because of the significant advantages for this type of flow when compared with the flow of uniform sized particles. The analysis of mixed regime flows introduces complications in terms of describing the mixture to be transported since a single particle size is no longer sufficient. A description of the vehicle is also required as well as the relative quantities of vehicle, bed load and suspended load.

This research makes a contribution to the understanding of mixed regime flows. Both a quantitative and qualitative analysis is presented. The quantitative analysis is based on a mechanistic model of the flow. The qualitative analysis describes the complexity of the flow phenomenon. The transition conditions from one regime to another, the physical change in the transported fluid due to the applied shear rate and the periodic flow that exists for sliding bed flow demonstrate this complexity.

Simplifying assumptions to make a quantitative analysis possible introduce the need for semi-empirical equations. The constants required for solid to pipe wall friction factor, velocity distribution and concentration distribution equations can only be found from experimental results. A detailed experimental investigation of mixed regime flow was undertaken to assess the various equations available in the literature and to assist in the development of new equations. These equations form part of the analytical model of mixed regime flow. These equations form part of the

analytical model of mixed regime flow. The experimental results are also used to evaluate the final model.

This chapter serves to summarise the main concepts discussed in this thesis. The decisions made and conclusions drawn are presented. Recommendations for future research work are also presented.

The major contribution made by the thesis is the development of a consistent computerised mathematical model for the flow of mixed regime slurries. Important aspects include :

1. The linking of *in situ* concentration (C_{vd}) and delivered concentration (C_{vt}) with the *in situ* value being used for calculation of the energy gradient.

2. The prediction of energy gradient for stationary bed flow, sliding bed flow and fully suspended flow.

3.The prediction of three dimensional concentration and velocity profiles for slurry flow in circular conduits for all flow conditions.

4. A thorough investigation of the mechanism involved in the turbulent suspension of particles and interfacial wave and slug formation.

5. The development of a sophisticated test facility for the measurement of slurry flow parameters.

6. The development of a novel technique for measuring data which ensures that the data is evaluated during the experimental stage.

7.1 MIXED REGIME FLOW

7.1.1 Mixed regime flow must not only comprise a mixture of well graded particles but must contain particles smaller than the maximum size for laminar settling (d_{Lmax}).

7.1.2 Fine particles are suspended from the bed surface drag due to laminar flow in the sublayer.

7.1.3 Coarse particles, protruding through the laminar sublayer, are suspended by turbulent bursts. Particles will not be suspended *en mass* but simultaneously at many discrete locations throughout the pipeline.

7.1.4 Dunes will form in a pipeline for Froude numbers less than unity. Dunes move downstream at a fraction of the mean velocity. The dune amplitude is a fraction of the pipe diameter while dune length is of the order of several pipe diameters.

7.1.5 For stationary bed flow for Froude numbers greater than unity, a plane bed is observed.

7.1.6 Sliding bed motion is caused by percolation through the stationary bed and the applied interface shear.

7.1.7 Sliding bed flow can be modelled as a two-fluid system, the bed mixture forming a denser fluid than the suspended mixture.

7.1.8 Interface waves occur due to the adverse pressure gradients caused by turbulence.

7.1.9 Interface waves are spaced several pipe diameters apart but have a width of the order of one pipe diameter.

7.1.10 Interface waves grow initially due to the low pressure at the wave crest, caused by an increase in velocity of the suspended mixture as it flows through the reduced area, overcoming the stabilizing effect of gravity.

7.1.11 A secondary mechanism producing exponential amplitude growth is associated with a pressure variation 180° out of phase with the waves in the pipe. This produces a Kelvin-Helmholtz instability. If sufficient bed material exists the wave amplitude grows until it fills the pipe completely and slug flow occurs. If insufficient bed material exists the bed will be dispersed and heterogeneous flow will occur.

7.1.12 The waves or slugs move downstream at approximately the slurry mean velocity.

7.1.13 Slug flow is dispersed by the entrainment of the suspended mixture into the upstream end of the slug eventually producing a continuous stream of suspended material. Heterogeneous flow then occurs.

7.1.14 Heterogeneous flow can only exist if all particles are maintained in turbulent suspension.

7.2 THE VEHICLE AND ITS ANALYSIS

7.2.1 The vehicle fraction of a mixture is comprised of at least all particles with diameter less than the particle size for unhindered laminar settling in the fluid phase (d_{Lmax}).

7.2.2 For a vehicle modelled as a non Newtonian fluid, the vehicle concentration is found from the ratio of particles smaller than d_{Lmax} . The rheological equations must be derived for that part of a mixture with d less than d_{Lmax} screened out of the total sample.

7.2.3 For a vehicle modelled as a Newtonian fluid the vehicle concentration is equal to the suspended solid concentration (C_{vtf}) . The viscosity is found from an equation of the form $\eta_r = fn(C_{vtf})$.

7.2.4 For Newtonian vehicle rheology the vehicle relative viscosity is calculated from the equation

$$\eta_r = \left[1 - \frac{C_{vtf}}{C_b}\right]^{-2.5} \quad . \qquad (2.23)$$

7.2.5 Kaolin clay is best described by a yield pseudoplastic rheology.

7.2.6 For turbulent flow kaolin clay surries can best be described by a combination of the Colebrook-White and Torrence friction factor equations. Both values should be calculated and the higher value assumed.

7.2.7 For a vehicle with unknown rheology the mixture relative viscosity should be calculated as a function of the suspended material concentration. The Colebrook-White equation should be used to predict turbulent flow friction factors.

7.3 THE ANALYTICAL MODEL

7.3.1 Particle size distribution is best represented analytically by a particle size and a mass fraction of that particle size. This is usually divided into equal mass fraction increments, e.g. if m_i = 0.1 then ten diameters are required to describe the distribution (d_5, d_{15}, d_{25}, ..., d_{95}) .

7.3.1 The concentration distribution can be calculated using the equation

$$C_v(y) = C_a \left[\frac{D/y - 1}{D/y_a - 1}\right]^{z_1} \qquad (3.33)$$

$$\text{where } z_1 = \frac{V_t}{\kappa u_{*I}} \quad . \qquad (3.34a)$$

The concentration distribution varies in the xy plane only and is constant in the z direction.

7.3.3 The suspended load volume is a function of the ratio of velocity required for turbulent suspension of a particular particle size and the mean mixture velocity.

7.3.4 The energy gradient is calculated from a force balance on the prevailing flow conditions over a unit length of pipeline.

7.3.5 For stationary bed flow the driving force is equal to the fluid shear force on the pipe wall above the bed, plus the interface shear force acting on the bed interface, plus the weight component of the suspended slurry.

7.3.6 For sliding bed flow the driving force is equal to the fluid shear force acting on the pipe wall above the sliding bed, plus the fluid shear force acting between the bed and the pipe wall, plus a solid sliding friction force between the bed and the pipe wall, plus the weight component of the slurry.

7.3.7 For fully suspended flow the driving force equals the fluid shear force acting on the total pipe perimeter plus the weight component of slurry.

7.3.8 Stationary bed flow occurs until the driving force on the bed, made up of the interface shear stress acting on the interface and the pressure differential along the bed, overcomes the resisting force of the bed, made up of the friction force between the bed and the pipe wall and the weight of the bed acting down the pipe slope.

7.3.9 Fully suspended flow occurs when the driving force for fully suspended flow becomes greater than the driving force for sliding bed flow.

7.3.10 The velocity distribution is symmetrical about the vertical axis.

7.3.11 The maximum velocity occurs at the point of zero shear.

7.3.12 The maximum velocity is calculated from the universal velocity distribution associated with the top of the pipe and a von Karman constant derived from the expirical correlation of Einstein and Chien (1954).

7.3.13 The velocity distribution is calculated using the velocity defect law from the location and value of the maximum velocity. The distribution shape is found by ensuring that the input mixture flow rate equals the calculated mixture flow rate by varying the constant (the von Karman constant in single phase flow) in the velocity defect law.

7.3.14 The velocity and concentration distributions are integrated numerically over a concentric computational grid which is independent of the existing flow regime and symmetrical about the vertical axis.

7.3.15 *In situ* concentration is found by ensuring that the input delivered concentration and the calculated delivered concentration are equal. For stationary and sliding bed flow the *in situ* and delivered concentrations differ. No slip between the particles and fluid phase is accounted for.

7.4 EXPERIMENTAL INVESTIGATION

7.4.1 Tests were conducted at constant concentration and varying mean mixture velocity.

7.4.2 Each data point was subject to a stabilization check before a measurement was initiated.

7.4.3 Each data point reading was made from the average of 11 groups of 3 readings. The sub group of three readings was made at the maximum read rate of the data acquisition unit. The 11 groups of readings were made at 10 second intervals.

7.4.4 The average value adopted from the 11 groups of readings was checked for drift over the time taken to make the reading. The maximum drift allowed being 10%.

7.4.5 All transducers could be calibrated in position on the test facility.

7.4.6 The expected highest error in the measurement of pipe diameter is below 0.3%.

7.4.7 The expected highest error in the measurement of differential pressure is 1% at a measured differential head of 10mm and less than 1% for larger differential heads.

7.4.8 The expected maximum error in the measurement of slurry temperature is 0.1%.

7.4.9 The expected highest error in the measurement of velocity is 5% for the 50mm and 63mm nominal diameter pipelines and 1% for the 90mm and 160mm nominal diameter pipelines.

7.4.10 The expected maximum error in the measurement of delivered concentration is 4.5% for the 50mm and 63mm nominal diameter pipelines and 1% for the 90mm and 160mm nominal diameter pipelines.

7.4.11 The expected highest error in the measurement of *in situ* concentration is 1%.

7.4.12 The experimental test facility constructed for this research is a complicated apparatus that requires careful operation to achieve good results.

7.4.13 The data acquisition philosophy adopted ensures the best quality results and gives the system operator information to assist in the decision of data acceptance.

7.4.14 The test facility proved successful in the measurement of the required parameters for mixed regime flow.

7.5 EXPERIMENTAL RESULTS

7.5.1 The materials tested for this research include :

1. Coal fired power station ash, both bottom ash and fly ash.
2. Ocean bed material.
3. Mine tailings.
4. Kaolin clay.
5. Beach sand.
6. Beach sand and kaolin mixtures.

7.5.2 Clear water energy gradients were predicted with highest expected error of 10% for energy gradients of 10mm/m . For energy gradients above 100mm/m the highest expected error is below 1%.

7.5.3 For bottom ash flow observations were difficult due to the dark slurry colour. Flow instabilities were apparent at low velocities.

7.5.4 Field 1 fly ash formed a typical mixed regime slurry with at least 70% of the mixture contributing to the vehicle. Slight high frequency fluctuations were visible at concentrations above 20% by volume.

7.5.5 Field 3 fly ash formed a typical non settling mixture which is assumed to represent the vehicle for field 1 fly ash.

7.5.6 The ocean bed material formed a stationary or sliding bed of coarse material at all velocities. No periodic flow was apparent.

The energy gradient remains constant for mean mixture velocity between 2 m/s and 5 m/s at the concentration tested ($C_{vd} \simeq 12\%$) .

7.5.7 Uranium mine tailings formed typical mixed regime slurries. No stationary bed flow occurred at the concentrations tested ($C_{vd} \geq 20\%$) . The slurry demonstrated highly periodic flow at low velocity ($V_m < 2$ m/s) . The energy gradient remained relatively constant for velocities between 0.5 m/s and 2.0 m/s for tests with $C_{vd} > 30\%$.

7.5.8 Kaolin clay slurries demonstrated characteristic floc structures in the delivery hopper before a test was conducted. The flow was homogeneous and turbulent for all points tested.

7.5.9 Beach sand forms a purely heterogeneous mixture. The particles are poorly graded and no vehicle component exists. Dune, wave and slug flow all occur and are easily discernible. At concentrations about 42% by volume a stable sliding bed occurs at all velocities and the energy gradient remains constant.

7.5.10 Kaolin-sand mixtures from typical mixed regime slurries. Dune, wave and slug flow are demonstrated although the range and strength of these phenomena is mediated by the kaolin component.

7.5.11 The minimum particle size and not the grading coefficient or mean particle size determines whether the beneficial qualities of mixed regime flow will exist.

7.5.12 The characteristic particle size for a slurry is taken to be the d_{10} particle size as a consequence of conclusion 7.6.11. The suspended component in the two-fluid multicomponent model is assumed to be pseudohomogeneous. The d_{10} particle size will ensure that this occurs for mixtures with fine components.

7.5.13 For an equivalent energy gradient the carrying capacity (or solid mass flow rate) is always higher for a kaolin-sand mixture than for the sand alone. The specific power consumption is consequently lower.

7.5.14 The kaolin-sand mixtures demonstrate stable, non pulsatile sliding bed flow for delivered concentration above 30%.

7.5.15 In the 90mm nominal diameter pipeline no pulsatile flow phenomena occurred for kaolin-sand mixtures at any mean mixture velocity for delivered concentration in excess of 40%.

7.5.16 Particle bed velocity is directly related to the velocity distribution shape. The flatter the velocity distribution the closer are the values of mean and bed velocity.

7.5.17 A horizontally mounted gamma ray densitometer always overestimates heterogeneous *in situ* concentration.

7.5.18 The actual *in situ* concentration measurement approaches the gamma ray densitometer measurement with increasing mixture flow rate or decreasing particle size.

7.6 ANALYTICAL MODEL EVALUATION

7.6.1 The log standard error is a successful tool for comparing observed and calculated quantities.

7.6.2 The interface friction factor is given by the equation

$$\sqrt{\frac{2}{f}} = 1.475 \ln \frac{D}{d_{85}} + 1.36 \quad . \tag{2.118}$$

7.6.3 The coefficient of sliding friction is assumed constant for a particular mixture. It is measured by the tangent of the angle that a pipe of similar roughness must be tilted to initiate motion of the stationary bed.

7.6.4 The maximum bed packing concentration was assumed to be constant where $C_b = 0.67$.

7.6.5 Particle shape factor is less than unity for naturally occurring particles and may be an inverse function of particle size.

7.6.6 The Meyer-Peter and Muller (1948) and the Einstein (1950) bed load model overpredict *in situ* concentration and hence underpredict the suspended material concentration at all velocities.

7.6.7 The Wilson and Watt (1974) equation, for the velocity for turbulent suspension, is used to describe the relative quantities of bed load and suspended load.

7.6.8 The Wilson and Watt (1974) equation underpredicts *in situ* concentration at low delivered concentration but predicts *in situ* concentration successfully for intermediate and high delivered concentration.

7.6.9 The empirical correlation for *in situ* concentration of Wani *et al.* (1983) predicts well for a first approximation. The scatter in the calculated results is high.

7.6.10 The present correlation predicts the energy gradient for the local data base with a log standard error of 0.00442 and for the imported data base with a log standard error of 0.00351.

7.6.11 The lowest log standard error value for the calculation of the energy gradient is the model ascribed to Wasp *et al.* (L.S.E. = 0.00442) for the local data base and the model ascribed to Lazarus (L.S.E. = 0.00333) for the imported data base.

7.6.12 The Wasp *et al.* model was developed specifically for mixed regime slurries with a high proportion of fine material. Most of the tests in the local data base are of this type so it is justified that this model predicts best over this limited range.

7.6.13 The log standard error values for the prediction of energy gradient are of the same order of magnitude for the present model and for the lowest values obtained from the other correlations presented. The present correlation predicts better over a

broader range of tests as shown by the percentage of the number of tests for which it predicted a minimum log standard error.

Equation	Percentage of total of 71 sets of tests
Pseudofluid	1.5%
Wasp *et al.*	24.0%
Wilson	4.0%
Lazarus	32.5%
Present	38.0%

7.6.14 The present correlation predicts energy gradient better at low and intermediate concentration than at high concentration.

7.6.15 The sliding bed flow equation of Newitt *et al.* (1955) predicts the energy gradient for mixtures where pure sliding bed flow occurs.

7.6.16 The present correlation is the only correlation that predicts the stationary, sliding and fully suspended flow regimes. The correlation predicts sliding bed for 72% of the points where stationary bed was observed. The correlation predicts sliding bed flow for 52% of the points where suspended flow was observed. The subjective nature of observing the transition from one regime to another must be taken into account when accessing these results.

7.6.17 Concentration and velocity profiles can be predicted by the present model. Although these are not confirmed by experiment they seem reasonable and are of the shape that would be expected.

7.6.18 The correlation presented can be used as a design tool by selecting the input conditions in accordance with the continuity equation. It is the only model at present that predicts energy gradient, *in situ* concentration and velocity and concentration profiles for all flow regimes.

7.7 FUTURE RESEARCH RECOMMENDATIONS

7.7.1 The method of calculating the maximum velocity and its position needs to be evaluated. This will require experimental measurements.

7.7.2 The velocity distribution produced by the model should be evaluated and compared with experimental measurements at all flow regimes.

7.7.3 Particle-particle interactions at high concentration need to be investigated so that a concentration distribution for each particle size group can be produced for all flow regimes.

7.7.4 The concentration distribution produced by the model should be evaluated and compared with experimental measurements at all flow regimes.

7.7.5 The energy term associated with high concentration sliding bed flow (thin film lubrication between particles and pipe wall) should be investigated and the reasons for the slope of the data being different from that predicted should be ascertained.

7.7.6 A method for accurately measuring the maximum bed concentration and the sliding friction coefficient should be found. These terms are functions of particle size distribution, *in situ* concentration and mean mixture velocity.

7.7.7 Pulsatile flow should be investigated fully. A surface tension term or equivalent measure must be found to allow for a shear stress between the bed material and suspended material. The stability criteria can then be checked. The relative velocity between the bed and the suspended material must be evaluated and the energy term associated with the interfacial shear determined. Transition criteria between the different periodic flow regimes must also be ascertained. A mechanistic model of the periodic flow phenomenon can be developed if the governing equations produced for the system are too difficult to solve.

REFERENCES AND BIBLIOGRAPHY

Abbas, M.A., Crowe, C.T. (1986) 'The effect of particle size and concentration on the flow properties of a homogeneous slurry'. *Proc. Int. Symp. on Slurry Flow, A.S.M.E. Winter Annual Meeting* p.1-8

Acaroglu, E.R., Graf, W.H. (1968) 'The modes of sediment transport and their related bed forms in conveyance systems'. *Intl. Assoc. of Scientific Hydrology Bulletin* v.13, p.123-135

Acrivos, A., Chang, E. (1986) 'A model for estimating transport quantities in two-phase materials'. *Phys. of Fluids* v.29 n.1, p.3-4

Ahmadi, G., Ma, D. (1986) 'A kinematic model for granular flow including intestial fluid effects'. *Proc. Int. Symp. on Slurry Flow, A.S.M.E. Winter Annual Meeting* p.25

Alger, G.R., Simons, D.B. (1968) 'Fall velocity of irregular shaped particles'. *Proc. A.S.C.E. (Jou. Hyd. Div.)* v.94 n.HY3, p.721-737

Allesandrini, A., Lapasin, R. (1985) 'A class of rheological models for concentrated suspensions : their application to clay/kaolin aqueous systems'. *Chem. Eng. Commun.* v.37, p.27-40

Ashida, K., Fujita, M. (1986) 'Stochastic model for particle suspensions in open channels'. *Jou. of Hydroscience and Hyd. Engnr.* v.4 n.2, p.21-46

Asszonyi, C., Kapolyi, I., Kantas, C., Meggyes, T. (1972) 'An experimental method to produce a size distribution ensuring maximum pipeline capacity'. *Proc. Hydrotransport 2 B.H.R.A.* p.D3-23/32

Ayukawa, K. (1970) 'Velocity distribution and pressure drop of heterogeneously suspended flow in hydraulic transport through a horizontal pipe'. *Proc. Hydrotransport 1 B.H.R.A.* p.F3-33/43

Aziz, N.M., Prasad, S.N. (1985) 'Sediment transport in shallow flows'. *Proc. A.S.C.E. (Jou. Hyd. Div.)*, v.111 n.10, p.1327-1343

Babcock, H.A. ((1970) 'The sliding bed flow regime'. *Proc. Hydrotransport 1 B.H.R.A.* p.H1-1/H1-16

Bagnold, R.A. (1954) 'Experiments on a gravity-free dispersion of large solid spheres in a Newtonian fluid under shear'. *Proc. Roy. Soc. London* v.225 Ser. A, p.49-63

_____. (1955) 'Some flume experiments on large grains but little denser than the transporting fluid, and their implications'. *Proc. Inst. Civil Eng.* v.4 part 3, p.174-205

_____. (1956) 'The flow of cohesionless grains in fluids'. *Proc. Roy. Soc. London* v.249 Ser A. n.964, p.235-297

_____. (1973) 'The nature of saltation and of 'bed-load' transport in water'. *Proc. Roy. Soc. London* v. 332 Ser A, p.473-504

Baker, P.J., Jacobs, B.E.A. (1979) *A guide to slurry pipeline systems.* Cranfield : B.H.R.A.

Bantin, R.A., Streat, M. (1972) 'Mechanism of hydraulic conveying at high concentration in vertical and horizontal pipes'. *Proc. Hydrotransport 2 B.H.R.A.* p.B2-11/B2-24

Batchelor, G.K., Janse van Rensburg, R.W. 'Structure formation in bidisperse sedimentation'. *J. Fluid Mech.* v.166, p.379-407

Beazley, K.M. (1971) 'Non-Newtonian technology in the China Clay Industry'. *The Chem. Engineer*, January, p.16-19

Beck, M.S., Mendies, P.J., Walecki, T., Gatland, H.B. (1974) 'Measurement and control in hydraulic transport systems using cross correlation measurement systems and fluidic diverters'. *Proc. Hydrotransport 3, B.H.R.A.* p.F5-69/8p

Berman, N.S. (1986) 'Velocity fluctuations in non-homogeneous drag reduction'. *Chem. Eng. Commun.* v.42, p.37-51

Binder, R.C., Busher, J.E. (1946) 'A study of flow of plastics through pipes'. *Proc. A.S.M.E. (Jou. App. Mech.)*, June, p.A101-A105

Binnie, A.M., Kud, T.-C. (1966) 'The mean velocity of nylon spheres transported in a horizontal water pipe'. *Brit. J. Appl. Phys.* v.17, p.945-949

Blasius, H. (1913) *Mitt. Forschungsarb.*, n.131

Blench, T., Galay, V.J., Peterson, A.W. (1980) 'Steady fluid-solid flow in flumes'. *Proc. Hydrotransport 1 B.H.R.A.* p.89-100

Bonapace, A.C. (1968) 'The hydraulic transport of granular materials of uniform size composition in horizontal pipes'. Reprinted from : *Coal, Gold and Base Minerals of Southern Africa*, Fuel Research Institute, Report No. 4.

_____. (1974) 'Conditions of particle equilibrium at the boundary of a stream'. *Proc. Hydrotransport 3 B.H.R.A.* p.E3-29/43

_____. (1981) 'Critical lift velocity of a particle placed at the boundary of a stream'. *The South African Mechanical Engineer*, v.31, p.111-127

Bonnington, S.T. (1959) 'Experiments on the hydraulic transport of mixed-size solids'. *B.H.R.A. Report, RR 637*

Boothroyde, J., Jacobs, B.E.A., Jenkins, P. (1979) 'Coarse particle hydraulic transport'. *Proc. Hydrotransport 6, B.H.R.A.* p.E1-1/24

Borshchevskii, Yu.T. (1963) 'Velocity pulsations in two phase streams'. *Intl. Chem. Engineering* v.3 n.2, p.235-239

Brady, J.F. (1985) 'The Rheology of concentrated suspensions of spheres in simple shear flow by numerical simulation'. *J. Fluid Mech.* v.155, p.105-129

Brinkworth, B.J. (1968) *An introduction to experimentation*, English University Press, London.

Briscoe, B.J., Radwan, H., Streat, M. (1983) 'Model experiments on sliding friction for application in hydraulic conveying of solids'. *Can. J. Chem. Eng.* v.61, p.769-775

Brooke Benjamin, T. (1986) 'On the Boussinesq model for two-dimensional wave motions in heterogeneous fluids'. *J. Fluid Mech.* v.165, p.445-474

Brook, N. (1987) 'Fluid transport of coarse solids'. *To be published in Mining Science and Technology* 21p.

Brown, N.P., Shook, C.A. (1982) 'A probe for particle velocities : The effect of particle size'. *Proc. Hydrotransport 2 B.H.R.A.* p.339-348

_____., Shook, C.A., Peters, J., Eyre, D. (1983) 'A probe for point velocities in slurry flow'. *Can. J. Chem. Engnr.* v.61, p.597-602

Bruhl, H., Kazanskij, I. (1976) 'New results concerning the influence of fine particles on sand water flows in pipe'. *Proc. Hydrotransport 4 B.H.R.A.* p.B2-19/B2-28

Cairns, R.C., Lawther, K.R., Turner, K.S. (1960) 'Flow characteristics of dilute small particle suspensions; A study on the influence of effective density ratio and concentration upon horizontal settling velocity'. *Brit. Chem. Engineering*, December, p.849-856

Caldwell, D.H., Babbitt, H.E. (1941) 'The flow of muds, sludges and suspensions in circular pipes'. *Am. Inst. Chem. Engnrs* v.33, p.237-266

Charleton, A.J., Cheng, D. C-H. (1977) 'Pipeline design for industrial slurries'. *Chem. Engineering*, April, p.95-100

_____., French, R.J., James, J.G., Broad, B.A., Streat M. (1978) 'Hydraulic transport of large particles using conventional and high concentration conveying'. *Proc. Hydrotransport 5, B.H.R.A.* p.D2-15/28

Carstens, M.R., Altinbilek, H.D. (1972) 'Bed-material transport and bed forms'. *Proc. A.S.C.E. (Jou. Hyd. Div.)*, v.98 n.HY5, p.787-794

_____. (1979) 'A theory for heterogeneous flow of solids in pipes'. *Proc. A.S.C.E. (Jou. Hyd. Div.)* v.95 n.HY1, p.275-286

Castillo,. C., Williams, M.C. (1979) 'Rheology of very concentrated coal suspensions'. *Chem. Eng. Commun.* v.3, p.529-547

Chan, K.W., Baird, M.H.I., Round, G.F. (1972) 'Behaviour of beds of dense particles in a horizontally oscillating liquid'. *Proc. Roy. Soc. London* v.330 Ser A. p.537-559

Charles, M.E., Charles, R.A. (1971) 'The use of heavy media in the pipeline transport of particulate solids'. *Advances in Solid-Liquid Flow in Pipes and its Application' (I. Zandi, Ed.)* Oxford : Pergamon p.187-197

Cheng, D.C-H. (1970) 'A design procedure for pipeline flow of non-Newtonian dispersed systems'. *Proc. Hydrotransport 1, B.H.R.A.* p.J5-77/95

_____., Whittaker, W. (1972) 'Application of the Warren Spring Laboratory pipeline design method to settling suspensions'. *Proc. Hydrotransport 2, B.H.R.A.* p.C3-21/39

Chhabra, R.P., Richardson, J.F. (1983) 'Hydraulic transport of coarse gravel particles in a smooth horizontal pipe'. *Chem. Eng. Res. Des.* v.61, p.313-317

Chhabra, R.P., Richardson, J.F. (1985) *Chem. Eng. Res. Des.* v.63, p.390-397

Chien, N. (1956) 'The present status of research on sediment transport'. *Trans. A.S.C.E.* v.121, p.833-868

Christiansen, E.B., Barker, D.H. (1965) 'The effect of shape and density on the free settling of particles at high Reynolds numbers'. *Jou. A.E. Ch. E.* v.11 n.1, p.145-151

Clarke, B. (1967) "Rheology of coarse settling suspensions'. *Trans. Inst. Chem. Engrs.* v.45, p.T251-T256

Clift, R., Clift, D.H. (1982) 'Continuous measurement of the density of flowing slurries'. *Proc. Fifth Annual Transportation of Solids using Centrifugal Pumps Seminar.* Grovetown : Georgia Iron Works, U.S.A.

_____., Wilson, K. C., Addie, G.R., Carstens, M.R. (1982) 'A mechanistically-based method for scaling pipeline tests for settling slurries'. *Proc. Hydrotransport 8, B.H.R.A.* p.91-101

Colebrook, C.F. (1939) 'Turbulent flow in pipes, with particular reference to the transition between smooth and rough pipe laws'. *J. Int. Civil Engrs.* v.11, p.133-156

Cross, M.M. (1965) 'Rheology of non-Newtonian fluids : A new flow equation for pseudolatic systems'. *J. of Colloid Science* v.20, p.417-437

_____. (1970) 'Kinetic interpretation of non-Newtonian flow'. *J. of Colloid and Interface Science* v.33 n.1, p.30-35

_____. (1975) 'Viscosity-concentration-shear rate relations for suspensions'. *Rheologica Acta* v.14, p.402-403

C.S.I.R. Report ME1386 (1975) 'Loop tests on gold slime slurry', *Fluid Mechanics Division*, Pretoria, South Africa

Dabak, T., Yucel, O. (1986) 'Shear viscosity of dense-phase slurries at varying shear-rates'. *Proc. Int. Symp. on Slurry Flow, A.S.M.E. Winter Annual Meeting* p.31-39

Daily, J.W., Roberts, P.R. (1966) 'Rigid particle suspensions in turbulent shear flow : Some size effects with spherical particles'. *J. Mech. Assoc. Pulp and Paper Ind.* v.49 n.3, p.115-125

Davis, R.H., Serayssol, J-M., Hinch, E.J. (1986) 'The elasto-hydrodynamic collision of two spheres'. *J. Fluid Mech.* v.163, p.479-497

Dedegil, M.Y. (1986) 'Drag coefficient and settling velocity of particles in non-Newtonian suspensions'. *Proc. Int. Symp. on Slurry Flow, A.S.M.E. Winter Annual Meeting* p.9-15

Doron, P., Granica, D., Barnea, D. (1986) 'Slurry flow in horizontal pipes - experimental and modelling [*sic.*]'. Paper produced by the Department of Fluid Mechanics and Heat Transfer. Tel-Aviv University, Israel.

du Plessis, M.P., Ansley, R.W. (1967) 'Settling parameter in solids pipelining'. *Proc. A.S.C.E. (Jou. Pipeline Div.)* v.93 n.PL2, p.1-17

Duckham, C.B. (1972) 'Local and general pipe laminar to turbulent transition problems for viscous and non-Newtonian slurries in pipelines'. *Proc. Hydrotransport 2 B.H.R.A.* p.B3-25/B3-40

Duckworth, R.A., Argyros, G. (1972) 'Influence of density ratio on the pressure gradient in pipes conveying suspensions of solids in liquids'. *Proc. Hydrotransport 2 B.H.R.A.* p.D1-1/D1-11

_____. (1978) 'The hydraulic transport of materials by pipeline'. *The South African Mechanical Engineer* v.28, p.291-306

_____., Pullum, L., Lockyear, C.F. (1983a) 'The hydraulic transport of coarse coal at high concentration'. *J. of Pipelines* v.3, p.251-265

_____., Pullum, L., Lockyear, C.F., Lenard, J. (1983b) 'The hydraulic transport of coal'. *Bulk Solid Handling* v.3 n.4, p.817-824

_____., Lockyear, C.F., Pullum, L., Littlejohn, M.H. (1985) 'Transport of coal by pipeline parts I and II'. *End of Grant Report, No. 464*, NERDDP, Dept. of Resources and Energy, Australia.

_____., Pullum, L, Addie, G.R., Lockyear, C.F. (1986) 'The pipeline transport of coarse materials in a non Newtonian carrier fluid'. *Proc. Hydrotransport 10 B.H.R.A.* p.69-88

Dukler, A.E., Wicks, M., Cleveland, R.G. (1984) 'Frictional pressure drop in two-phase flow'. *Jou. A. I. Ch. E.* v.10 n.1, p.38-51

Durand, R. (1953) 'Basic relationships of the transportation of solids in pipes - experimental research'. *Proc. Minnesota Int. Hydraulics Convention* Int. Assoc. for Hydraulic Research, p.89-102

Durst, F., Milojevic, D., Schönung, B. (1984) 'Eulerian and Lagrangian predictions of particulate two-phase flows : a numerical study'. *Appl. Math. Modelling* v.8, p.101-115

Dutkiewicz, R.K., Cipolat, A. (1970) 'Pressure drop in horizontal pipes conveying solid-liquid mixtures'. *The South African Mechanical Engineer* v.20, p.68-71

Einstein, H.A. (1942) 'Formulas for the transportation of bed load'. *Trans. A.S.C.E.* v.107, p.561-593

_____. (1948) 'Determination of rates of bed load measurement', *Proc. Fed. Iterogency Sedimentation Conf.*, U.S. Dept. Interior

_____. (1950) 'The bed load function of sediment transportation in open channel flows'. *U.S. Dept. Agric., Soil Conservation Service*, Technical Bulletin : 1026

_____., Chien, N. (1954) 'Second approximation to the solution of the suspended load theory'. *The Missouri River Division Sediment Series* Report No. 3

_____., Abdel-Aal, F.M. (1972) 'Einstein bed-load function at high sediment rates'. *Proc. A.S.C.E. (Jou. Hyd. Div.)*, v.98 n.HY1, p.137-151

Ekmann, J.M., Wildeman, D.J., Chen, J.L.S. (1986) 'Laminar flow studies of highly loaded suspensions in horizontal pipes'. *Proc. Int. Symp. on Slurry Flow, A.S.M.E.* Winter Annual Meeting p.85-92

Elliott, D.E., Gliddon, B.J. (1970) 'Hydraulic transport of coal at high concentrations'. *Proc. Hydrotransport 1, B.H.R.A.* p.G2-25/56

Engelund, F. (1966) 'Hydraulic resistance of alluvial streams'. *Proc. A.S.C.E. (Jou. Hyd. Div.)*, v.92 n.HY2, p.315-326

Ercolani, D., Ferrini, F., Arrigoni, V. (1979) 'Electric and thermic probles for measuring the limit deposit velosity'. *Proc. Hydro-transport 6, B.H.R.A.* p.27-42

Faddick, R. (1982a) 'Settling slurries'. *Course preceeding Hydrotransport 8*, Johannesburg : B.H.R.A. Chapter 4

_____. (1982b) 'Mixed slurries'. *Course preceeding Hydrotransport 8*, Johannesburg : B.H.R.A. Chapter 6

Fichman, M., Pnueli, D. (1985) 'Sufficient conditions for small particles to hold together because of adhesian forces'. *Jou. Appl. Mech.* v.52, p.105-108

Field, W.G. (1968) 'Effects of density ratio on sedimentary simulitude'. *Proc. A.S.C.E. (Jou. Hyd. Div.)* v.94 n.HY3, p.705-719

Francis, J.R.D., Vickers, J.A. (1968) 'The motion of solitary particles on the fixed, granular bed of a stream'. *Proc. Conf. on Hyd. and Mixed Mech.* Inst. of Engnrs., Australia p.38-40

_____. (1970) 'Solitary particle movement in a rough-bedded stream'. *The South African Mechanical Engineer* v.20, p.72-75

_____. (1973) 'Experiments on the motion of solitary grains along the bed of a water-stream'. *Proc. Roy. Soc. London* v.332 Ser A. p.443-471.

Fukushima, Y., Fukuda, M. (1986) 'Analysis of turbulent structure of open-channel flow with suspended sediment'. *Jou. of Hydroscience and Hyd. Engnr.* v.4 n.2, p.47-54

Galvin, J.M. (1982) 'The physical, chemical and mineralogical properties of ashfill'. *Chamber of Mines Report* 8/82

Gandhi, R.L. (1976) 'An analysis of hold up phenomena in slurry pipelines'. *Proc. Hydrotransport 4 B.H.R.A.* p.A3-33/A3-50

Givler, R.C., Mikatarian, R.R. (1986) 'Numerical simulation of fluid-particle flows : Geothermal drilling applications'. *Proc. Int. Symp. on Slurry Flow, A.S.M.E. Winter Annual Meeting* p.51-59

Goedde, E. (1978) 'To the critical velocity of heterogeneous hydraulic transport'. *Proc. Hydrotransport 5 B.H.R.A.* p.B4-81/98

Govier, G.W., Aziz, K. (1981) '*The flow of complex mixtures in pipes*', FLORIDA : ROBERT E. KRIEGER Publishing Co.

Graf, W.H., Acaroglu, E.R. (1967) 'Homogeneous suspensions in circular pipes'. *Proc. A.S.C.E. (Jou. Pipeline Div.)* v.93 n.Pl2, p.63-69

_____. (1971) '*Hydraulics of sediment transport*'. New York : McGraw-Hill, Inc.

Grootscholten, P.A.M., de Jong, E.J. (1985) 'Particle-particle interactions in poly-sized solid-liquid suspensions'. *Chem. Eng. Science* v.40 n.1, p.151-154

Hadley, D.W., Weber, J.D. (1975) 'Rheological nomenclature'. *Rheologica Acta* v.14, p.1098-11

Hanes, D.M., Inman, D.L. (1985) 'Observations of rapidly flowing granular-fluid materials' *J. Fluid Mech.* v.150, p.357-380

Hanks, R.W. (1978) 'Low Reynolds number turbulent pipeline flow of pseudohomogeneous slurries'. *Proc. Hydrotransport 5 B.H.R.A.* p.C2-23/34

_____. (1979) 'The not so "generalised" Reynolds number'. *Proc. 4th Int. Tech. Conf. on Slurry Transportation* p.91-99

_____. (1980) 'The influence of non-Newtonian rheology in mixed homogeneous-heterogeneous slurry flow'. *Proc. 5th Int. Tech. Conf. on Slurry Transportation* p.251-260

_____. Hanks, K.W. (1982) 'A new viscometer for determining the effect of particle size distributions and concentration on slurry rheology'. *Proc. 7th Int. Tech. Conf. on Slurry Transportation* p.151-161

Hashimoto, H., Noda, K., Masuyama, T., Kawashima, T. (1980) 'Influence of pipe inclination on deposit velocity'. *Proc. Hydrotransport 7, B.H.R.A.* p.231-244

Hauge, H., Sharma, M.P. (1986) 'An investigation of coarse particle transport in inclined pipes'. *Proc. Int. Symp. on Slurry Flow, A.S.M.E. Winter Annual Meeting* p.113-118

Haywood, N.I., Cheng, D. C-H. (1984) 'Flow in pipes Part 2 : Multiphase flow'. *Phys. Technal.* v.15 n.6, p.291-314 passim

Hendrix, C.D. (1986) 'Sixteen ways to mess up an experiment'. *Chemtech.* April, p.228-231

Hisamitsu, N., Shoji, Y., Kosugi, S. (1978) 'Effect of added fine particles on flow properties of settling slurries'. *Proc. Hydro-transport 5, B.H.R.A.* p.D3-29/50

Horsley, R.R., Reizes, J.A. (1978) 'Variation in head loss gradient in laminar slurry pipe flow due to changes in zeta potential'. *The South African Mechanical Engineer* v.28, p.307-311

_____. (1982) 'Viscometer and pipe loop tests on gold slime slurry at very high concentrations by weight, with and without additives'. *Proc. Hydrotransport 8, B.H.R.A.* p.367-382

Howard, G.W. (1939) 'Transportation of sand and gravel in a four-inch pipe'. *Trans. A.S.C.E.* v.104, p.1334-1380

Hunt, J.N. (1969) 'On the turbulent transport of a heterogeneous sediment.' Quart. *Jou. Mech. and Appl. Math.* v.22 n.2, p.235-246

Ippen, A.T., Verma, R.P. (1953) 'The motion of discrete particles along the bed of a turbulent stream'. *Proc. Int. Assoc. Hyd. Res., 5th Congress* p.7-20

_____. (1971) 'A new look at sediment in turbulent streams'. *Jou. Bos. Soc. of Civ. Engnrs.* v.58 n.3, p.131-161

Ippolito, M., Sabatino, C. (1985) 'Velocity profiles of non-Newtonian suspensions in smooth pipes'. *Chem. Eng. Commun.* v.39, p.127-145

Ismail, H.M. (1951) 'Turbulent transfer mechanism and suspended sediment in closed channels'. *Trans. A.S.C.E.* v.117, p.409-446

Iwanami, S., Tachibana, M. (1970) 'Viscosity and pipeloss of fly ash slurry'. *Proc. Hydrotransport 1, B.H.R.A.* p.J3-45/63

Julian, F.M., Dukler, A.E. (1965) 'An eddy viscosity model for friction in gas-solids flow'. *Jou. A. I. Ch. E.* v.11 n.5, p.853-858

Kada, H., Hanratty, T.J. (1960) 'Effects of solids on turbulence in a fluid'. *Jou. A. I. Ch. E.* v.6 n.4, p.624-630

Kakka, R.S., Gandhi, R.L. (1983) 'Coarse coal slurry pipeline technology'. *Jou. of Pipelines* v.3 n.4, p.267-277

Kao, T-Y., Wood, D.J. (1974) 'Incipient motion of solids in solid-liquid transport system'. *Trans. AIME*, v.255, p.39-44

Kao, D.T.Y., Hwang, A.L.Y. (1980) Determination of particle settling velocity in heterogeneous suspension and its effect on energy loss prediction in solid-liquid freight pipelines'. *Jou. of Powder and Bulk Solids Tech.* v.4, p.31-40

Kawashima, T., Noda, K. (1970) 'Hydraulic transport of solids in an inclined pipe : Theoretical and experimental studies of pressure loss'. *Proc. Hydrotransport 1 B.H.R.A.* p.J6-97/J6-111

Kazanskij, I., Bruhl, H. (1972) 'Influence of high concentrated rigid particles on macroturbulence characteristics in pipe flow'. *Proc. Hydrotransport 2 B.H.R.A.* p.A2-15/A2-30

_____., Bruhl, H., Hinsch, J. (1974) 'Influence of added fine particles on the flow structure and the pressure losses in sand-water-mixture'. *Proc. Hydrotransport 3, B.H.R.A.* p.D2-11/21

_____. (1976) 'Some results of comparison of the pressure drop of sand-water-flow in pipes'. *Franzius Institute Report* TU Hanover

_____. (1978) 'Scale-up effects in hydraulic transport theory and practice'. *Proc. Hydrotransport 5, B.H.R.A.* p.B3-47/79

_____., Mathias, H.J., Luck, K. (1978) 'Behaviour of pseudo-plastic slurries in pipe flow'. *Proc. Hydrotransport 5 B.H.R.A.* p.C3-35/48

Kenchington, J.M. (1974) 'An assessment of methods of pressure drop prediction for slurry transport'. *Proc. Hydrotransport 3 B.H.R.A.* p.F1-1/F.2-21

_____. (1976) 'Prediction of critical conditions for pipeline flow of settling particles ina heavy medium'. *Proc. Hydrotransport 4, B.H.R.A.* p.D3-31/48

_____. (1978) 'Prediction of pressure gradient in dense phase conveying'. *Proc. Hydrotransport 5 B.H.R.A.* p.D7-91-102

Kennedy, J.F. (1963) 'The mechanics of dunes and antidunes in erodible-bed channels'. *Jou. of Fluid Mech.* v.16 n.4, p.521-544

Keska, J (1978) 'Measurement of the distribution and overall spatial solid body content in the process of hydrotransport of mixtures in pipe-lines [*sic.*]'. *Proc. Hydrotransport 5, B.H.R.A.* p.G5-59/72

Kesten, U., Klose, R. (1982) 'Automatic image analysis system to measure the particle size distributions of pipelined coal'. *Proc. Hydrotransport 8 B.H.R.A.* p.349-366

Kilner, F.A., Lazarus, J.H. (1971) '*Velocity profile analysis*', University of Cape Town : 3rd year Hydraulics course notes.

Klose, R.B. (1982) 'The hydraulic transport of coal suspensions with coarse particles'. *Proc. 7th Int. Tech. Conf. on Slurry Transportation* p.61-64

Kobayashi, N., Seo, S.N. (1985) 'Fluid and sediment interaction over a plane bed'. *Proc. A.S.C.E. (Jou. Hyd. Eng.)* v.111 n.6, p.903-921

Koka, V.R., Papachristodoulou, G., Trass, O. (1985) 'Settling stability of coal slurries prepared by wet grinding in the Szego mill'. *Can. Jou. of Chem. Eng.* v.63, p.585-590

Korbel, K., Michalik, A., Przewlocki, Parzonka, W., Wolanski, Z. (1976) 'Determination of the polyfractional solids distribution in a pipe'. *Proc. Hydrotransport 4 B.H.R.A.* p.A4-51/61

Kordyban, E. (1985) 'Some details of developing slugs in horizontal two-phase flow'. *Jou. A.I. Ch. E.* v.31 n.5, p.802-806

Kril, S.I. (1981) 'Energy expended by pressure-type slurry flow and generating a concentration distribution in the solids [SIC]'. *Fluid Mechanics - Soviet Research* v.10 n.2, p.142-147

_____. (1981) 'Critical flow in pipeline transport of solids'. *Fluid Mechanics - Soviet Research* v.10 n.3, p.96-105

Laursen, E.M. (1956) 'Sediment transport mechanics in stable channel design'. *Trans. ASCE* Paper 2918, p.195-203

Lawler, H.L., Pertuit, P., Tennant, J.D., Cowper, N.T. (1978) 'Application of stabilized slurry concepts of pipeline transportation of large particle coal'. *Proc. 3rd Int. Tech. Conf. on Slurry Transportation*, p.164-178

Lazarus, J.H., Neilson, I.D. (1978) 'A generalised correlation for friction head losses of settling mixtures in horizontal smooth pipelines'. *Proc. Hydrotransport 5, B.H.R.A.* p.B1-1/32

_____. (1980) 'Rheological characterisation for optimising specific power consumption of a phosphate ore pipeline'. *Proc. Hydrotransport 5, B.H.R.A.* p.133-148

_____. (1981) 'Mechanistic approach to pressure loss and sediment suspension' *Unpublished*, University of Cape Town, SA

_____. (1982) 'Optimum specific power consumption for transporting settling slurries in pipelines'. *Hydrotransport 8, B.H.R.A.* p.123-132

_____., Sive, A.W. (1984) 'A novel balanced beam tube viscometer and the rheological characterisation of high concentration fly ash slurries'. *Hydrotransport 9, B.H.R.A.* p.207-226

_____. (1985a) 'Rössing tailings system, Phase 1 : Preliminary calculations mechanistic approach' *Hydrotransport Research Unit Report*, University of Cape Town, SA

_____. (1985b) *'Hydraulic Transport of Solids'*, Postgraduate course notes, University of Cape Town, South Africa.

_____. (1986) 'Mechanistic model for mixed regime slurries in pipelines'. *To be published.*

_____., Slatter, P.T. (1986) 'Comparative rheological characterisation using a balanced beam tube viscometer and rotary viscometer'. *Hydrotransport 10, B.H.R.A.* p.291-302

_____., Slatter, P.T. (1987) 'A method for the rheological characterisation of tube viscometer data'. *To be published* 15p.

Le Fur, B., Martin, M. (1967) 'Laminar and transitional flow of drilling muds and various suspensions in circular tubes'. *Jou. of Fluid Mech.* v.30 n.3, p.449-464

Le Feuvre, A.R., Altinbilek, H.D., Carstens, M.R. (1970) 'Sediment - pickup function'. *Proc. A.S.C.E. (Jou. Hyd. Div.)* v.96 n.HY10, p.2051-2063

Lekoudis, S.G., Sengupta, T.K. (1986) 'Two-dimensional turbulent boundary layers over rigid and moving swept wavy surfaces'. *Phys. Fluids* v.29 n.4, p.964-970

Lipson, C., Sheth, N.J. (1973) *Statistical design and analysis of engineering experiments.* McGraw-Hill, New York.

Lockyear, C.F., Pullum, L., Lenard, J.A., Duckworth, R.A. (1983) 'The rheology of fine coal suspensions'. *Proc. 3rd National Conf. on Rheology* Melbourne, p.51-54

_____., Pullum, L., Duckworth, R.A., Littlejohn, M.H., Lenard, J.A. (1984) 'Prediction of pressure gradients for the transport of coarse coal in a fine coal carrier'. Presented, *Transp. Conf. Inst. of Engnrs. Australia* 6p.

Masliyah, J.H. (1979) *Chem. Eng. Science*, v.34, p.1166-1168

Matthew, G.D. (1986) 'Velocity profile and friction factor relationships for turbulent flow in smooth pipes - a reassessment of some earlier mixing length assumptions'. *Proc. Inst. Civ. Engrs., Part 2* v.81, p.277-290

Masuyama, T., Kawashima, T., Noda, K. (1978) 'Pressure loss of pseudo-plastic fluid flow containing coarse particles in a pipe'. *Proc. Hydrotransport 5, B.H.R.A.* P.D1-1/14

_____., Kawashima, T., Noda, K. (1982) 'Study on the pressure loss of pseudo-plastic fluid flow containing coarse particles in horizontal pipes'. *The Technology Reports of the Toholeu University* v.47, p.79-92

Maude, A.D., Whitmore, R.L. (1956) 'The wall effect and the viscometry of suspensions'. *Brit. Jou. Appl. Phys.* v.7, p.98-102

_____., Whitmore, R.L. (1958a) 'The turbulent flow of suspensions in tubes'. *Trans. Inst. Chem. Engrs.* v.36, p.296-310

_____., Whitmore, R.L. (1958b) 'A generalised theory of sedimentation'. *Brit. Jou. Appl. Phys.* v.9, p.477-482

Meyer-Peter, E., Müller, R. (1948) 'Formulas for bed load transport'. *Int. Assoc. Hyd. Research*, 2nd Meeting, Stockholm

Michaelides, E.E., Farmer, L.K. (1984) 'A model for slurry flows based on the equations of turbulence'. *Jou. of Pipelines* v.4 n.3, p.185-191

Michaelson, A.P., Thompson, J.L., Bruce, A.M. , Frost, R.C. (1982) 'Sewage sludge pumping - Recent research and application'. *Water Pollution Control* v.81 n.2, p.220-240

Michiyoshi, I., Matsumoto, R., Mizuno, K., Nakai, M. (1966) 'Flow of slurry through a circular pipe. Friction factor for tubes, Part 2'. *Int. Chem. Engr.* v.6 n.2, p.382-388

_____., Masumoto, R., Nakai, N., Kikuchi, S. (1966) 'Flow of slurry through circular tubes, Part 3. Velocity distribution in turbulent flow'. *Int. Chem. Engr.* v.6 n.3, p.534-539

Murphy, P.J., Aguirre, E.J. (1985) 'Bed load on suspended load'. *Jou. Hyd. Engr.* v.111 n.1, p.93-107

_____. (1985) 'Equilibrium boundary condition for suspension'. *Jou. Hyd. Engr.* v.111 n.1, p.108-117

Murphy, T.D. (1977) 'Design and analysis of industrial experiments'. *Chem. Engineering*, June, p.168-181

Murrell, J.N., Boucher, E.A. (1982) *Properties of liquids and solutions*; Chichester : John Wiley & Sons Ltd.

Nakagawa, H., Tsujimoto, T. (1975) 'Mechanism of motion of individual sediment particles'. *Trans. J.S.C.E.* v.7, p.99-100

Nasr-el-din, H., Shook, C.A., Colwell, J. (1986) 'The lateral variation of solids concentration in horizontal slurry pipeline flow'. *Proc. Int. Symp. on Slurry Flow, A.S.M.E. Winter Annual Meeting* p.175-180

Newitt, D.M., Richardson, J.F., Abbott, M., Turtle, R.B. (1955) 'Hydraulic converging of solids in horizontal pipes'. *Trans. Inst. Chem. Engrs.* v.33, p.93-113

_____., Richardson, J.F., Shook, C.A. (1962) *Proc. Symp. Interaction between Fluids and Particles*, I.C.E. London, p.87

Nicholson, J., O'Connor, B.A. (1986) 'Cohesive sediment transport model'. *Jou. Hyd. Engnr.* v.112 n.7, p.621-640

Noda, K., Takahashi, H., Kawashima, T. (1984) 'Relation between behaviour of particles and pressure loss in horizontal pipes'. *Proc. Hydrotransport 9 B.H.R.A.* p.191-205

Novak, P., Nalluri, C. (1972) 'A study into the correlation of sediment motion in pipe and open channel flow'. *Proc. Hydrotransport 2 B.H.R.A.* p.D4-33/51

_____., Nalluri, C. (1974) 'Correlation of sediment incipient motion and deposition in pipes and open channels with fixed smooth beds'. *Proc. Hydrotransport 3 B.H.R.A.* p.E4-45/56

O'Brien, M.P., Folsom, R.G. (1937) 'The transportation of sand in pipelines'. *University of California Publications in Engineering* v.3 n.7, p.343-384

Odrowaz-Pieniazek, S., Steele, K. (1986) 'Advances in slurry pumps. Part 2'. *The Chemical Engineer*, March, p.30-33

Okada, T., Hisamitsu, N., Ise, T., Takeishi, Y. (1982) 'Experiments on restart of reservoir sediment slurry pipeline'. *Proc. Hydrotransport 8 B.H.R.A.* p.399-414

Okuda, K. (1981) 'Trajectory and diffusion of particles in liquid-solid flow of slurry pipeline'. *Jou. of Pipelines* v.1 n.3, p.211-223

_____. (1986) 'Mechanism for suspension and dispersion for coarse solid particles in the hydraulic transport pipe'. *Proc. Hydrotransport 7 B.H.R.A.* p.291-300

Oroskar, A.R., Turian, R.M. (1980) 'The critical velocity in pipeline flow of slurries'. *Jou. A.E. Ch. E.* v.26 n.4, p.550-558

Parchure, T.M., Mehta, A.J. (1985) 'Erosion of soft cohesive sediment deposits'. *Jou. Hyd. Engnr.* v.111 n.10, p.1308-1326

Parzonka, W., Kenchington, J.M., Charles, M.E. (1981) 'Hydrotransport of solids in horizontal pipes : Effects of solids concentration and particle size on the deposit velocity'. *Can. Jou. Chem. Engnr.* v.59, p.291-296

Peters, J., Salazar, A., Shook, C.A. (1977) 'Startup of a pipeline containing settled solid particles'. *Can. Jou. Chem. Engnr.* v.55, p.506-509

Pike, R.W., Wilkins, B., Ward, H.C. (1965) 'Measurement of the void fraction in two-phase flow by x-ray attenuation'. *Jou. A.I. Ch. E.* v.11 n.5, p.794-800

Piotrowski, G. (1983) 'Interactive data acquisition and analysis - A design philosophy'. *Mechanical Engineering*, November, p.43-49

Ponce-Campos, C.D., Wall, D.G. (1984) 'A model for the calculation of hold-up in turbulent solid-liquid flow'. *Jou. of Pipelines* v.4 n.3, p.177-183

Poreh, M., Eakin, J.L., Brosh, A., Warshavsky, M. (1970) 'Drag reduction in hydraulic transport of solids'. *Proc. A.S.C.E. (Jou. Hydr. Div.)* v.96 n.HY4, p.903-909

Prasad, P. (1985) 'Waves at the interface between a clear liquid and a mixture in a two-phase flow'. *Jou. Fluid Mech.* v.150, p.417-426

Quader, A.K.M.A., Wilkinson, W.L. (1980) 'Correlation of turbulent flow rate-pressure drop data for non-Newtonian solutions and slurries in pipes'. *Int. Jou. Multiphase Flow* v.6, p.553-561

Reddy, V., McLaughlin, J.B., Nunge, R.J. (1985) 'A numerical study of pulsed turbulent pipe flow'. *Jou. of Fluids Engnr.* v.107, p.205-211

Reich, I., Vold, R.D. (1959) 'Flocculation-deflocculation in agitated suspensions, I. Carbon and ferric oxide in water'. *J. Phys. Chem.* v.63, p.1497

Richardson, J.F., Zaki, W.N. (1954) 'The sedimentation of a suspension of uniform spheres under conditions of viscous flow'. *Chemical Engineering Science* v.3, p.65-73

_____., Meikle, R.A. (1961a) 'Sedimentation and fluidisation Part 3, The sedimentation of uniform fine particles and of two-component mixtures of solids'. *Trans. Inst. Chem. Engrs.* v.39, p.348-356

_____., Meikle, R.A. (1961b) 'Sedimentation and fluidisation Part 4, Drag force on individual particles in an assemblage'. *Trans. Inst. Chem. Engrs.* v.39, p.357-362

_____., Simons, D.B. (1967) 'Resistance to flow in sand channels'. *Int. Assoc. Hyd. Research*, 12th Meeting, Fort Collins

Rizk, M.A., Elghobashi, S.E. (1985) 'The motion of a spherical particle suspended in a turbulent flow near a plane wall'. *Phys. Fluids* v.28 n.3, p.806-817

Roco, M.C., Shook, C.A. (1982) 'Computational approach for coal slurry pipelines'. *Proc. 7th Int. Tech. Conf. on Slurry Transportation* p.175-192

_____., Shook, C.A. (1983) 'Modelling of slurry flow : The effect of particle size'. *Can. Jou. Chem. Eng.* v.61, p.494-503

_____., Shook, C.A. (1984) 'A model for turbulent slurry flow'. *Jou. Pipelines* v.4, p.3-13

_____., Balakrishnam, N. (1985) 'Multi-dimensional flow analysis of solid-liquid mixtures'. *Jou. Rheology* v.29 n.4, p.431-456

_____., Shook, C.A. (1985a) 'Turbulent flow of incompressible mixtures'. *Jou. Fluids Engnr.* v.107, p.224-231

_____., Shook, C.A. (1985b) 'Critical deposit velocity in slurry flow'. *Jou. A.E. Ch. E.* v.31 n.8, p.1401-1403

Rose, H.E., Duckworth, R.A. (1969) 'Transport of solid particles in liquids and gasses'. *The Engineer* v.227 n.5903, p.392-396; v.227 n.5904, p.430-433; v.227 n.5905, p.478-483

Sakamoto, M., Mase, M., Nagawa, Y., Uchida, K., Kamino, Y. (1978) 'The hydraulic transport study of coarse materials including fine particles with hydrohoist'. *Proc. Hydrotransport 5, B.H.R.A.* p.D6-79/90

Samaga, B.R., Ranga Raju, K.G., Garde, R.J. (1986a) 'Bed load transport of sediment mixtures'. *Jou. Hyd. Engnr.* v.112 n.11, p.1003-1018

_____., Ranga Raju, K.G., Garde, R.J. (1986b) 'Suspended load transport of sediment mixtures'. *Jou. Hyd. Engnr.* v.112 n.11, p.1019-1035

Scarlett, B., Grimley, A. (1974) 'Particle velocity and concentration profiles during hydraulic transport in a circular pipe'. *Proc. Hydrotransport 3 B.H.R.A.* p.D3-23/37

Schlichting, H. (1955) *Boundary layer theory*, New York : McGraw-Hill Inc.

Schowalter, W.R. (1960) 'The application of boundary-layer theory to power-law pseudoplatic fluids : Similar solutions'. *Jou. A.I. Ch. E.* v.6 n.1, p.24-28

Schriek, W., Smith, L.G., Haas, D.B., Husband, W.H.W. (1973) 'Experimental studies on solids pipelining of Canadian commodities for The Canadian Transport Commission and The Transportation Development Agency'. *Report II, E73-10*, Saskatchewan Research Council.

Shahinpoor, M. (1981) 'On rapid flow of bulk materials'. *Bulk Solids Handling* v.1 n.3, p.487-500

Shemer, L. (1985) 'Laminar-turbulent transition in a slowly pulsating pipe flow'. *Phys. Fluids* v.28 n.12, p.3506-3509

Shen, H.H., Hopkins, M.A., Ackermann, N.L. (1986) 'Modelling collisional stresses in a dense fluid-solid mixture'. *Proc. Int. Symp. on Slurry Flow, A.S.C.E. Winter Annual Meeting* p.17-24

Shen, H.W., Wang, J.-S. (1970) 'Incipient motion and limiting deposit conditions of solid-liquid pipe flow'. *Proc. Hydrotransport 1 B.H.R.A.* p.H3-37/51

_____. Talk Committee for Preparation of the Sedimentation Manual (1970) 'Sediment transportation mechanics : J. Transportation of sediment in pipes'. *Proc. A.S.C.E. (Jou. Hyd. Div.)* v.96 n.HY7, p.1503-1586

Shenoy, A.V., Talathi, M.M. (1985) 'Turbulent pipe flow velocity profile model for drag-reducing fluids'. *Jou. A.I. Ch. E.* v.31 n.3, p.520-522

Shih, T.-H., Lumley, J.L. (1986) 'Second-order modelling of particle dispersion in a turbulent flow'. *Jou. Fluid Mech.* v.163, p.349-363

Shook, C.A., Daniel, S.M. (1965) 'Flow of suspensions of solids in pipelines, Part 1 : Flow with a stable stationary deposit'. *Can. Jou. Chem. Engnr.* v.43, p.56-61

_____., Daniel, S.M., Scott, J.A., Holgate, J.P. (1968) 'Flow of suspensions in pipelines, Part 2 : Two mechanisms of particle suspension'. *Can. Jou. Chem. Engnr.* v.46, p.238-244

_____., Bowles, R.C., Vassie, G.S. (1971) 'The effective viscosity of a turbulently suspended fluid-particle mixture'. *Can. Jou. Chem. Engnr.* v.49, p.544-547

_____., Haas, D.B., Husband, W.H.W., Schriek, W., Smith, L. (1972) 'Some experimental studies of the effect of particle and fluid properties upon the pressure drop of slurry flow'. *Proc. Hydrotransport 2, B.H.R.A.* p.D2-13/22

_____., Schriek, W., Smith, L.G., Haas, D.B., Husband, W.H.W. (1973) 'Experimental studies of the transport of sands in liquids of varying properties in 2 and 4 inch pipelines'. *Report VI, E73-20,* Saskatchewan Research Council

_____., Rollins, J., Vassie, G.S. (1974) 'Sliding in inclined slurry pipelines at shutdown'. *Can. Jou. Chem. Engnr.* v.52, p.300-305

_____. (1976) 'Developments in hydrotransport'. *Can. Jou. Chem. Engnr.* v.54, p.13-25

_____., Gillies, R., Haas, D.B., Husband, W.H.W., Small, M. (1982) 'Flow of coarse and fine sand slurries in pipelines'. *Jou. of Pipelines* v.3 n.1, p.13-21

_____. (1985) 'Experiments with concentrated slurries of particles with densities near that of the carrier fluid'. *Can. Jou. Chem. Engnr.* v.63, p.861-869

Sinclair, C.G. (1962) 'The limit deposit-velocity of heterogeneous suspensions. *Proc. Symp. Interaction between Fluids and Particles, London:* Inst. Chem. Engnrs. p.78-86

Sive, A.W., Lazarus, J.H. (1985) 'Final report on the hydraulic transport of fly ash slurries'. *Hydrotransport Research Unit Report No. COM5/85,* University of Cape Town

_____., Lazarus, J.H. (1986) 'A comparison of some generalised correlations for the head loss gradient of mixed regime slurries'. *Proc. Hydrotransport 10, B.H.R.A.* p.149-175

_____., Lazarus, J.H. (1987) 'Hydraulic transport systems design for high concentration fly ash slurries'. Proc. Ash - a valuable resource, C.S.I.R., South Africa v.4, 18p

Slatter, P.T. (1986) 'The rheological characterisation of non Newtonian slurries using a novel balanced beam tube viscometer'. *MSc Dissertation*, University of Cape Town

_____. (1987) 'Kaolin viscometer results'. *Private communication.* University of Cape Town.

Slattery, J.C. (1962) 'Approximations to the drag force on a sphere moving slowly through either an Ostwold-De Waele or a Sisko Fluid'. *Jou. A.I. Ch. E.* v.8 n.5, p.663-667

Smith, R.A. (1955) 'Experiments on the flow of sand-water slurries in horizontal pipes'. *Trans. Inst. Chem. Engrs* v.33, p.85-92

Smoldyrev, A. Ye. (1982) '*Pipeline transport - principles of design*'. Rochville, U.S.A. : Terraspace Inc. (Translated from Russian)

Soo, S.L., Regalbuto, J.A. (1960) 'Concentration distribution in two-phase pipe flow'. *Can. Jou. Chem. Engnr.* v.38, p.160-166

_____. (1986) 'Slurry flow modelling and effect of concentration'. *Proc. Int. Symp. on Slurry Flow, A.S.M.E. Winter Annual Meeting* p.1-8

Spells, K.E. (1965) 'Correlations for use in transport of aqueous suspensions of fine solids through pipes'. *Trans. Inst. Chem. Engnrs.* v.33, p.79-84

Steinour, H.H. (1944a) 'Rate of sedimentation : Nonflocculated suspensions of uniform spheres'. *Ind. Eng. Chem.* v.36 n.7, p.618-624

_____. (1944b) 'Rate of sedimentation : Suspensions of uniform size angular particles'. *Ind. Eng. Chem.* v.36 n.9, p.840-847

Stepanoff, A.J. (1964) 'Pumping solid-liquid mixtures'. *Mechanical Engineering* v.86, p.29-35

Streicher, D.J. (1984) 'Optimisation for hydraulic transport of solids in pipes'. *MSc Thesis*, University of Cape Town.

Streat, M., Televantos, Y., Carleton, A.J. (1976) 'Pilot-plant studies of hydraulic conveying of coarse materials at high concentration in pipelines. *Proc. Hydrotransport 4 B.H.R.A.* p.F2-21/F2-30

_____. (1982) 'A comparison of specific energy consumption in dilute and dense phase conveying of solid-water mixtures'. *Proc. Hydrotransport 8, B.H.R.A.* p.111-122

_____. (1986) 'Dense phase flow of solid-water mixtures in pipelines : A state-of-the-art review', *Proc. Hydrotransport 10, B.H.R.A.* p.39-49

Sumer, B.M., Oguz, B. (1978) 'Particle motions near the bottom in turbulent flow in an open channel'. *Jou. Fluid Mech.* v.86 n.1, p.109-127

_____., Deigaard, R. (1981) 'Particle motions near the bottom in an open channel. Part 2'. *Jou. Fluid Mech.* v.109, p.311-337

Tadros, T.F. (1985) 'Rheology of concentrated suspensions'. *Chemistry and Industry*, 1 April, p.210-218

Takaoka, T., Hisamitsu, N., Ise, T., Takeishi, Y. (1981) 'Blockage of slurry pipeline'. *Bulk Solids Handling* v.1 n.3, p.479-486

Task Committee on Preparation of Sedimentation Manual (1962) 'Sediment Transportation Mechanics : Introduction and properties of sediment'. *Proc. A.S.C.E. (Jou. Hyd. Div.)*, v.88 n.HY4, p.77-107

_____. (1963) 'Sediment Transportation Mechanics : Suspension of Sediment'. *Proc. A.S.C.E. (Jou. Hyd. Div.)*, v.89 n.HY5, p.45-76

_____. (1966) 'Sediment Transportation Mechanics : Initiation of Motion'. *Proc. A.S.C.E. (Jou. Hyd. Div.)*, v.92 n.HY2, p.292-314

_____. (1970) 'Sediment Transportation Mechanics : J. Transportation of sediment in pipes'. *Proc. A.S.C.E. (Jou. Hyd. Div.)*, v.96 n.HY7, p.1503-1586

_____. (1971) 'Sediment Transportation Mechanics : F. Hydraulic relations for alluvial streams'. *Proc. A.S.C.E. (Jou. Hyd. Div.)*, v.97 n.HY1, p.101-141

of solids in

: studies of
ı pipelines.

ı dilute and
ransport 8,

pelines : A
49

ı turbulent

in an open

ıistry and

ockage of

'Sediment
'. *Proc.*

ısion of

tion of

_____. (1970) 'Sediment Transportation Mechanics : J. Transportation of sediment in pipes'. *Proc. A.S.C.E. (Jou. Hyd. Div.)*, v.96 n.HY7, p.1503-1586

_____. (1971) 'Sediment Transportation Mechanics : F. Hydraulic relations for alluvial streams'. *Proc. A.S.C.E. (Jou. Hyd. Div.)*, v.97 n.HY1, p.101-141

_____. (1971) 'Sediment Transportation Mechanics : H. Sediment discharge formulas'. *Proc. A.S.C.E. (Jou. Hyd. Div.)*, v.97 n.HY4, p.523-567

_____. (1971) 'Sediment Transportation Mechanics : Fundamentals of sediment transportation'. *Proc. A.S.C.E. (Jou. Hyd. Div.)*, v.97 n.HY12, p.1979-2002

Taylor, H.M., Leonard, E.F. (1965) 'Axial dispersion during pulsating pipe flow'. *Jou. A.I. Ch. E.* v.11 n.4, p.686-689

Taylor, R.P., Coleman, H.W., Hodge, B.K. (1985) 'Prediction of turbulent rough-wall skin friction using a discrete element approach'. *Jou. Fluids Engnr.* v.107, p.251-257

Televantos, Y., Shook, C., Carlton, A., Streat, M. (1979) 'Flow of slurries of coarse particles at high solids concentrations'. *Can. Jou. Chem. Engnr.* v.57, p.255-262

Thomas, A.D. (1975a) 'Factors affecting the hydraulic performance of slurries'. *Proc. Conf. Thermofluids, Brisbane* Inst. of Eng. Australia p.96-100

_____. (1975b) 'December monthly project report'. M.D. Research Co., Aust. 12p.

_____. (1976a) 'Some results of applying scale-up equations to predict slurry pressure drop in large pipes'. *Unpublished* M.D. Research Co., Aust. 12p.

_____. (1976b) 'Scale-up methods for pipeline transport of slurries'. *Int. Jou. Mineral Processing* v.3, p.51-69

_____. (1977a) 'Particle size effects in turbulent pipe flow of solid-liquid suspensions'. *Proc. 6th Aust. Hyd. and Fluid Mech. Conf.* Adelaide p.113-116

_____. (1977b) 'Variation of deposit velocity with pipe size for horizontal turbulent flow of slurries composed of discrete particles in Newtonian fluids'. *Unpublished* 19p.

_____. (1978) 'Coarse particles in a heavy medium - Turbulent pressure drop reduction and deposition under laminar flow'. *Proc. Hydrotransport 5, B.H.R.A.* p.D5-63/78

_____. (1979a) Predicting the deposit velocity for horizontal turbulent pipe flow of slurries'. *Int. Jou. Multiphase Flow* v.5, p.113-129

_____. (1979b) 'Pipelining of coarse coal as a stabilized slurry - another viewpoint'. *Proc. 4th Int. Tech. Conf. on Slurry Transportation* p.196-205

Thomas, D.G. (1961) 'Transport characteristics of suspensions : Minimum transport velocity for flocculated suspensions in horizontal pipes'. *Jou. A.I. Ch. E.* v.7 n3, p.423-430

_____. (1962) 'Transport characteristics of suspensions, Part 6. Minimum transport velocity of large particle size suspensions in round horizontal pipes'. *Jou. A.E. Ch. E.* v.8 n.3, p.373-378

_____. (1963a) 'Non Newtonian suspensions, Part 1. Physical properties and laminar transport characteristics'. *Ind. Engnr. Chem.* v.55 n.11, p.18-29

_____. (1963b) 'Transport characteristics of suspensions, Part 7. Relation of hindered-settling floc. characteristics to rheological parameters'. *Jou. A.I. Ch. E.* v.9 n.3, p.310-316

_____. (1964a) 'Periodic phenomena observed with spherical particles in horizontal pipes'. *Science* v.144, p.534-536

_____. (1964b) 'Transport characteristics of suspensions, Part 9. Representation of periodic phenomena on a flow regime diagram for dilute suspension transport'. *Jou. A.I. Ch. E.* v.10 n.3, p.303-308

Toda, M., Konno, H., Saito, S. (1980) 'Simulation of limit-deposit velocity in horizontal liquid-solid flow'. *Proc. Hydrotransport 7, B.H.R.A.* p.347-358

Torrence, B. McK. (1963) 'Friction factors for turbulent non-Newtonian fluid flow in circular pipes'. *The South African Mechanical Engineer* v.13, p.89-91

Tsuji, Y., Morikawa, Y., Fujiwara, Y. (1985) 'Pipe flow with solid particles fixed in space'. *Int. Jou. Multiphase Flow* v.11 n.2, p.177-188

Turian, R.M., Yuan, T.-F. (1977) 'Flow of slurries in pipelines'. *Jou. A.I. Ch. E.* v.23 n.3, p.232-243

Valentik, L., Whitmore, R.L. (1965) 'The terminal velocity of spheres in Bingham plastics'. *Brit. Jou. Appl. Phys.* v.16, p.1197-1203

Vanoni, V.A. (1946) 'Transportation of suspended sediment by water'. *Trans. A.S.C.E.* v.111, p.67-133

Verkerk, C.G. (1982) 'Investigation into the design of slurry pipelines with reference to low and high concentration slurries'. *M.Sc. Dissertation*, Johannesburg : University of Witwatersrand

Vocadlo, J.J., Charles, M.E. (1972) 'Prediction of pressure gradient for the horizontal turbulent flow of slurries'. *Proc. Hydrotransport 2, B.H.R.A.* p.C1-1/12

_____. (1976) 'Role of some parameters and effective variables in turbulent slurry flow'. *Proc. Hydrotransport 4 B.H.R.A.* p.D4-49/D4-51

Wadell, H. (1935) 'Volume, shape, and roundness of quartz particles'. *Jou. of Geology* v.43, p.250-280

Wagner, K. (1982) 'Consideration of the effect of a wide particle size distribution on calculations for hydraulic conveying'. *Bulk Solids Handling* v.2 n.2, p.249-252

Wakefield, A.W. (1986) 'Design of stable coarse-slurry pipelines'. *Bulk Solids Handling* v.6 n.4, p.755-758

Wallace, J.M., Brodkey, R.S., Eckelmann, H. (1977) 'Pattern-recognised structures in bounded turbulent shear flows'. *Jou. Fluid Mech.* v.83, p.673-693

Wallis, G. B. (1969) '*One-dimensional two-phase flow*'. New York : McGraw-Hill Inc.

Wan, Z. (1985) 'Bed material movement in hyperconcentrated flow'. *Jou. of Hyd. Engnr.* v.111 n.6, p.587-1002

Wani, G.A., Sarkar, M.K., Pitchumani, B. (1982) 'Pressure drop prediction in multisize particle transportation through horizontal pipes'. *Jou. of Pipelines* v.3 n.1, p.23-33

_____., Mani, B.P., Suba Rad, D., Sarkar, M.K. (1983) 'Studies on hold-up and pressure gradient in hydraulic conveying of settling slurries through horizontal pipes'. *Jou. of Pipelines* v.3 n.3, p.215-222

Ward, S.G., Whitmore, R.L. (1950) 'Studies of the viscosity and sedimentation of suspensions, Part 2 : The viscosity and sedimentation of suspensions of rough powders'. *Brit. Jou. Appl. Phys.* v.1 n.12, p.325-328

Wasp, E.J., Regan, T.J., Withers, J., Cook, P.A.C., Clancey, J.T. (1963) 'Cross-country coal pipe line hydraulics'. *Pipe Line News* v.35, p.20-28

_____., Aude, T.C., Kenny, J.P., Seiter, R.H., Jacques, R.B. (1970) 'Deposition velocities, transition velocities, and spatial distribution of solids in slurry pipelines'. *Hydrotransport 1, B.H.R.A.* P.H4-53/76

_____., Aude, T.C., Seiter, R.H., Thompson, T.L. (1971) 'Hetero-homogeneous solids/liquid flow in the turbulent regime'. *Advances in solid-liquid flow in pipes and its application (I. Zandi, Ed.)* Oxford: Pergamon p.199-210

Wasserman, M.L., Slattery, J.C. (1964) 'Upper and lower bounds on the drag coefficient of a sphere in a power-model fluid'. *Jou. A.I. Ch. E.* v.10 n.3, p.383-388

Weber, M. (1986) 'Improved Durand-equation for multiple application'. *Proc. Int. Symp. on Slurry Flow, A.S.M.E. Winter Annual Meeting* p.61-66

Webster, I.W., Sauermann, H.B. (1978) 'Pressure gradient scale-up methods for slurry pipelines'. *The South African Mechanical Engineer* v.28, p.312-318

Weltmann, R.N., Green, H. (1943) 'Rheological properties of colloidal solutions, pigment suspensions and oil mixtures'. *Jou. Appl. Phys.* v.14, p.569-576

White, C.M. (1940) 'The equilibrium of grains on the bed of a stream'. *Proc. Roy. Soc. London* v.174 Ser. A, p.322-338

Wiedenroth, W. (1979) 'Methods for the determination of the transport concentration and some problems associated with the use of radiometric density meters'. *Proc. Hydrotransport 6 B.H.R.A.* p.89-104

Willetts, B.B. (1970) 'The influence of lift due to circulation on saltation and suspension of solid particles in streams'. *Proc. Hydrotransport 1 B.H.R.A.* p.H3-37/51

Wilson, K.C. (1966) 'Bed load transport at high shear stress'. *Proc. A.S.C.E. (Jou. Hyd. Div.)* v.92 n.HY6, p.49-59

_____. (1970) 'Slip point of beds in solid-liquid pipeline flow'. *Proc. A.S.C.E. (Jou. Hyd. Div.)* v.96 n.HY1, p.1-12

_____., Streat, M., Bantin, R.A. (1972) 'Slip-model correlation of dense two-phase flow'. *Proc. Hydrotransport 2, B.H.R.A.* P.B1-1/10

_____. (1972) 'A formula for the velocity required to initiate suspension in pipeline flow'. *Proc. Hydrotransport 2, B.H.R.A* p.E2-23/36

_____., Watt, W.E. (1974) 'Influence of particle diameter on the turbulent support of solids in pipeline flow'. *Proc. Hydrotransport 3, B.H.R.A.* p.D1-1/9

_____. (1974) 'Co-ordinates for the limit of deposition in pipeline flow'. *Proc. Hydrotransport 3, B.H.R.A.* P.E1-1/13

_____. (1976) 'A unified physically-based analysis of solid-liquid pipeline flow'. *Proc. Hydrotransport 4, B.H.R.A.* p.A1-1/16

_____., Judge, D.G. (1977) 'Application of analytic model to stationary-deposit limit in sand-water slurries'. *2nd Int. Symp. on Dredging Tech. B.H.R.A.* p.J1-1/11

_____., Judge. D.G. (1978) 'Analytically-based nomographic charts for sand-water flow'. *Proc. Hydrotransport 5, B.H.R.A.* p.A1-1/12

_____. (1979) 'Deposition-limit nomograms for particles of various densities in pipeline flow'. *Proc. Hydrotransport 6, B.H.R.A.* p.1-12

_____., Judge, D.G. (1980) 'New techniques for the scale-up of pilot-plant results to coal slurry pipelines'. *Jou. of Powder and Bulk Solids Tech.* v.4 n.1, p.15-22

_____. (1980) 'Analysis of slurry flow with a free surface'. *Proc. Hydrotransport 7 B.H.R.A.* p.123-132

_____. (1981) 'Analysis of slip of a particulate mass in a horizontal pipe'. *Bulk Solids Handling* v.1 n.2, p.295-299

_____., Thomas, A.D. (1985) 'A new analysis of the turbulent flow of non-Newtonian fluids'. *Can. Jou. Chem. Engnr.* v.63, p.539-546

_____. (1986) 'Modelling the effects of non-Newtonian and time-dependent slurry behaviour'. *Proc. Hydrotransport 10 B.H.R.A.* p.283-289

_____. (1987) 'Analysis of bed load motion at high shear stress', *Jou. of Hyd. Engnr.* v.113 n.1, p.97-103

Wood, D.J. (1979) 'Pressure gradient requirements for re-establishment of slurry flow'. *Proc. Hydrotransport 6 B.H.R.A.* p.217-228

Worster, R.C. (1955) 'Some tests on the flow along pipes of mixtures of fly ash and water'. *B.H.R.A. Report No. 507* Cranfield 10p.

Yagi, T., Okude, T., Miyazaki, S., Koreishi, A. (1972) 'An analysis of the hydraulic transport of solids in horizontal pipelines'. *Report of the Port and Harbour Research Institute* v.11 n.3, 34p.

Yang, W.-C. (1984) 'Mechanistic models for transitions between regimes of fluidization'. *Jou. A.I. Ch. E.* v.30 n.6, p.1025-1027

Yen, J.G., Aandi, I. (1969) 'Transport of slurries in heterogeneous regime'. *Preprint No. 69-B-70 A.I.M.E.* 28p.

Young, D.F. (1961) 'Drag and lift on spheres within cylindrical tubes'. *Trans. A.S.C.E.* v.162, Part I, p.1235-1248

Zandi, I. (1971) 'Hydraulic transport of bulky materials'. *Advances in Solid-Liquid Flow in Pipes and its Application* (I Zandi, ed.) Oxford : Pergamon p.1-34

Zenz, F.A. (1964) 'Conveyability of materials of mixed particle size'. *I.E.E.C. Fund.* v.3 n.1, p.65-75

Zhaoyin, W., Ning, Q. (1984) 'Experiment study of two-phase turbulent flow with hyperconcentration of coarse particles'. *Scientia Sinica (Series A)* v.27 n.12, p.1317-1327

Zilker, D.P., Cook, G.W., Hanratty, T.J. (1977) 'Influence of the amplitude of a solid wavy wall on a turbulent flow, Part 1. Non-separated flows'. *Jou. Fluid Mech.* v.82 n.1, p.29-51